DISSERTATION

submitted to the

Combined Faculties of Natural Sciences and Mathematics
University of Heidelberg, Germany

for the degree of

Doctor of Natural Sciences (Dr. rer. nat.)

presented by

MSc Jan Frederik Hartmann

born in Speyer, Germany

Oral examination: 18.10.2018

Methane Dynamics in Lakes

Referees:

Prof. Dr. Margot Isenbeck-Schröter

Prof. Dr. Frank Keppler

Kurzfassung

Im Rahmen dieser Arbeit wurde eine schnelle und sensitive Methode zur kontinuierlichen Bestimmung der Konzentrationen von Methan (CH_4) und der stabilen Kohlenstoff-Isotopie von CH_4 ($\delta^{13}C$-CH_4) in Wässern entwickelt. Das Gas wird mittels Vakuum durch eine Membran aus dem Wasser extrahiert und mit einem portablen *cavity ring-down spectroscopy Analyser* analysiert (M-CRDS). Das M-CRDS wurde mithilfe von synthetischen Wasserstandards kalibriert und zeigte während Labor- und Feldmessungen eine sehr gute Übereinstimmung mit konventionellen Messmethoden. Das M-CRDS erlaubt somit kontinuierliche und zeitlich-hochauflösende Analysen von CH_4 Konzentrationen und $\delta^{13}C$-CH_4 Werten in Oberflächengewässern.

Die neuentwickelte Methode (M-CRDS) wurde an drei verschiedenen Seen erfolgreich eingesetzt: Willersinnweiher (Deutschland), Stechlinsee (Deutschland) und Erkensee (Schweden). Diese Untersuchungen zeigen erstmals die große Variabilität von CH_4 in der Wassersäule und den Sedimenten. Die Studien an den drei Seen mit unterschiedlichen Nährstoffgehalten verdeutlichen, dass die anaerobe und aerobe Oxidation von CH_4 eine bedeutende Senke für CH_4 in den Sedimenten bzw. der Wassersäule darstellt und die Emission von CH_4 in die Atmosphäre weitgehend verhindert.

Ungeachtet dessen wurde im Epilimnion aller Seen eine CH_4-Übersättigung im Vergleich zur Atmosphäre beobachtet. Diese Übersättigung resultierte zumeist aus dem lateralen Transport von CH_4 aus der Uferzone der Seen oder dem Eintrag durch Grundwasser, wie z.B. am Willersinnweiher. Zudem wurde u.a. am Stechlin eine Methanproduktion durch photoautotrophe Organismen im oxischen Epilimnion beobachtet. Diese Produktion ist möglicherweise direkt an die Dynamik von Algenblüten gekoppelt. Die zeitliche und räumliche Variabilität von CH_4 im Wasser ist somit durch die Produktion und die Emission von CH_4 gesteuert. Die Studien zeigen, dass windinduzierte Veränderungen in den oberflächennahen Schichten von Seen auch in zeitlich hochvariablen Emissionsraten von CH_4 resultieren. Die Untersuchungen haben gezeigt, dass sowohl die Eutrophierung als auch die Klimaerwärmung einen essentiellen Einfluss auf die CH_4-Produktion in Seen haben. Dabei werden die CH_4-Emissionen von limnischen Gewässern in die Atmosphäre in Zukunft ansteigen – mit weitreichenden Konsequenzen für den Klimawandel.

Abstract

Within the framework of this study a fast and sensitive method for the continuous determination of methane (CH_4) and its stable carbon isotopic values ($\delta^{13}C\text{-}CH_4$) in surface waters was developed. The gas is extracted by applying a vacuum to a gas-liquid exchange membrane and measured by a portable cavity ring-down spectroscopy analyser (M-CRDS). The M-CRDS was calibrated and characterised for CH_4 concentration and $\delta^{13}C\text{-}CH_4$ with synthetic water standards. Deployments in the laboratory as well as during fieldwork showed a very good agreement of CH_4 measured simultaneously by the M-CRDS and conventional analytical methods. Therefore, the M-CRDS provides the continuous analyses of dissolved CH_4 concentrations and $\delta^{13}C\text{-}CH_4$ values of surface water at a very high temporal resolution.

The newly developed method (M-CRDS) was successfully deployed at three lakes with different trophic states: Lake Willersinnweiher (Germany), Lake Stechlin (Germany) and Lake Erken (Sweden). The studies revealed for the first time high spatial and temporal variability of CH_4 behaviour in the water column and the sediments. In addition, these studies showed that the presence of anaerobic (AOM) and aerobic (MOx) oxidation of methane in the sediment and within the water column, respectively, is a very effective barrier to CH_4 emission into the atmosphere in thermal stratified lakes.

Nonetheless, CH_4 oversaturation with respect to the atmosphere was observed in the surface water layer of all three lakes during all seasons of the year. Most surface water CH_4 concentrations are derived by horizontal transport processes from littoral zones. Groundwater-fed lakes such as Lake Willersinnweiher might be enriched in CH_4 by groundwater contributing to its methane pool. Surface water CH_4 could also be produced *in-situ* by the photoautotroph community, directly linked to algae dynamics and algae abundances. The temporal and spatial variability of CH_4 is thereby unambiguously controlled by CH_4 accumulation within the oxic water layer and its CH_4 loss to the atmosphere. These studies also demonstrated that wind-induced changes in the upper water column of lakes lead to highly variable CH_4 emissions from lakes. Growing eutrophication and climate warming will both have major effects on the CH_4 pool of lakes. Accordingly, CH_4 emissions from freshwater environments will further increase in the future with far-reaching consequences for climate change.

Acknowledgements

First and foremost I would like to thank my thesis supervisor Margot Isenbeck-Schröter for all her support she gave me over the years that I have been a member of her research group. She got me into her group 9 years ago, gave me total freedom to work in all fields of my interest and challenged and encouraged me all at the same time. Many thanks also to Frank Keppler for his support during the research and the publication work as well as for agreeing to be my second thesis referee.

A special thank you goes to Torben Gentz of the AWI for his sympathetic ear and helpful advices mostly in times of endless methodical problems and struggle - especially during the development of the new method. Furthermore, Torben helped me to establish the first contacts to the crews at Lake Stechlin and Lake Erken, managed to get me on RV Heincke and – not to forget – offered me his outrageously expensive synthetic water standards free of charge ;).

Getting through this project would not have been possible without the research group "Hydrogeochemistry and Hydrogeology" in Heidelberg. Thank you. You are my second family! Christian Scholz shared his extensive knowledge and experience in laboratory and fieldwork. Stefan Rheinberger is THE contact person when having any trouble and always a reliable source of information and help - and also of fantastic, but often bad jokes and puns. In all the years in Heidelberg, Simon Ritter became a very good friend, proofreader, discussion partner and fellow sufferer. Together with Florian Freundt, Sami AlNajem and Lukas Klose: you are not only fantastic colleagues but you have turned out to be good friends and sports partners. Silvia Rheinberger is the good soul of the group and I was so lucky to have her as my roommate over all these years. My bachelor and master students Markus Ohnemus (very first fieldwork / experiences with the M-CRDS), Felix Rabe (hard fieldwork at Lake Stechlin) and in particular Yannic Wellach (fantastic work at Lake Willersinnweiher) and Amanda Schiller (essential calibration and characterisation work during the development of the new method) played a key part in this work.

Many thanks also to my various collaboration partners: Markus Greule supported the calibration work, Thomas Klintzsch provided important results from laboratory incubations, Hans-Peter Grossart (IGB) supported and pushed

the field measurements at Lake Stechlin and Marco Günthel (University of Edinburgh), Georgiy Kirillin (IGB) as well as Armin Penske (IGB) supplied me with essential results from fieldwork.

Finally, and most importantly, I want to thank my friends and family – especially my parents – your support in every respect during this thesis, but also during my whole life made this happen. Special thanks to Charlotte for supporting, understanding and loving me unconditionally the way I am!

Abbreviations

Common used abbreviations used in this work. Parameter for calculations and element names are explained in the text.

Abbreviation*	Description	**Abbreviation**	Description
CH_4	methane	**AOM**	anaerobic oxidation of CH_4
$\delta^{13}C$-CH_4	stable carbon isotopic composition of methane	**DAOM**	denitrification-dependent anaerobic oxidation of CH_4
CRDS	cavity ring-down spectroscopy	**MOx**	aerobic oxidation of CH_4
M-CRDS	membrane-coupled cavity ring-down spectroscopy (analyser)	**OM**	organic matter
GC-FID	gas chromatography with flame ionization detector	**OMP**	oxic methane production
GC-C-IRMS	gas chromatography combustion isotope ratio mass spectrometry	**SCR**	sedimentary carbon conversion rates
ICOS	off-axis integrated cavity output spectrometer	**SMTZ**	sulphate-methane transition zones
M-ICOS	membrane-coupled off-axis integrated cavity output spectrometer	**SRB**	sulphate reducing bacteria
UWMS	underwater mass spectrometry	**SRR**	sulphate reduction rates
		TEA	terminal electron acceptor
AWI	Alfred-Wegener Institute, Helmholtz Centre for Polar and Marine Research, Bremerhaven (Germany)		
IGB	Leibniz-Institute of Freshwater Ecology and Inland Fisheries, Berlin (Germany)		

Contents

Introduction 3

1. Establishment and Optimisation of the new Method (M-CRDS) 17

1.1. Method Calibration 23

1.1.1. Procedure 23

1.1.2. Results 24

1.2. Method Characterisation 29

1.2.1. Procedure 29

1.2.2. Results 30

1.3. Potential sources of errors 35

1.4. First field application 39

1.4.1. Procedure 39

1.4.2. Results 40

2. Field studies 45
2.1. Lake Willersinnweiher 47
2.1.1. Study site 47
2.1.2. Material and Methods 49
2.1.3. Results 55
2.1.4. Discussion 65
2.1.5. Conclusions 83
2.2. Lake Stechlin 85
2.2.1. Study site 87
2.2.2. Material and Methods 89
2.2.3. Results 91
2.2.4. Discussion 97
2.2.5. Conclusions 107
2.3. Lake Erken 109
2.3.1. Study site 109
2.3.2. Material and Methods 111
2.3.3. Results 115
2.3.4. Discussion 121
2.3.5. Conclusion 131
3. Conclusions and Prospective Research 133
3.1. The M-CRDS 135
3.2. Methane in lake environments and future prospects 137
4. Related Scientific Work 143
5. List of Figures 147
6. List of Tables 159
7. References 161
8. Appendix 183

Introduction

Methane (CH_4) is an atmospheric greenhouse gas playing an important role in climate research, as its global warming potential is estimated to be 86 times the potential of carbon dioxide (CO_2) in the coming decades (IPCC-Report 2013). Atmospheric CH_4 contributes to global warming both directly as well as indirectly via the production of ozone in the troposphere and water vapour in the stratosphere (Dlugokencky et al. 2011). Recent atmospheric CH_4 concentrations are up to 2.5 times higher than during preindustrial times, which is mainly attributed to anthropogenic sources. Thus, CH_4 accounts for about one-fifth of the human-induced climate warming (Stocker et al. 2001; IPCC-Report 2013; Kirschke et al. 2013; Saunois et al. 2016).

Methane sources

In general, atmospheric CH_4 originates from both natural and anthropogenic sources (Figure 1). While anthropogenic contributions stem from burning of fossil fuels and intense agriculture, natural CH_4 is either of thermogenic, pyrogenic or biogenic origin. The latter makes up the largest share in the CH_4 budget (Kirschke et al. 2013; Saunois et al. 2016). Biogenic CH_4 mainly derives from bacterial degradation of organic matter (OM) in anoxic environments at low temperatures (< 75°C), whereas thermogenic CH_4 is formed by the thermocatalytic breakdown of complex organic molecules at high(er)

temperatures. Pyrogenic CH_4 is the result of incomplete combustion of biomass and soil carbon (Clayton 1991; Kirschke et al. 2013). The main source for atmospheric CH_4 is the biogenic CH_4 production by methanogenic archaea (80 % – 90 %) (e.g. Cicerone and Oremland 1988).

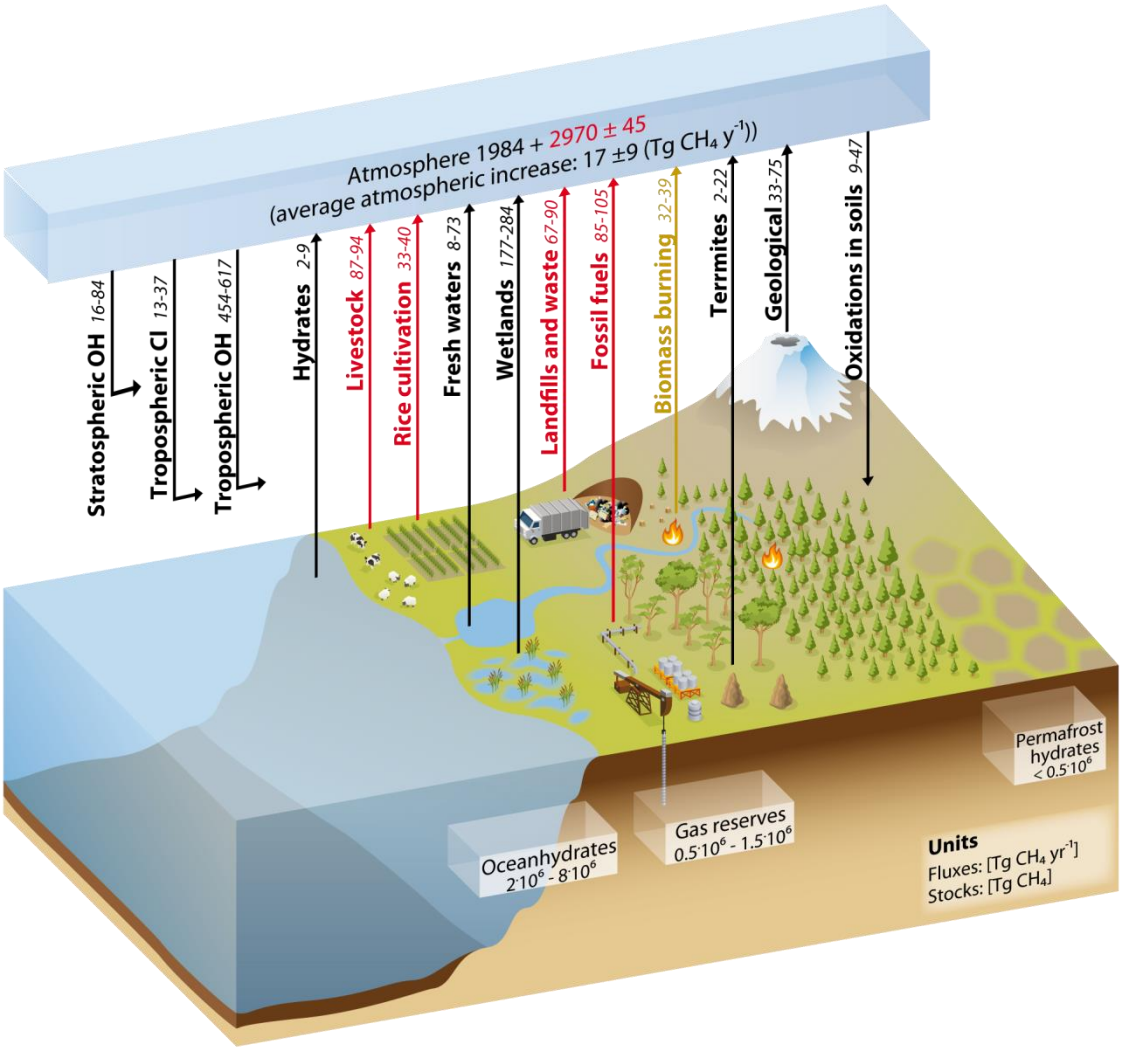

Figure 1: Global sources and sinks of CH_4 (modified after IPCC-Report 2013). Methane fluxes are given in [Tg yr^{-1}]. Natural fluxes are black, anthropogenic fluxes are red and combined natural and anthropogenic fluxes are light brown.

For long, biogenic methanogenesis in anoxic environments was believed to follow the redox sequence of OM oxidation after the depletion of oxygen, nitrate, manganese, ferric iron and sulphate as terminal electron acceptors (TEAs) (Froelich et al. 1978; Berner 1981). However, more recent studies show that the microbial community is rather controlled by the competition for the compounds used by those organisms than by the (Gibbs) energy yield by utilizing specific TEAs (Sørensen 1982; Jørgensen and Bak 1991; Thullner et al.

2007). Methane-producing archaea (methanogens) metabolize only very specific compounds and are dependent on other organisms (e.g. fermentative organisms) converting complex substrates to easily degradable substrates. In general, biomass is decomposed to acetate, formate as well as hydrogen (H_2) and CO_2 under anaerobic conditions (Figure 2). Methane is then produced from these products by methanogenic archaea (e.g. Söhngen 1906).

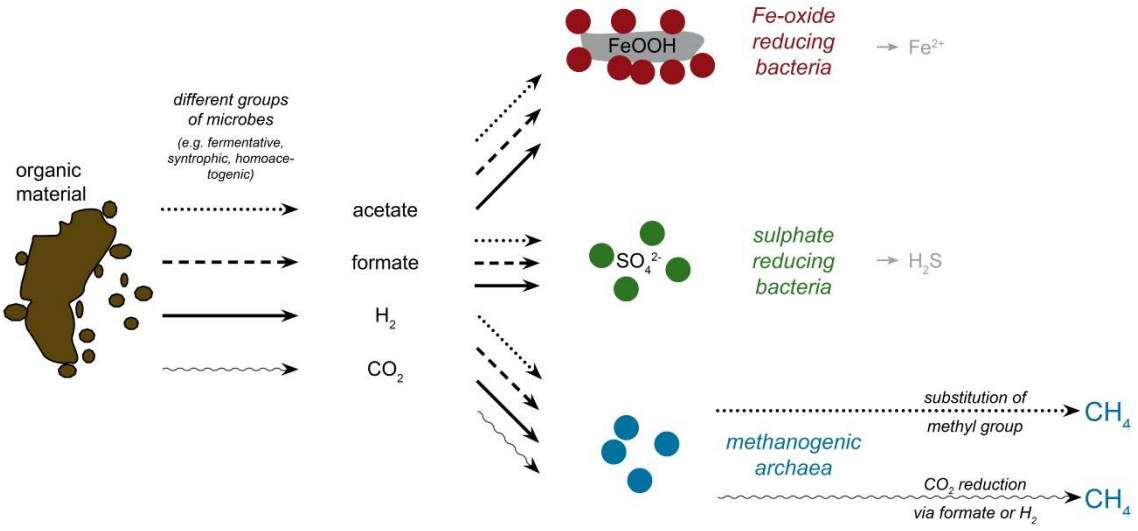

Figure 2: The pathways of organic matter decomposition under anoxic conditions. Methanogenesis during the anaerobic decomposition of organic matter base on either acetate (via substitution of the methyl group) or CO_2 reduction (via H_2 or formate). Modified after Appelo and Postma (2005).

The metabolisms are based on either the hydrogenotrophic pathway via H_2 and CO_2 (eq. [1]) or formate (eq. [2]) or the acetoclastic pathway with acetate as substrate (eq. [3]) (Conrad 1989; Ferry 2011).

CO_2 reduction pathway

via H_2 oxidation

$$\mathbf{4\,H_2 + CO_2 \rightarrow CH_4 + 2\,H_2O} \qquad [1]$$

via formate oxidation

$$\mathbf{4\,HCOOH + 4H^+ \rightarrow CH_4 + 3\,CO_2 + 2\,H_2O} \qquad [2]$$

*Acetoclastic pathway (methyl group transfer indicated with *)*

$$CH_3{}^{*}COOH \rightarrow CH_4{}^{*} + CO_2 \quad [3]$$

Methanogenic pathways depend on the availability of the compounds used by the methanogens, which vary between specific environments. The compounds are classified in competitive and non-competitive substrates (Whiticar 1999). Non-methanogens such as nitrate (NO_3^-), iron (Fe) or sulphate (SO_4^{2-}) reducing bacteria metabolize competitive substrates and outcompete the methanogens. Non-competitive substrates are not favoured by other bacteria and are preferably used by methanogens. Substrate competition mainly occurs in sulphate-rich (> 200 μM) environments (e.g. marine sediments), where sulphate reducing bacteria (SRB) are active. Below the depth of sulphate depletion, methanogenesis is often coupled to carbonate reduction (hydrogenotrophic pathway) (e.g. Conrad 1989). In contrast, freshwater environments are generally characterised by low sulphate concentrations and SRB are inactive or absent. Here, up to 70 % of total CH_4 is produced by acetotrophic methanogens (Cicerone and Oremland 1988) and subsequent CO_2 reduction under anaerobic conditions. Methanogenesis by carbonate reduction might become increasingly important with rising shortage of other substrates. Methane produced by methylotrophic pathways via methanol, methylated amines and organic sulphur compounds play a minor role in biogenic methanogenesis (Lovley and Klug 1983; Ferry 2011; Penger et al. 2012).

For decades, methanogenesis was believed to occur only under strictly anoxic conditions, although studies of the oceanic water column showed supersaturated CH_4 concentrations with respect to the atmospheric partial pressure in well oxygenated surface layers (e.g. Lamontagne et al. 1973, 1974; Brooks and Sackett 1973; Burke et al. 1988). However, these results contradicted the paradigm that CH_4 production is not supposed to occur in oxic waters ("methane paradox"). Methane accumulation within the oxic water layer was explained by e.g. methanogenesis in anoxic micro-environments in ocean particles (Karl and Tilbrook 1994). More recently, studies provided evidence that methanogenesis also occurs under aerobic conditions by yet unknown physiological processes. Keppler et al. (2006) showed that methane is produced in terrestrial plants under oxic conditions. Also, it was recently shown that CH_4 is produced in continental oxic waters (Grossart et al. 2011; Tang et al. 2016).

Here, CH_4 is strongly suggested to stem from a biological source, contributing about 4 % of the atmospheric CH_4. The pathways suggested for aerobic CH_4 production in water comprise CH_4 formation by anoxic micro-niches (Oremland 1979; Grossart et al. 2011), algal metabolites (Lenhart et al. 2015) as well as by-product of methyl-phosphonate decomposition (Karl et al. 2008). Methane occurrence and production appears to be related to photoautotrophic production and growth (Grossart et al. 2011; Bogard et al. 2014; Tang et al. 2014). It can be deduced that CH_4 production under oxic conditions might be significantly influenced by changes in the interplay between biological, chemical and physical processes in the environment.

The various pathways of CH_4 formation can be characterised and distinguished by the determination of the stable isotopic composition of CH_4 (δ^{13}C-CH_4) (Schoell 1980, 1988; Coleman et al. 1981; Conrad 2005; Laukenmann et al. 2010). The isotopic ratio between the stable carbon isotopes ^{13}C and ^{12}C is conventionally expressed in the δ notation in per mille (‰) relative to the *Vienna Pee Dee Belemnite* (V-PDB) standard, using the equation [4] (Craig 1957; Hornberger 1995).

$$\boldsymbol{\delta^{13}C} = \left[\frac{\left(\frac{\boldsymbol{^{13}C}}{\boldsymbol{^{12}C}}\right)_{\boldsymbol{sample}}}{\left(\frac{\boldsymbol{^{13}C}}{\boldsymbol{^{12}C}}\right)_{\boldsymbol{standard}}} - \mathbf{1} \right] * \mathbf{1000}‰ \qquad [4]$$

The isotopic signature of CH_4 sources is thereby significantly dependent on isotope fractionation during the methanogenic reactions and the isotope signature of the used substrate. Fractionation factors for the biogenic methanogenesis vary considerably with various conditions and environments, and differ significantly between the pathways (Conrad 2005). In general, biogenic CH_4 has low δ^{13}C-CH_4 values due to enrichment of light ^{12}C by microbial isotope fractionation (Rosenfeld and Silverman 1959; Games et al. 1978). Thermogenic CH_4 is relatively enriched in ^{13}C compared to biogenic CH_4. δ^{13}C-CH_4 values generally range from − 25 to − 55‰ for thermogenic, − 50 to − 70‰ for methanogenesis via the acetoclastic pathway and − 60 to – 110‰ via the hydrogenotrophic pathway by CO_2 reduction (Cicerone and Oremland 1988; Wahlen 1993; Neef et al. 2010; Monteil et al. 2011). The various pathways or groups of CH_4 formation are classified including the H isotope variations in

CH_4 (Figure 3). Stable H isotope ratios are given as the ^1H / ^2H ratio relative to the *Vienna Standard Mean Ocean Water* (V-SMOW) standards (δD) (Hornberger 1995).

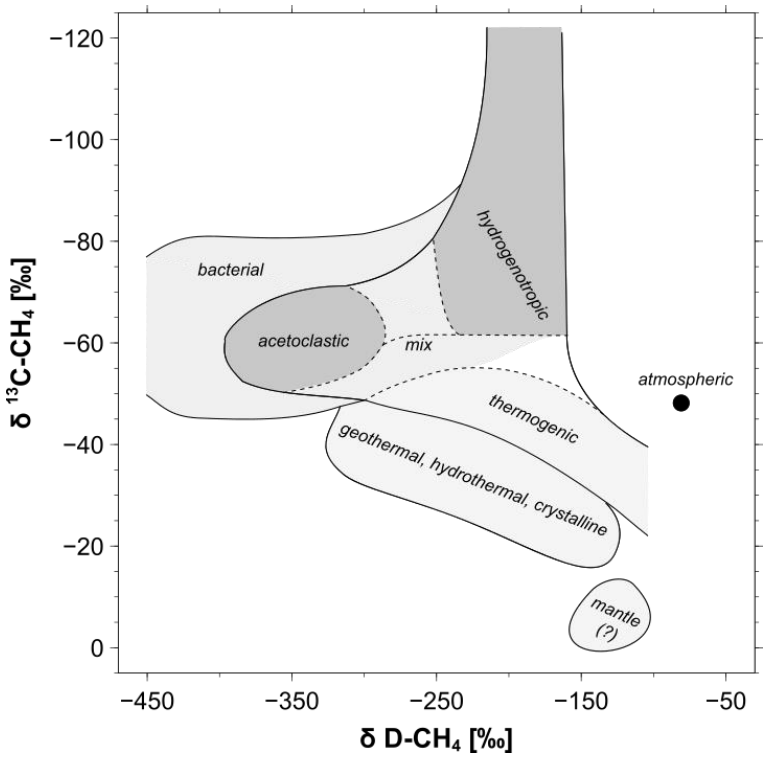

Figure 3: Classification of the various pathways of CH_4 formation using the stable isotopic composition of CH_4 ($\delta^{13}C$ and δD values). Modified after Oremland et al. (1987) and Whiticar (1999).

Methane sinks

The major atmospheric CH_4 sink is the oxidation by hydroxyl radicals (•OH), producing methyl radicals ($\bullet CH_3$) and water (H_2O) in the troposphere (eq. [5]) (Nicolet 1970; Chameides and Walker 1973; Crutzen and Zimmermann 1991).

$$\mathbf{CH_4 + \bullet OH \rightarrow \bullet CH_3 + H_2O} \qquad [5]$$

This oxidation is subsequently followed by different pathways and methyl radicals ($\bullet CH_3$) react to formaldehyde, CO and finally to CO_2 and H_2O (Chameides and Walker 1973; Crutzen 1973; Crutzen and Zimmermann 1991). Oxidation by hydroxyl radicals thereby accounts for 90% of the atmospheric CH_4 sink. Minor sinks are consumption by methanotrophic bacteria (e.g. Curry 2007) as well as reactions with chlorine radicals in the stratosphere and in the

marine air-water boundary layer (e.g. Cicerone and Oremland 1988; Allan et al. 2007).

In aquatic systems, CH_4 is oxidised by methanotrophs via anaerobic and aerobic pathways. Anaerobic oxidation of methane (AOM) is known to be coupled to the reduction of nitrate (eq. [6]) and nitrite (eq. [7]) (Raghoebarsing et al. 2006; Ettwig et al. 2008; Deutzmann et al. 2014; Norði and Thamdrup 2014; Shen et al. 2017), to the reduction of manganese (eq. [8]) and / or iron (eq. [9]) (Beal et al. 2009; Amos et al. 2011; Crowe et al. 2011; Norði et al. 2013; He et al. 2018) or to the reduction of sulphate (eq. [10]) (Martens and Berner 1974; Reeburgh 1976).

AOM coupled to the reduction of nitrate (eq. [6]) and nitrite (eq. [7])

$$\mathbf{5}\,\boldsymbol{CH_4} + \mathbf{8}\,\boldsymbol{NO_3^-} + \mathbf{8}\,\boldsymbol{H^+} \rightarrow \mathbf{5}\,\boldsymbol{CO_2} + \mathbf{4}\,\boldsymbol{N_2} + \mathbf{14}\,\boldsymbol{H_2O} \quad [6]$$

$$\mathbf{3}\,\boldsymbol{CH_4} + \mathbf{8}\,\boldsymbol{NO_2^-} + \mathbf{8}\,\boldsymbol{H^+} \rightarrow \mathbf{3}\,\boldsymbol{CO_2} + \mathbf{4}\,\boldsymbol{N_2} + \mathbf{10}\,\boldsymbol{H_2O} \quad [7]$$

AOM coupled to the reduction of manganese (eq. [8]*) and iron (eq.* [9]*)*

$$\boldsymbol{CH_4} + \mathbf{4}\,\boldsymbol{MnO_2} + \mathbf{7}\,\boldsymbol{H^+} \rightarrow \boldsymbol{HCO_3^-} + \mathbf{4}\,\boldsymbol{Mn^{2+}} + \mathbf{5}\,\boldsymbol{H_2O} \quad [8]$$

$$\boldsymbol{CH_4} + \mathbf{8}\,\boldsymbol{Fe(OH)_3} + \mathbf{15}\,\boldsymbol{H^+} \rightarrow \boldsymbol{HCO_3^-} + \mathbf{8}\,\boldsymbol{Fe^{2+}} + \mathbf{21}\,\boldsymbol{H_2O} \quad [9]$$

AOM coupled to the reduction of sulphate (eq. [10]*)*

$$\boldsymbol{CH_4} + \boldsymbol{SO_4^{2-}} \rightarrow \boldsymbol{HCO_3^-} + \boldsymbol{HS^-} + \boldsymbol{H_2O} \quad [10]$$

The AOM coupled to the reduction of sulphate is a common feature in marine sediments due to high pore-water SO_4^{2-} concentrations (Martens and Berner 1974; Reeburgh 1976). Methane is oxidised with SO_4^{2-} as electron acceptor by methane-oxidizing archaea and sulphate-reducing bacteria consuming upward migrating CH_4 in sulphate-methane transition zones (SMTZ) (Hinrichs et al. 1999; Boetius et al. 2000). Pronounced SMTZ have been observed for very few specific freshwater environments only (Schubert et al. 2011; Timmers et al. 2016). Freshwater environments are limited in available sulphate and AOM is

usually coupled to the reduction of nitrate and nitrite or to the reduction of iron and/or manganese.

Aerobic oxidation of methane is found in the oxic zones of the sediments and / or in oxic water layers and are an effective barrier to CH_4 release into the atmosphere (Bastviken et al. 2008). Methanotrophs oxidise CH_4 to CO_2 in the presence of oxygen utilizing CH_4 as their carbon and energy source (eq. [11]) (e.g. Söhngen 1906).

Aerobic oxidation of methane

$$\boldsymbol{CH_4 + 2\ O_2 \rightarrow CO_2 + 2\ H_2O} \qquad [11]$$

Detailed pathways of aerobic microbial CH_4 oxidation are complex and vary due to the diversity of methanotrophs and wide range of habitats (Trotsenko and Murrell 2008). Aerobic methane oxidation might be further mediated by the light exposure and the dominating types of methanotrophs (Utsumi et al. 1998; Dumestre et al. 1999; Murase et al. 2005; Grossart et al. 2011; Tang et al. 2014; Oswald et al. 2015)

Methane emissions

Even though CH_4 produced in aquatic systems is largely consumed by anaerobic and aerobic methanotrophs (30 to 99 %) (Bastviken et al. 2008), significant amounts of CH_4 are emitted from natural wetlands, sediments or freshwaters (e.g. Bastviken et al. 2011; Ortiz-Llorente and Alvarez-Cobelas 2012; Wik et al. 2016; Holgerson and Raymond 2016). Processes leading to CH_4 emissions from a stratified lake are the emissions by ebullition, plant ventilation, water column storage and diffusion (Chanton and Whiting 1995; Bastviken et al. 2004) (Figure 4).

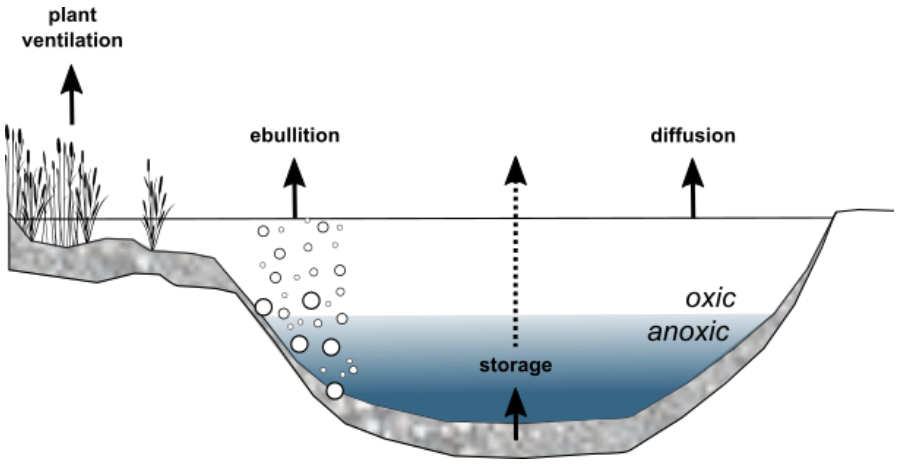

Figure 4: The CH_4 emission pathways in a stratified lake (modified after Bastviken et al. 2004).

Plant ventilation occurs in the littoral areas where aeration in the *aerenchyma* (air channels in the plant) lead to intense exchange between water / sediment and the atmosphere (Seiler and Holzapfel-Pschorn 1984; Schütz et al. 1989b; Ernst 1990). Root-associated methane emissions have been reported as the most important pathway of CH_4 emissions in wetlands, and especially in rice paddies (Schütz et al. 1989b; Hamilton et al. 2014).

Ebullition is the transport of gas bubbles super-saturated with CH_4 from sediments through the water column to the atmosphere (Chanton and Whiting 1995) and occurs in marine (Schneider von Deimling et al. 2010; Gentz et al. 2014) and lacustrine (Leventhal and Guntenspergen 2004; McGinnis et al. 2006; DelSontro et al. 2011) environments. The quantity of emission depends on the water depth, the bubble size, the water temperature, and the CH_4 concentrations in the water, as gaseous CH_4 tends to rapidly equilibrate with ambient water. The main triggers of ebullition are pressure changes within the water column / sediment-interface e.g. by subtidal pumping or ship passages (Riedl et al. 1972; van der Loeff 1981; Maeck et al. 2014). The importance and possible consequences of ebullition for total emissions remains unclear, as fast and sensitive methods capturing ebullition and the rise of gas bubbles are not available yet.

In stratified lakes, CH_4 accumulates in the anoxic deep water layer during summer. Stored CH_4 is released during the autumn overturn period by vertical water mass mixing, resulting in high emission rates of CH_4 into the atmosphere (e.g. Bastviken et al. 2004). The sudden release of CH_4 previously sealed off

from the atmosphere was also observed during spring overturns along with thawing ice coverage (e.g. López Bellido et al. 2009). This so-called "storage flux" (Bastviken et al. 2004) is mostly diminished by CH_4 oxidation in the water column as a function of the speed of vertical mixing which results in oxic conditions throughout the entire water column. Methane oxidation rates during autumn overturn are a subject of controversial discussion. Results range from oxidation of 45 to 95 % of CH_4 stored in the deeper water layers (Kankaala et al. 2007; López Bellido et al. 2009; Schubert et al. 2012; Encinas Fernández et al. 2014), while the relative contribution of storage flux to total lake emission is highest for small lake environments.

Aquatic CH_4 emissions by diffusion base on the gas exchange at the air–water interface due to differences in gas partial pressure between water ($p_{CH_{4_{water}}}$) and air ($p_{CH_{4_{air}}}$). The diffusive flux of CH_4 (F_{CH_4}) [mol m^{-2} d^{-1}] in the upper mixed layer (epilimnion) is calculated by equation [12]:

$$\boldsymbol{F_{CH_4} = k\left(C_{CH_{4_{water}}} - C_{CH_{4_{air}}}\right)} \quad [12]$$

with $C_{CH_{4_{water}}}$ as the CH_4 concentration of the surface water layer [mol m^{-3}], $C_{CH_{4_{air}}}$ as the saturation concentration in equilibrium with the overlying atmosphere [mol m^{-3}] and k as the gas transfer or piston velocity [m d^{-1}]. Calculated emissions consequently depend on the estimation of the gas transfer velocity which is affected by the near-surface turbulence (e.g. MacIntyre et al. 2010). Further factors are the presence of microbubbles (Eugster et al. 2011; Prairie and del Giorgio 2013; McGinnis et al. 2015), water currents (Zappa et al. 2003; Borges et al. 2004), rainfall (Ho et al. 1997) and suspended matter (Dyer et al. 2004).

Methane-sensing technologies[1]

Methane fluxes from aquatic environments to the atmosphere have often been studied (e.g. Abril and Iversen 2002b; Bastviken et al. 2004; McGinnis et al. 2011, 2015; Schubert et al. 2012; Call et al. 2015), but emission rates still have large uncertainties as flux pathways are complex and difficult to quantify (Kirschke et al. 2013; Saunois et al. 2016). Direct measurements above the air–water

[1] Following section partly consists of the introduction in Hartmann et al. 2018.

interface avoid the determination of the gas transfer velocity and allow estimations of total aquatic CH_4 emissions. The diffusive flux of CH_4 is generally analysed by eddy covariance stations (continuous measurements) (e.g. Kaimal 1975) or by floating chambers (single point measurements) (Frankignoulle 1988). However, most flux estimations are based on (single) measurements at very few stations per lake and do not include emission variability, while CH_4 concentrations are known to vary spatially and temporally within the surface water layer (Schilder et al. 2013; Blees et al. 2015; Call et al. 2015; Natchimuthu et al. 2017; Paranaíba et al. 2018). Therefore, CH_4 dynamics in freshwater environments are still not taken into account in regional and global CH_4 mass balances (Hofmann 2013; Schilder et al. 2013).

A fast, sensitive, and continuously-measuring method to determine *in-situ* both CH_4 concentration and $\delta^{13}C\text{-}CH_4$ values in water environments is therefore desirable when addressing the complex pathways and transformations of CH_4 in aquatic ecosystems. First studies presenting simultaneous data for dissolved CH_4 and $\delta^{13}C\text{-}CH_4$ in aquatic systems are based on the spray chamber-method (Gülzow et al. 2013; Maher et al. 2015). However, those methods are suitable for long term measurements only, as the spray chamber-method is based on the gas-equilibrium between water and analysed headspace, leading to measurement times of several minutes to hours (Webb et al. 2016). Recently, fast *in-situ* methods for the determination of dissolved CH_4, such as underwater mass spectrometry (UWMS) and a membrane contactor for gas / liquid exchange coupled with an off-axis integrated cavity output spectrometer (M-ICOS) were introduced by Schlüter and Gentz (2008) and Gonzalez-Valencia et al (2014), respectively. These methods are limited to CH_4 concentration only. Wankel et al. (2013) further improved UWMS by developing a near real-time analyser for $\delta^{13}C\text{-}CH_4$ measurements in the deep-ocean. However, this analyser can only be used in environments with CH_4 values above 0.1 mM and 0.5 mM for the determination of CH_4 concentration and $\delta^{13}C\text{-}CH_4$ values, respectively; concentrations which occur, for example, in hydrothermal vent systems or cold seeps (e.g. Dando et al. 1995; Botz et al. 1999).

Thus, for surface waters and shallow freshwater environments with low CH_4 concentrations, methods to determine short term $\delta^{13}C\text{-}CH_4$ variations are not available to date. These instruments would offer a better understanding of the

different pathways, sources and sinks of CH_4 and, consequently, help to improve the quantification of the local and global CH_4 budgets.

Aquatic CH_4 dynamics have often been studied on a weekly, or monthly basis (Abril and Iversen 2002b; Middelburg et al. 2002; Biswas et al. 2007; Blees et al. 2015; Maher et al. 2015), but lack high spatial and temporal resolution as traditional in-situ devices were strongly limited by the number of discrete samples.

In the frame of this thesis, a method for continuous and simultaneous measurements of CH_4 concentrations and $\delta^{13}C\text{-}CH_4$ values in water was developed and optimized during laboratory work and preliminary fieldwork. The development mainly focused on the response time and the accuracy of the new method. Therefore, a membrane-coupled system was chosen for further development due to its promising short response times for CH_4 and $\delta^{13}C\text{-}CH_4$ values. Once the system was established, it was applied in fieldwork at different lake environments (oligotrophic, mesotrophic and eutrophic) and for various applications (single measurements, continuous profiling and continuous analysis). To ensure the correctness of this new method, all measurements were accompanied by conventional analytical methods.

Outline of this thesis

The thesis is divided into four main chapters. The first chapter (Chapter 1) introduces the new membrane-coupled CRDS system (M-CRDS). Results are shown for calibration and characterisation work in the laboratory and field. The detection limit for the simultaneous determination of CH_4 and $\delta^{13}C\text{-}CH_4$ values is 3.6 nM CH_4, which is significantly lower than reported CH_4 concentrations in many freshwater environments. The M-CRDS was successfully applied and tested for suitability during fieldwork at Lake Stechlin (Germany). The results from the fieldwork at various lake environments are shown in the second chapter of this thesis (Chapter 2). The M-CRDS was applied at three different lake environments: Lake Willersinnweiher (Germany), Lake Stechlin (Germany) and Lake Erken (Sweden). All three studies focussed on different aspects of CH_4 dynamics in lakes, such as sedimentary processes, sediment-water interactions and temporal and spatial variations within the water column. Conclusions as well as prospective future development efforts for the M-CRDS and research objectives are presented in Chapter 3. The thesis ends with a Chapter (Chapter 4) on related scientific work that was conducted within the framework of this study.

1. Establishment and Optimisation of the new Method (M-CRDS)

The following chapter mainly consists of the publication "A fast and sensitive method for the continuous *in-situ* determination of dissolved methane and its δ^{13}C-isotope ratio in surface waters" which was published 2018 as Open Access in *Limnology & Oceanography: Methods* (Hartmann et al. 2018). The chapter was rearranged and supplemented by additional results from laboratory and fieldwork.

The experimental setup for continuous and simultaneous measurements of CH_4 concentration and $\delta^{13}C$-CH_4 values in water is shown in Figure 6. The major parts are indicated by capital letters (A-K). The setup can be subdivided into a water and a gas system. The water system mainly contains a pump and filtering units as well as the membrane contactor. The gas system consists of a vacuum pump, a dilution chamber and the CRDS analyser (G2201-i, *Picarro*©, USA). The membrane-coupled CRDS - collectively called "M-CRDS" - is built as a modular structured system, allowing a quick replacement of individual pieces, as all parts are easily exchangeable within minutes. Due to the compact and robust construction, the M-CRDS is suitable for applications in the field or on, e.g., ship-expeditions.

In the water system, the water flow is generated by a submersible pump (Part A, MP1, *Grundfoss*, Denmark) and filtered by different filtering units (Part B, Causagard / Causpure, *Infiltec*, Germany) of decreasing mesh sizes of 200 µm, 100 µm, 25 µm and/or 5 µm. The mesh sizes depend on the requirements of the sampled aquatic system to ensure longevity of the measuring setup. Several sensors log *in-situ* water temperature [°C] at the submersible pump as well as water temperature [°C] at the membrane, redox potential [V], pH, O_2 [%] and conductivity [S/m] in a bypass (Part C, *WTW*, Germany). Samples for reference measurements during laboratory experiments were also taken from that bypass.

Dissolved CH_4 is extracted by a membrane contactor (Part E, LIQUI-CEL mini module©, *3M Industrial Group*, USA) as described by Noble and Stern (1995). The water flow through the membrane contactor is adjusted by a high-quality mass flow controller (Part D, Series 358, *Analyt-MTC*, Germany) to 500 ± 5 mL min^{-1} to achieve best response times. The flow rate, and consequently the response time, is generally limited by the membrane contactor to 500 mL min^{-1} as higher water flow rates might deform the pores due to increased hydrostatic pressure, which results in decreasing gas exchange through the membrane (Boulart et al. 2010; Wankel et al. 2013). The membrane contactor is set to a vertical position and the flow enters the bottom and exits the top to assure a bubble-free water-air-boundary at the membrane surface.

In the gas system, vacuum is applied to the membrane contactor using a membrane pump (Part G, N920KT.29.18, *KNF*, Germany) to minimise equilibration times for gas exchange between water and the analysed headspace. The flow rate of extracted gas is ~50 ml min^{-1}. Even though the membranes are hydrophobic with small pores, water vapour is removed by the vacuum mode (up to 5 %). In a first approach, the water vapour was trapped by a small-sized, robust cryo-trap based on thermoelectric cooling that was developed and built in-house (Figure 5).

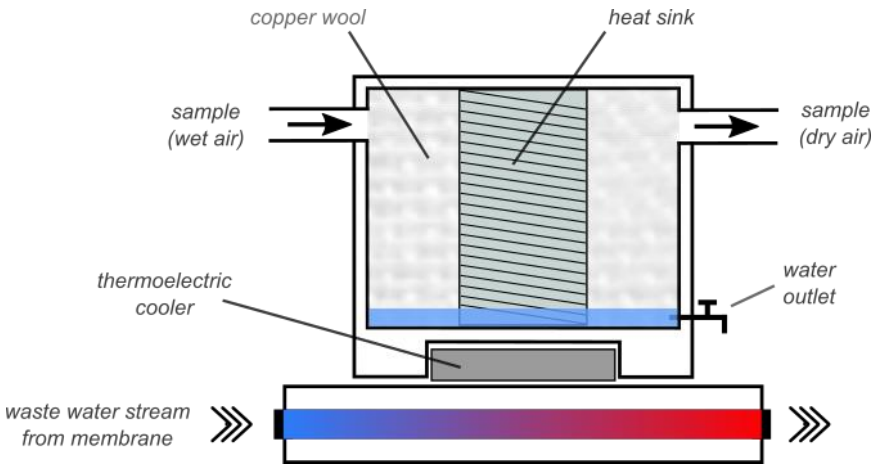

Figure 5: Schematic of the cryo-trap based on thermoelectric cooling. The wet gases enter the cryo-trap, water vapour is frozen at the heat sink as well as at the copper wool and dried gases are subsequently directed to the analyser. The heat sink was cooled by a Peltier element (*QuickCool*, QC127).

The gas enters the cryo-trap at the gas inlet, water vapour is frozen at the heat sink and dried gas is subsequently directed to the analyser. The heat sink was cooled by a Peltier element (*QuickCool*, QC127). The waste water stream that passed the membrane contactor dissipated the waste heat of the Peltier element to avoid additional peripheral equipment. The gas inlet as well as the layout of the heat sink was modified several times, as the gas inlet was clogged by frozen water vapour within minutes. The shape of the heat sink was optimised regarding its material, heat transfer, surface expansion and drain separation, but remained unsuccessful. As the clogged cryo-trap was ruling out stable long-term measurement, the cryo-trap has been removed. The vacuum pump and tubes are now flushed via two automatic 3-way-valves (Part F_1 and F_2) with ambient air for 7 min (every 4 h) avoiding condensation in the system and guaranteeing a constant vacuum. This further improved the system with respect to field measurements with limited power supply.

As the CRDS' operational range is limited to a maximum concentration of 1000 ppm, a small-sized and own-built dilution chamber was applied to dilute highly concentrated sampling gases with synthetic air (20.5 ± 0.5 mol% O_2 in N_2, *AirLiquide*, Germany). The dilution is regulated via two high quality mass flow controllers (Parts H_1 (up to 5 mL min^{-1}) & H_2 (up to 500 mL min^{-1}), Series 358, *Analyt-MTC*, Germany) in a concentration-depended manner. Reference gases for prior calibration, during and following the experiments are introduced via 3-way-valves (Part I, Swagelok, Germany). Since all gas samples are dried by a

Nafion© drying tube (Nafion MD110, *PermaPure LLC*, USA) before measurements to ensure higher accuracy (Part J), water vapour concentrations are less than 0.2 % in the analyser, where the software internal water correction algorithm shows its best applicability (Rella et al. 2013). Gases are subsequently directed to the portable CRDS analyser and analysed for CH_4 concentration and $\delta^{13}C\text{-}CH_4$ (Part K). The *Picarro*© G2201-i measures $^{12}CH_4$, $^{13}CH_4$ and H_2O individually and quasi-simultaneously at a very high temporal resolution (1 Hz) and provides $\delta^{13}C$ values in‰ relative to the Vienna Pee Dee Belemnite standard. Picarro© uses built-in pressure and temperature control systems as well as automatic water vapour correction to ensure a high stability of its portable analyser. Effects of water vapour on the measurement were corrected automatically by the *Picarro*© software. The manufacturer states concentration precision for the analysis of CH_4 in the "high precision mode" of 5 ppbv ± 0.05 % (^{12}C) and 1 ppbv ± 0.05 % (^{13}C), while a concentration range from 1.8 ppm to 12 ppm is covered. The given precision of $\delta^{13}C\text{-}CH_4$ is <0.8‰. Higher concentration ranges (up to 1000 ppm) are covered by the "high range mode", providing a precision of 50 ppbv ± 0.05 % (^{12}C) and 10 ppbv ± 0.05 % (^{13}C). During all measurements, the analyser was operated inside a *Zargesbox* houding with built-in venting system and uninterruptible power supply system to ensure a continuous operation during the measurements. Both the gas system and the entire setup of the M-CRDS was improved to field measurements with limited power supply and, hence, the M-CRDS can be operated either by 220 V or 24 V (using car batteries) power supply. The runtime of the car batteries might be influenced by the ambient temperatures but lasts a minimum of 7 h during field work.

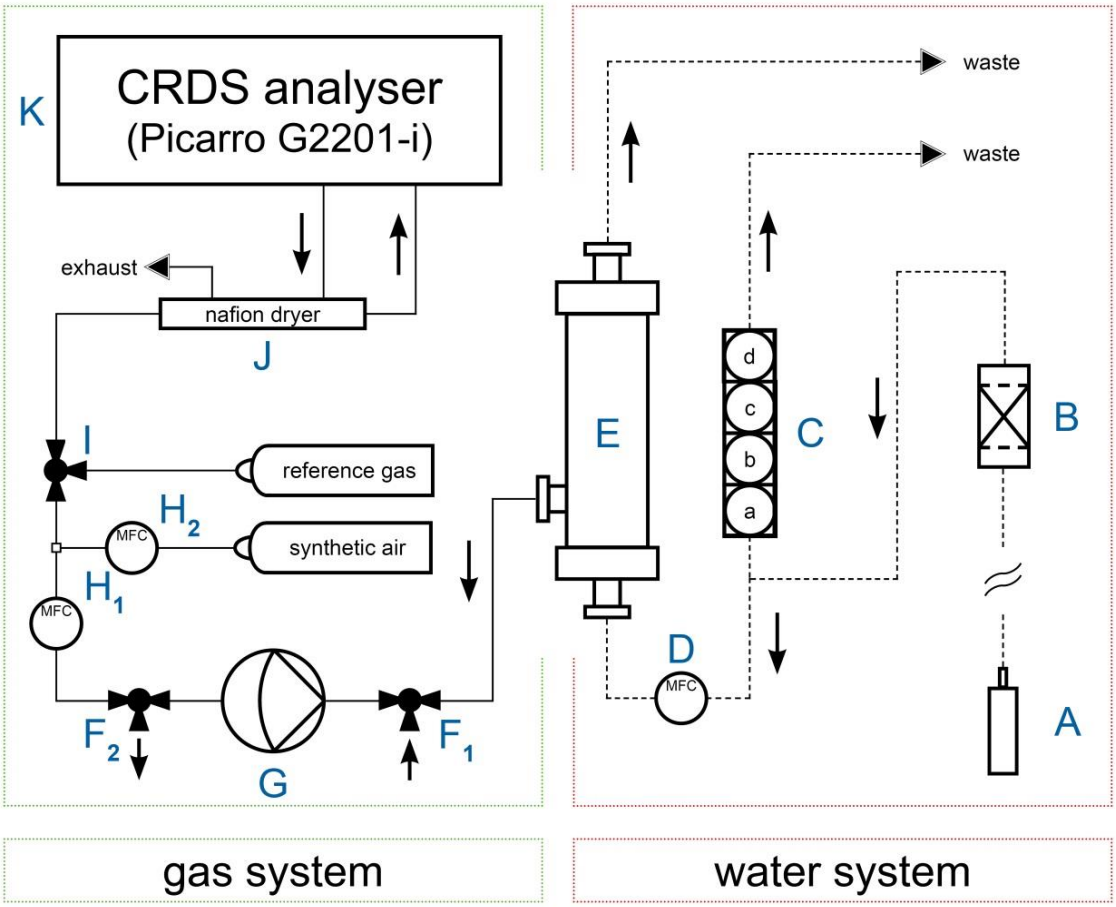

Figure 6: Schematic overview of the CRDS analyser combined with a membrane contactor setup for continuous and simultaneous determination of dissolved CH_4 concentration and $\delta^{13}C\text{-}CH_4$ in water. In the water system, water is pumped by a submersible pump (A), filtered (B) and analysed by several sensors in a bypass (C). Main water flow is adjusted by a mass flow controller (D) and directed to the membrane contactor (E). In the gas system part, gases are extracted by the membrane pump (G). The vacuum pump and tubes are flushed via two automatic 3-way-valves (Part F_1 and F_2) with ambient air avoiding condensation in the system. Depending on the CH_4 concentration, the gas sample can be diluted with synthetic air by two mass flow controllers (H_1 for gas sample flow and H_2 for synthetic air flow). Reference gases for calibration prior, during and following the experiments are introduced via 3-way-valves (I). Gases are dried by a Nafion drying tube (J) prior to analysis by the CRDS analyser (K).

1.1. Method Calibration

1.1.1. Procedure

Data obtained by the M-CRDS cannot be corrected by headspace calculations since the extraction of CH_4 from the water is based on the application of a vacuum. Therefore, the M-CRDS is calibrated for CH_4 concentration using synthetic water standards including CH_4 at certain concentrations (*SubSeaSpec UG*, Germany) as described by Schlüter and Gentz (2008). For this approach, several 60 L water reservoirs were filled with tap water and continuously flushed with reference gas. Each reservoir was flushed with different CH_4 concentration (5 ppm, 100 ppm and 1000 ppm CH_4 in methane-free synthetic air, *AirLiquide*, Germany) and pumped to the membrane contactor subsequently as described in Figure 1. A multi-channel pump was used to generate samples of different CH_4 concentrations through mixing of standard water from the water reservoirs and methane-free synthetic air (20 mol% O_2 in N_2, *AirLiquide*, Germany) flushed tap water (zero water). In order to quality assure the $\delta^{13}C$-CH_4 values, water samples from lakes, ponds as well as groundwater with different stable carbon isotopic values were measured both by M-CDRS and GC-C-IRMS since certified aquatic $\delta^{13}C$-CH_4 standards are not yet available. All values were averaged over 10 min measurement interval.

Subsamples of the water mixtures of different CH_4 concentrations (4 nM CH_4 to 500 nM CH_4) were independently measured in the laboratories of the *University of Heidelberg* (Germany) and the *Alfred-Wegener Institute* (AWI), Helmholtz Centre for Polar and Marine Research located in Bremerhaven (Germany) via the headspace technique (Kampbell et al. 1989) by gas chromatography (GC-FID, *ThermoFinnigan*, Waltham, USA) and gas chromatography combustion

isotope ratio mass spectrometry (GC-C-IRMS, Deltaplus XL, *Thermo Finnigan*, Bremen, Germany) analyses.

The CH_4 concentration and $\delta^{13}CH_4$ ratios in water samples were measured using 255 ml serum vials, closed with butyl rubber stoppers and aluminium crimp caps. Each serum vial was shaken vigorously for 120 s to reach equilibration between the water and the gas headspace. Promptly, CH_4 concentration in the headspace was measured by GC-FID and CH_4 concentration in the water determined using Henry's law (Wiesenburg and Guinasso 1979) and solubility coefficients for CH_4 according to Weiss (1974) and Yamamoto et al. (1976).

Prior to this study, the $\delta^{13}C$-CH_4 ratios for several environmental samples were determined by GC-C-IRMS for calibration purposes. "Interfering compounds were separated by GC and CH_4 trapped on Hayesep D. The sample was then transferred to the IRMS system (ThermoFinnigan Delta^{plus} XL, *Thermo Finnigan*, Bremen, Germany) via an open split. The working reference gas was carbon dioxide of high purity (carbon dioxide 4.5, *Messer Griesheim*, Frankfurt, Germany) with a known $\delta^{13}C$ value of -23.634‰ ± 0.006‰ versus V-PDB (calibrated at MPI for Biogeochemistry in Jena, Germany). All $\delta^{13}C$-CH_4 values were corrected using two CH_4 working standards (*isometric instruments*, Victoria, Canada). The known $\delta^{13}C$-CH_4 values of the two working standards in‰ vs. V-PDB were -23.9 ± 0.2 and -54.5 ± 0.2. All samples were normalized by two-scale anchor calibration according to Paul et al. (2007) and show an average standard deviation of the analytical measurements in the range of 0.1‰ to 0.3‰."[2]

1.1.2. Results

The calibration results of the M-CRDS using synthetic CH_4-water standards (water enriched with CH_4) are shown in Figure 2. Concentration data was averaged over the 10-min measurement interval. The CH_4 measured by the M-CRDS setup [ppm/cm] and the dissolved CH_4 concentrations gained by the well-established GC-FID analysis are highly correlated ($R^2 = 0.999$). The concentration of dissolved CH_4 can be derived from the obtained data of the M-CRDS setup via the linear best fit function y = 1.441 x (Figure 7).

[2] cited from joint work by Frank Keppler and Markus Greule in Hartmann et al. (2018)

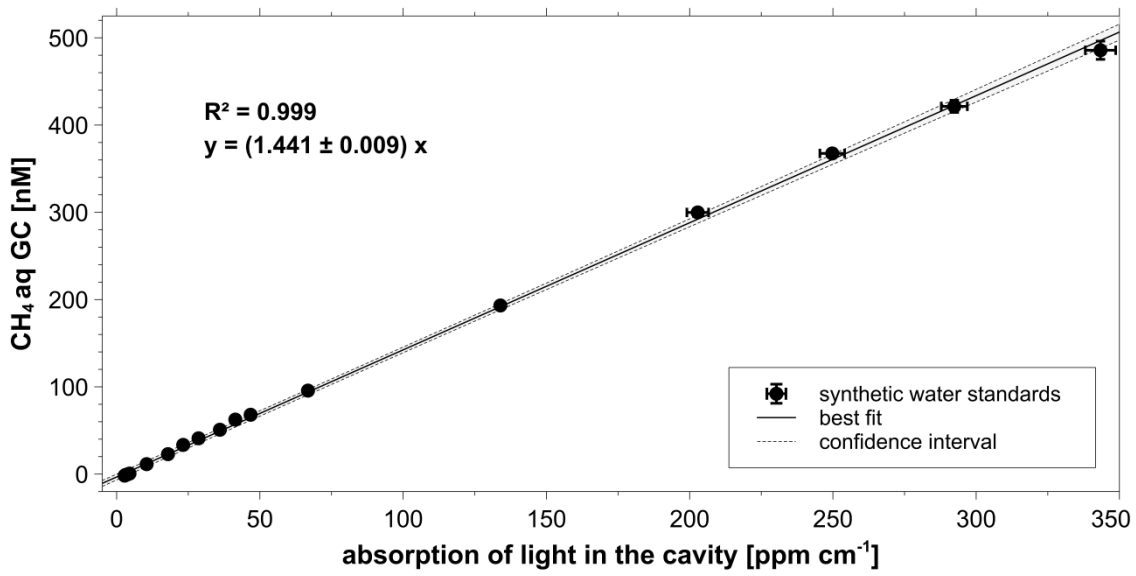

Figure 7: The results of the calibration of the M-CRDS for CH_4 concentration using synthetic water standards (n = 21). Error bars (1-σ) of measurements mainly lie within symbols and reflect the noise within the measurement interval (10 min). Best fit was calculated by geometric mean regression (Sokal and Rohlf 1995).

Analyses of $\delta^{13}C\text{-}CH_4$ values in the synthetic water standards as well as in the reference gases, used to produce those standards, show nearly identical and constant isotopic values. Due to a lack of aquatic $\delta^{13}C\text{-}CH_4$ reference standards, water samples from lakes, ponds as well as groundwater with different stable carbon isotopic values were measured both by M-CDRS and GC-C-IRMS (Figure 8). The mean offset between the $\delta^{13}C\text{-}CH_4$ values measured by the M-CRDS and the GC-C-IRMS is 0.5‰ ± 1.1‰. Isotopic values were averaged over the 10 min measurement interval.

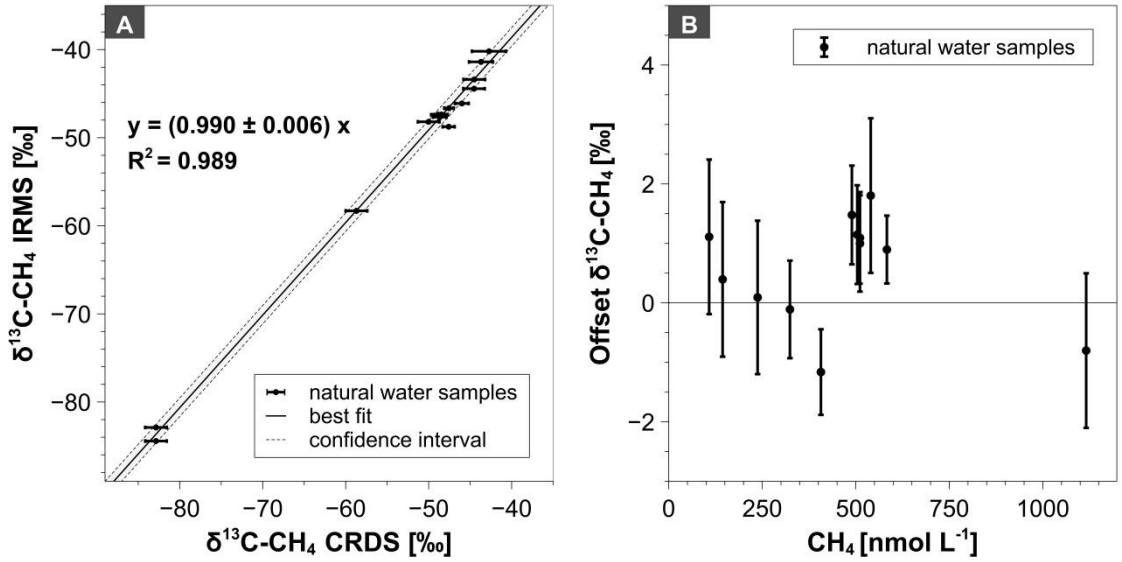

Figure 8: The δ^{13}C-CH_4 values of natural water samples (n = 15) with different stable carbon isotopic values measured both by M-CDRS and GC-C-IRMS (a). Error bars (1-σ) of measurements reflect the noise within the measurement interval (10 min). Offset of δ^{13}C-CH_4 values for natural water samples (n = 15) with different δ^{13}C-CH_4 values and CH4 concentration were measured by M-CRDS in comparison with GC-C-IRMS (b).

In these laboratory experiments, the concentration of CH_4 in the synthetic water standards reflects the combination of the synthetic water standards and the variable amounts of background atmospheric concentration (used to produce the dilution water). Isotope source signatures were determined using Keeling plot analyses (Keeling 1958). The Keeling plot of the isotopic composition [‰] versus the inverse concentration $1/CH_4$ [L nmol^{-1}] of the analysed samples provides the isotope ratio of the CH_4 source. The extrapolated intercept of the straight line in the Keeling plot corresponds to the situation when the concentration is very high and dominated by CH_4 ($1/CH_4 = 0$) and thus reveals the isotope ratio of the CH_4 source. The reference gas that was used to produce synthetic water standards represents the source of CH_4 in the Keeling plot, whereas the dilution water, used for the dilution of the synthetic water standards, displays the background concentration (Figure 9). The Keeling plot intercept within 95% confidence interval was estimated by model II (reduced major axis) regression to obtain the source signature of δ^{13}C-CH_4 (Sokal and Rohlf 1995; Pataki et al. 2003). A detailed discussion of the Keeling plot method for environmental applications is presented in Keppler et al. (2016) and Pataki et al. (2003).

The calibration data points (solid circles) correlate very well (R^2 = 0.9949). The calculated source signature of $\delta^{13}C\text{-}CH_4$ (solid star) results in -32.0‰ ± 1.5‰, which is agrees well with the $\delta^{13}C\text{-}CH_4$ signature of the reference gas (-33.6‰ ± 0.3‰). The results show, that stable carbon isotope fractionation during water-gas transfer in the membrane contactor was not observed and can therefore be excluded.

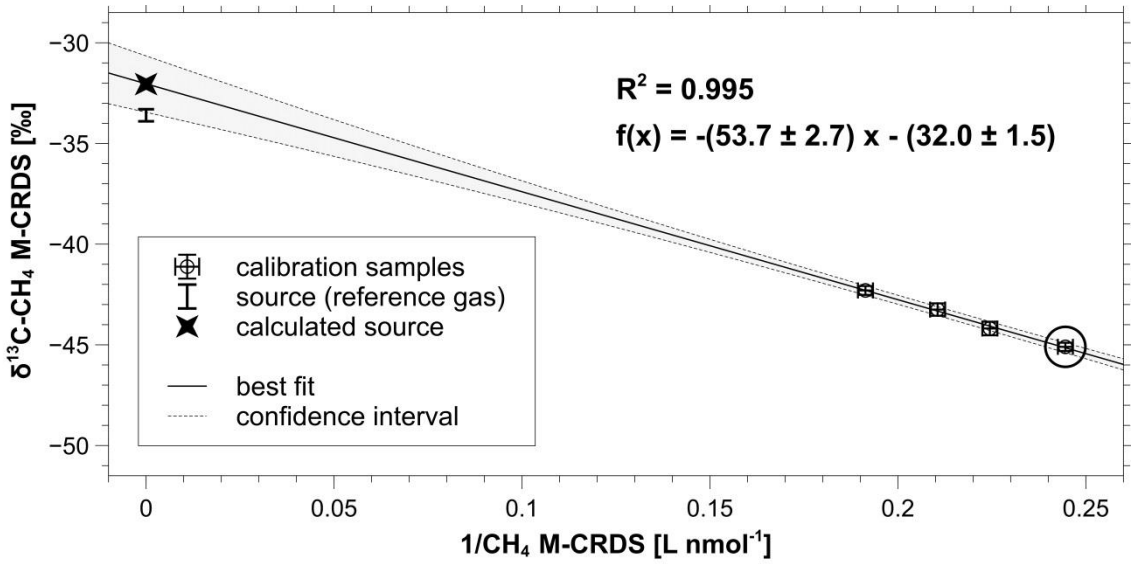

Figure 9: Keeling plot analysis of the samples used for the calibration of CH_4 concentration and $\delta^{13}C\text{-}CH_4$ by synthetic CH_4-water standards. The reference gas that was used to produce synthetic water standards represents the source of CH_4 in the Keeling plot, whereas the dilution water, used for the dilution of all synthetic water standards, displays the background concentration (encircled). The extrapolated intercept of the best fit in the Keeling plot (also shown in equation of the geometric mean regression) provides the isotope ratio of the water CH_4 source (-32.0‰). Error bars (1-σ) of measurements reflect the noise within the measurement interval (10 min) and mainly lie within symbols.

1.2. Method Characterisation

1.2.1. Procedure

Measuring accuracy, precision and the response time for the simultaneous determination of the concentration and δ^{13}C-CH_4 in water were validated via measuring water reservoirs and water sampling bags with constant CH_4 concentration and δ^{13}C-CH_4 values by M-CRDS, GC-FID and GC-C-IRMS. The response time of the M-CRDS was assessed by switching between two water reservoirs with different CH_4 concentrations and δ^{13}C-CH_4 for low to high and high to low concentration transitions (Johnson 1999; Webb et al. 2016). The response time is given as the time constant τ of exponential decay during the concentration transitions using equation [13] (Johnson 1999).

$$\boldsymbol{C = A + B\, e^{\frac{-t}{\tau}}} \qquad [13]$$

where C is the gas phase from the membrane contactor, t is time [s], and A, B, and τ are constants found for each fit. Although this model is mainly used for equilibration devices (Johnson 1999), the time constant τ is a primary factor to evaluate the performance of the devices during maximum to minimum and minimum to maximum transitions.

Since CH_4 measurements by CRDS are dependent on the air composition of the sampled gas (Nara et al. 2012), tests were conducted to examine the effects of O_2 in the sampling gas on the measurement of CH_4 concentration. Therefore, the extracted air was analysed for O_2 concentration by an optical oxygen sensor (FiBox 4, *PreSense*, Germany). Gas solubility is highly temperature dependent (Henry 1803). Therefore, the impact of changes in the water temperature within

the tubing on the membrane properties was examined, using a water reservoir (200 L) at constant temperature, CH_4 concentration and ^{13}C-CH_4. The tubing was heated using a water-bath with temperature control and both *in-situ* temperatures at the membrane and at the submersible pump were measured to examine the warming of the water in the tubes.

1.2.2. Results

All laboratory tests performed suggest that the M-CRDS setup is a sensitive and fast method, suitable for the simultaneous determination of dissolved CH_4 concentration and $\delta^{13}C$-CH_4 values in water. Determined measurement parameters are given in Table 1.

Table 1: Results of the characterisation of the M-CRDS for CH_4 concentration and $\delta^{13}C$-CH_4

Measurement parameters	Values
CH_4 detection limit (for the simultaneous determination of CH_4 and $\delta^{13}C$-CH_4)	3.6 nM
response time τ (continuous mode)	57 s ± 5 s
measuring precision (CH_4) (1-σ)	1.1 %
measuring accuracy (CH_4)	1.3 %
measuring precision ($\delta^{13}C$-CH_4) (1-σ)	1.7‰
measuring accuracy ($\delta^{13}C$-CH_4)	0.8‰

The detection limit for the simultaneous determination of CH_4 and $\delta^{13}C$-CH_4 values is 3.6 nM CH_4, which is significantly lower than reported CH_4 concentrations in many freshwater environments (Abril and Iversen 2002a; Juutinen et al. 2009; Grossart et al. 2011; Bussmann et al. 2013). The measuring accuracy of the M-CRDS for CH_4 concentration and $\delta^{13}C$-CH_4 values is 1.3 % and 0.8‰, respectively (n = 20). The precision (1-σ) is 1.1 % for CH_4 concentration and 1.7‰ for $\delta^{13}C$-CH_4 (n=20) compared to the validation by GC-FID and GC-C-IRMS since certified aquatic CH_4 and $\delta^{13}C$-CH_4 standards are not available. The precision of $\delta^{13}C$-CH_4 values increases with increasing CH_4 concentrations from less than 1.5‰ for CH_4 concentrations < 250 nM to 0.5‰ (> 600 nM) (Figure 10). The mean difference of $\delta^{13}C$-CH_4 values determined by

the M-CRDS and the GC-C-IRMS is 0.76 ± 1.19‰. All samples were measured for at least 15 min to achieve stable measured values and have been averaged over 10 min.

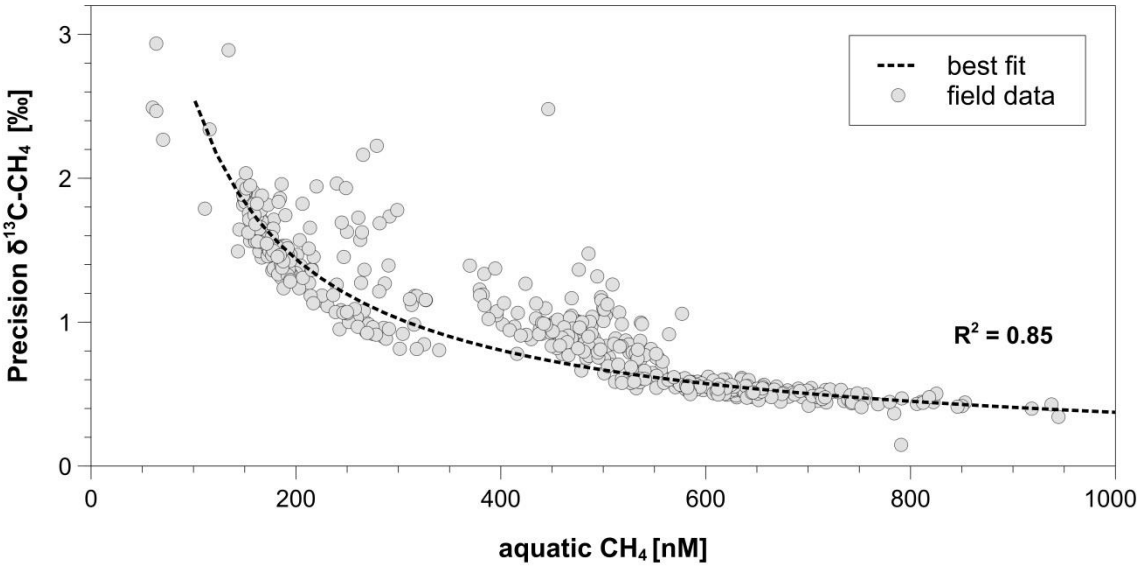

Figure 10: Precision of δ^{13}C-CH_4 values of the M-CRDS versus the CH_4 concentration of natural water samples (n = 520) analysed during fieldwork. Error bars (1-σ) of measurements reflect the noise within the measurement interval (10 min).

In addition response times τ for the simultaneous determination of CH_4 concentration and δ^{13}C-CH_4 values were calculated according to Johnson (1999). A detailed discussion of response times τ for air-water equilibration devices is presented in Webb et al. (2016). The Johnson et al. equilibration model has been applied for ^{12}C and ^{13}C, but shows no significant different time constants ($\tau\ ^{12}C$ = 56.68 ± 5.41 s and $\tau^{13}C$ = 56.36 ± 4.74 s). Time constants for ^{12}C and ^{13}C are equal and, hence, response time for total CH_4 is 57 ± 5 s (n = 8) for surface waters (Figure 11). A concentration dependence of the determined response time was not observed. However, response times τ might change with concentration differences that are unusual for surface waters or shallow freshwater environments, e.g. at hydrothermal vents or cold seeps. Within the framework of this thesis, no investigation has been carried out in more uncommon aquatic environments.

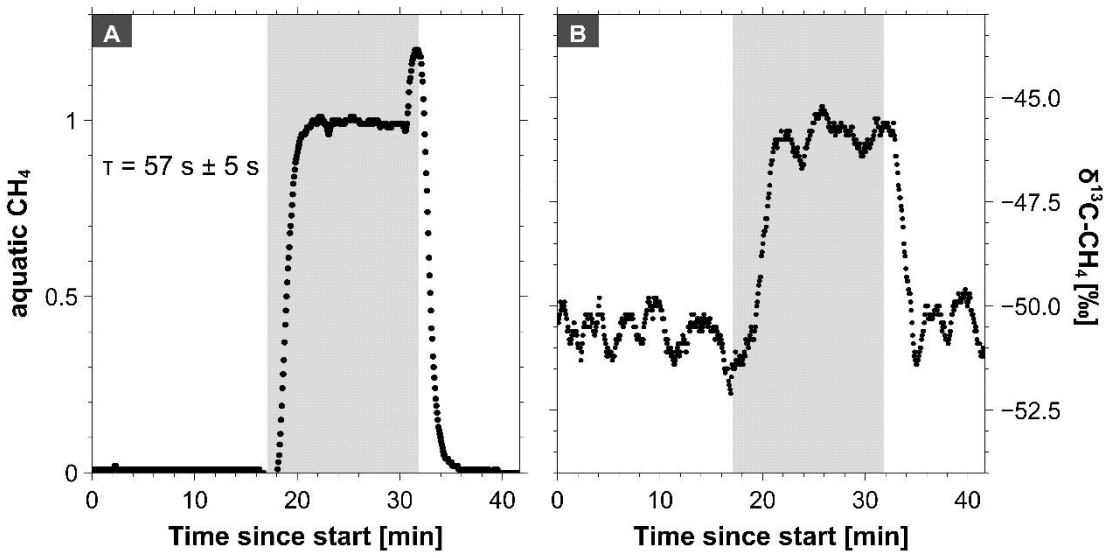

Figure 11: Exemplary response time of CH_4 concentration (a) and $\delta^{13}C$-CH_4 values (b) for low to high and high to low concentration transitions. Concentrations are normalised to 0 (1st reservoir, 130 nM) and 1 (2nd reservoir, 170 nM). Response times of the M-CRDS were assessed by the calculation of the time constant τ [s] (Johnson 1999) (n=8). $\delta^{13}C$-CH_4 data has been smoothed to 30 s averaging interval. High concentration measurement marked in grey. Spikes in CH_4 concentration arise from increased retention time of waters in the membrane contactor due to switching between water reservoirs.

The response time for determination of CH_4 and $\delta^{13}C$-CH_4 in water with "conventional" equilibration devices is generally based on Henry's law, establishing the equilibrium between water and the analysed headspace (Henry 1803). Consequently, response times for concentration transitions in equilibration devices are increased by long equilibration times for CH_4 due to the lower solubility of CH_4 in water. Isotopic values are further affected by isotopic mixing, which requires complete equilibration between water and headspace (Faure 1986; Webb et al. 2016).

The M-CRDS avoids the occurrences of long equilibration times for CH_4 as well as memory and isotopic mixing effects occurring with "conventional" equilibration devices. The system extracts the analysed gases by a vacuum and therefore eliminates the time-consuming establishment of the equilibration between water and analysed headspace. As a consequence, the M-CRDS provides more than two times faster analyses for the simultaneous determination of CH_4 concentration and $\delta^{13}C$-CH_4 values compared to previously published methods (Rhee et al. 2009; Gülzow et al. 2013; Li et al. 2015; Webb et al. 2016) (Table 2) and, more importantly, shows identical response times for low to high and high to low concentration transitions,

whereas significant equilibration delays for $\delta^{13}C\text{-}CH_4$ values occur for "conventional" air-water equilibration devices for transitions from high to low concentration levels due to isotope mixing effects (Faure 1986; Webb et al. 2016). These improvements show that the M-CRDS response times are mainly limited by the rise / fall-time of the CRDS analyser due to the more demanding isotopic measurement rather than the gas-extraction step.

Table 2: Comparison of response times for the simultaneous determination of CH_4 and $\delta^{13}C\text{-}CH_4$ in water from other studies for different devices (after Webb et al. (2016)) compared with response times calculated for the M-CRDS (this study).

Device	Response Time τ [s]	Study
Weiss-type (small)	2248	Li et al. (2015)
General Oceanics	2041 ± 247	Webb et al. (2016)
Shower head	1657 ± 69	Webb et al. (2016)
Weiss-type (large)	1200	Rhee et al. (2009)
Marble	893 ± 12	Webb et al. (2016)
Bubble-type	678	Gülzow et al. (2011)
Liqui-Cel (medium)	417 ± 126	Webb et al. (2016)
Liqui-Cel (small)	177 ± 126	Webb et al. (2016)
Liqui-Cel (large)	117 ± 6	Webb et al. (2016)
Liqui-Cel (small) in vacuum mode	57 ± 5	this study

1.3. Potential sources of errors

Several laboratory tests were done to validate the developed method for a range of external factors that potentially contribute to variability in the future field measurements.

Rella et al. (2013) have examined direct spectroscopic interference between water vapour (H_2O) and CH_4 causing a bias in the CH_4 measurements. Therefore, all gas samples are dried by a Nafion© drying tube (Nafion MD110, *PermaPure LLC*, USA) before measurements to ensure higher accuracy, as water vapour is removed by the vacuum mode (up to 5 %). Although water vapour concentrations were reduced to less than 0.2 % in the analyser, the measurement precision was tested by analysing a reference gas with water vapour contents of 0.06 % to 2.25 %. The obtained bias for corrected CH_4 concentration is 2 ppb / % H_2O and a bias for isotopic ratio was not measurable. Thus, assuming way higher water vapour contents of 1-2 % in the samples as reported (0.1 %), the uncertainty of the software internal water correction algorithm is still significantly lower than the actual measuring precision (Figure 12).

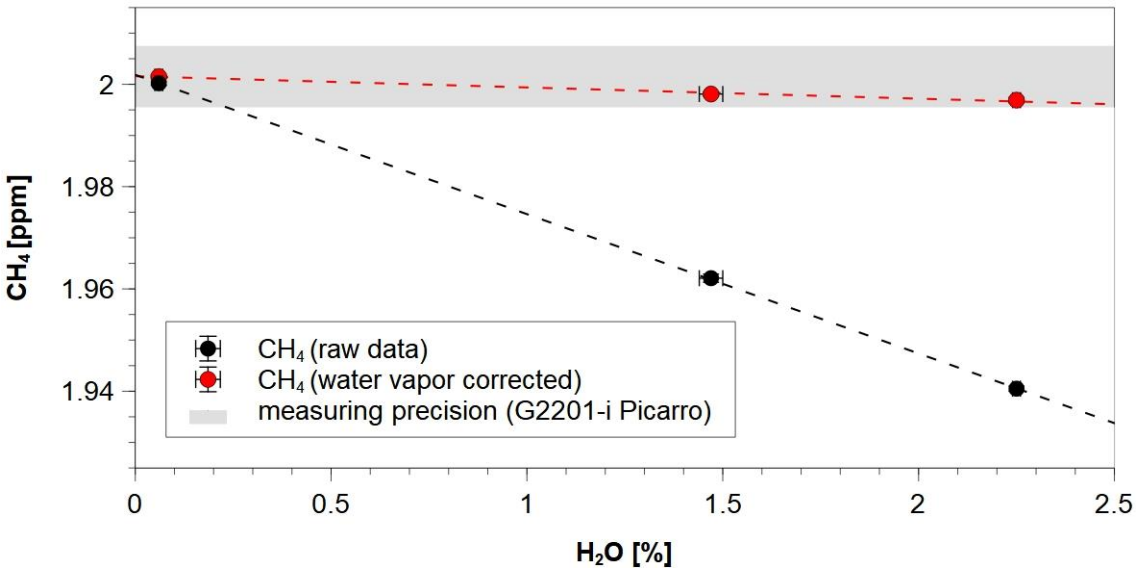

Figure 12: Bias in the CH_4 measurements due to spectroscopic interference between water vapour (H_2O) and CH_4 in reference gas in respect to the water vapour content. The uncertainty of the software internal water correction algorithm is significantly lower than the actual measuring precision (6 ppb). Error bars (1-σ) reflect the precision of the M-CRDS.

Further, Nara et al. (2012) showed potential interferences of the extracted gas matrix on the CH_4 concentration and $\delta^{13}C$-CH_4 measurements by the CRDS. Hence, we examined the effects of the oxygen concentration in the extracted air. Changes in aquatic O_2 saturation of approximately 80 % result in a change in O_2 excess concentration in the extracted air of up to 8000 ppm. Nara et al. (2012) show resulting pressure-broadening effects on CH_4 measurements for ambient air concentrations, which is significantly lower than the measuring accuracy and precision (1.3 % and 1.1 %, respectively) of the M-CRDS and no significant isotopic bias for ^{13}C-CH_4 measurements by CRDS analysis. The natural samples used for the $\delta^{13}C$-CH_4 calibration / validation of the M-CRDS also show a broad range in oxygen concentration (0 % up to 130 % oxygen saturation) in the water samples (Figure 13).

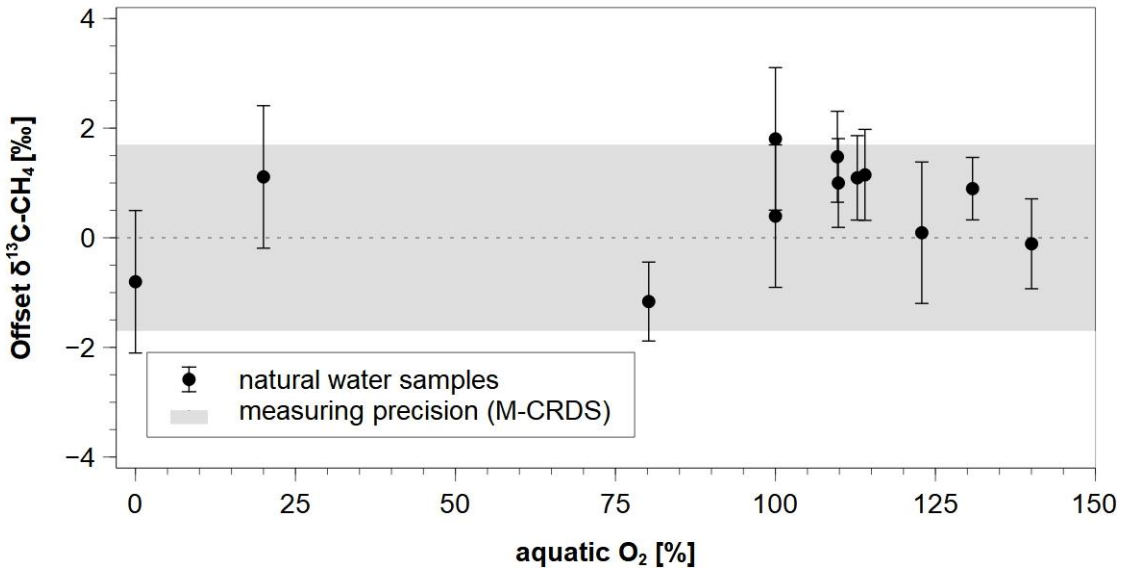

Figure 13: Bias in the δ^{13}C-CH_4 measurements due to effects of the gas matrix on the stable carbon isotopic values. Effects of changes in aquatic O_2 concentration are were not detected or significantly lower than the actual measuring precision (1.7‰). Error bars (1-σ) reflect the precision of the M-CRDS.

The validation measurements by GC-C-IRMS show no effects of the gas matrix on the stable carbon isotopic values for the natural water samples. However, the analysis of waters with other organics or sulphur containing compounds might strongly affected by interferences on the CRDS measurement that are usually indicated by the in-built ChemDetect™ sensing contaminants in samples. Nevertheless, field measurements will undoubtedly require sampling for validation measurements with GC and GC-C-IRMS for field and long-term measurements.

Since gas solubilities as well as the extraction by the membranes are highly temperature dependent, the impact of changes in the water temperature on the membrane properties was examined. The temperature difference between the *in-situ*-water temperature at the membrane and the temperature at the submersible pump was examined for a range of 0 °C to 12 °C. The observed temperature dependency for the measurements was weak (Figure 14) and insignificant compared to the measuring accuracy and precision of 1.3 % and 1.1 %, respectively. Significant effects of temperature differences (e.g. due to warming of the water in the tubing) on the analysed CH_4 concentration and / or extraction efficiency can therefore be neglected for surface waters and moderate climates.

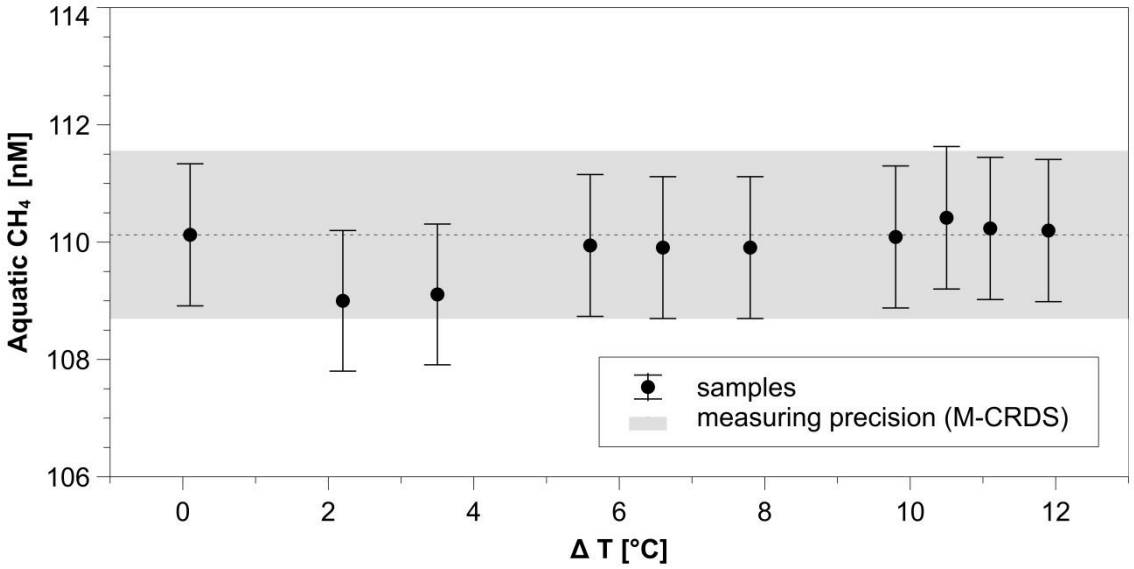

Figure 14: Measured CH_4 concentration versus the temperature difference between the water temperature at the membrane and the temperature at the submersible pump during laboratory experiments. Error bars (1-σ) reflect the precision of the M-CRDS (1.1 %).

1.4. First field application

1.4.1. Procedure

The M-CRDS was applied and tested for suitability during fieldwork at Lake Stechlin (Germany) in July and August 2015. Lake Stechlin is a dimictic meso-oligotrophic lake about 80 km northeast of Berlin, Germany. The M-CRDS was deployed from a large floating platform that is constantly installed in the lake (*LakeLab*: http://www.lake-lab.de). Vertical CH_4 concentration profiles through the entire water column were measured with the M-CRDS setup. To verify the applicability of the system for field measurement the same CH_4 profiles were measured quasi-simultaneously at the *LakeLab* by the M-CRDS, a membrane contactor for gas / liquid exchange coupled with an off-axis integrated cavity output spectrometer (M-ICOS) (Gonzalez-Valencia et al. 2014), and with a GC-FID (Shimadzu, Japan) in the laboratory (Grossart et al. 2011). The M-ICOS system was calibrated and operated according to Gonzalez-Valencia et al. (2014). Samples for GC-FID analyses were independently sampled by a hydrocast and measured immediately thereafter (1-2 h) in the laboratories of the *Leibniz-Institute of Freshwater Ecology and Inland Fisheries* (IGB, Germany) via the headspace technique (Kampbell et al. 1989). The working reference gas for CH_4 was analysed prior and at the end of the profile measurements.

Based on the results of the vertical CH_4 concentration profiles, subsequent 24-hour measurements were performed at the depth of maximum CH_4 concentration in the oxic water column at the LakeLab. The working reference gas for CH_4 (5 ppm CH_4 and 500 ppm CO_2 in synthetic air) was analysed every 8 h during the measurements. Water flow was regulated to a constant flow of 500 ± 5 mL min^{-1} all time.

1.4.2. Results

Methane in Lake Stechlin

The water column of Lake Stechlin (Germany) was analysed for CH_4 via M-CRDS, M-ICOS and GC-FID (vie headspace technique) in July and August 2015 (Figure 15). Maximum CH_4 concentrations of M-CRDS (577 nM), GC-FID (574 nM) and M-ICOS (613 nM) at 7 m water depth coincided with the thermocline in Lake Stechlin (Figure 15). Maximum CH_4 concentrations at Lake Stechlin generally vary between 0.6 and 0.85 mM at 7 to 7.5 m water depth during the summer months (June to August). Epilimnetic CH_4 concentrations were constant (~500 nM), whereas CH_4 decreased at the thermocline and shows constant hypolimnetic CH_4 concentrations (~150 nM). Elevated CH_4 concentrations in the well-oxygenated upper 10 m of the water column were recorded repeatedly in Lake Stechlin and other lakes (Grossart et al. 2011; Bogard et al. 2014; Tang et al. 2014; McGinnis et al. 2015; Donis et al. 2017). The $\delta^{13}C\text{-}CH_4$ depth profile showed $\delta^{13}C\text{-}CH_4$ values of -35.2‰ at 8 m water depth, whereas epilimnetic and hypolimnetic $\delta^{13}C\text{-}CH_4$ were relatively stable at about -50‰ (Figure 15b). Highest and lowest $\delta^{13}C\text{-}CH_4$ values of this field campaign are in good agreement with previously published $\delta^{13}C\text{-}CH_4$ values for depth profiles in Lake Stechlin (Tang et al. 2014).

Based on the results of the CH_4 concentration and $\delta^{13}C\text{-}CH_4$ profiles by the M-CDRS and the weekly routine sampling procedure for CH_4 concentration at Lake Stechlin, 24-hour measurements were performed to detect short-term changes in CH_4 concentration and $\delta^{13}C\text{-}CH_4$ at the water depth of maximum CH_4 concentration (7 m water depth). The presented data are the first demonstrating short-term variations of concentration and $\delta^{13}C\text{-}CH_4$ in surface waters (Figure 15).

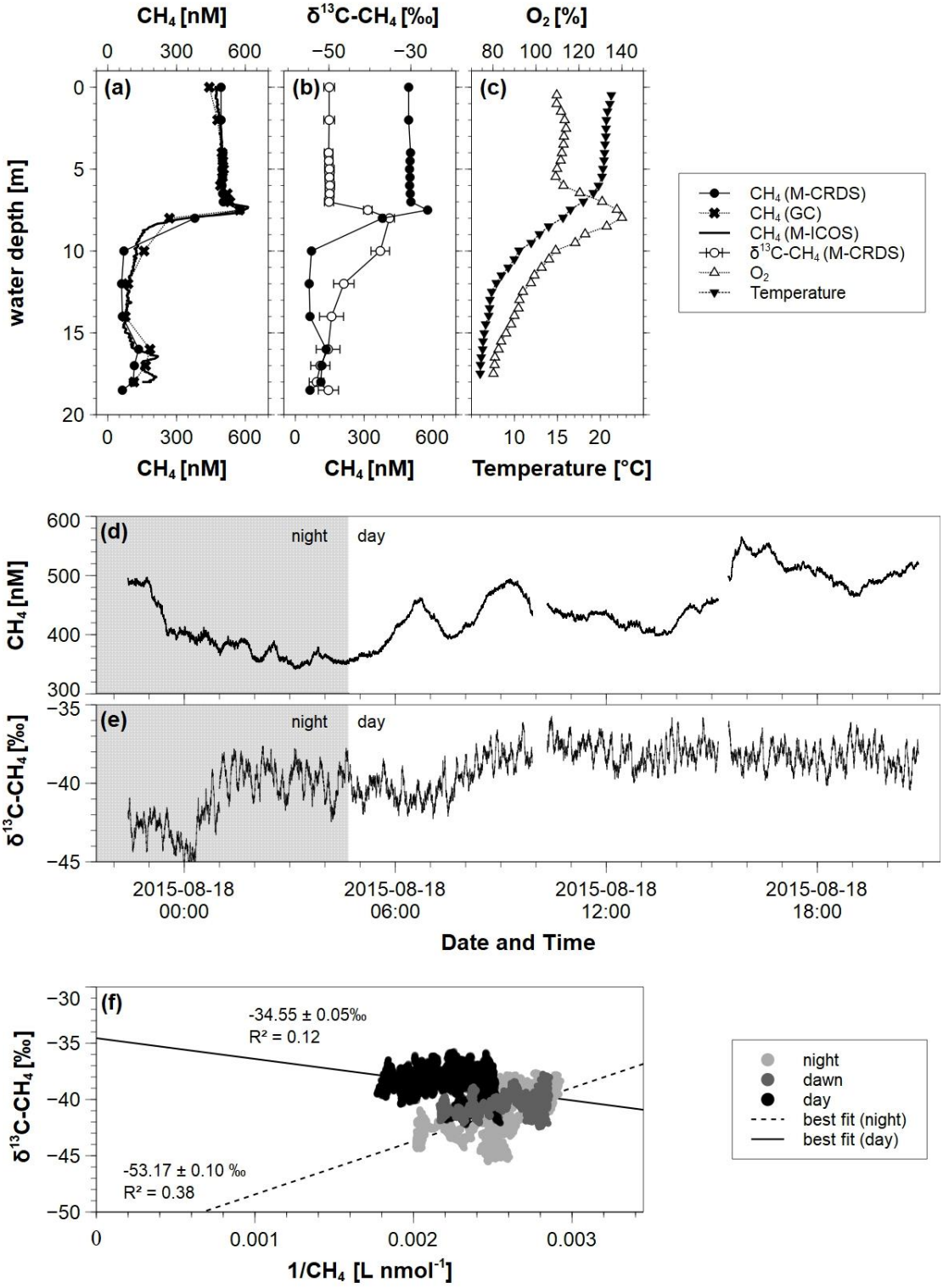

Figure 15: Results from first field application of the M-CRDS. Depth profiles for CH_4 were analysed by M-CRDS, M-ICOS and GC-FID analysis (a), for CH_4 and $\delta^{13}C$-CH_4 (b) and for temperature and O_2 in July 2015 (c). Results of the 24-hour measurement performed at the depth of maximum CH_4 concentration (7 m) at the LakeLab (Lake Stechlin) from August 17th to 18th, 2015 reveal high temporal variations in CH_4 concentration (d) and $\delta^{13}C$-CH_4 (e). Night time marked in grey. Keeling-Plot analysis of the 24-hour measurement (f). The extrapolated intercepts of the best fit in the Keeling plot provide the isotope ratios of the CH_4 sources (-34.55 ± 0.05‰ and -53.17 ± 0.10‰) (Sokal and Rohlf 1995; Pataki et al. 2003).

The data reveal temporal variations of CH_4 concentration (Figure 15d) and $\delta^{13}C\text{-}CH_4$ (Figure 15e) at 7 m water depth during the 24-hour measurement at Lake Stechlin. Methane concentration decreased during night time from 495 to 350 nM and increased again after sunrise and during the day up to 565 nM. The $\delta^{13}C\text{-}CH_4$ values also showed temporal variations and decreased with decreasing CH_4 concentration from -42‰ to -45‰ and increased rapidly during the early night and after sunrise up to -40‰ and -38‰, respectively. The isotopic values remain rather constant over the day. Temperature differences between the *in-situ* water temperature at the membrane and the temperature at the submersible pump were less than 3.0 °C. Effects of the temperature differences on the analysed CH_4 concentration and $\delta^{13}C\text{-}CH_4$ values can be neglected for these temperature ranges.

The Keeling plot results indicate that CH_4 at 7 m depth (thermocline) might be a mixture of two end members during the 24-hour measurement (Figure 6c). During night time, a ^{13}C depleted CH_4 source was found with a $\delta^{13}C\text{-}CH_4$ value of -53‰, whereas the $\delta^{13}C\text{-}CH_4$ signature of the CH_4 source during daytime is less depleted in ^{13}C (-35‰). Although the correlation coefficient of the best fit is weak, the calculated results agree very well with the $\delta^{13}C\text{-}CH_4$ signatures of the data obtained from the $\delta^{13}C\text{-}CH_4$ depth profile as a $\delta^{13}C\text{-}CH_4$ value of ~ -35‰ is found around 8 m, whereas epilimnetic and hypolimnetic $\delta^{13}C\text{-}CH_4$ values are around - -50‰ (Figure 15b).

Temporal variations in CH_4 concentration and $\delta^{13}C\text{-}CH_4$ values at Lake Stechlin might therefore be either controlled by local methane production / oxidation or physical variations in the thermocline. Turbulence and internal seiching is a common phenomenon in stratified lakes and reported for Lake Stechlin (Kirillin and Engelhardt 2008; Kirillin et al. 2009; Giling et al. 2016). Lake hydrological dynamics dominated by internal seiches may have partly caused upwelling of colder deep water with lower CH_4 concentration and more negative $\delta^{13}C\text{-}CH_4$ (see Figure 15b). However, turbulence sensors were not deployed and, hence, seiche-driven mixing in the thermocline was not measured during our campaign. An alternative explanation for the short-term variations in CH_4 concentration and $\delta^{13}C\text{-}CH_4$ values at Lake Stechlin could be both CH_4 production by methanogens or other processes (generating ^{13}C depleted CH_4) and CH_4 oxidation by methanotrophs (generating ^{13}C enriched CH_4) along with photosynthesis (Oswald et al. 2015). Mid-water CH_4 production is a widely

occurring phenomena, also previously reported for the oxygen-rich Lake Stechlin water column (Grossart et al. 2011; Tang et al. 2014). Lateral input of CH_4 from the littoral zone into Lake Stechlin cannot be fully ruled out, despite it was excluded by previous studies, e.g. Tang et al. (2014).

Therefore, future high resolution and simultaneous analyses of CH_4 concentration and $\delta^{13}C$-CH_4 values by the M-CRDS are critically needed for detailed studies of the origin and fate of mid-water CH_4 in Lake Stechlin (Tang et al. 2016) as the mechanisms and pathways of CH_4 transformation in oxic waters are highly complex and still not fully resolved yet.

Performance of the M-CRDS

The offset between the CH_4 concentration measured by the M-CRDS in comparison with GC-FID and M-ICOS is shown in Figure 16. The M-CRDS data correlate with the independently measured data by GC-FID and M-ICOS with $R^2 = 0.995$ and $R^2 = 0.998$, respectively, which is only slightly lower than the correlation coefficient between M-CRDS and GC-FID analysis via headspace technique during laboratory calibration ($R^2 = 0.999$).

The mean offset between the CH_4 concentrations measured by M-CRDS and other conventional analytical methods is -5.7 nM ± 41.6 nM for GC-FID and -7.8 nM ± 24.7 nM for M-ICOS. Epilimnetic CH_4 concentration correlate well with the data by GC-FID ($R^2 = 0.998$) and M-ICOS ($R^2 = 0.999$), whereas differences between all methods exist in samples below the thermocline. Here, the mean offsets ranged from -19.5 nM ± 26.2 nM (M-ICOS) to -28.4 nM ± 19.0 nM (GC-FID) but showed no systematic offset.

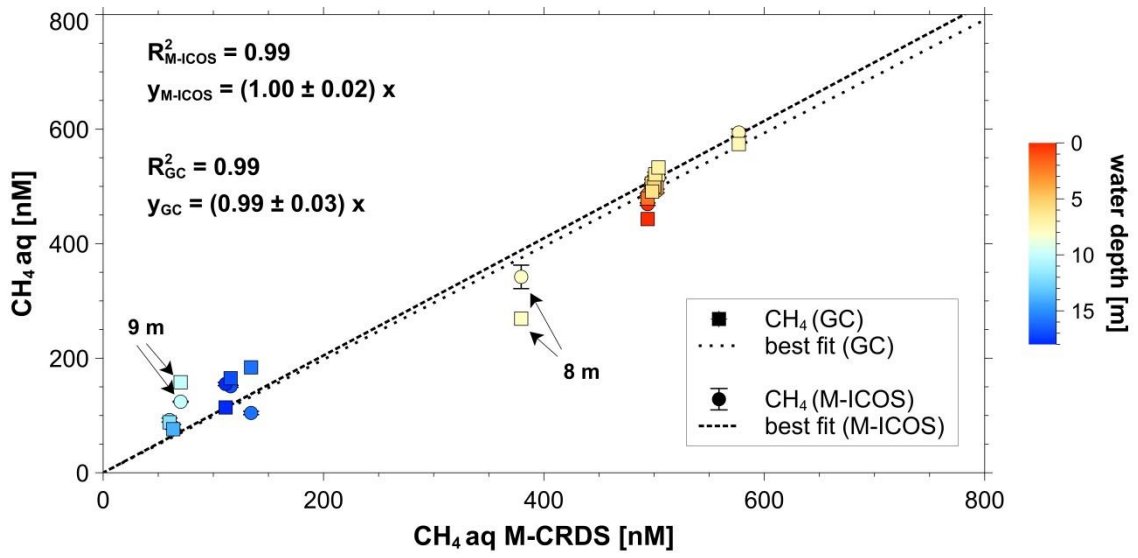

Figure 16: Offset between CH_4 concentrations measured by M-CRDS in comparison with GC-FID (squares) and M-ICOS (dots) (d). Error bars (1-σ) of measurements mainly lie within symbols and reflect the noise within the measurement interval (10 min).

Differences for metalimnetic samples are best explained by the independent sampling of all three used methods, as the M-ICOS requires its own portable pumping system and the GC samples were taken independently by a hydrocast within routine sampling procedure at the same time. Since the concentration gradient is highest in the thermocline, variations of the sampled water depth directly result in changes in the measured CH_4 concentration. The deviations from the laboratory calibration of the M-CRDS point out that validation and recalibration by GC-FID measurements are required for future field measurements.

However, the presented data clearly confirm the suitability of the M-CRDS for *in-situ* analyses of CH_4 concentration and $\delta^{13}C\text{-}CH_4$ within surface water and lake environments. The future application of the M-CRDS for the determination of dissolved CH_4 and $\delta^{13}C\text{-}CH_4$ values will offer a better understanding of the different pathways, sources and sinks of CH_4 and, consequently, help to improve the local and global CH_4 budget.

2. Field studies

The newly developed method (M-CRDS) was deployed at three different lake environments: Lake Willersinnweiher (SW Germany), Lake Stechlin (NO Germany) and Lake Erken (E Sweden).

Lake Willersinnweiher is a small, eutrophic artificial hardwater lake in the plain of the Upper Rhine Graben. Two decades ago, the former gravel pit was restored by planting vegetation at the lake shore to reduce the problem of eutrophication. The lake is dominated by groundwater that is enriched in sulphate (SO_4^{2-}). Former studies showed high sulphide concentrations in the anoxic hypolimnion and intense SO_4^{2-} reduction within the sediments of Lake Willersinnweiher (Schröder 2004). The interaction of carbon and sulphur cycling in the sediments suggest that CH_4 is playing an essential role in carbon cycling of Lake Willersinnweiher. The objective of this study was to assess the impact and effects of CH_4 within the water column and sediments of Lake Willersinnweiher, as direct coupling between sulphate and CH_4 cycling generally results in anaerobic CH_4 transition zones that are uncommon in freshwater environments.

Lake Stechlin is an oligo- to mesotrophic hardwater lake in north-eastern Germany. The Lake is of glaciogenic origin and fed by direct precipitation and groundwater CH_4 concentrations of up to 1.4 μM in the well-oxygenated upper

10 m of the water column were recorded repeatedly in Lake Stechlin (Grossart et al. 2011; Tang et al. 2014). At the start of this thesis, very few studies on CH_4 accumulation and production in oxic waters had been published (Karl et al. 2008; Grossart et al. 2011; Tang et al. 2014). Instead, most existing studies focused on anoxic CH_4 production. Therefore, the M-CRDS and additional *in-situ* field analyses were combined to study and quantify the processes of the CH_4 dynamics and production in the oxic surface water of Lake Stechlin.

Lake Erken located 60 km northeast of Stockholm (Sweden) and the largest lake among the three analysed lakes and. The lake is meso-eutrophic and fed by precipitation and several streams. Lake Erken is covered with ice for around four months per year, while summer thermal stratification usually develops in late spring. Nutrients within the water column decreases rapidly and stay low during the summer due to phytoplankton blooms (Pechlaner 1970a; Pettersson 1980, 1985). Sediment resuspension in relatively shallow and littoral areas is known to result from wind-induced hydrodynamic forces (Weyhenmeyer et al. 1995). Thus, enhanced release of sedimentary CH_4 might result in increased transport processes from littoral zones. Field application at Lake Erken therefore focussed on the spatial and temporal variability of CH_4 and $\delta^{13}C\text{-}CH_4$ values in the surface water layer.

2.1. Lake Willersinnweiher

2.1.1. Study site

In this study, sampling was performed at Lake Willersinnweiher in the plain of the Upper Rhine Graben near Ludwigshafen, Germany (49.499950 °N; 8.397138 °E) (Figure 17). Lake Willersinnweiher is one of four former gravel pits which were built for the excavation of gravel and sand from the upper aquifer sediments of Pleistocene age. The lake has a size of 17 ha, is composed of two smaller basins and has a mean depth of about 8 m and a maximum depth of 20 m (Sandler 2000). Lake Willersinnweiher is classified as a holomictic, eutrophic hardwater lake (Wollschläger et al. 2007), has no surface influx or effluents and is fed by direct precipitation and groundwater. The average water residence time was estimated to 3.7 a (Wollschläger et al. 2007). A dominance of sulphate (SO_4^{2-}) with concentrations up to 2.4 mM was observed in the groundwater in former studies (e.g. Schröder 2004). Groundwater infiltrating the lake at the south-eastern shore has further passed at least one of the lakes located upstream of Lake Willersinnweiher (Wollschläger et al. 2007).

Coupling between groundwater and surface water as well as high bioproduction in the summer season result in high sulphide concentrations in the anoxic hypolimnion of Lake Willersinnweiher. Seasonal and spatial variations of the depth of the redoxcline and the fluxes of the redox sensitive elements manganese, iron and sulphur were observed in the sediments as well as the water column and correlate with the lake depth (Schröder 2004). Schröder (2004) further suggested that CH_4 cycling plays an essential role within the sediments of Lake Willersinnweiher, since the flux balances indicate

an imbalance between the cycles of carbonate and sulphur, demonstrating that an additional CO_2 source within the sediment is required.

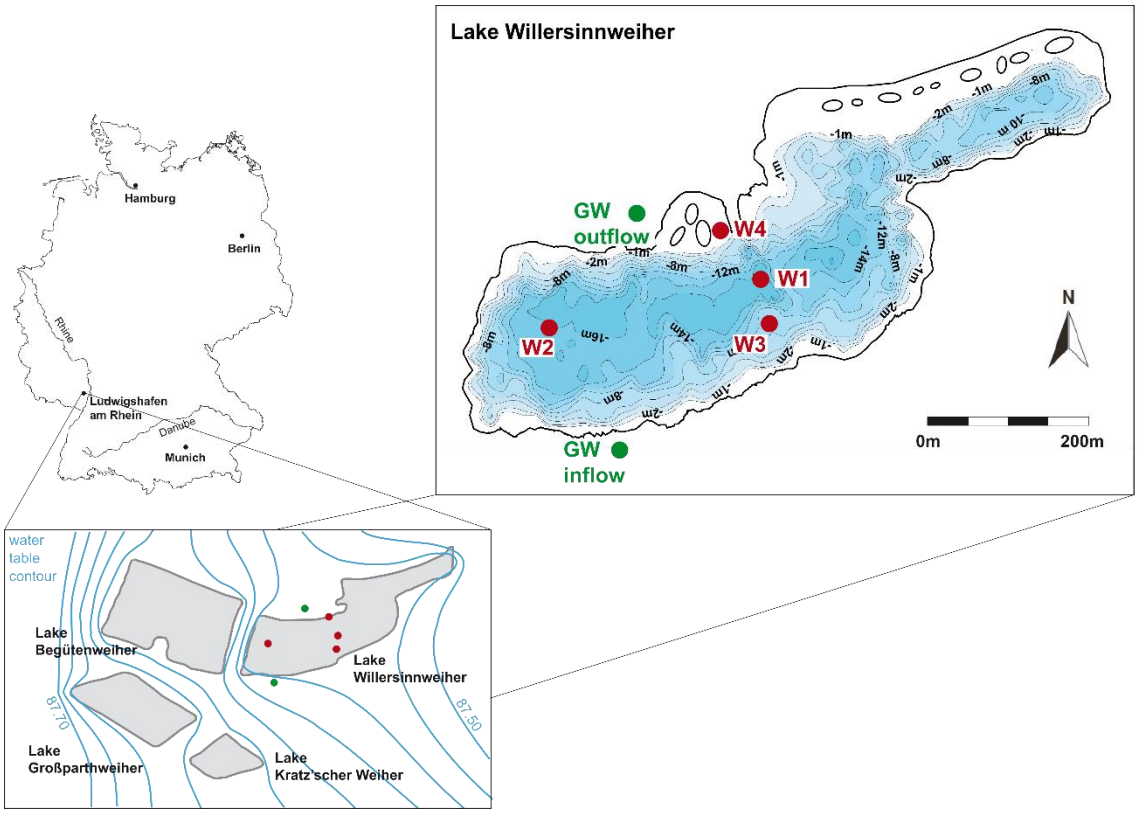

Figure 17: Location of Lake Willersinnweiher in Germany and sampling locations (W1-W4) at Lake Willersinnweiher as well as groundwater wells GW-inflow and GW-outflow, sampled in May 2017, October 2017 and February 2018. Groundwater table contour modified after Wollschläger et al. (2007).

2.1.2. Material and Methods

Sampling sites

Sampling of the water column was carried out at four sites (W1 - W4) with different lake depths. Groundwater was sampled at groundwater wells upstream and downstream of Lake Willersinnweiher in May 2017, October 2017 and February 2018 (Figure 17 and Table 3). Sediments were sampled at the four sites (W1-W4) in May 2017 (Figure 17).

Table 3: Locations sampled at Lake Willersinnweiher. Water depth for groundwater wells are expressed as groundwater level below gauge top.

Sample ID	Latitude	Longitude	Lake depth [m]
W1	49°30.015' N	8°23.835' E	19
W2	49°29.980' N	8°23.613' E	16
W3	49°29.988' N	8°23.827' E	9
W4	49°30.047' N	8°23.792' E	1.5
			GW level [m] below gauge top (February 2018)
Groundwater inflow	49°29.898' N	8°23.689' E	2.2
Groundwater outflow	49°30.062' N	8°23.711' E	3.9

Lake water and pore-water analyses

Depth profiles of CH_4 concentration and $\delta^{13}C\text{-}CH_4$ in the water column were performed by the M-CRDS system (Chapter 1) at all four sites. Each depth was measured for 20 min and CH_4 and $\delta^{13}C\text{-}CH_4$ values were averaged over the measurement interval of 10 min. For quality control, the working reference gas for CH_4 (10 ppm CH_4 in synthetic air) was analysed prior and at the end of the measurements. Groundwater samples were analysed using the headspace technique and gas chromatography analyses (GC-FID, *ThermoFinnigan*, Waltham, USA).

The M-CRDS was verified for CH_4 concentrations by subsamples from Lake Willersinnweiher measured in the laboratory. Samples were taken from the side stream of the M-CRDS system and analysed for CH_4 concentrations via the headspace technique (Kampbell et al. 1989) by GC-FID according to the procedure descripted in Chapter 1.1.1. Water temperature [°C], pH and dissolved oxygen [%] were examined in the side stream of the M-CDRDS. Samples for the analysis of dissolved ions in the lake water and groundwater were filtered with a 0.45 µm cellulose acetate filter and samples for iron (Fe) and manganese (Mn) were acidified with 200 µL HNO_3 (6 M). All samples were stored dry and cool (4 °C) until further analysis. Dissolved Fe and Mn were determined using an ICP-OES (*Agilent* ICP-OES 720, USA). The concentrations of sulphate (SO_4^{2-}) and nitrate (NO_3) in all samples were analysed by ion chromatography (Dionex ICS 1100, *Thermo Fisher Scientific*, USA). Total sulfide was determined photometrically (DREL 2800, *Hach,* USA) using the Sulfide Test Spectroquant© (*Merck*, Germany) immediately after sampling in the field. Dissolved carbon (DIC and DOC) was measured using the *Shimadzu* TOC-V CPH (*Shimadzu*, Japan).

Pore-water analyses were performed on two parallel cores (core length ~ 20 - 40 cm) of lake sediment recovered at all four locations using a manual gravity corer. From one core, pore-water was extracted by rhizons (*Rhizosphere Research Products*, USA) with a pore size of 0.15 µm (Seeberg-Elverfeldt et al. 2005). The second core was used to determine the concentration of CH_4 in the pore-water. Lake sediment (5 ml) of a defined sediment depth was transferred into a glass vial together with 5 ml of 1 M NaOH solution and stored dry and dark until further analysis by GC-FID and GC-BID (Barrier Ionization Discharge Detector, *Shimadzu*, Japan) in the laboratory. For density and porosity determination, sediment samples were weighed before and after drying for 24 h at 105 °C. Pore-water samples were analysed in the same way as the lake water samples.

Calculations

Saturation indices (SI) of $CaCO_3$ in the water of Lake Willersinnweiher were calculated with *PHREEQC* (Parkhurst and Appelo 1999). Diffusive fluxes were calculated from concentration gradients according to Fick's first law assuming steady-state conditions (eq. [14]):

$$\boldsymbol{J = -\, D_W \frac{\partial C}{\partial x}} \quad [14]$$

where J is the diffusive flux [mmol m^{-2} d^{-1}], D_W is the diffusion coefficient [m^2 s^{-1}] in water, C is the concentration [mol m^{-3}], and x is the depth [m]. The porosity has to be taken into account for pore-water calculations and fluxes were corrected using the filled porosity ∅ [dimensionless] and the diffusion coefficient D_S for the sediment (eq. [15]).

$$\boldsymbol{J = -\emptyset * D_S \frac{\partial C}{\partial x}} \quad [15]$$

with D_S as the diffusion coefficient [m^2 s^{-1}] for pore-waters, dependent on the tortuosity θ [dimensionless] (eq. [16]).

$$\boldsymbol{D_S = \frac{D_w}{\theta^2}} \quad [16]$$

D_w is the molecular diffusion coefficient in water [m^2 s^{-1}] taken from Broecker and Peng (1974) and the tortuosity θ was calculated using equation [17] according to Boudreau (1996)

$$\boldsymbol{\theta = 1 - ln(\emptyset^2)} \quad [17]$$

Total sedimentary conversion rates of organic carbon (SCR_{calc}) [mmol m^{-2} d^{-1}] were calculated as the sum of equivalents, based on the electron transfer of the terminal electron acceptors (TEAs) and products using equation [18] to [21]. Minimum (SCR_{calc}^{min} in eq. [22]) and maximum conversion rates (SCR_{calc}^{max} in eq. [23]) were calculated for a complete reaction via the methanogenic pathway of either eq. [19] or eq. [20], respectively.

$$MnO_2 + 2\,e^- + 4\,H^+ \rightleftharpoons Mn^{2+} + 2\,H_2O \quad [18]$$

$$CO_2 + 8\,e^- + 8\,H^+ \rightleftharpoons CH_4 + 2\,H_2O \quad [19]$$

$$CH_2O + 4\,e^- + 4\,H^+ \rightleftharpoons CH_4 + H_2O \quad [20]$$

$$SO_4^{2-} + 8\,e^- + 9\,H^+ \rightleftharpoons HS^- + 4\,H_2O \quad [21]$$

$$SCR_{calc}^{min} = 1 * J_{CH_4}^{eq} + 0.25 * J_{Mn}^{eq} + 1 * J_{SO_4}^{eq} \quad [22]$$

$$SCR_{calc}^{max} = 1 * J_{CH_4}^{eq} + 0.5 * J_{Mn}^{eq} + 2 * J_{SO_4}^{eq} \quad [23]$$

Diffusive CH_4 emissions (F_{CH_4}) [mmol m^{-2} d^{-1}] were estimated by the wind-mediated gas transfer across the surface water-atmosphere boundary layer via eq. [24]:

$$F_{CH_4} = k_{CH_4}\,(C_{CH_4\,water} - C_{CH_4\,atmosphere}) \quad [24]$$

where k_{CH_4} is the transfer velocity [m s^{-1}], $C_{CH_4\,water}$ is the CH_4 concentration [mol m^{-3}] in the water and $C_{CH_4\,atmosphere}$ is the CH_4 concentration [mol m^{-3}] of the water in equilibrium with atmospheric CH_4 concentrations. $C_{CH_4\,atmosphere}$ was determined using the partial pressure of CH_4 above the surface water layer $p_{CH_4 atmosphere}$ [bar] (measured data) and Henry's law solubility constant H^{cp} [mol m^{-3} bar^{-1}] (eq. [25]). H^{cp} was calculated from the Bunsen coefficient β with R as the gas constant [L bar K^{-1} mol^{-1}] and T^{STP} as the temperature [K] for standard temperature and pressure (STP) (eq. [26]). The Bunsen coefficient β was determined from equation [27] with temperature T [°K], salinity S [‰] and the parameters A_i and B_i (Table 4) (Wiesenburg and Guinasso 1979). Sander (2015) provides a good review of the calculations used to convert the various Henry's law solubility constants for water.

$$C_{CH_4 atmosphere} = H^{cp} * p_{CH_4 atmosphere} \quad [25]$$

$$H^{cp} = \beta * \frac{1}{RT^{STP}} \quad [26]$$

$$ln(\beta) = A_1 + A_2\left(\frac{100}{T}\right) + A_3 * ln\left(\frac{T}{100}\right) + S * \left[B_1 + B_2\left(\frac{T}{100}\right) + B_3\left(\frac{T}{100}\right)^2\right] \quad [27]$$

Table 4: Constants for the calculation of Bunsen Solubility Coefficient β (Wiesenburg and Guinasso 1979).

A_1	A_2	A_3	B_1	B_2	B_3
-68.8862	101.4956	28.7314	-0.076146	0.043970	-0.0068672

The gas transfer velocity k_{CH_4} [m s^{-1}] was obtained by calculations based on equations [28] to [30] (Jähne et al. 1987; Wanninkhof 1992).

$$k_{CH_4} = k_{600} * \left(\frac{600}{Sc_{CH_4}}\right)^n \quad [28]$$

$$k_{600} = 2.07 + 0.215 * U_{10}^{1.7} \quad [29]$$

$$Sc_{CH_4} = 1897.8 - 114.28 * t + 32902 * t^2 + 0.039061 * t^3 \quad [30]$$

n is a factor dependent on the wind speed and determined as $n = -2/3$ for wind speeds < 3.7 m s^{-1} and $n = -1/2$ for higher wind speeds (Jähne et al. 1987). The k_{600} [m s^{-1}] is k for CO_2 (20°C) and used to normalize k by the Schmidt number of 600 (Sc_{CH_4}) for better comparison of transfer velocities for any gas (Jähne et al. 1987). k_{600} was calculated by equation [29] with U_{10} as the wind speed [m s^{-1}] at 10 m height (Cole and Caraco 1998) using equation [30] with t as temperature [°C] (Matthews et al. 2003). At Lake Willersinnweiher, wind speeds were obtained from a nearby weather station (49.51° N / 8.55° E).

A CH_4 mass balance (P_{net}) [mmol m^{-3} d^{-1}] of Lake Willersinnweiher was calculated based on CH_4 fluxes in the sediments and the water column. A surface water production was calculated for steady state conditions ($\frac{\partial C}{\partial t} = 0$) according to Donis et al. (2017) (eq. [31]) with parameters from Table 5.

$$\boldsymbol{P_{net} = \frac{\partial C}{\partial t} + (A_P F_S + MOx) - (A_S F_L + A_P F_Z)} \quad [31]$$

Table 5: Parameters used for the CH_4 mass balance at Lake Willersinnweiher.

Flux	Description	Value	Unit
P_{net}	Net CH_4 production for steady state conditions	-	[mmol m^{-3} d^{-1}]
$\frac{\partial C}{\partial t}$	Changes in the CH_4 concentration in the surface water between sampling	0	[mmol m^{-3} d^{-1}]
A_P	Lake planar area	$1.7 * 10^5$	[m^2]
F_S	CH_4 emission from surface to atmosphere	- (obtained from eq. [24])	[mmol m^{-2} d^{-1}]
MOx	Methane oxidation	- *summer stratification:* 0.1 d^{-1} (Tang et al. 2014), 0.5 d^{-1} (Oswald et al. 2015) *winter circulation*: 0 d^{-1} (Denfeld et al. 2016)	[mmol m^{-3} d^{-1}]
A_S	Sediment surface (in contact with the surface water layer)	$5.45 * 10^4$	[m^2]
F_L	Diffusion from pelagic and littoral sediments	- (obtained from sedimentary CH_4 release from Figure 20 and porosity data shown in the appendix)	[mmol m^{-2} d^{-1}]
F_Z	Diffusion from metalimnion	0	[mmol m^{-2} d^{-1}]

2.1.3. Results

Groundwater background at Lake Willersinnweiher

The groundwater of the in- and outflow at lake Willersinnweiher is anoxic all year and pH values ranged from 7.3 in summer to 8.3 in winter. The groundwater upstream showed major contents of Ca, DIC and SO_4^{2-} (Ca-HCO_3^--SO_4^{2-} type water) (Figure 18, Table 6). Significant dissolved Mn and Fe concentrations were observed for all sampling periods while NO_3^- was detectable in autumn only. Methane groundwater concentrations upstream of Lake Willersinnweiher ranged from 0.84 µM in spring and 2.4 µM in winter to 2.4 µM in late summer. The $\delta^{13}C$-CH_4 values are - 6.3‰ for the late summer and - 10‰ for the winter time.

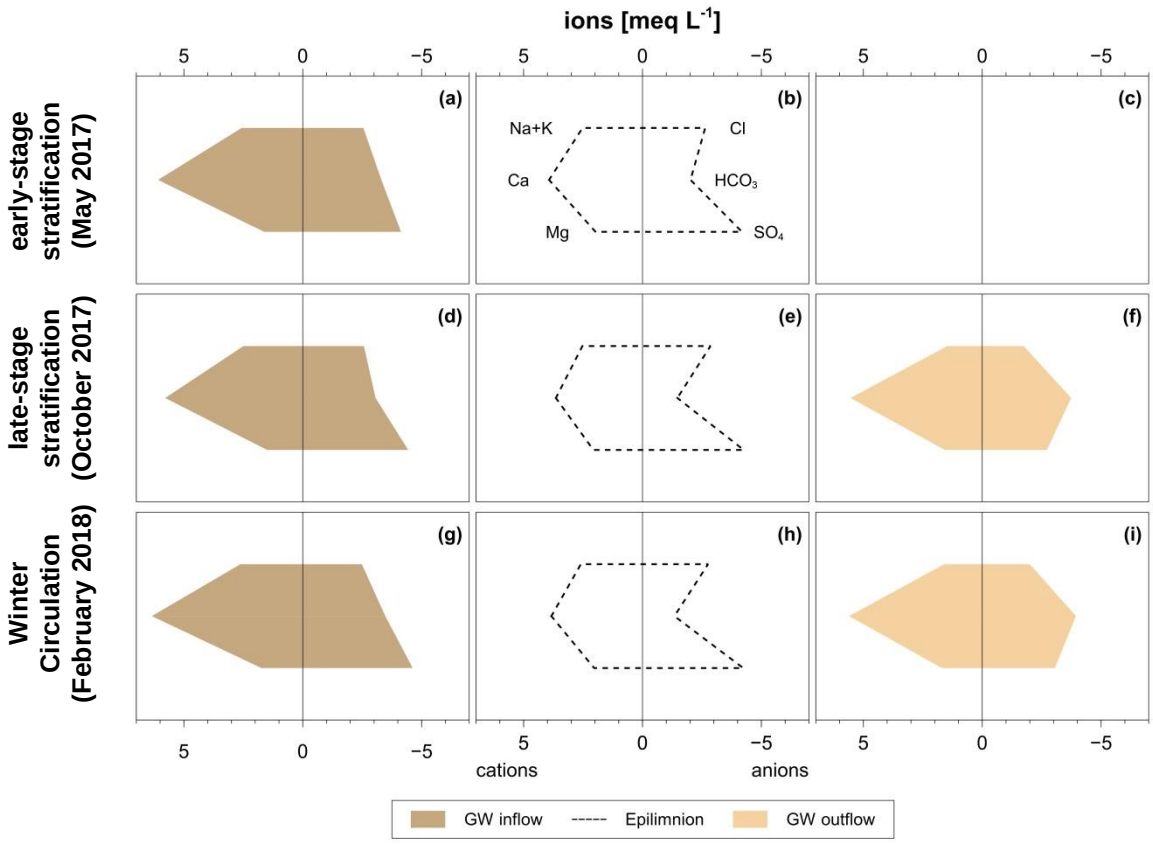

Figure 18: *STIFF*-diagrams of groundwater inflow and outflow as well as lake water for early-stage thermal stratification (a-c), late-stage thermal stratification (d-f) and winter circulation (g-i). The groundwater of the upstream (inflow) of Lake Willersinnweiher is classified as Ca-HCO_3^-- SO_4^{2-} type water, downstream (outflow) of Lake Willersinnweiher as Ca-HCO_3 type water. The groundwater outflow was not analysed for early-stage thermal stratification.

The epilimnion of Lake Willersinnweiher was oxic and all redox sensitive elements were depleted compared to the groundwater upstream, while dissolved Fe and Mn were near or below the detection limit. Groundwater outflow concentrations of major elements differ from groundwater inflow concentrations at any time of the year (Table 6). Sulphate concentrations are significantly lower and DIC concentrations are significantly higher in the groundwater outflow than in the inflow (Ca-HCO_3^- type water). The CH_4 concentration in the groundwater outflow was lower than in the inflow for late-stage thermal stratification and winter circulation. Furthermore, winter $\delta^{13}C$-CH_4 values were lighter in the inflow and heavier in the outflow compared to autumn values. Dissolved Fe and Mn concentrations between groundwater inflow and outflow are similar (Table 6).

Table 6: Concentrations of major elements in epilimnion as well as groundwater inflow and outflow of Lake Willersinnweiher for early-stage thermal stratification, late-stage thermal stratification and winter circulation. Groundwater outflow was not analysed for CH_4 concentrations during early-stage thermal stratification.

GW well	O_2	pH	Ca	DIC	SO_4^{2-}	Fe	Mn	NO_3^-	CH_4	$\delta^{13}C$ CH_4
	[mM]					[µM]				[‰]
Early-stage stratification										
In	n.d.*	7.3	3.04	3.31	2.07	39.7	11.4	n.d.	0.84	-
Lake	0.35	8.8	1.85	1.51	2.12	0.18	0.18	24.0	0.13	-52.4
Out	-	-	-	-	-	-	-	-	-	-
Late-stage stratification										
In	n.d.	7.3	2.89	3.06	2.22	39.0	10.7	10.2	2.42	-7.1
Lake	0.30	8.3	1.92	1.35	1.77	n.d.	n.d.	3.5	0.55	-51.2
Out	n.d.	7.3	2.77	3.74	1.36	43.0	15.5	5.48	2.15	-19.3
Winter circulation										
In	n.d.	8.02	3.18	3.47	2.31	43.0	11.8	n.d.	1.28	-10.9
Lake	0.42	-	2.01	2.04	2.08	0.14	0.53	n.d.	0.06	-50.1
Out	n.d.	8.28	2.80	3.94	1.53	45.8	15.0	n.d.	0.13	1.10

* n.d. indicates below detection limit

Seasonal water characteristics

Early-stage thermal stratification

Lake Willersinnweiher showed early-stage thermal stratification during the measurements in May 2017 (Figure 19). The epilimnion extends over the uppermost 4 m and the metalimnion reached down to 6 m. Average epilimnetic water temperature was 14 °C for profundal sites and 18 °C for more shallow sites. Gradients in epilimnetic water temperature show weak thermal stratification. In the metalimnion, temperatures decreased with depth to ~ 8 °C at 7 m (Figure 19). The epilimnion was well-oxygenated and O_2 concentrations decreased with depth. The oxycline was found at 12 m water depth. The pH in Lake Willersinnweiher followed the profiles of temperature and O_2 and showed pH values of 8.8 to 9 within the surface waters. Values decreased within the metalimnion and range from 7.4 and 7.6 in the hypolimnion. Epilimnetic Ca and DIC concentrations were substantially lower than hypolimnetic concentrations. Dissolved Fe and Mn concentrations were low in the epilimnion and highest in the bottom waters. Elevated dissolved Mn concentrations were found in the transition zone between the metalimnion and hypolimnion. Sulphate concentrations were constant throughout the entire water column while sulphide concentrations were below the detection limit (< 0.06 mM).

The water column of Lake Willersinnweiher showed maximum CH_4 concentrations of 2500 to 3000 nM at maximum water depths (Figure 19f). The isotopic composition of CH_4 ranged from - 75‰ to - 80‰ at the depths of maximum CH_4 concentrations. Generally, the $\delta^{13}C\text{-}CH_4$ values decreased with increasing CH_4 concentrations at deeper sampling points (Figure 19f). Minimum CH_4 concentrations were found in the upper hypolimnion with concentrations of 5 - 12 nM and $\delta^{13}C\text{-}CH_4$ values around - 50‰. Methane concentrations in the metalimnion and epilimnion were 130 nM for profundal sites. Littoral sites are different and show higher CH_4 concentrations and lighter $\delta^{13}C\text{-}CH_4$ values. The $\delta^{13}C\text{-}CH_4$ depth profile showed the highest $\delta^{13}C\text{-}CH_4$ values of - 43‰ at 7 m water depth, whereas epilimnetic $\delta^{13}C\text{-}CH_4$ was relatively stable at about -50‰. Methane concentration and $\delta^{13}C\text{-}CH_4$ values showed high temporal variations at 7 m.

Late-stage thermal stratification

Lake Willersinnweiher was thermally stratified during the measurements in October 2017 (Figure 19 g). The epilimnion reached down to 7 m and the metalimnion was between 7 m and 10 m water depth. Average epilimnic temperatures were 15 °C and decreased to 8 °C in the anoxic hypolimnion. The metalimnion separated the well-oxygenated epilimnion from the anoxic hypolimnion. Anoxic conditions were found below 12 m water depth. Epilimnic pH of 8.3 was considerably higher than pH values in the hypolimnion. Calcium and DIC concentrations in the epilimnion were lower than in the hypolimnion. Dissolved Fe and Mn concentrations in the epilimnion were below detection limit. Maximum dissolved Fe and Mn concentrations were found at the transition between metalimnion and hypolimnion. Sulphate concentrations were constant with depth and the highest sulphide concentrations were detected in the bottom near waters.

Epilimnetic CH_4 concentrations were considerably higher in late summer at all sites than in spring. The $\delta^{13}C\text{-}CH_4$ varied around - 52‰ in the epilimnion. Minimum $\delta^{13}C\text{-}CH_4$ values were found in the metalimnion along with highest $\delta^{13}C\text{-}CH_4$ values. Methane concentrations showed maximum concentrations of 107 µM in the hypolimnion of Lake Willersinnweiher (Figure 19). Minimum $\delta^{13}C\text{-}CH_4$ values of - 78‰ were found at depths of maximum CH_4 concentration.

Winter circulation

During the winter sampling, no variation in major elements with depth was observed, indicating a full circulation of the water column at Lake Willersinnweiher during the winter (Figure 19). Methane oversaturation with respect to atmospheric CH_4 concentrations (> 3 nM) was found in the entire water column.

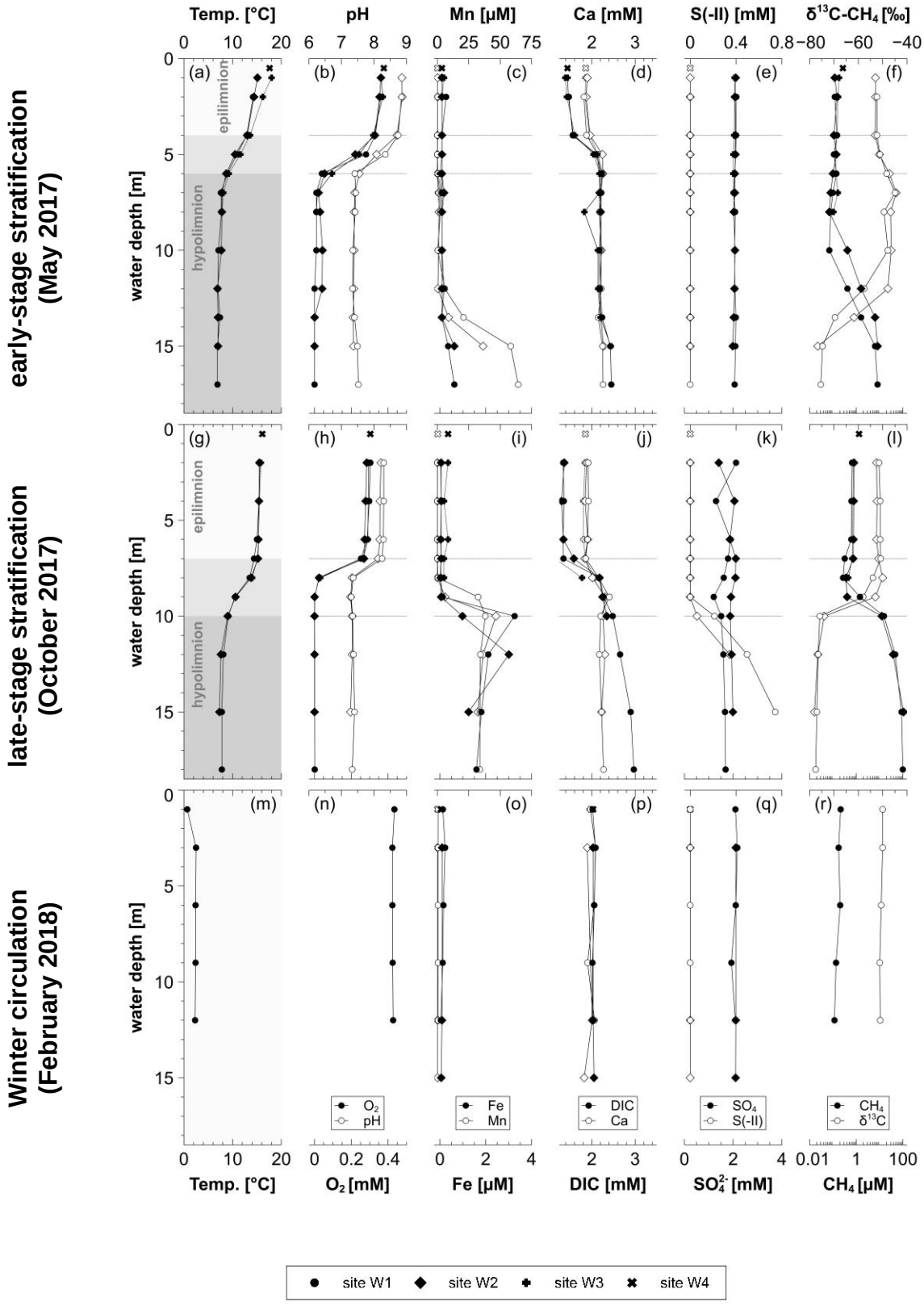

Figure 19: The water column of Lake Willersinnweiher at all sites (W1 to W4) for the early-stage thermal stratification (a-f), late-stage thermal stratification (g-l) and winter circulation (m-r).

Fluxes in the water column

The estimations of the fluxes from the sources and sinks of dissolved species within water layers of Lake Willersinnweiher shows significant temporal and spatial differences (Table 7).

During early-stage stratification, Ca and DIC fluxes from the metalimnion into the epilimnion were ~ 4 mmol m^{-2} d^{-1} and ~ 8 mmol m^{-2} d^{-1}, respectively. The difference between DIC and Ca fluxes (ΔJ_{DIC-Ca}) was ~ 4 mmol m^{-2} d^{-1} for the epilimnion of Lake Willersinnweiher. Downward fluxes for Mn and O_2 into the oxycline were relatively consistent for the profundal sites and higher than in more littoral sites. Upward diffusion of CH_4 to the oxycline ranged from 0.5 - 86 µmol m^{-2} d^{-1} during early-stage stratification. Calculated CH_4 emissions from the surface water of Lake Willersinnweiher into the atmosphere were around 12 µmol m^{-2} d^{-1} for the profundal and 28 µmol m^{-2} d^{-1} for the littoral sites. Methane production rates for the epilimnion of Lake Willersinnweiher were calculated to 39 ± 27 µmol m^{-3} d^{-1}.

Generally, fluxes during late-stage stratification are higher than in spring. Calcium and DIC fluxes were around 4 mmol m^{-2} d^{-1} and 10 mmol m^{-2} d^{-1}, respectively, resulting in a difference of ~ 6 mmol m^{-2} d^{-1}. In summer, Mn fluxes were considerably higher and showed values of 1.6 - 2 mmol m^{-2} d^{-1} for the profundal sites. Calculated CH_4 fluxes reached values of 120 µmol m^{-2} d^{-1} at the littoral and up to 275 µmol m^{-2} d^{-1} at the profundal sites. Summer CH_4 emissions were 5 to 10-fold higher than the spring values. Summer production rates were ~ 170 ± 105 µmol m^{-3} d^{-1}.

For the winter circulation no fluxes in the water column were determined (Table 7). Methane emissions from the surface water of Lake Willersinnweiher into the atmosphere were estimated to 2 µmol m^{-3} d^{-1}.

Table 7: Calculated fluxes into the epilimnion for DIC and Ca^{2+} (upwards) and into the oxycline for CH_4 (upwards) and Mn and O_2 (downwards) in the water column. Methane emission from the epilimnion and internal CH_4 production in Lake Willersinnweiher were estimated from surface water CH_4 concentrations. Note: Production rates are given in [µmol m^{-3} d^{-1}].

site	Fluxes in the water column						Emission	Internal Production
	Ca	DIC	ΔJ_{DIC-Ca}	CH_4	Mn	O_2	CH_4	CH_4
	— (into epilimnion) —			— (into oxycline) —				
	— [µmol m^{-2} d^{-1}] —							[µmol m^{-3} d^{-1}]
Early-stage stratification								
W1	3130	7510	4380	44.6	901	10300	12	39 ± 27
W2	4960	9580	4620	85.8	1040	11800	15	
W3	3450	7460	4010	0.5	79	9180	19	
W4	-	-	-	-	-	-	28	
Late-stage stratification								
W1	4700	11200	6510	985	2010	11600	126	169 ± 105
W2	4050	10300	6220	1240	1630	19800	152	
W3	3750	10700	6980	1.2	16	20100	155	
W4	-	-	-	-	-	-	275	
Winter circulation								
W1	0	0	0	0	0	0	2	0
W2	0	0	0	0	0	0		
W3	0	0	0	0	0	0		
W4	-	-	-	-	-	-		

Sediment pore-water characteristics and pore-water fluxes

Analyses of pore-water were obtained for the period of early-stage stratification in May 2017 only. The sediments of Lake Willersinnweiher showed condensed geochemical redox zonation of all the measured terminal electron acceptors (TEAs) at all sites (Figure 20).

Manganese is released within the entire sediment column, with maximum concentrations of 200 µM found at profundal sites. Pore-water Mn concentrations peaked within the uppermost 2 to 8 cm of the sediments, while Mn concentrations increased again with depth below 20 cm at site W2. The ferruginous zone was absent within the sediments of Lake Willersinnweiher. Significant concentrations of dissolved Fe were found at site W2 for depths below 20 cm, only. Pore-water SO_4^{2-} decreased within the uppermost 10 cm and dissolved sulphide built up below to concentrations of up to 2.5 mM at site W2. Maximum HS^- concentrations were found around 5 to 10 cm. DIC significantly increased with depth to concentrations of up to 8 mM. Methane concentrations in bottom waters of Lake Willersinnweiher ranged from 0.02 mM to 0.5 mM, which is up to 2 orders of magnitude higher than in the hypolimnion. Pore-water CH_4 generally increased with sediment depth to maximum values of 5 mM at site W2. Site W1 showed a different pattern with a distinct local maximum at 5 cm and decreasing concentrations below. In general, the redox zonation was less pronounced and pore-water concentrations were lower at littoral sites than at profundal sites (Figure 20).

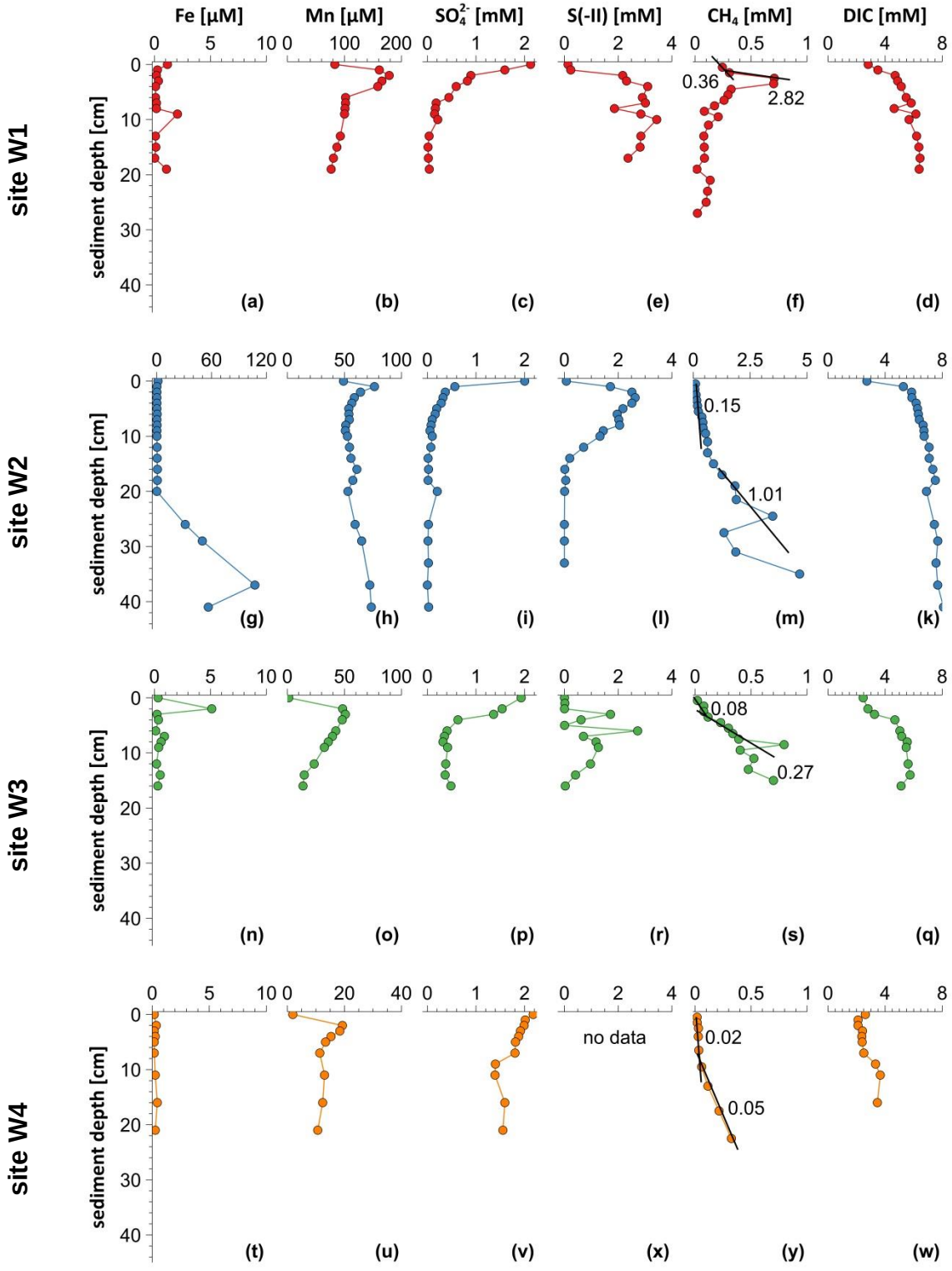

Figure 20: Geochemical pore-water profiles of selected elements at site W1 (a-f), site W2 (g-m), site W3 (n-s) and site W4 (t-w) in the sediments of Lake Willersinnweiher for the early-stage stratification (May 2017). Sedimentary fluxes of CH_4 are indicated by bold lines and are given in mmol m^{-2} d^{-1}.

Methane was considerably released across the sediment-water interface into the bottom water at all sites (Figure 20). Methane release from the sediment to the water body ranged from 0.02 - 1.32 mmol m^{-2} d^{-1} at shallow sites and profundal sites, respectively.

Conversion rates of organic carbon within the sediments were calculated based on pore-water fluxes of the TEAs and products using eq. [18] to [23] (Table 8). Pore-water fluxes of Mn, SO_4^{2-}, DIC and CH_4 generally decreased with increasing lake depth. Fluxes of CH_4 and SO_4^{2-} show maximum values of 1.86 and 4.61 mmol m^{-2} d^{-1}, respectively, whereas maximum Mn reduction rates are substantially lower. Turnover rates of OM calculated as the sum of equivalent rates for each element, based on the electrons exchanged during production (release of CH_4 and Mn) and internal consumption (SO_4^{2-}) consequently decrease with increasing lake depth. Turnover rates for CH_4 and SO_4^{2-} in the sulphate-methane-transition (SMT) zones ranged from 0.04 - 0.96 mmol m^{-2} d^{-1} and 0.28 - 4.61 mmol m^{-2} d^{-1}, respectively.

Table 8: Sedimentary conversion rates of organic carbon (SCR) calculated from redox-processes (via eq. [18] to [23]) and DIC fluxes within the sediments of Lake Willersinnweiher for early-stage stratification. Rates are given in mmol m^{-2} d^{-1}.

site	Pore-water fluxes			Calculated rates		Calculated from DIC fluxes	
	Mn	SO_4^{2-}	CH_4	SCR_{calc}	+-	$J_{observed}$ -	+-
	[mmol m^{-2} d^{-1}]						
W1	0.26	2.59	1.86	5.84	1.33	3.27	0.58
W2	0.13	4.61	0.87	7.84	2.32	3.49	0.62
W3	0.08	2.23	0.27	3.65	1.13	5.23	0.92
W4	0.00	0.29	0.05	0.49	0.14	1.23	0.22

2.1.4. Discussion

Lakes are significant reservoirs of terrestrial carbon and the fate of carbon is thereby determined by various processes within the sediments and the water column (e.g. Cole et al. 2007; Tranvik et al. 2009). This study presents the different pathways of carbon cycling within Lake Willersinnweiher and shows the interaction of carbon and sulphur cycling within the sediments. Production and consumption of carbon compounds, particularly with regard to CH_4, within the sediments and the water column are discussed and quantified. Further estimations of CH_4 cycling in the surface water and emissions to the atmosphere allow a whole-lake CH_4 mass balance for Lake Willersinnweiher.

Carbon cycling in the sediments

Diffusive fluxes across the sediment-water interface into the bottom water reveal the lake sediments as the major source of DIC and CH_4 in the hypolimnion of Lake Willersinnweiher. In contrast, for sulphate the sediments in Lake Willersinnweiher act as a sink. Lake Willersinnweiher is sulphur dominated and sulphate reduction is the main pathway of OM conversion in the sediments with maximum rates of 4.61 mmol m^{-2} d^{-1} (site W2). However, sulphur recycling was previously reported for the sediments of Lake Willersinnweiher (Schröder 2004) and calculated sulphate reduction rates (SRR) might therefore represent minimum values for the sediments in Lake Willersinnweiher. Calculated SRR values of 0.2 – 4.5 mmol m^{-2} d^{-1} are consistent with previously reported values for Lake Willersinnweiher (1.5 – 4 mmol m^{-2} d^{-1}, Schröder 2004) as well as other eutrophic and/ or SO_4^{2-}-enriched lakes (0.4 – 50 mmol m^{-2} d^{-1}, Holmer and Storkholm 2001; Schubert et al. 2011; Norði et al. 2013) and marine sediments (0.5 – 27 mmol m^{-2} d^{-1}, Jørgensen and Kasten 2006). Methanogenesis at Lake Willersinnweiher accounted for 10 – 40 % of the OM degradation and the proportion of sedimentary CH_4 formation increased with increasing lake depth (Figure 21a). This is in very good agreement with previous studies accounting 20 – 42% of OM degradation to methanogenesis in profundal sediments (Kelley et al. 1990; den Heyer and Kalff 1998; Liikanen et al. 2003).

The calculation of sedimentary carbon conversion rates (SCR) based on the rates of Mn, CH_4 and SO_4^{2-} and neglected reduction rates of the energetically more

favourable electron acceptors O_2, NO_3 and Fe, since O_2 and NO_3 are consumed within the uppermost 1 cm of the sediments and Fe is fixed as iron-sulphides in the sulphur-dominated sediments of Lake Willersinnweiher (Schröder 2004). Values obtained for sedimentary diffusional fluxes of SO_4^{2-}, DIC and CH_4 are in very good agreement with calculated fluxes previously reported for Lake Willersinnweiher (Schröder 2004) and very similar to rates found in mesotrophic to eutrophic lakes at this time of year (Sweerts et al. 1991; Liikanen et al. 2003). Fluxes of Mn, SO_4^{2-}, DIC and CH_4 are generally increasing with increasing bathymetric depth of the sampled site (Figure 21A).

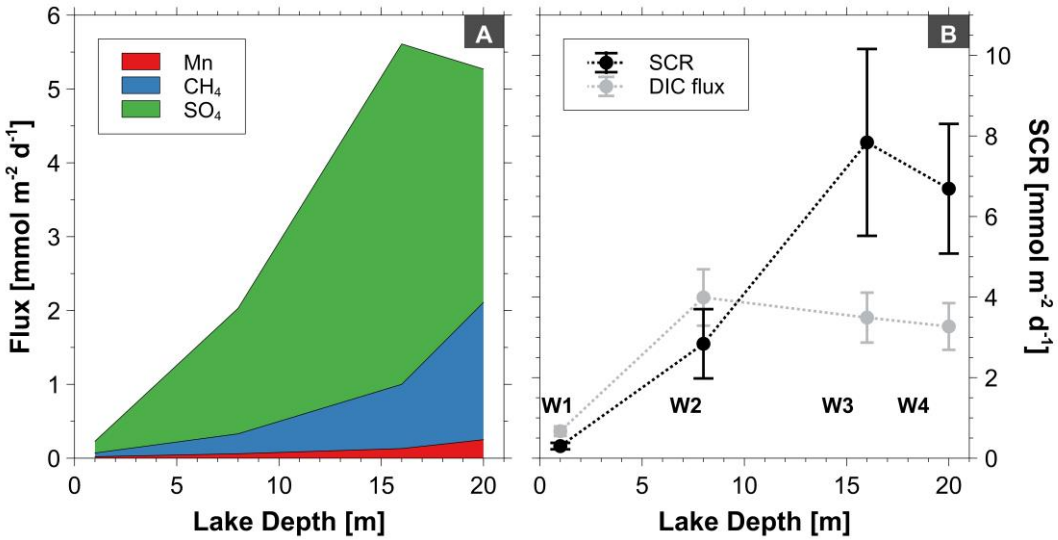

Figure 21: Stacked fluxes of Mn, CH_4 and SO_4^{2-} in the sediments versus the respective lake depth of the sediments in Lake Willersinnweiher (A). Sedimentary conversion rates of OM (SCR) (calculated as the sum of internal production (CH_4 and Mn) and internal consumption (SO_4^{2-})) and calculated DIC fluxes with lake depth of the sampled sediments in Lake Willersinnweiher (B). Calculated rates are in the range of observed DIC fluxes in the sediments. Sulphate reduction is the main pathway of OM conversion in the sediments of Lake Willersinnweiher. Methane cycling plays an essential role within sediments of Lake Willersinnweiher.

Hence, OM conversion rates calculated as the sum of internal production (release of CH_4 and Mn) and internal consumption (SO_4^{2-}) are substantially higher at profundal sites than at the littoral site, indicating more intensive decomposition of OM by heterotrophic microorganisms in the deeper areas of Lake Willersinnweiher. Calculated SCR of up to 5.5 mmol m^{-2} d^{-1} are in the range of rates reported for other freshwater sediments (den Heyer and Kalff 1998; Liikanen et al. 2003). The SCRs of Lake Willersinnweiher are in the same scale as the observed DIC fluxes in the littoral site but differ for the profundal

sites (Figure 21B). Pore-water DIC flux might be underestimated due to the precipitation of carbonates in the sediments of Lake Willersinnweiher, which limits the pore-water DIC concentrations and consequently leads to underestimated DIC fluxes. An additional explanation might be the method of pore-water sampling. Profundal sites are characterised by intense degradation of OM and, consequently, higher DIC concentrations than at littoral sites. Since pore-water extraction by rhizons generally leads to an underestimate of DIC due to degassing of CO_2 during vacuum extraction (Schrum et al. 2012), this effect might be most obvious for the higher concentration ranges found along with enhanced decomposition of OM. Future analysis of pore-water pH and CO_2 (g) as well as sediment squeezing might therefore result in more accurate DIC concentrations, not influenced by the method of pore-water extraction.

Interaction of carbon and sulphur cycling in the sediments

Groundwater entering Lake Willersinnweiher is a part of the groundwater system within the Upper Rhine Graben. Lake Willersinnweiher is significantly affected by SO_4^{2-}-rich groundwater (> 2 mM) due to the oxidation of pyrite in the quaternary river Rhine sediments in the catchment upstream of Lake Willersinnweiher (Schröder 2004). Turnover processes in the sediments result in lower SO_4^{2-} outflow concentrations and, hence, Lake Willersinnweiher is a sink for sulphur.

In the sediments of Lake Willersinnweiher, direct coupling between sulphur and carbon cycling was found. The presence of SO_4^{2-} generally limits sedimentary CH_4 formation as carbon compounds are favourably metabolized by non-methanogens. In SO_4^{2-}-rich zones, sulphate reducing bacteria (SRB) and methanogens compete for available H_2 and acetate. On the other hand, methanogenic archaea generally benefit from the acetate produced by SRB from substrates like lactate (Cappenberg 1974, 1975; Winfrey and Zeikus 1977). As considerable pore-water concentrations of free sulphide were found, SRB out-compete the methanogens for available H_2 in the sediments of Lake Willersinnweiher. Methane is consequently produced via the hydrogenotrophic pathway (carbonate reduction) at greater sediment depths where SO_4^{2-} is depleted and SRB are inactive. However, sulphate-methane-interaction is not only affecting CH_4 formation, but also CH_4 consumption in the sediments. Sulphate minima generally coincide with the depth of CH_4 minima, indicating

the presence of anaerobic oxidation of methane (AOM) in the upper sediment layers (Niewöhner et al. 1998; Borowski et al. 1999). Here, CH_4 is most likely oxidised with SO_4^{2-} as electron acceptor by methane-oxidizing archaea (anaerobic methanotrophs, ANME) and sulphate-reducing bacteria consuming upward migrating CH_4 (Hinrichs et al. 1999; Boetius et al. 2000). Sulphate-methane transition zones (SMTZ) were determined at all sites (Figure 22). Furthermore, site W3 showed two distinct SMTZ in 5 cm and 10 cm depth that might be a result from the seasonal variations of the depth of the redoxcline that was previously reported by (Schröder 2004).

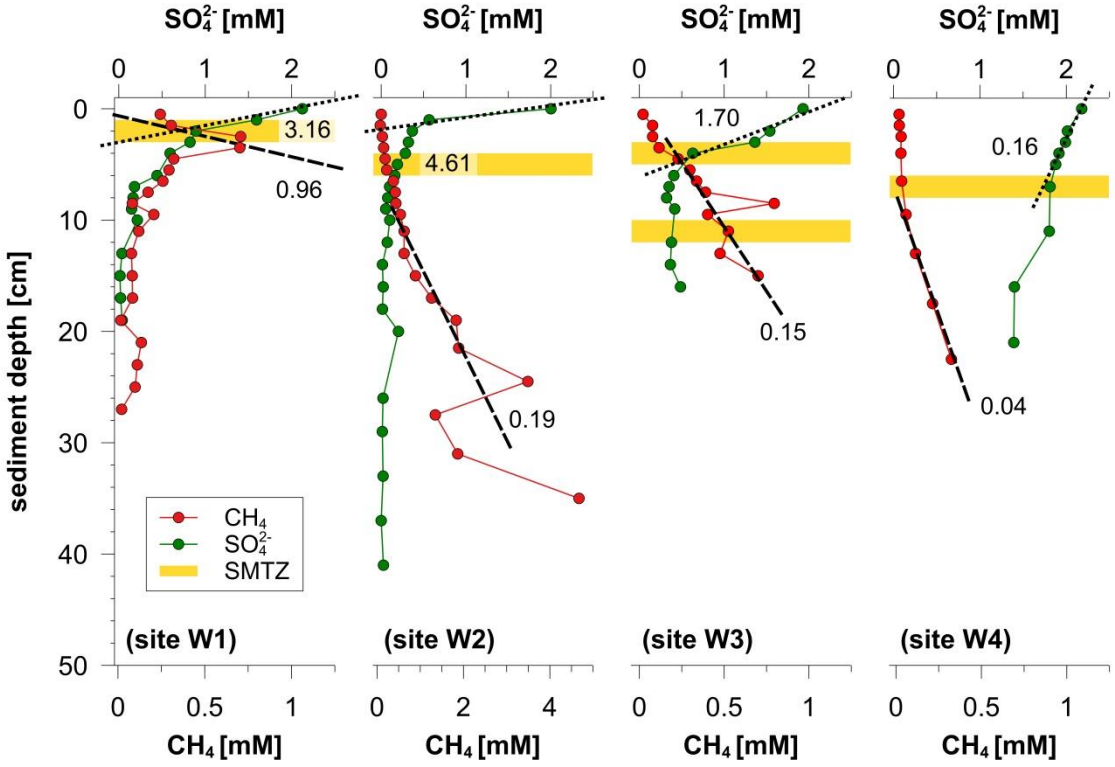

Figure 22: Sulphate and methane concentrations in the pore-water at different sediment depths of the sites W1-W4 of Lake Willersinnweiher. The sulphate-methane transition zones (SMTZ) are characterised by minimum SO_4^{2-} and CH_4 concentrations in the pore-water. Data indicate the presence of anaerobic oxidation of methane (AOM) by methane-oxidizing archaea and sulphate-reducing bacteria in the upper sediment layers, consuming upward migrating CH_4. Rates for CH_4 and SO_4^{2-} consumption are indicated by the dashed and dotted lines, respectively, and are given in mmol m^{-2} d^{-1}.

SMTZ is a common feature first described for marine sediments due to high pore-water SO_4^{2-} concentrations (Martens and Berner 1974; Reeburgh 1976), whereas pronounced SMTZ have been observed for very few specific freshwater environments only (Schubert et al. 2011; Timmers et al. 2016). AOM in freshwater environments is usually coupled to the reduction of nitrate and

nitrite (Raghoebarsing et al. 2006; Ettwig et al. 2008; Deutzmann et al. 2014; Norði and Thamdrup 2014; Shen et al. 2017) or to the reduction of iron and / or manganese (Beal et al. 2009; Amos et al. 2011; Crowe et al. 2011; Norði et al. 2013; He et al. 2018). However, NO_3 concentrations are negligible in the pore-water and dissolved Fe is trapped as (oxyhydr-)oxides or sulphides in the sediments of Lake Willersinnweiher (Schröder 2004). AOM by the oxidation of Mn-oxides might be an additional pathway in the sediments of Lake Willersinnweiher as Mn-oxides as electron acceptors are energetically more favourable than SO_4^{2-}. Intense Mn-cycling and Mn-dependent sulphide-oxidation in the sediments was reported for Lake Willersinnweiher during winter (Schröder 2004). Dissolved Mn was found in the pore-water of Lake Willersinnweiher and might therefore indicate AOM by Mn-oxides. The impact of Mn-oxides as electron acceptors might be quantitatively significant but subordinated to AOM via SO_4^{2-} in the sediments of Lake Willersinnweiher. The interaction of methanogenesis, sulphur cycling and recycling of DIC produced by AOM leads to a carbon cycling at the top of the methanogenic zone. As a consequence, CH_4 could be formed from DIC via CO_2 reduction (subordinated from methanogenesis) (Figure 23). However, future investigations of $\delta^{13}C$, δD and $\delta^{34}S$ values are desirable and would provide further evidence of AOM in the sediments of Lake Willersinnweiher by covering all major constituents in carbon cycling.

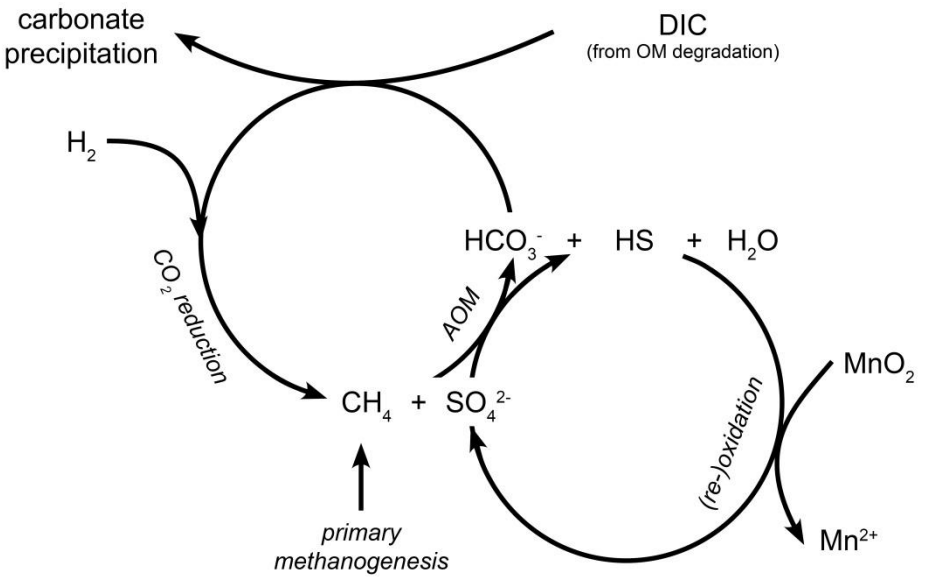

Figure 23: The interaction of carbon and sulphur cycling in sediments. Modified after Borowski et al. (1997) for the conditions at Lake Willersinnweiher.

Sedimentary release

About 60 - 90 % of the produced and upwards migrating CH_4 is consumed by AOM before reaching the water column (Figure 24). The percentage of CH_4 oxidised in the SMTZ accounted for 45 % to up to 65 % for profundal and littoral sites, respectively. Nevertheless, considerable release of CH_4 and DIC across the sediment-water interface into the bottom water was found and fluxes were significantly increasing with rising lake depth. This indicates that the release of CH_4 is linked to AOM efficiency in the SMTZ. This might be controlled by the different nature of OM degradation and the substrate availability for archaea and SO_4^{2-} reducers changing with lake depth (Boetius et al. 2000).

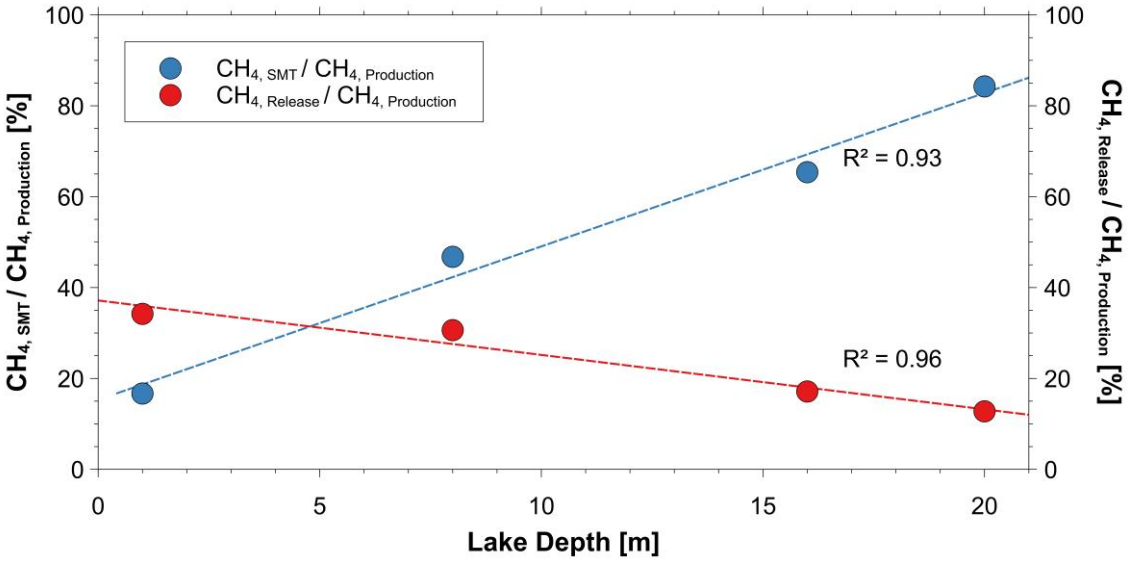

Figure 24: Percentage of produced CH_4 released across the sediment-water interface into the bottom water as well as well as AOM efficiency (percentage of produced CH_4 oxidised in SMTZ in the sediments) with respect to the lake depth of the sediments in Lake Willersinnweiher.

Calculating the total loss of CH_4 by the turnover in the SMTZ and the release into the bottom water does not add up to 100 % of the produced CH_4 within the sediments. Deviations from this calculation decrease with increasing lake depth from 50 % (littoral) to 3 % (profundal). Schröder (2004) showed seasonal variations in the fluxes of TEAs and the depth of the redox front within the sediments of Lake Willersinnweiher. Increasing temperatures during early-stage stratification will lead to considerable and fast changes in pore-water chemistry and turnover rates with time. Furthermore, secondary methanogenesis and intense sulphur cycling within the sediments also lead to

non-steady state conditions in AOM settings (e.g. Dale et al. 2008). Hence, calculations from concentration gradients according to Fick's first law assuming steady-state conditions result in underestimations of CH_4 turnover within the sediments.

Aerobic CH_4 oxidation (MOx)

Despite pronounced AOM in the sediments, oxidation of CH_4 was also obvious in the water column of Lake Willersinnweiher (Figure 25). In general, SMTZ in the sediments considerably diminishes CH_4 release into the water column of Lake Willersinnweiher. However, CH_4 is still significantly released across the sediment-water interface into the bottom water. Upward migrating CH_4 is consumed towards the oxycline (redoxcline). Minimum CH_4 concentrations (5 - 10 nM) coincide well with decreasing O_2 concentrations in the metalimnion. Calculated upward fluxes for CH_4 (up to 1.2 mmol m^{-2} d^{-1}) in the oxic/anoxic transition zone during late-stage stratification are in the same range with AOM rates in the SMTZ (~ 1.0 mmol m^{-2} d^{-1}). Methane fluxes at the redoxcline show maximum values in the summer months and are in agreement with rates reported for other eutrophic lakes (e.g. Oswald et al. 2015). Downward fluxes for O_2 (1 mmol m^{-2} d^{-1}) are higher than Mn and CH_4 fluxes and, hence, Mn, S(-II) and CH_4 are completely oxidised by O_2. Dissolved Mn presumably precipitates as rhodochrosit at the redoxcline and Mn-carbonate formation might therefore be coupled to CO_2 that is produced during CH_4 oxidation within the water column. Analysis of $\delta^{13}C$ values in carbonates could provide evidence for the coupling of Mn and CH_4 cycling at the oxycline of Lake Willersinnweiher.

$\delta^{13}C$-CH_4 values increase towards the oxycline, indicating the uptake of lighter CH_4 by aerobic microbial oxidation within the water column of Lake Willersinnweiher (Barker and Fritz 1981) (Figure 25). Aerobic CH_4 oxidation might therefore also depend on the interaction between oxygenic phototrophs and aerobic methanotrophs, as recently shown for Lake Rotsee (Switzerland) by Oswald et al. (2015). Methane oxidation thereby seems to be mediated by both the light intensity (Dumestre et al. 1999; Murase et al. 2005; Oswald et al. 2015) and the oxygen concentrations (Rudd et al. 1976) within the water column. Aerobic CH_4 oxidation within the water column of Lake Willersinnweiher acts therefore as an effective barrier to minimize CH_4 release into the surface water and the atmosphere.

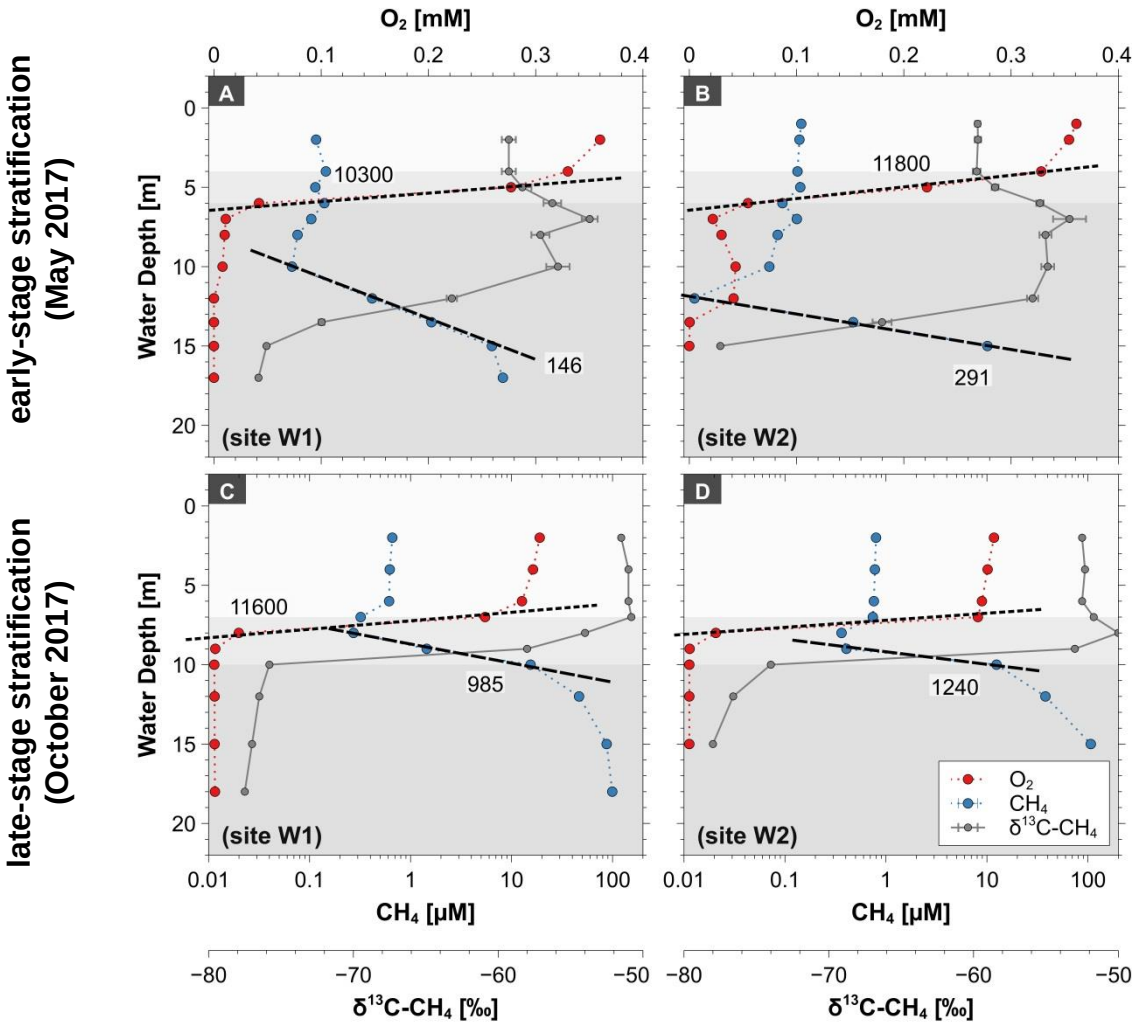

Figure 25: O_2 and CH_4 concentrations at the redoxcline in Lake Willersinnweiher during early-stage stratification (A-B) and late-stage stratification (C-D). Aerobic oxidation of methane consumes upward migrating CH_4 released from the sediments. Rates for CH_4 and O_2 consumptions are indicated by the dashed and dotted lines, respectively, and are given in mmol m^{-2} d^{-1}.

Surface water

The redoxcline at Lake Willersinnweiher decouples the surface water from the deep water reservoirs. Methane oversaturation in the surface water requires a methane source located in the upper oxic layer as upward migrating sedimentary CH_4 is consumed towards the oxycline (Figure 25). The Keeling plot for water samples supports this assumption and shows different sources of CH_4 for the epilimnion and hypolimnion of Lake Willersinnweiher (Figure 26). The extrapolated intercepts of the best fit in the Keeling plot provide the isotope ratio of sub-thermocline CH_4 which ranged from -75.6‰ to -77.8‰. In contrast, waters from the epilimnion show intercepts of -56.8‰ to -49.4‰ revealing methanogenic sources within the upper water column of Lake Willersinnweiher (Figure 26).

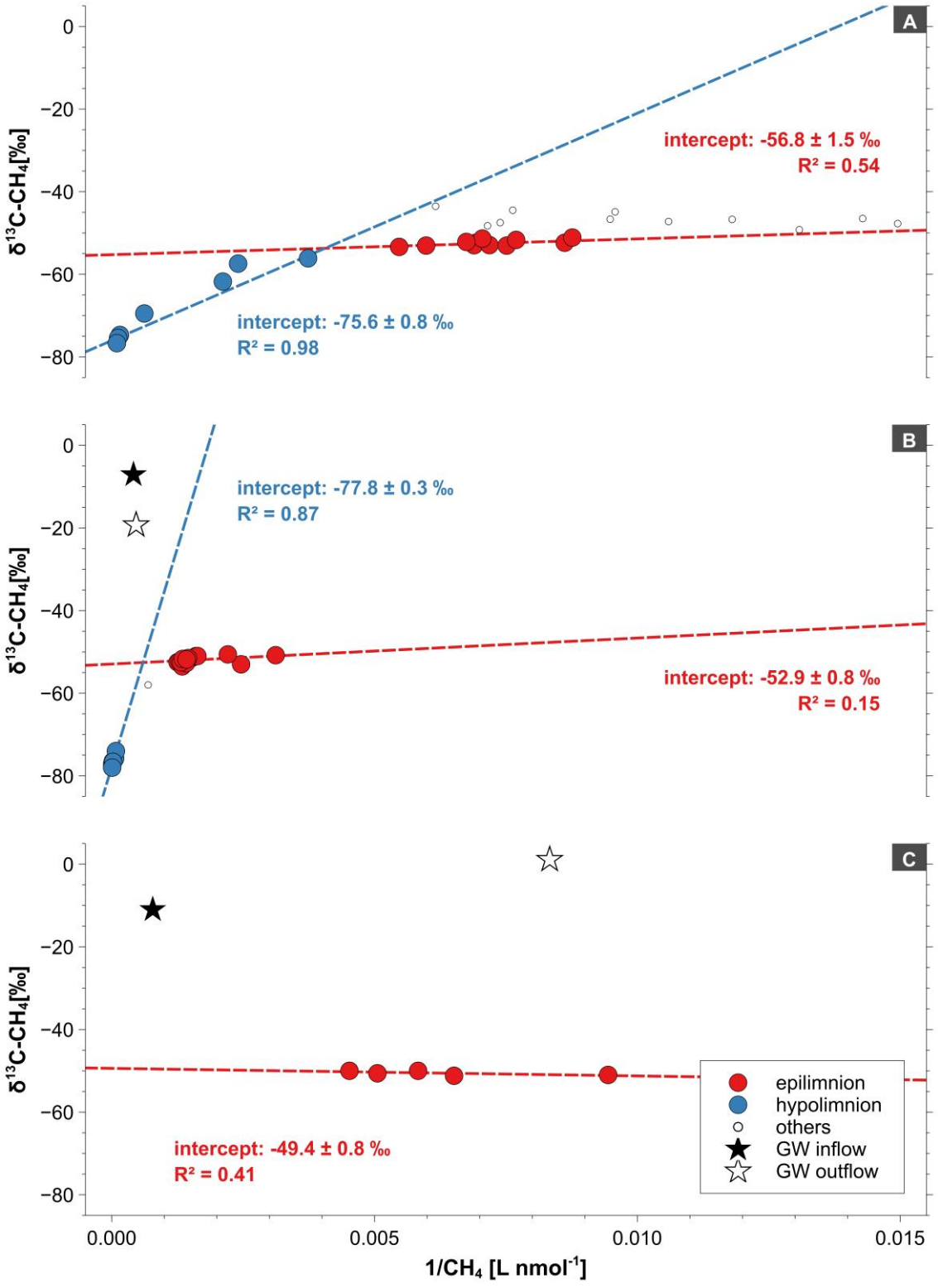

Figure 26: Keeling-Plot for the water samples from Lake Willersinnweiher for early-stage thermal stratification (A), late-stage thermal stratification (B) and winter circulation (C). The extrapolated intercepts of the best fit in the Keeling plot provide the isotope ratio of the different sources of CH_4 in Lake Willersinnweiher. Error bars (1-σ) of measurements reflect the noise within the measurement interval (10 min) and mainly lie within symbols. Best fit and intercepts were estimated by geometric mean regression.

The sources of CH_4 in the water column might be (1) transport of CH_4 from littoral sediments, (2) groundwater contribution and / or (3) internal oxic methane production (OMP) (Grossart et al. 2011; Bogard et al. 2014; Tang et al. 2014; McGinnis et al. 2015; Donis et al. 2017).

(1) Lateral transport of CH_4

Concentration gradients from littoral to profundal sites and lateral transport of CH_4 from littoral sediments was shown for lake environments (Murase et al. 2005; Hofmann et al. 2010; Encinas Fernández et al. 2016; DelSontro et al. 2017). Surface water CH_4 concentrations in Lake Willersinnweiher were higher in the littoral than profundal and might result in CH_4 transport to the centre of the lake. However, the data of this study cannot provide any evidence for this assumptions as no systematic transect of water column profiles over lake width was conducted.

(2) Groundwater contribution

Groundwater contribution into the epilimnion of Lake Willersinnweiher (2) is likely as groundwater infiltrating the lake at the south-eastern shore is enriched in CH_4 (up to 2.4 µM). Relatively little is known about naturally occurring background CH_4 concentrations in groundwater in the URG to date and the source of CH_4 in the groundwater of the upstream of Lake Willersinnweiher is unknown and could originate from various sources (Table 9).

Groundwater $\delta^{13}C\text{-}CH_4$ values ranged between -18‰ and 1.6‰ and are rarely reported for groundwaters (Schloemer et al. 2016). Increasing $\delta^{13}C\text{-}CH_4$ values generally indicate intense microbial CH_4 oxidation (Barker and Fritz 1981). Hence, $\delta^{13}C\text{-}CH_4$ values might not provide any evidence about the actual source of CH_4 in the groundwater.

Table 9: Potential pathways for CH_4 accumulation in groundwater upstream of Lake Willersinnweiher

Source	Pathway	Pro	Contra
lignite bearing sediments and / or thermogenic origin	diffusion from deeper aquifers	relatively light $\delta^{13}C$-CH_4 values	requires pathways for ascending waters
organic-rich sediments of old river branches	anoxic methanogenesis within the aquifer	substrates available	limited in the presence of SO_4^{2-}
(freshwater) carbonates	methanogenesis via CO_2 reduction	substrates available	producing relatively heavy $\delta^{13}C$-CH_4 values limited in the presence of SO_4^{2-}
contamination site	anoxic methanogenesis / methanogenesis during the degradation of organic contaminants	substrates available	contamination sites not documented
surface	infiltration from e.g. gravel pits	open gravel pit < 1km upstream	no CH_4 data available
lakes upstream	anoxic methanogenesis in littoral sediments	seasonal variations	no CH_4 data available

Lignite bearing sediments are known as groundwater CH_4 sources in deeper aquifers of the URG (e.g. Gründger et al. 2015). Reported coalbed $\delta^{13}C$-CH_4 values range from about -80‰ to -16‰ (e.g. Rice 1993). Furthermore, natural thermogenic $\delta^{13}C$-CH_4 is usually in the range of - 50‰ to - 25‰. Methane from both sources might migrate into the groundwater. Although, ascent of deep fluids into shallow aquifers was shown for very specific areas linked to graben structures (AlNajem 2016; Freundt 2017), fracture zones and flow paths of upward ascending waters in the direct proximity are not reported. Diffusion from deeper aquifers of Miocene or Oligoncene age is therefore unlikely to cause CH_4 concentrations in the surface near groundwater.

Methanogenesis via CO_2 reduction depends on the substrates available. Carbonate reduction is the dominant pathway for reservoirs with high DIC concentrations. However, substrates might be fully metabolized by non-methanogens (e.g. SRB) since groundwater is significantly enriched in SO_4^{2-}.

Organic-rich sediments from old branches of the river Rhein (e.g. Roxheimer Altrhein) span over a large area upstream of Lake Willersinnweiher. These sediments might provide substrates for methanogens within the surface-near aquifer. However, methanogenesis is substantially limited in the presence of SO_4^{2-} and CH_4 originating from these sediments might have been fully oxidised to within the lakes upstream before reaching Lake Willersinnweiher.

Methane is produced by anoxic methanogenesis and as product of oxidative biodegradation of (highly volatile chlorinated) hydrocarbons in contamination sites (Hunkeler et al. 2005; Azadpour-Keeley et al. 2005; Wickert et al. 2009; Schmidt et al. 2010). The isotopic composition of CH_4 is thereby controlled by the $\delta^{13}C$-ratio of the original substrate. Wickert et al. (2009) reported elevated CH_4 concentrations (up to 2.5 µM) downstream of an CHC-contaminated site in the URG, compared to background concentrations of 0.3 µM. Methanogenesis as a result of a contamination is likely but, however, these sites are not documented for the nearby environment.

The infiltration of surface water into groundwater is possible since an open gravel pit is located less than 1 km upstream of Lake Willersinnweiher (49°29.81' N 8°22.62' E). However, pathways of infiltration and methanogenesis in the gravel pit was not analysed in the frame of this study.

Methane concentrations of the groundwater inflow and outflow of Lake Willersinnweiher showed (seasonal) variations that could only be explained by temporally variable CH_4 production or oxidation. Wollschläger et al. (2007) have shown that groundwater infiltrating the lake at the south-eastern shore has passed at least one of the lakes located in the catchment of Lake Willersinnweiher. This suggests that groundwater CH_4 most likely results from the lakes upstream. Here, lake water infiltrates into the aquifer through the porous littoral sediments before entering Lake Willersinnweiher. Sediments are significantly enriched in CH_4 compared to lake water and show seasonal variation in CH_4 production that became apparent during further studies at Lake Willersinnweiher (first results not shown in the frame of this study) and other lake environments (e.g. Holmer and Kristensen 1996; Nusslein and Conrad 2000). Methane oxidation in the groundwater might be coupled to the reduction of NO_3^-, NO_2^-, Fe and Mn as O_2 is absent or limited within the groundwater (Raghoebarsing et al. 2006; Ettwig et al. 2008; Deutzmann et al. 2014; Norði and Thamdrup 2014; Shen et al. 2017). Denitrification-dependent

AOM (DAOM) is coupled to a microbial consortium that was found in different freshwater ecosystems worldwide (Raghoebarsing et al. 2006), but its occurrence and distribution in aquifers has not yet been described. Agricultural usage leads to an intense contribution of NO_3^- into the groundwater (up to 4.5 mM upstream of Lake Willersinnweiher) and might also result in (seasonal) variations in DAOM. However, processes in the aquifers between lakes upstream and Lake Willersinnweiher are complex and have not yet been sufficiently studied. Further investigations of the lake waters upstream as well as along the groundwater flow path are crucial for the understanding of the complex groundwater–surface water interactions in Lake Willersinnweiher.

Groundwater contribution of CH_4 to the epilimnion plays a key role in CH_4 budget of Lake Willersinnweiher, since CH_4 oversaturation occurred all year. Nonetheless, surface water CH_4 concentrations are higher during summer stratification than during winter circulation.

(3) Oxic CH_4 production (OMP)

Estimations of epilimnic CH_4 production calculated according to Donis et al. (2017) include groundwater input and assuming common MOx rates reported for e.g. Lake Stechlin (0.1 d^{-1}; Tang et al. 2014), Lake Rotsee (0.5 d^{-1}; Oswald et al. 2015) or Lake Cromwell (1.0 d^{-1}; Bogard et al. 2014). The results show *in-situ* CH_4 production of 65 ± 50 nM d^{-1} for early-stage and 280 ± 200 nM d^{-1} for late stage stratification. These values are in good agreement with estimated values of 40 nM d^{-1} to 90 nM d^{-1} for Lake Stechlin (Grossart et al. 2011; Tang et al. 2014), 110 ± 60 nM d^{-1} for Lake Halwill (Donis et al. 2017), 230 ± 10 nM d^{-1} for Lake Cromwell (Bogard et al. 2014) and up to 225 ± 170 nM d^{-1} for Lake Stechlin presented in this thesis (Chapter 2.2.). Elevated CH_4 concentrations in well-oxygenated surface water and OMP (mostly generating ^{13}C depleted CH_4) was reported repeatedly for different lake types (Grossart et al. 2011; Bogard et al. 2014; Tang et al. 2014; McGinnis et al. 2015; Donis et al. 2017). Methane production in oxic freshwaters thereby appears to be associated with, inter alia, photoautotrophs (Grossart et al. 2011; Bogard et al. 2014; Tang et al. 2014; Yao et al. 2016) or algae (Lenhart et al. 2015). Biological studies were not carried out at Lake Willersinnweiher, but a detailed study focussing on short-term variations of CH_4 due to changes in the physical, chemical and/or biological conditions in freshwater environments as well as

biochemical pathway(s) of methane production in oxic waters is shown in Chapter 2.2.

Biological activity further affects inorganic carbon cycling in the surface water of Lake Willersinnweiher. Surface water Ca^{2+} and DIC concentrations are substantially lower than below the thermocline. The epilimnion is oversaturated with respect to calcite in the surface water of Lake Willersinnweiher in the summer months with stable thermal stratification (Figure 27). The precipitation of $CaCO_3$ results from the incorporation of CO_2 by biota (primarily bacteria or algae) along with O_2 oversaturation within the surface water layer. The loss of CO_2 consequently shifts the chemical equilibrium to decreasing Ca^{2+} and DIC concentrations and elevated pH values within the surface water. Biogenically induced calcite precipitation is known to play an important role in eutrophic hard-water lakes (e.g. Brunskill 1969; Kelts and Hsü 1978; Effler and Drlscoll 1985; Müller et al. 2016). The rates of biologically induced calcification in the epilimnion are in very good agreement with values previously reported for Lake Willersinnweiher (Schmid 2002) and other groundwater-fed lakes e.g. Williams Lake (Minnesota, USA) (McConnaughey et al. 1994).

As a consequence, surface water of Lake Willersinnweiher acts as a source for CH_4 and a sink for CO_2 with respect to emissions to the atmosphere. Methane oversaturation in Lake Willersinnweiher can be considered as a mixture of both groundwater contribution and *in-situ* OMP. Notwithstanding the source of CH_4 in the surface water, CH_4 might not be fully oxidised which may further result in significant CH_4 emissions from Lake Willersinnweiher.

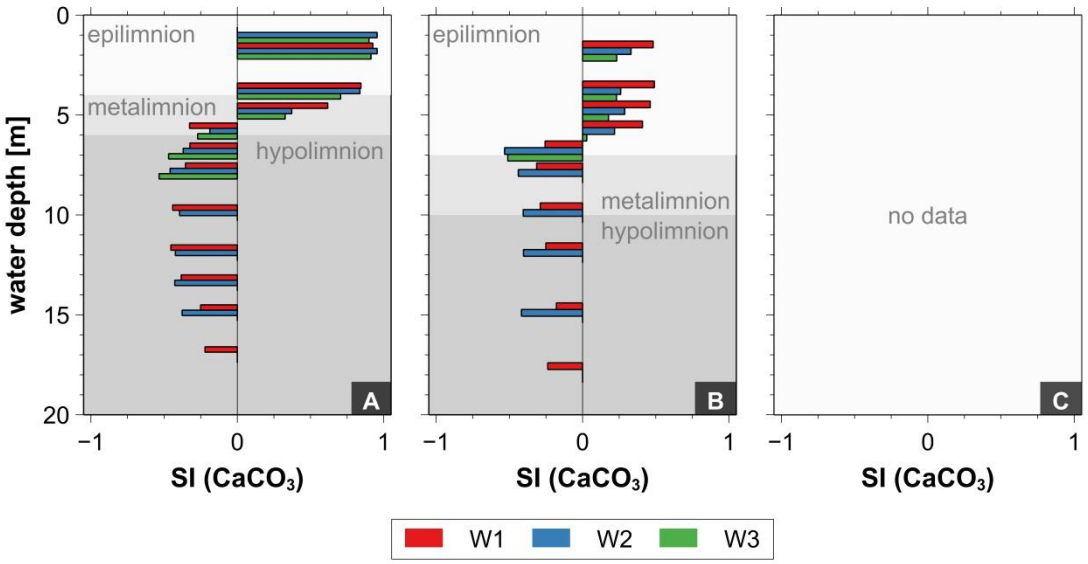

Figure 27: Calculated $CaCO_3$ solubility by *PHREEQC* (Parkhurst and Appelo 1999) for early-stage (A) and late-stage stratification (B) of Lake Willersinnweiher. No pH data was available for the winter circulation (C). $CaCO_3$ precipitates in surface water and dissolves in deeper waters of Lake Willersinnweiher.

Emissions

Methane emission rates for early-stage are lower than rates found for late-stage stratification. Lake Willersinnweiher is an all year source for atmospheric CH_4 as considerable emissions during winter circulation were found (2 µmol m^{-2} d^{-1}). Calculated emission rates are in very good agreement with emission data reported for common lake environments (Bastviken et al. 2008; Podgrajsek et al. 2014; Donis et al. 2017; Roland et al. 2017). However, mass-balance based emission data of this study lacks enhanced CH_4 emissions by ebullition (e.g. Bastviken et al. 2008) or plant ventilation (Chanton and Whiting 1995) in the littoral areas of Lake Willersinnweiher as well as continuous and direct CH_4 flux measurements via floating chamber or eddy covariance tower as CH_4 emissions are strongly affected by the wind speed and epilimnetic CH_4 concentration. The immediate effects of changes in the interplay between biological and physical processes in the lakes' environment on aquatic CH_4 accumulation and, consequently, on CH_4 methane emissions are presented in Chapter 2.2. Furthermore, all estimations are based on calculations from steady state conditions for single measurements in May 2017, October 2017 and February 2018, making future investigations of detailed seasonal variations in open-water and pore-water concentrations as well as fluxes desirable. The

presented data therefore represents a very conservative estimate of CH_4 emission of Lake Willersinnweiher.

Emissions during the summer stratification mainly result from OMP and groundwater input in the epilimnion as upward migrating CH_4 from deeper water is removed by aerobic oxidation at the oxycline in the water column. Summer stratification prevents CH_4 in the hypolimnion from outgassing and CH_4 consequently accumulates in the anoxic deep waters. Stored CH_4 is then released during the autumn overturn period by vertical water mass mixing, resulting in high emission rates of CH_4 (e.g. Bastviken et al. 2004). This phenomenon was also observed during spring overturns along with thawing ice coverage (e.g. López Bellido et al. 2009). Methane stored in the hypolimnion is oxidised to great extent in the water column. Oxidation is thereby dependent on the speed of vertical water column mixing. MOx rates during autumn overturn are a subject of controversial discussion and range from 45 to 95 % of CH_4 stored in the deeper water layers (Kankaala et al. 2007; López Bellido et al. 2009; Schubert et al. 2012; Encinas Fernández et al. 2014).

Methane mass balances for early and late-stage stratification and as well as winter circulation therefore allow very rough estimates of the annual total emissions of Lake Willersinnweiher. Estimations assume no production during the winter circulation (December to April) and a linear increase of CH_4 concentration in the surface water of Lake Willersinnweiher from April to November. Data for air temperature and wind speed suggests the autumn overturn in the last weeks of November, when temperature decreased to 0 °C and temporarily higher wind speeds (>10 m s^{-1}) might have caused mixing event(s) within the complete water column (Encinas Fernández et al. 2014) (Figure 28a). Methane emission rates for the autumn overturn calculated for minimum and maximum CH_4 oxidation rates range from 1.0 to 10 mmol m^{-2} d^{-1} and total annual emissions sum up to 11 mmol m^{-2} d^{-1} (Figure 28). These values are in good agreement with overturn emission rates measured at e.g. Lake Mindelsee (SW Germany) (12 mmol m^{-2} d^{-1} overturn and 15 mmol m^{-2} d^{-1} annual emissions), a temperate lake in Southern Germany with similar trophic state and size as Lake Willersinnweiher (Encinas Fernández et al. 2014). Calculated overturn emissions of Lake Willersinnweiher thereby account for 5 % to up to 50 % of the annual CH_4 emissions (depending on the respective assumed CH_4 oxidation rates in Lake Willersinnweiher) which is in good agreement with

most reported values of up to 40 - 50 % (Michmerhuizen et al. 1996; Riera et al. 1999; Liikanen et al. 2003; Bastviken et al. 2004; López Bellido et al. 2009; Encinas Fernández et al. 2014; Jammet et al. 2017).

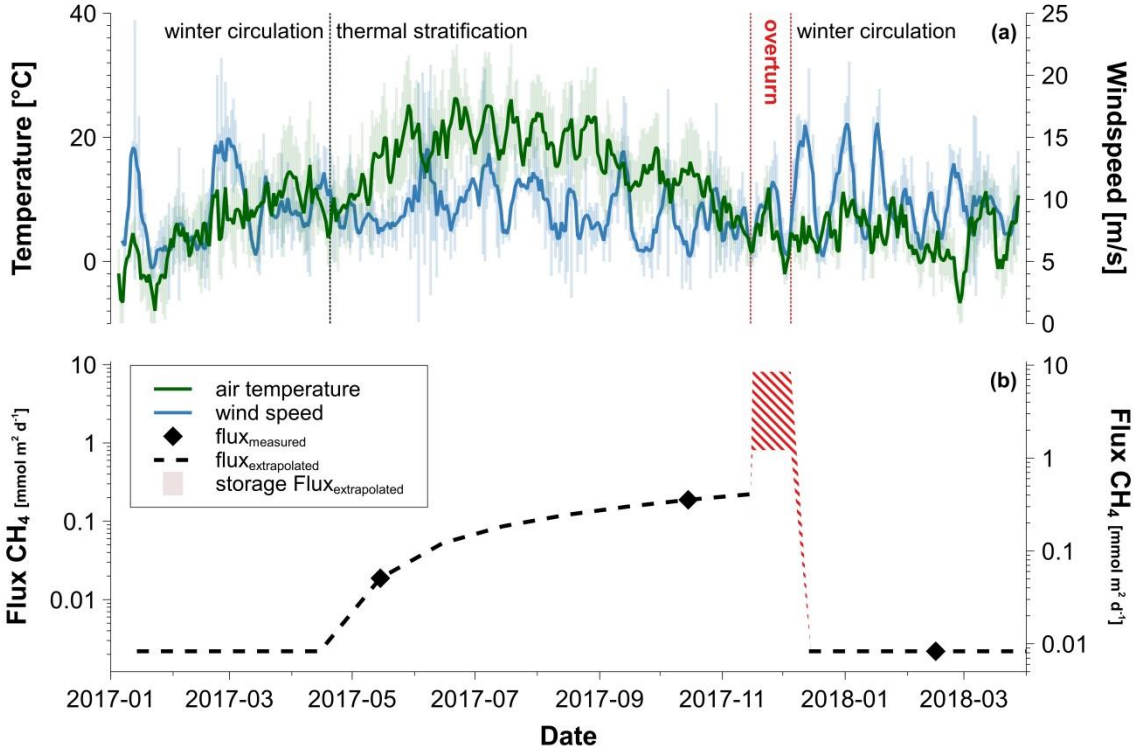

Figure 28: Air temperature and maximum wind speed at Lake Willersinnweiher for 2017 and 2018 (a). Annual CH_4 emissions from Lake Willersinnweiher based on calculations from campaigns during early-stage and late-stage stratification as well as winter circulation (b). Methane emissions during autumn overturn were conservatively estimated by calculations based on literature data (e.g. Encinas Fernández et al. 2014). Methane emission rates for autumn overturn were calculated for minimum (45°%) and maximum (95 %) CH_4 oxidation rates reported in the literature. Wind speed and air temperature data was obtained from a nearby weather station (49.51° N / 8.55° E). Note: y-axis (Flux CH_4) in logarithmic scale.

2.1.5. Conclusions

This study has shown the various sources and sinks of CH_4 within the water column and the sediments of Lake Willersinnweiher (Figure 29). Calculations of CH_4 fluxes in the sediments and water column of Lake Willersinnweiher allow detailed CH_4 mass balances for early-stage stratification (May 2017), late-stage stratification (October 2017) and winter circulation (February 2018).

The fate of carbon in Lake Willersinnweiher is mainly determined by turnover processes in the sediments, where DIC and CH_4 is considerably produced. Methane is consumed to a great extent by microbial anoxic oxidation of methane (AOM) via SO_4^{2-} reduction in the sulphate-methane transitions zone (SMTZ) before reaching the water column. SMTZ are uncommon in freshwater environments and occur at Lake Willersinnweiher due to high SO_4^{2-} concentrations of the groundwater input. AOM efficiency in the SMTZ is generally decreasing with increasing lake depth and the release of CH_4 into the bottom water is consequently higher in the profundal areas of Lake Willersinnweiher. Methane released into the water column is considerably oxidised by O_2 at the redoxcline in profundal areas of Lake Willersinnweiher, whereas aerobic oxidation seems to be inhibited by both the light intensity and the oxygen concentrations in the littoral areas. Aerobic CH_4 oxidation at the redoxcline of Lake Willersinnweiher is an effective barrier to CH_4 release into the atmosphere.

The redoxcline at Lake Willersinnweiher decouples surface water from deep water reservoirs. Methane oversaturation in the surface water was observed and results in significant CH_4 emissions during summer stratification. Sources of CH_4 in the epilimnion might be a mixture of both groundwater contribution and *in-situ* OMP. Notwithstanding the source of CH_4 in the surface water, CH_4 might not be fully oxidised and further result in significant CH_4 emissions from Lake Willersinnweiher. The calculated overturn emissions of Lake Willersinnweiher account for 5 % to up to 50 % of the annual CH_4 emissions (depending on assumed CH_4 oxidation rates in Lake Willersinnweiher).

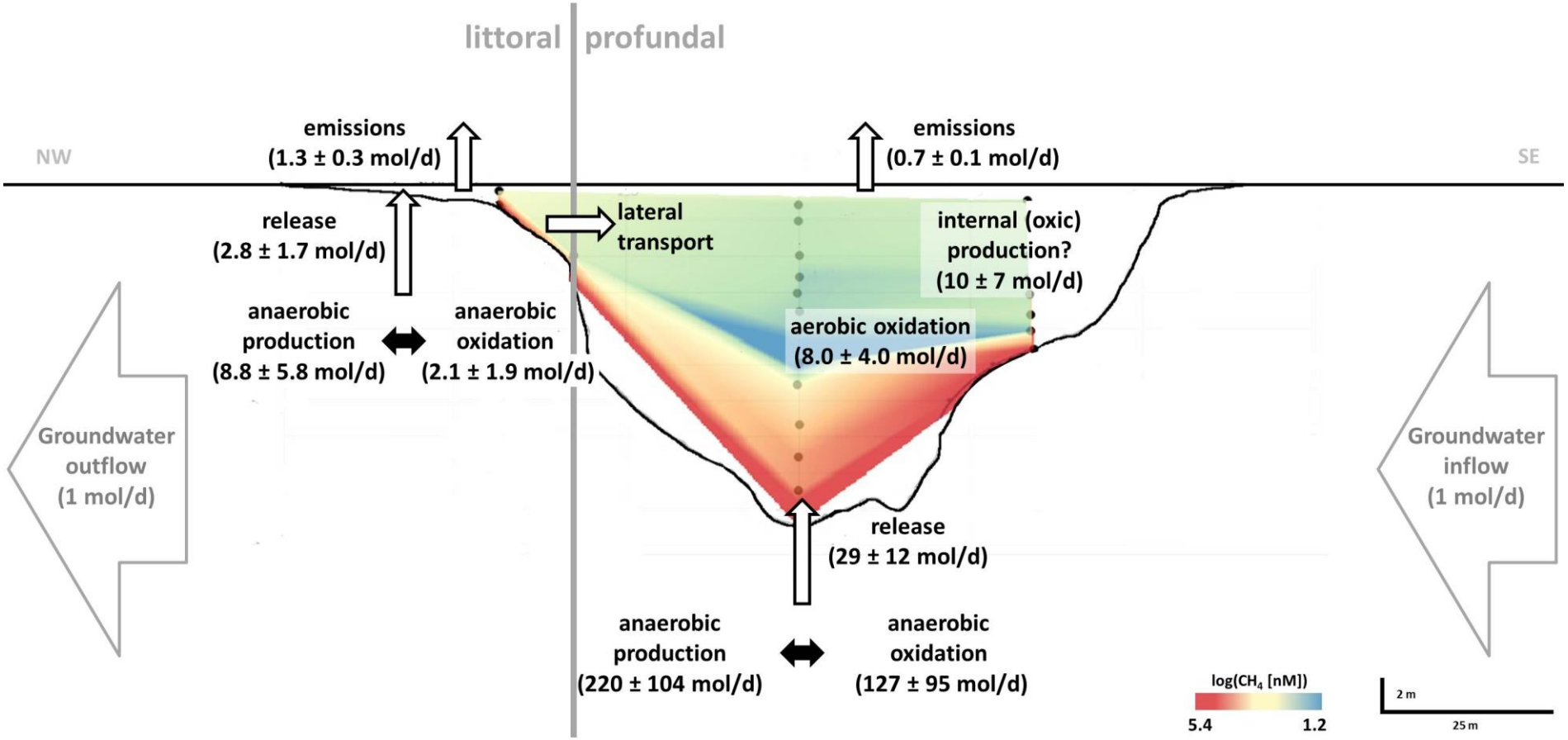

Figure 29: Methane mass balance for May 2017 in Lake Willersinnweiher. Interpolated CH_4 logarithmic concentration in the water column (*QGIS Desktop 2.18.4,* TIN (*triangular irregular network*) method) as well as the estimated rates for production and consumption of CH_4 within the water column and the sediments of Lake Willersinnweiher during early-stage stratification (May 2017). Data for whole-lake CH_4 mass balance is presented in the appendix.

2.2. Lake Stechlin

The following chapter mainly bases on the manuscript "Evidence for *in-situ* production of methane in the oxic surface water of an oligotrophic lake" (current working title) which is prepared for publication in *Nature Communications*. The Chapter was supplemented by additional results gained during fieldwork. Sections concerning laboratory incubations were conducted by Thomas Klintzsch (Heidelberg University). Quotations of joint work are indicated by footnotes. Methane flux was measured every 4 h by a floating chamber attached to a portable CH4 analyser (Los Gatos, USA) and flux data was calculated by Marco Günthel (University of Edinburgh). Turbulence data was provided by Georgiy Kirillin (Leibnitz-Institute of Freshwater Ecology and Inland Fisheries, Berlin). Weather data was obtained from the Umweltbundesamt and water quality data from the multi-parameter probes were provided by Armin Penske (Leibniz-Institute of Freshwater Ecology and Inland Fisheries, Berlin).

The studies at Lake Stechlin are part of a collaboration with Prof. Hans-Peter Grossart from the Leibnitz-Institute of Freshwater Ecology and Inland Fisheries, Berlin (IGB).

2.2.1. Study site

Lake Stechlin is a dimictic and oligo- to mesotrophic hardwater lake in north-eastern Germany (53°09′ N, 13°01′ E) (Figure 30). The Lake was formed after the withdrawal of the glacier tongues at the end of the Weichselian glaciation ~ 12 000 years ago. Lake Stechlin has a mean depth of 22.8 m, a surface area of 4.3 km^2 (Casper 1985) and is fed by direct precipitation and groundwater. The water residence time is supposed to be more than 40 a (Holzbecher et al. 1999). Methane concentrations of up to 1.4 µM in the well-oxygenated upper 10 m of the water column were recorded repeatedly in Lake Stechlin (Grossart et al. 2011; Tang et al. 2014). Additionally, studies show low pore-water CH_4 concentrations of about 0.04 mM in the upper sediment, and sediment-methane ebullition can be neglected (Casper et al. 2005; Conrad et al. 2007; McGinnis et al. 2015).

Lake Stechlin has been intensively studied for decades and a large experimental setup ("LakeLab") of the Leibniz-Institute of Freshwater Ecology and Inland Fisheries (IGB) was installed in the south western bay in 2011/2012. The LakeLab consists of 24 lake-water basins ("mesocosms") that are isolated from the rest of the lake (LakeLab: http://www.lake-lab.de). The mesocosms are used for a large number of different ecological experiments.

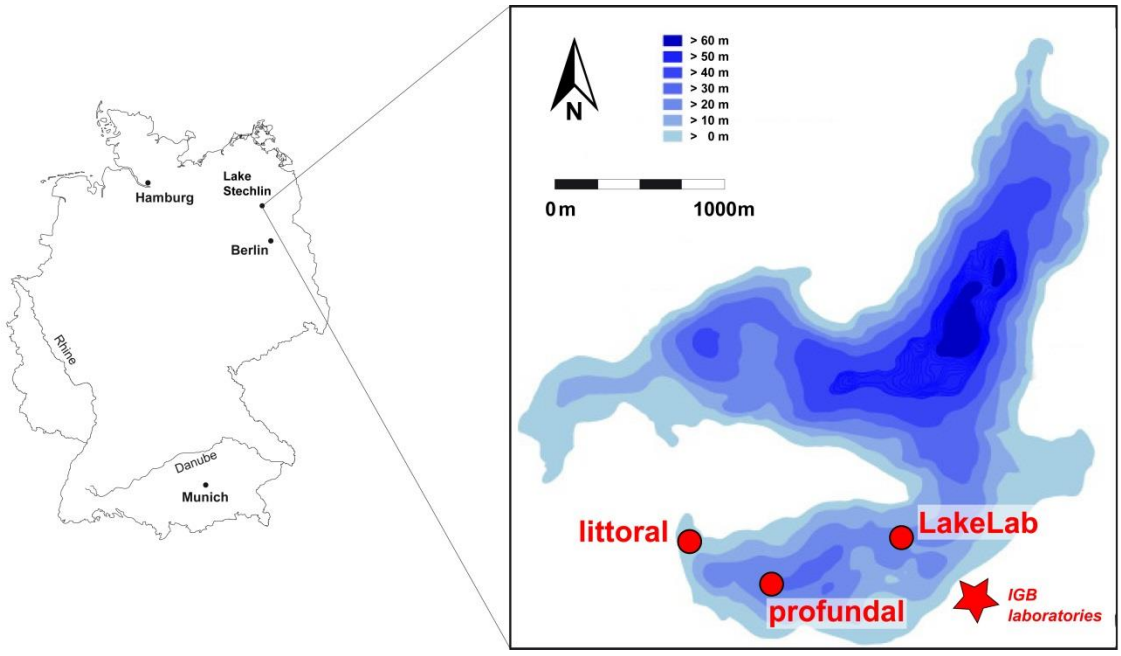

Figure 30: Position of the sampling locations (LakeLab, profundal and littoral) in June 2017 and the Leibniz-Institute of Freshwater Ecology and Inland Fisheries, Berlin (IGB). Bathymetric map of Lake Stechlin was modified after Aichner et al. (2017).

2.2.2. Material and Methods

In-situ measurements

Depth profiles of CH_4 concentration and $\delta^{13}C\text{-}CH_4$ were performed by the M-CRDS system (Chapter 1) from 14.06.2017 to 26.06.2017. The M-CRDS was deployed from a large floating platform that is constantly installed at the lake (LakeLab). Vertical CH_4 concentration profiles through the upper 10 m of the water column were measured with the M-CRDS setup every 4 hours. Nine depths (0.5 m to 9.95 m) were measured for 20 min each and CH_4 concentration as well as $\delta^{13}C\text{-}CH_4$ values were averaged over a measurement interval of 10 min. The submersible pump and tubing were mounted on an automatic winch of the lake lab, enabling continuous measurements of depth profiles during the campaign. Temperature differences between the water temperature at the membrane and the *in-situ* temperature at the submersible pump due to warming of the water in the tubing were lower than 4 °C and, therefore, effects on the CH_4 concentration could be neglected. Water flow was regulated to a constant flow of 500 ± 5 mL min^{-1} all time. For quality control, the working reference gas for CH_4 (5 ppm CH_4 and 500 ppm CO_2 in synthetic air) was analysed every 8 h during the measurements.

In addition, the conditions in the lake were simultaneously measured by two *in-situ* probes mounted 0.5 m above the submersible pump on the automatic profiler. A multi-parameter probe (6600 V2, *YSI*, USA) measured temperature [°C], pH and dissolved oxygen (DO) [%]. The photoautotroph community was continuously characterized by an additional probe (FluoroProbe, *BBE moldanke*, Germany) measuring total biomass (chlorophyll) and types (accessory pigments for green algae, cyanobacteria, diatoms and cryptophytes).

Geochemical analyses

All samples taken in the water column and from sediment cores were treated and analysed following the procedure described for samples from Lake Willersinnweiher, except that all samples were frozen (-4 °C) until further analysis in the laboratories of the Heidelberg University.

Calculations

Diffusive fluxes were calculated from concentration gradients according to the procedure described for Lake Willersinnweiher in Chapter 2.1.

Net CH_4 production rates (P_{Net} [mmol m^{-3} d^{-1}]) for non-steady state conditions were calculated by the recently published model for balancing epilimnic CH_4 under steady state conditions by Donis et al. (2017) (eq. [32]). $\frac{\partial C}{\partial t}$ was set as the changes in the *in-situ* CH_4 concentration in the surface water over the 4 h intervals.

$$\boldsymbol{P_{net} = \frac{\partial C}{\partial t} + (A_P F_S + MOx) - (A_S F_L + A_P F_Z)} \quad [32]$$

$\frac{\partial C}{\partial t}$ is the CH_4 concentration difference between sampling, F_S the CH_4 emission from surface to atmosphere, MOx the CH_4 oxidation, A_S the sediment surface area and A_P represents the lake planar area. Methane oxidation rates were obtained from former studies on CH_4 production in Lake Stechlin (Grossart et al. 2011; Tang et al. 2014). Used parameters are shown in Table 10.

Table 10: Parameters used for the calculation of the CH_4 mass balance at Lake Stechlin

Flux	Description	Value	Unit
$\boldsymbol{P_{net}}$*	Net CH_4 production for non-steady state conditions	-	[mmol m^{-3} d^{-1}]
$\boldsymbol{\frac{\partial C}{\partial t}}$ *	Changes in the summed CH_4 concentration in the surface water over the 4 h intervals	-	[mmol m^{-3} d^{-1}]
$\boldsymbol{F_S}$*	CH_4 emission from surface to atmosphere	-	[mmol m^{-2} d^{-1}]
$\boldsymbol{MOx}$**	Methane oxidation	0.89 (day) 0.10 (night)	[mmol m^{-3} d^{-1}]
$\boldsymbol{A_S}$	Sediment surface (in contact with the surface water layer)	$1.1 * 10^5$	[m^2]
$\boldsymbol{F_L}$ *	Diffusion from littoral sediments	0.2	[mmol m^{-2} d^{-1}]
$\boldsymbol{A_P}$	Lake planar area	$4.3 * 10^6$	[m^2]
$\boldsymbol{F_Z}$ *	Diffusion from metalimnion	-	[mmol m^{-2} d^{-1}]

* **based on presented results**
** **obtained from Tang et al. (2014)**

2.2.3. Results

Water characteristics

Lake Stechlin was thermally stratified and well-oxygenated during the measurements in June 2017. The average temperature in the upper 6 m was 18 °C (epilimnion). Water temperatures decreased in the metalimnion to ± 8 °C at 9 m. The water column was oxic down to the sediments with maximum concentrations at 7 m water depth. Iron, Mn and Ca did not change significantly with water depth. The pH in Lake Stechlin followed the profiles of O_2 and showed maximum pH values of 8.7 at 7 m and decreased within the metalimnion and ranged between 7.4 and 7.6 in the hypolimnion. Epilimnetic DIC and SO_4^{2-} concentrations were lower than hypolimnetic concentrations. Orthophosphate concentrations were below detection limit (< 0.08 µM) in the upper water column and increase with depth in the hypolimnion to up to 0.6 µM.

Methane concentrations in the epilimnion were relatively constant with values of 510 nM, maximum concentrations were found at the thermocline (630 nM). Methane concentration decreased with water depth to minimum values of 140 nM at 14 m and showed higher concentrations above the sediment surface. The isotopic composition of CH_4 was about - 49.5‰ in the epilimnion and increased to - 45‰ at depths of minimum CH_4 concentration. Sediment near water layers showed $\delta^{13}C$-CH_4 values of - 50‰.

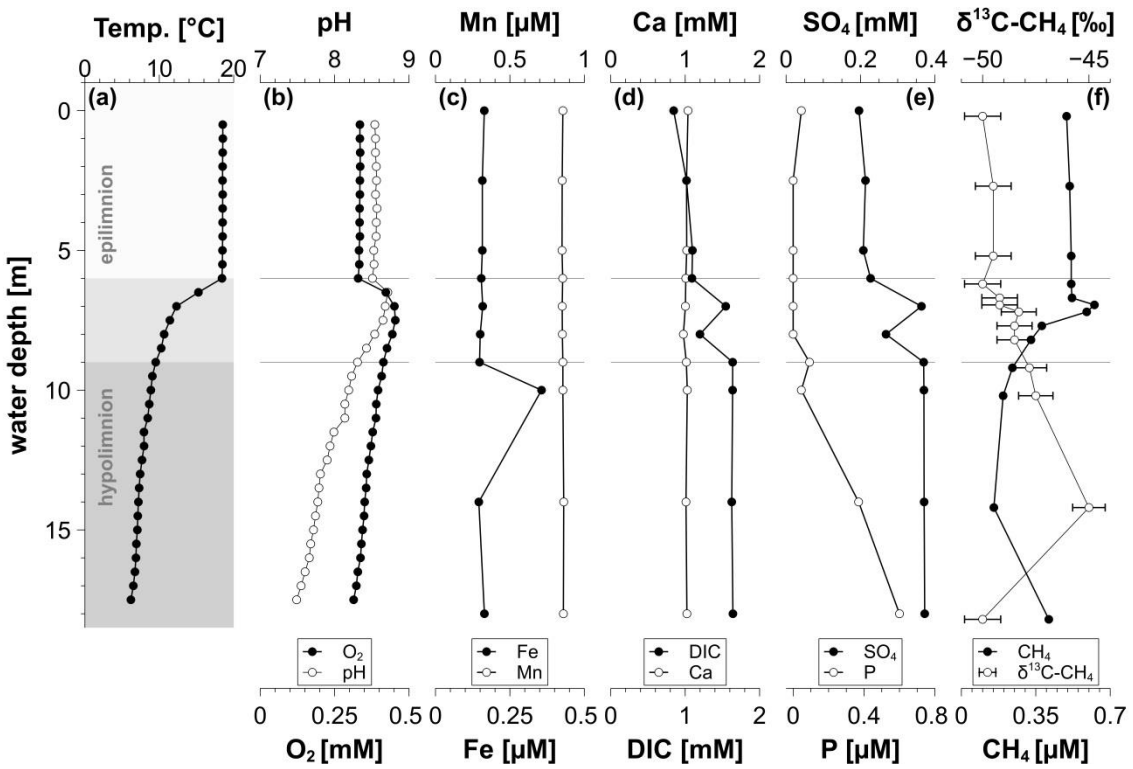

Figure 31: The water column at the LakeLab, exemplarily shown for June 15th 2017 (Lake Stechlin).

Physical conditions at Lake Stechlin

Long-term measurements were dominated by changeable weather conditions (Figure 32). Wind speed generally followed a daily diurnal cycle. Near-surface turbulence showed turbulent to high-turbulent conditions in the uppermost 2.5 m water column extending downwards to the thermocline for moderate and gusty wind. Average epilimnic temperatures were 20 °C and up to 23 °C for sunny and windless days (Figure 32A and C). Dissolved oxygen (DO) ranged from 115 % to 145 % with maximum saturation at 7 m water depth (Figure 32D). Oxygen oversaturation was observed throughout the upper 10 m of Lake Stechlin.

Phytoplankton

The photoautotroph community in Lake Stechlin was dominated by cyanobacteria (Figure 32). The field campaign covered the two final weeks of a fading cyanobacteria bloom with maximum pigment abundance at the thermocline of 22 µg L^{-1} (Figure 32E). While cyanobacteria pigments were fading, diatom pigments were rising up to 2.4 µg L^{-1} above the thermocline during the second week of measurements (Figure 32F). The abundancy of green

algae shows values scattering around 2.5 ± 2.4 µg L^{-1} in the upper 4 m (Figure 32G), while cryptophytes show maximum concentration of up to 7 µg L^{-1} at 7 - 8 m water depth during the measurements in June 2017 (Figure 32H).

Methane in Lake Stechlin

Methane in the water column

The simultaneous and continuous depth profiles of CH_4 concentration and $\delta^{13}C$-CH_4 values show high spatial and temporal variations (Figure 32I and K). Methane oversaturation with respect to atmospheric equilibrium (> 3 nM) in the epilimnion was found at any time and CH_4 maxima (up to 950 nM) at 7 m water depth coincide well with the upper boundary of the thermocline and DO oversaturation (Figure 32E and D). Epilimnic CH_4 concentrations generally ranged from 350 to 950 nM during the measurement period of 12 days. Methane concentrations at the thermocline (7 m) showed large variations ranging from 450 to 950 nM. Metalimnic CH_4 was relatively constant with time and showed concentrations of ~ 200 nM. Surface water $\delta^{13}C$-CH_4 values were generally higher (> -48‰) than below the thermocline (< -48‰).

Methane fluxes to the atmosphere

The CH_4 emission to the atmosphere showed maximum fluxes up to 2.7 mmol m^{-2} d^{-1} for turbulent to high-turbulent conditions, mainly at mid-day, and minimum fluxes of <0.5 mmol m^{-2} d^{-1} during windless periods (Figure 32A). The water-to-air CH_4 fluxes followed the diurnal patterns of wind (0 to 8 m s^{-1}) and turbulence (-9.3 to -5.8 W kg^{-1} $\log_{10}$ TKE dissipation).

Methane fluxes at the thermocline

Methane upward fluxes from thermocline into the epilimnion ranged from 0.002 - 0.006 mmol m^{-2} d^{-1} and showed maximum values of 0.01 - 0.02 mmol m^{-2} d^{-1} during windy and/ or high-turbulent conditions (Figure 32B).

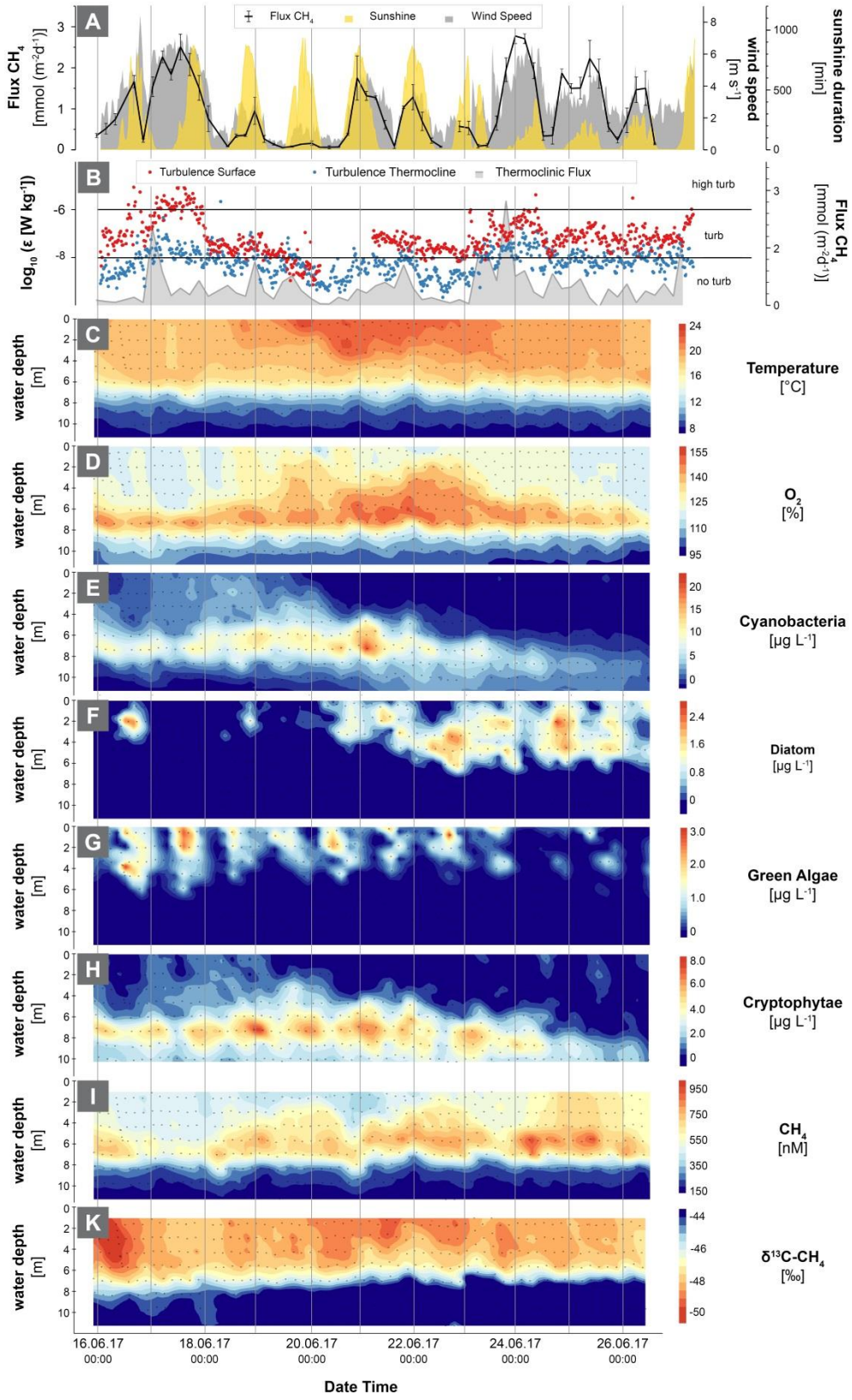

Figure 32: Continuous 2-week depth profiles at the LakeLab at Lake Stechlin. Average wind speed, CH_4 fluxes and sunshine duration (A), turbulence at 2 m and 7 m water depth as well as fluxes at the thermocline (B), temperature (C), oxygen saturation (D), cyanobacteria (E), diatoms (F) green algae (G), cryptophytae (H), CH_4 concentration (I) and $\delta^{13}C$-CH_4 values (K) interpolated from measurements at Lake Stechlin in June 2017. Grey points indicate the sampling time and depths.

Sediment pore-water characteristics and CH_4 pore-water fluxes

At all sites, dissolved Fe was absent in the pore-water of the upper part of the sediments. Dissolved Mn concentrations showed maximum concentrations of 9 µM at the LakeLab and 4 µM in the pore-water of profundal and littoral sediments. At the littoral site, dissolved Mn peaked in the pore-water within the uppermost 5 cm whereas dissolved Mn concentrations decreased with depth below 30 cm for the profundal and LakeLab site. Pore-water SO_4^{2-} generally decreased with sediment depth. Sulphate was absent below 5 cm and 20 cm for the LakeLab site as well as the littoral and profundal site, respectively. Sulphide concentrations showed local maxima at the LakeLab and the profundal site, whereas total S (-II) concentrations increased to up to 0.25 mM with depth at the littoral site (Figure 33).

Pore-water CH_4 generally increased with depth to maximum values of 1.5 to 2 mM at all sites. Sediments at the LakeLab showed a local maximum between 5 and 15 cm and rather constant CH_4 concentrations below. Methane production within sediments varied considerably between 0.22 mmol m^{-2} d^{-1} for profundal sediments and 1.87 mmol m^{-2} d^{-1} for the LakeLab site. Methane release from the sediment into the bottom water was 0.20 mmol m^{-2} d^{-1} and equal for the littoral and profundal sites, whereas the flux was 1.87 mmol m^{-2} d^{-1} at the LakeLab site (Figure 33d, k and q). $\delta^{13}C$-CH_4 values from littoral sediment sites decreases downwards from - 58‰ in the upper pore-waters to - 63‰ in 27 cm sediment depth.

DIC increased with depth from 1.5 - 5 mM at the LakeLab and the littoral site, whereas maximum DIC concentrations of 2.5 mM were significantly lower at the profundal site (Figure 33). Orthophosphate increased with depth to up to 15 µM for littoral and profundal sediments. The LakeLab site showed peak concentrations of 55 µM between 5 and 15 cm sediment depth and decreasing concentrations below.

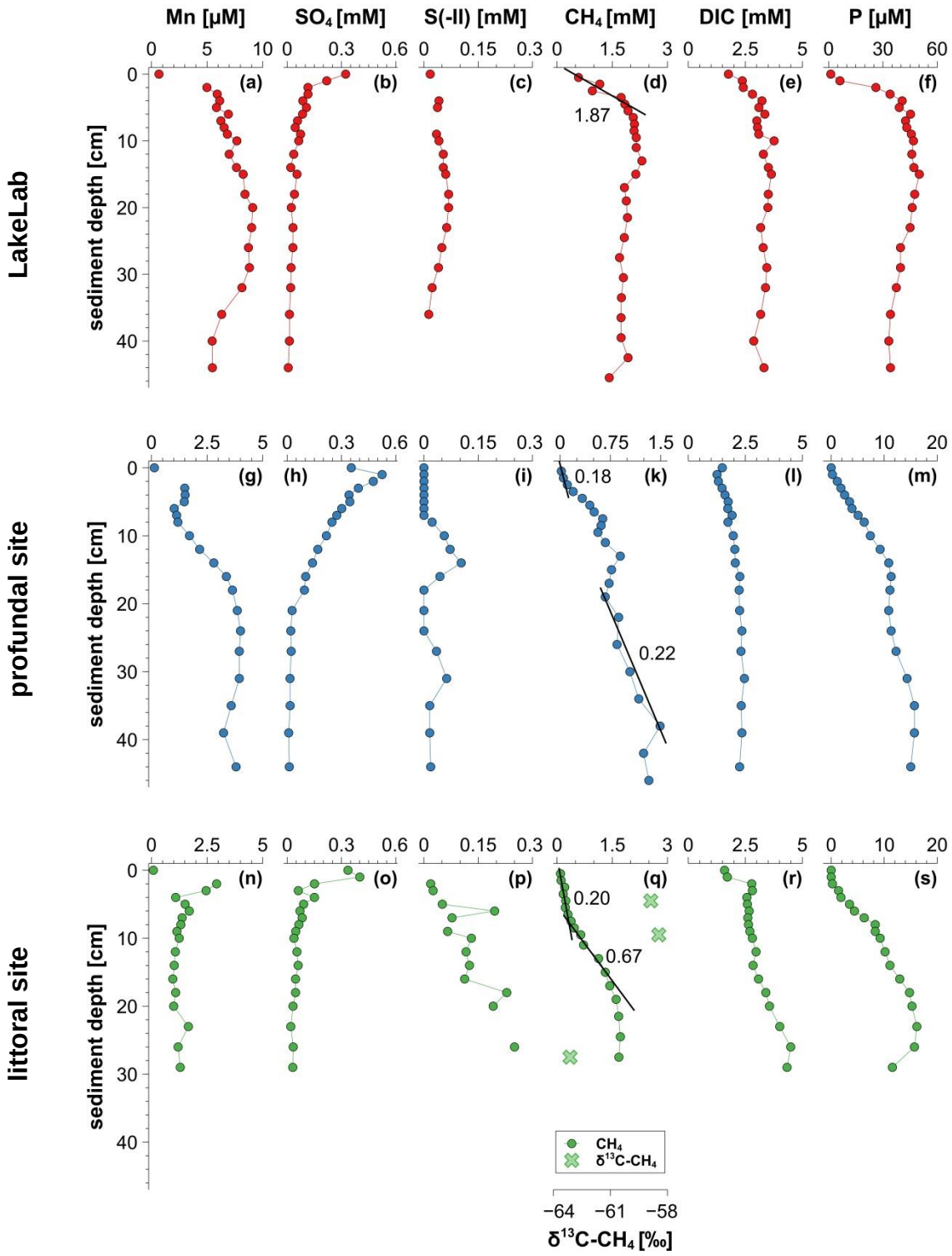

Figure 33: Geochemical profiles of selected elements in the pore-water of the sediments at the LakeLab (a-f), at the profundal site (g-m) and the littoral site (n-s) of Lake Stechlin in June 2017. Pore-water CH_4 concentration and CH_4 diffusive fluxes calculated with Fick's 1st law. Pore-water fluxes are given in mmol m^{-2} d^{-1}.

2.2.4. Discussion

Methane accumulation in the upper water layer of lakes is a common phenomenon directly affected by the emission to atmosphere, internal production, internal consumption and input from anoxic zones (Karl et al. 2008; Tang et al. 2016). The presented data highlight the temporal and spatial dynamics of CH_4 in the water column of Lake Stechlin and the immediate effects of changes in the interplay between biological and physical processes in the oxic surface water layer of aquatic systems. Sources of CH_4 in the water column might be CH_4 input from littoral sediments and / or internal oxic methane production (OMP).

Methane in the sediments of Lake Stechlin

Input of CH_4 from littoral or benthic sediments has been shown for specific lake environments (Hofmann et al. 2010; Encinas Fernández et al. 2016). At Lake Stechlin, near bottom water is considerably influenced by sedimentary methanogenesis, whereas the pathways of CH_4 production and CH_4 oxidation vary between profundal and littoral sites. Sediments at Lake Stechlin are iron-dominated and the broad SO_4^{2-} reduction in the profundal sediments, zone indicate that methanogens are outcompeted by sulphate reducing bacteria (SRB) in the upper 20 cm. Below this depth, SRB become inactive and methanogenesis is most likely coupled to carbonate reduction (e.g. Conrad 1989). Opposing gradients of CH_4 and SO_4^{2-} along with increasing sulphide concentrations might further indicate the presence of sulphate-methane transition zones (SMTZ) and the anaerobic oxidation of CH_4 (AOM) with SO_4^{2-} as electron acceptors in the upper sediment layer (Hinrichs et al. 1999; Boetius et al. 2000). Consequently, upward migrating CH_4 is consumed before reaching the bottom water of Lake Stechlin. In contrast, profundal sediments at the LakeLab showed more condensed geochemical redox zonations. Here, OM conversion might be enhanced by the anthropogenic input of carbon and nutrients such as (ortho-)phosphates or methylated substrates from the mesocosm experiments. Anthropogenic enhanced carbon input consequently leads to high sedimentary CH_4 production rates in the upper sediment layer. Methanogenesis is the dominant process of OM degradation, as available dissolved SO_4^{2-} is consumed within the uppermost 5 cm of the sediment.

Methane formation via non-competitive methanogenic pathways, e.g. by utilizing methylated substrates, is possible. AOM in the upper sediment layer might be coupled to Mn or SO_4^{2-} reduction. Diffusion of CH_4 into the bottom water was an order of magnitude higher than at other profundal sites. However, released CH_4 is consumed by aerobic CH_4 oxidation (MOx) in the oxic hypolimnion before reaching the surface water layer of Lake Stechlin.

Carbon cycling pathways in littoral sediments are different to profundal sediments. Manganese and SO_4^{2-} are depleted below 5 cm sediment depth. Methane formation is the main TEA for OM oxidation at littoral sites. Pore-water $\delta^{13}C$-CH_4 values in the lower parts of the sediments suggest that methanogenesis is based on the either hydrogenotrophic, or acetoclastic pathway or both (Oremland et al. 1987; Whiticar 1999). In the upper layer, higher $\delta^{13}C$-CH_4 indicates intense AOM most likely coupled to the reduction of Mn. Littoral sediments might also be ventilated by the submerged vegetation, which could consequently lead to an underestimation in CH_4 fluxes across the sediment-water interface.

Organic-rich littoral sediments are therefore considered as possible sources of laterally transported CH_4. showed fluxes into the bottom water of 0.2 mmol m^{-2} d^{-1}. However, former studies found no significant horizontal gradients in CH_4 concentrations from littoral to profundal sites (e.g. Tang et al. 2014). In addition, CH_4 oversaturation was found within the oxygen-rich mesocosm water, sheltered from the input of littorally produced CH_4 (Tang et al. 2016). However, mesocosmic CH_4 might be influenced by the LakeLab since anthropogenic influence was already shown for the sediments. Algal growth on the inner and outer enclosure walls of the LakeLab is present and CH_4 formation might consequently be coupled to anoxic micro-niches (Oremland 1979; Grossart et al. 2011). However, the inner walls are frequently cleaned from biofilm e.g. by underwater vacuum cleaners. Outer wall biofilms might also have a minor influence on surface water CH_4 formation, since CH_4 oversaturation was found in the surface water layer of Lake Stechlin (Grossart pers. comm.). Furthermore, oversaturated CH_4 concentrations in oxic waters as well as OMP was shown for other lake environments (Juutinen et al. 2009; Bogard et al. 2014; Blees et al. 2015; Donis et al. 2017). Methane transported from littoral sites or produced on the enclosure walls of the LakeLab might therefore be excluded as the main source for the accumulation of CH_4 in the

surface water layer at Lake Stechlin. Consequently, surface water CH_4 needs to be significantly produced within in the oxic water layer.

CH_4 in the oxic surface water

The CH_4 mass balance based on internal consumption and input from anoxic zones and adds up to an internal oxic CH_4 production (OMP) of 232 ± 177 nM d^{-1} in the surface water layer of Lake Stechlin. However, OMP showed large variations with time (Figure 34).

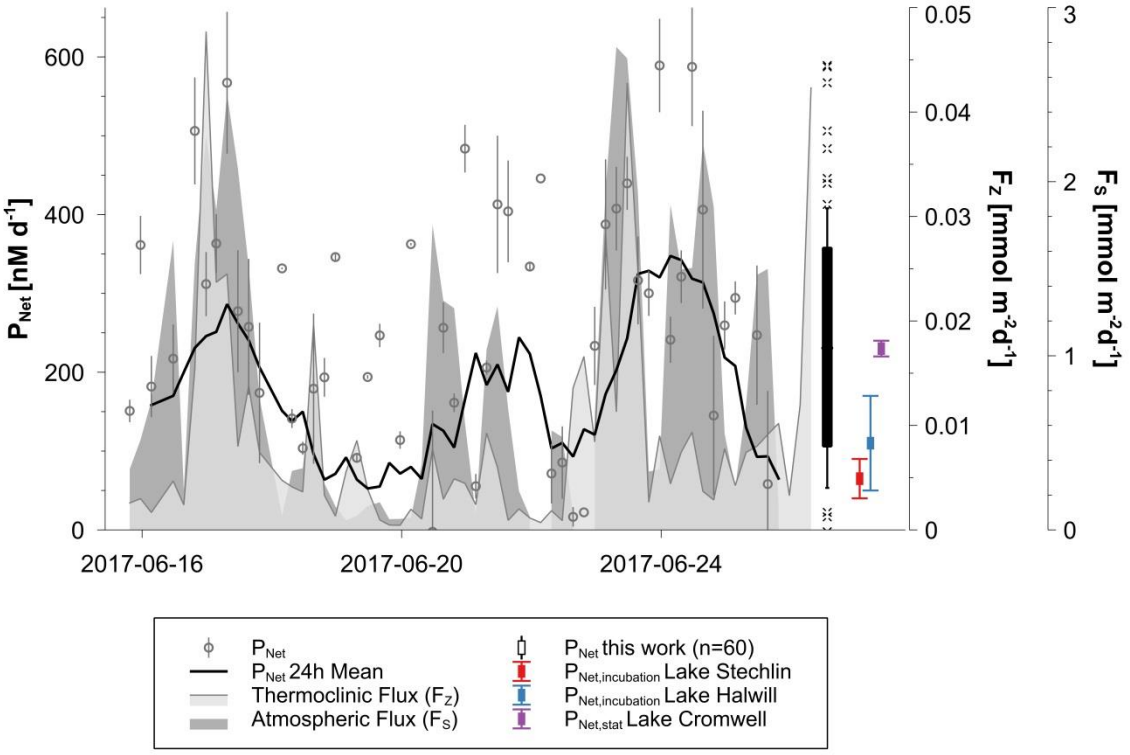

Figure 34: Net oxic CH_4 production for non-steady state conditions (225 ± 170 nM d^{-1}), water-to-Air CH_4 Flux (F_S, light grey), upwards diffusion from the thermocline (F_Z, dark grey) as well as mean values of CH_4 production for Lake Stechlin, Lake Halwill (Donis et al. 2017) and Lake Cromwell (Bogard et al. 2014). Error bars represent 1-σ standard deviation.

Data smoothed to a 24 h averaging interval tend to follow the water-to-air CH_4 fluxes. The deployment of floating chambers for CH_4 emission measurements is known to enhance gas transfer through disturbance of the surface boundary layer by small waves, especially during higher wind speeds (e.g. Matthews et al. 2003). Methane fluxes to the atmosphere may therefore be slightly overestimated in the calculation of CH_4 production. However, the results for OMP of 232 ± 177 nM d^{-1} in Lake Stechlin cover the range of previously reported

data for Lake Stechlin (40 nM d^{-1} to 90 nM d^{-1}) (Grossart et al. 2011; Tang et al. 2014) as well as for estimations for other lakes in the temperate zone and with similar trophic state of 110 ± 60 nM d^{-1} for Lake Halwill (Donis et al. 2017) and up to 230 ± 10 nM d^{-1} for Lake Cromwell (Bogard et al. 2014).

Previously published estimations on OMP were exclusively based on in-lake incubation experiments or calculations from steady state conditions, not covering the temporal variability of CH_4 concentrations within the surface water, as CH_4 dynamics are not captured by conventional analytical methods. This study presents the first CH_4 production data considering the highly dynamic conditions in the surface water. In the high-resolution field study, the main components of the CH_4 mass balance such as aquatic CH_4 concentration and CH_4 emissions to the atmosphere were analysed. Methane oxidation rates, however, are resulting from studies on CH_4 oxidation and its photoinhibition dependence at Lake Stechlin (Grossart et al. 2011; Tang et al. 2014). Estimations of CH_4 oxidation rates are based on incubation experiments and thereby particularly prone to error in temporal resolution. Simultaneous measurements of the *in-situ* concentration and $\delta^{13}C$ values of CH_4 and CO_2 in water are not available yet, but will be essential for a higher temporal and spatial resolution of the sinks for CH_4 in limnic systems.

High resolution mass balance for the surface water of Lake Stechlin shows no significant correlation with suggested factors controlling the oxic CH_4 production (Grossart et al. 2011; Tang et al. 2014) such as radiation, but, however, might be disguised by wind-induced effects on CH_4 concentration in the surface water (Figure 35).

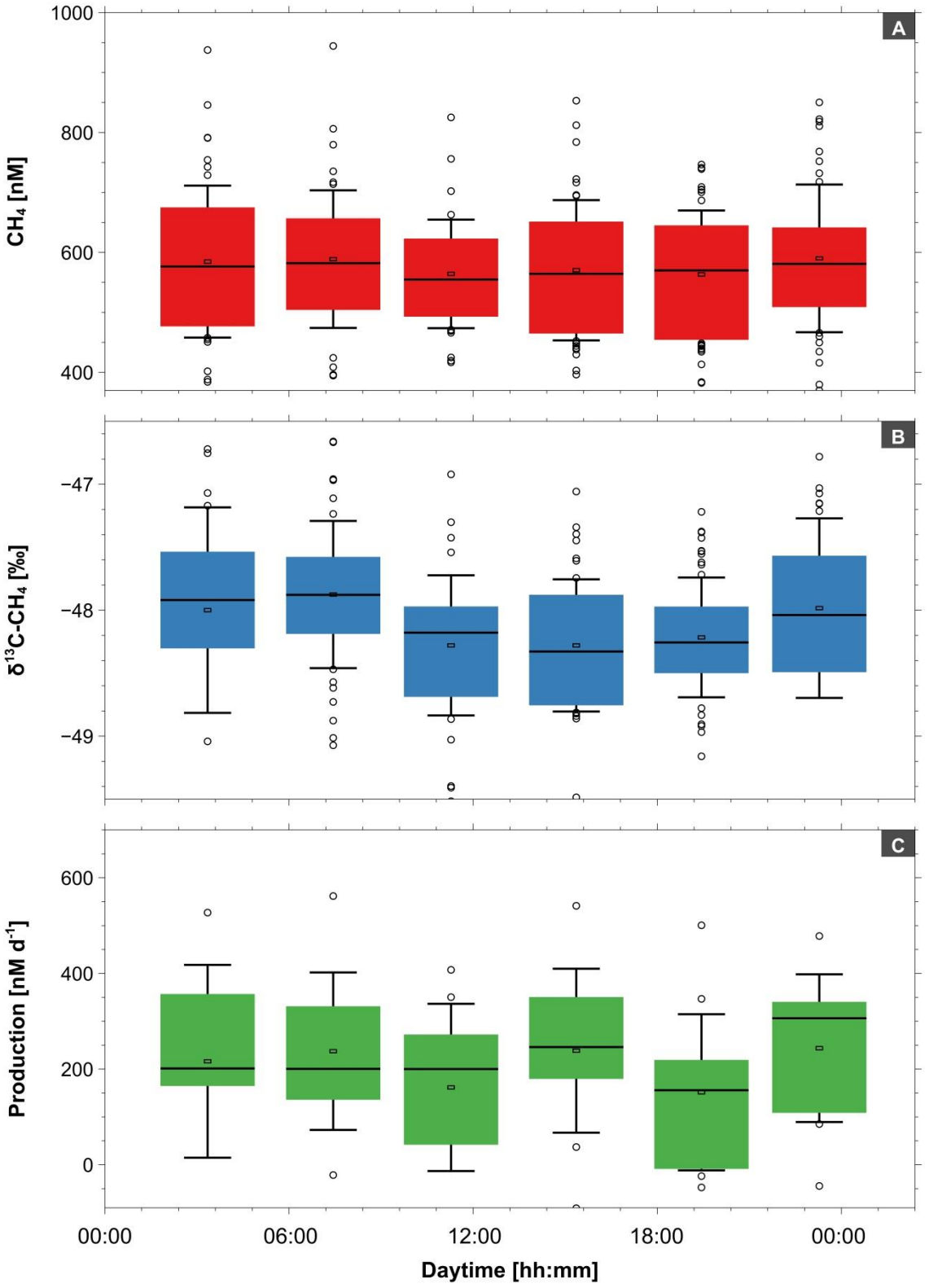

Figure 35: Box-Whisker-Plots (*whisker mode:* 1 SD) for surface water CH_4 concentration (A), $\delta^{13}C$-CH_4 values (B) and oxic CH_4 production rates (C) with respect to the time of day. No significant correlations were found for oxic CH_4 production with suggested factors controlling the oxic CH_4 production such as radiation.

Oxic CH_4 production and the photoautotrophic community

Although CH_4 accumulation and CH_4 production in the oxic surface water became obvious over recent years, only vague attributions can be made concerning the source and pathways for oxic CH_4 production in water. Methane occurrence and production in lakes was further suggested to be related to photoautotrophic production and growth, but lacked the conclusive evidence (Grossart et al. 2011; Bogard et al. 2014; Tang et al. 2014). This study now clearly demonstrates that aquatic CH_4 concentrations at Lake Stechlin are directly linked to algal dynamics and algae abundances. The *in-situ* results of CH_4 accumulation and pigment presence of cyanobacteria and diatoms showed spatial and temporal coverage (Figure 32 and Figure 36). Cyanobacteria chlorophyll correlates (person correlation) with CH_4 concentration within the cyanobacteria bloom, whereas the diatom chlorophyll concentration showed significant correlation with CH_4 concentration inside the diatom bloom in the surface water of Lake Stechlin. Green algae and cryptophytes showed inverse or no correlation, respectively, most likely due to the dominance of cyanobacteria and diatom bloom events (Figure 32). Temporally missing correlation between phytoplankton and CH_4 accumulation is best explained by wind-induced loss of CH_4 by emission to the atmosphere. Furthermore, the simultaneous and immediate CH_4 production along with culture growth is very unlikely. The algae metabolism might cause a delay in the CH_4 production that is not captured by the 4 h sampling intervals and disguised by wind-induced changes in aquatic CH_4 concentration.

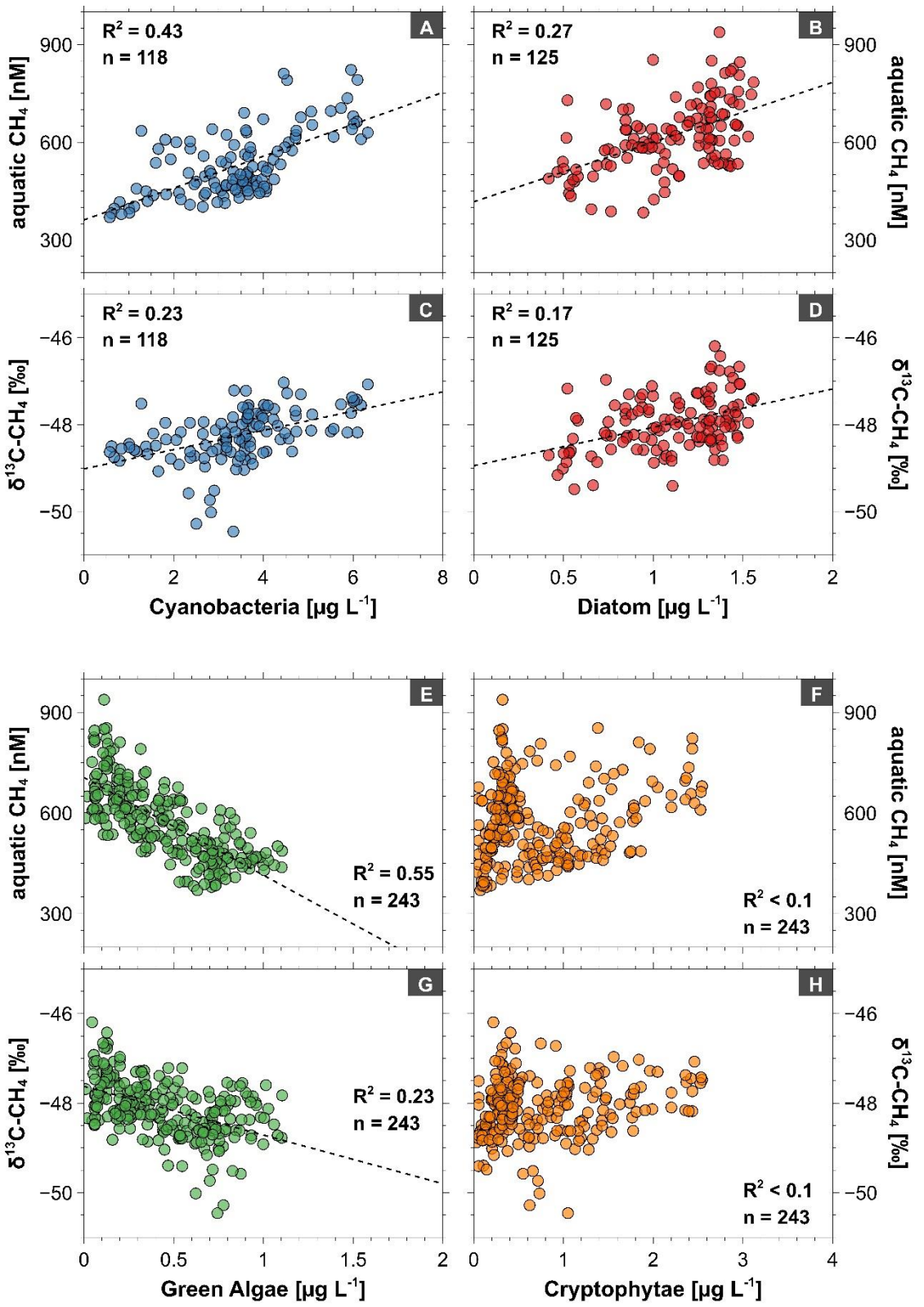

Figure 36: Correlation of *in-situ* results of cyanobacteria within the cyanobacteria bloom (A,B), diatom within the diatom bloom (C,D), green algae (E,F) and cryptophytae (G,H) with the CH_4 concentration and $\delta^{13}C$-CH_4 values in the surface water layer of Lake Stechlin. Temporally missing correlation between phytoplankton and CH_4 accumulation is most likely due to wind-induced loss of CH_4 by emission to the atmosphere.

"Field data are mirrored in laboratory incubations, where produced CH_4 was consistent with the biomass yield in all cultures. Representatives of all major phytoplankton classes in Lake Stechlin (diatoms, green alga, cryptophytes, all isolated from the lake) and cyanobacteria (from culture collections) were investigated for their potential CH_4 production. Alga cultures were incubated with ^{13}C-labeled bicarbonate ($NaH^{13}CO_3$) as carbon source. All such treated cultures showed conversion of $NaH^{13}CO_3$ into $^{13}CH_4$, that was indicated by increasing $\delta^{13}CH_4$ values in head space CH_4 with respect to untreated cultures. (Figure 37).

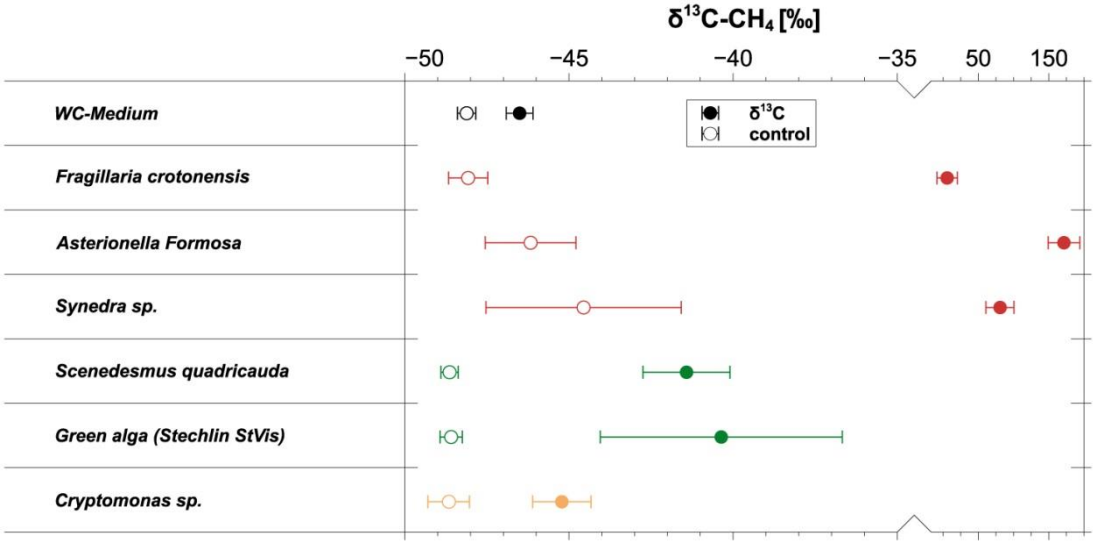

Figure 37: Laboratory incubation results for diatoms (red), green algae (green) and cryptophytes (orange). Incubation of cyanobacteria was not evaluated within the frame of this study. $\delta^{13}C$-CH_4 values of headspace CH_4 from cultures ($NaH^{13}CO_3$) and WC-medium (control) incubated with or without (control) a treatment of $NaH^{13}CO_3$ (filled and empty dots, respectively). Laboratory incubations were conducted by Thomas Klintzsch (Heidelberg University).

The increase of $\delta^{13}C$-CH_4 values ranged from 3.44 ± 0.88‰ in cultures of cryptomonas up to 214 ± 23‰ in *Asterionella formosa*. All $NaH^{13}CO_3$ treated alga cultures produced CH_4 enriched in ^{13}C, and thus providing isotopic evidence that major phytoplankton classes in Lake Stechlin (green algae, cyanobacteria, diatoms, cryptophytes) *per se* produce CH_4 under oxic conditions."[3] Hence, CH_4 is directly formed by those organisms. While the in-situ lake production rates of algae and cyanobacteria in Lake Stechlin are still unknown, this study now confirms previously published studies suggesting CH_4 accumulation and production to be related to photoautotrophic production and growth (Grossart et al. 2011; Bogard et al. 2014; Tang et al. 2014).

[3] cited from joint work by Thomas Klintzsch in Hartmann et al. (2018, in preparation)

Surface water – atmosphere interactions

This study shows that opposing impacts on aquatic CH_4 concentrations in the epilimnion are prevalent. Methane is significantly produced and considerably emitted from in the surface water layer of Lake Stechlin. Open-water CH_4 emissions of 0.05 - 2.78 mmol m^{-2} d^{-1} are consistent with emissions of 0.95 - 2.7 mmol m^{-2} d^{-1} for Lake Stechlin reported earlier (McGinnis et al. 2015). The CH_4 emissions are up to five times higher than the estimated mean water-to-air CH_4 fluxes from freshwater lakes presented by Bastviken et al. (Bastviken et al. 2011). Several authors supposed the presence of microbubbles enhancing CH_4 fluxes at Lake Stechlin for wind speeds ≥ 2 m/s as turbulence increase the exposure of gas-supersaturated water (Eugster et al. 2011; Prairie and del Giorgio 2013; McGinnis et al. 2015). These are very similar results, as CH_4 emission rates correlated significantly with wind speeds of ≥ 1.5 m/s (R^2 = 0.615) (Figure 38). The diurnal pattern of maximum and minimum fluxes mainly at mid-day and midnight, respectively, might therefore be the result from enhanced turbulence transfer within the surface water due to more windy conditions (Bastviken et al. 2004, 2010).

Moreover, and this is crucial, increasing wind speeds also control total CH_4 concentrations in the surface water layer (R^2 = 0.36). Wind-induced increase in CH_4 emission rates reduces the CH_4 concentrations in the uppermost 5 m and, hence, fuels the diffusion from the thermocline by increasing the CH_4 concentration gradients within the surface water layer (Figure 38). Upward-directed CH_4 fluxes from the thermocline to the surface water layer reached up to 0.02 mmol m^{-2} d^{-1} for windy and high turbulent regimes. This reinforces a decrease of CH_4 concentrations in the surface water layer by an upwelling of colder deep water with lower CH_4 concentration and slightly more negative $\delta^{13}C$-CH_4 values (Figure 39) (Kirillin and Engelhardt 2008; Kirillin et al. 2009; Hartmann et al. 2018). Consequently, both aquatic CH_4 concentrations and emissions from the surface water to the atmosphere are immediately affected by wind speed.

The results demonstrate that CH_4 concentrations and emissions are not predictable from single and/or random measurements as generally used for gas flux calculations. Estimations of the local CH_4 budget, therefore, need to be reconsidered with respect to the high dynamics of CH_4 production the oxic

surface water layers, which consequently, also affects CH_4 emission to the atmosphere.

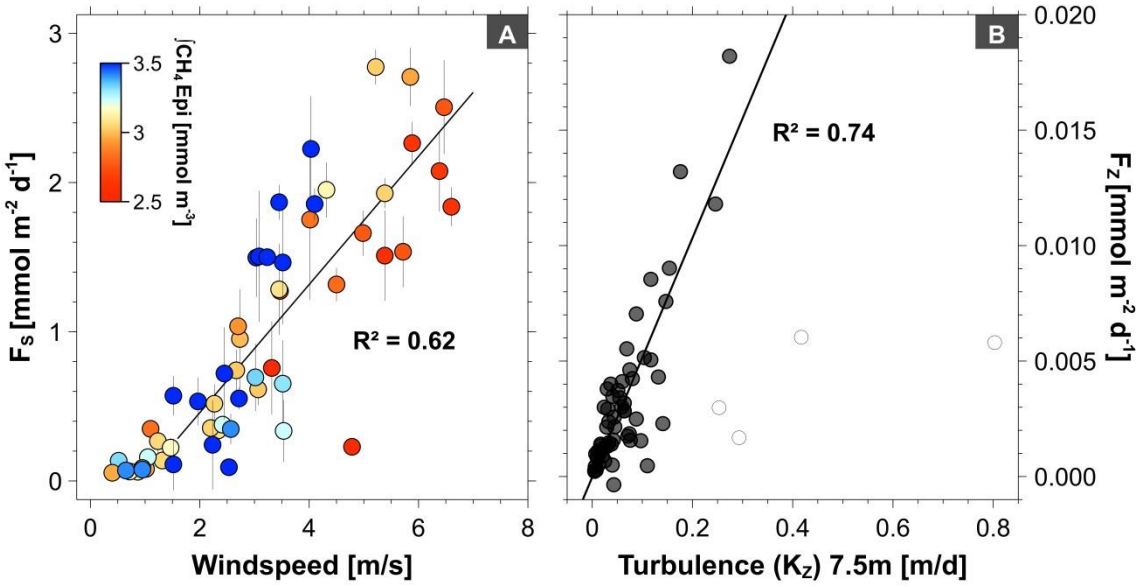

Figure 38: Correlation of the wind speed with CH_4 flux and summed epilimnic CH_4 concentration (A). Increasing wind speed (> 2 m/s) leads to decreasing CH_4 concentration in the water column and increasing CH_4 emissions. Diffusion from the thermocline to the surface water by wind-induced turbulence (B). Reduced CH_4 concentration in the uppermost 5 m by lowering the CH_4 concentration gradients within the surface water layer due to an upwelling of colder deep water with lower CH_4 concentration and slightly lighter $\delta^{13}C$-CH_4 values. Outliers in (b) are drawn as empty circles. Error bars represent the standard deviation.

2.2.5. Conclusions

This study clearly shows the temporal and spatial variability of aquatic CH_4 that is unambiguously controlled by CH_4 loss to the atmosphere and photoautotrophic CH_4 production within the oxic water layer. Whereas recently published studies have demonstrated active CH_4 production in well oxygenated waters (Grossart et al. 2011; Tang et al. 2014; Donis et al. 2017), but remained hypothetic with respect to the CH_4 sources or metabolic pathways, this study now provides the first evidence from laboratory and field measurements that all major phytoplankton classes in the surface water of Lake Stechlin produce CH_4 under oxic conditions. These results could drastically change our understanding of the behaviour of CH_4 in aquatic systems since CH_4 production in oxic water layers might be significantly influenced by future changes in the interplay between biological, chemical and physical processes in lake environments. The results further demonstrate that CH_4 concentration and emissions are not predictable from single and/or random measurements and, hence, estimations of the local methane budget need to be reconsidered with respect to the highly dynamic behaviour of CH_4 in surface waters.

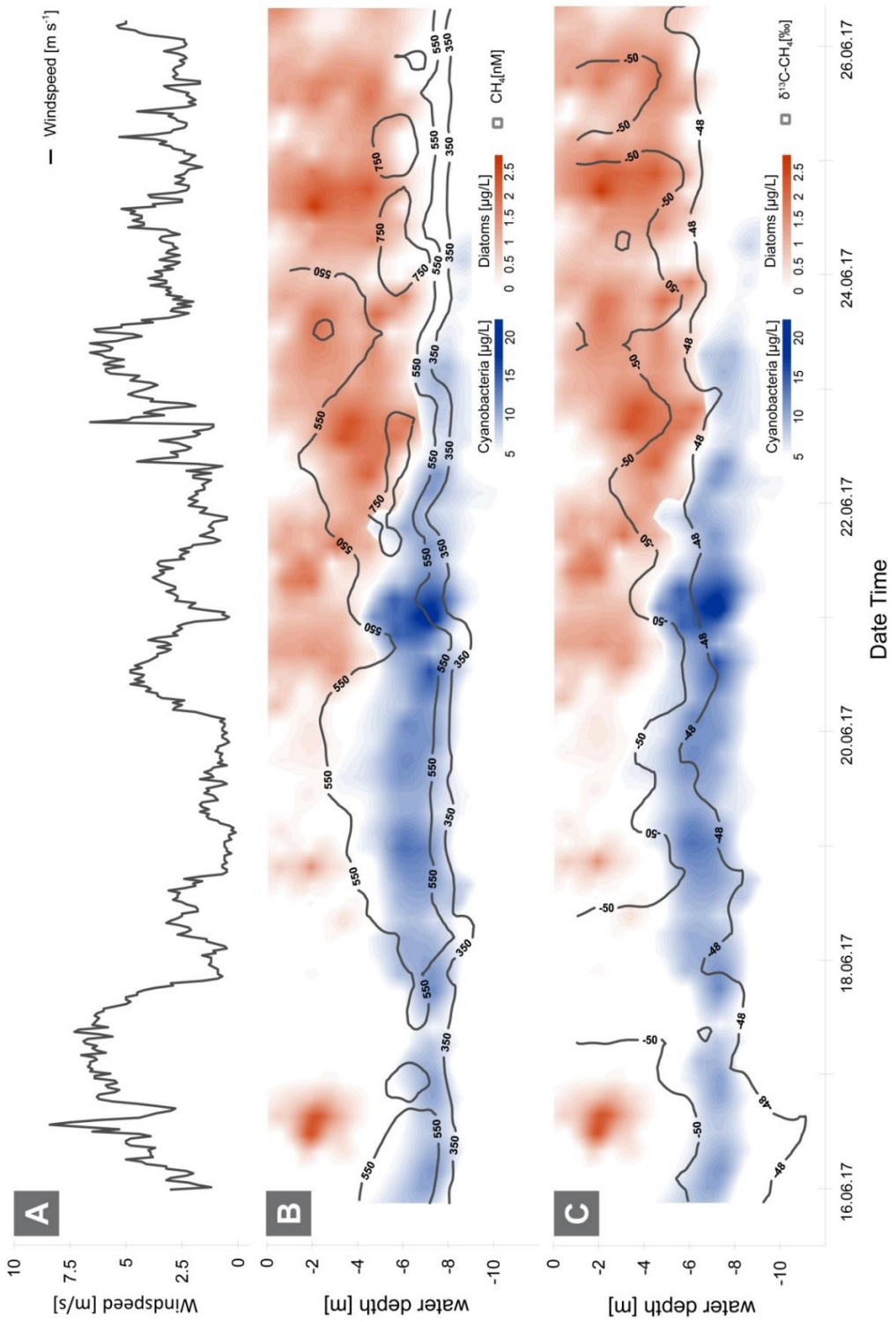

Figure 39: Wind speed (A), *in-situ* results of cyanobacteria (blue) and diatoms (red), the CH_4 concentration (B) and the $\delta^{13}C$-CH_4 values (C) in the water column. When merged together, the data of CH_4 accumulation and pigment presence of cyanobacteria and diatoms showed good spatial and temporal coverage. Temporally missing correlation between phytoplankton and CH_4 accumulation is best explained by wind-induced loss of CH_4 by emission to the atmosphere.

2.3. Lake Erken

2.3.1. Study site

Lake Erken (59°51‘ N, 18°35‘ E) is an alkaline, mesotrophic and discontinuously dimictic lake 60 km north-east of Stockholm (Sweden) (Figure 40). Lake Erken has a total area of 24 km², a mean depth of 9 m and a maximum depth of 21 m. The water residence time is about 7 a (Widell 1965). The drainage area is 140 km² and mostly dominated by coniferous forest. The lake is covered with ice for 16 to 18 weeks per year (December/January to April/May). Summer stratification usually develops in late May. Phytoplankton blooms occur regularly in the ice-out period, while nutrients decrease rapidly and e.g. phosphorus is limited by May (Pechlaner 1970b; Pettersson 1980, 1985; Malmaeus et al. 2006).

Sediment resuspension in relatively shallow and littoral areas is known to result from wind-induced hydrodynamic forces (Weyhenmeyer et al. 1995). The predominant winds generally arrive from the east due to the proximity to the Baltic coast. Wind direction [°] and wind speed [m s^{-1}], photosynthetically active radiation (PAR) [W m^2] as well as water temperature [°C] were collected and provided by the meteorological station at *Malma Islet* (Figure 40).

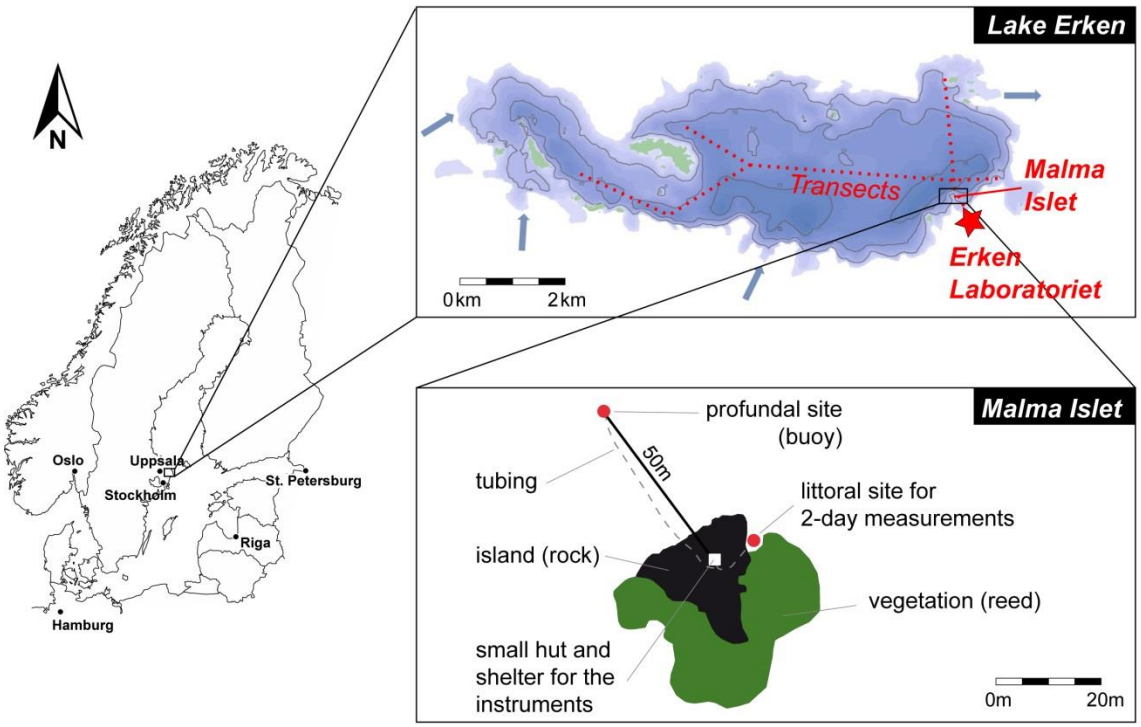

Figure 40: Lake Erken, 60 km north east of Stockholm, Sweden. Position of the sampling locations (*Malma Islet* and littoral site in front of *Erken Laboratoriet*), transects (red dotted) and sampling sites for continuous measurements near *Malma Islet* at Lake Erken, sampled in July 2017. The bathymetric map of Lake Erken was modified after Eidborn (2015).

2.3.2. Material and Methods

Sampling sites

At Lake Erken, the M-CRDS was operated at a small island (*Malma Islet* 59°50.345‘ N, 18°37.774‘ E) in front of the *Erken Laboratoriet* (*University of Uppsala*, Sweden) (Figure 40). During the first two days, the water was pumped from the island shore from 1.0 m water depth. Thereafter, the submersible pump was deployed at a buoy in 2.5 m water depth 50 m offshore north of the island (Figure 40). Additionally, a depth profile of CH_4 concentrations and $\delta^{13}C$-CH_4 was performed by the M-CRDS system at the buoy immediately thereafter. Discrete water samples for GC-FID analyses were taken along two defined 7000 m and 2300 m long transect lines in 0.5 m water depth with a lateral resolution of ~20 - 1500 m (Figure 40, Table 11) to detect spatial variations in CH_4 concentration in the upper water layer of Lake Erken. Sediment sampling was carried out at the site of the continuous measurement (buoy) and within the bay in front of the *Erken Laboratoriet*.

Table 11: Locations sampled at Lake Erken. Profundal "buoy site" and shallow shore site at *Malma Islet* was analysed by M-CRDS and GC-FID, transect locations were analysed by GC-FID only. Cores were taken at the buoy site and at the Littoral site in front of Erken Laboratoriet.

Sample ID	Latitude	Longitude	Lake depth [m]	Sampled depth [m]
Buoy (profile)	49°30.015' N	8°23.835' E	15	0 - 15
Buoy (continuous)	49°30.015' N	8°23.835' E	15	2.5
Malma Islet shore (littoral)	59°50.358′ N	18°37.773′ E	1.0	1.0
Littoral site (bay in front of *Erken Laboratoriet*)	49°29.980' N	8°23.613' E	2.0	2.0
Transect locations				
1	59°50.395' N	18°31.145' E		0.5
2	59°50.276' N	18°32.596' E		0.5
3	59°51.830' N	18°33.070' E		0.5
4	59°50.452' N	18°34.214' E		0.5
5	59°50.305' N	18°36.367' E		0.5
6	59°50.535' N	18°37.264' E		0.5
7	59°50.287' N	18°37.390' E		0.5
8	59°50.244' N	18°37.426' E		0.5
9	59°50.269' N	18°38.269' E		0.5
10	59°50.960' N	18°37.527' E		0.5
11	59°51.119' N	18°37.419' E		0.5
12	59°50.575' N	18°37.430' E		0.5
13	59°50.380' N	18°37.419' E		0.5
14	59°50.244' N	18°37.426' E		0.5
15	59°50.215' N	18°37.466' E		0.5
16	59°50.172' N	18°37.480' E		0.5
17	59°50.118' N	18°37.530' E		0.5
18	59°50.110' N	18°37.548' E		0.5
19	59°50.850' N	18°37.584' E		0.5

Lake water and pore-water analyses

For 10 days, CH_4 concentrations were continuously and simultaneously measured by the M-CRDS and an underwater mass spectrometry (UWMS) (Schlüter and Gentz 2008). Discrete water samples for the validation of the CH_4 concentration measurements were taken from the bypass of the M-CRDS. $\delta^{13}C$-CH_4 of the water was analysed by the M-CRDS, only. All discrete water samples were independently analysed in the laboratories of the *Institute of Earth Sciences at University of Heidelberg* (Germany) and the *Alfred-Wegener Institute* (AWI), Helmholtz Centre for Polar and Marine Research located in Bremerhaven (Germany) via the headspace technique (Kampbell et al. 1989) by GC-FID according to the procedure descripted in Chapter 1.1.1.

All samples taken in the water column and from sediment cores were treated and analysed identical to the procedure described for Lake Willersinnweiher (Chapter 2.1.2).

Calculations

Diffusive fluxes were calculated from concentration gradients according to the procedure described in Chapter 2.1.

2.3.3. Results

Sediment pore-water characteristics and CH_4 pore-water fluxes

The pore-water of littoral and profundal sediments at Lake Erken showed differently pronounced geochemical redox zones (Figure 41).

Pore-water Mn concentrations in littoral and profundal sediments peaked at 2 cm and 4 cm sediment depth, respectively. Maximum Mn concentrations of 90 μM at the profundal site were around 10 times higher than at the littoral site. Pore-water Mn was detected in the entire sediment column at both sites. Iron concentrations were with maximum concentrations of 50 μM and 0.5 μM lower than Mn concentrations at both sites. Dissolved Fe was low at the littoral site and an order of magnitude higher at the profundal sites. Profundal sediments showed a strong peak from 0 to 10 cm depth with up to 45 μM of dissolved Fe. Furthermore, the littoral sediments showed increasing Fe concentrations below 20 cm to up to 40 μM at 30 cm depth. Pore-water SO_4^{2-} decreased with sediment depth in the uppermost 5 cm at all sites. Concentrations decreased within the uppermost 2 cm at the profundal site, whereas SO_4^{2-} showed a local maximum at 2 cm and decreasing concentrations below (Figure 41). Total sulphide was below the detection limit at both sites. Pore-water CH_4 concentrations increased with depth to maximum values of 0.7 mM in the profundal sediments, whereas the littoral sediments showed maximum CH_4 concentrations of 0.4 mM in 15 cm sediment depth. Methane production in pelagic sediments was equal for profundal and littoral sites, whereas CH_4 release into bottom water was 8 times higher at the littoral site than at the profundal sites (Figure 41).

At both sites, DIC increased to maximum concentrations of 3 mM with depth. Littoral sediments showed an increase within the uppermost 10 cm and constant values below, whereas DIC at the profundal site peaked at depth at the same depth of dissolved Fe within the upper 10 cm and below 20 cm sediment depth. Total dissolved phosphorus showed maximum concentrations between 5 and 15 cm depth of the littoral core. Profundal total dissolved P followed the pattern of Fe and DIC and peaked at 8 and 30 cm depth.

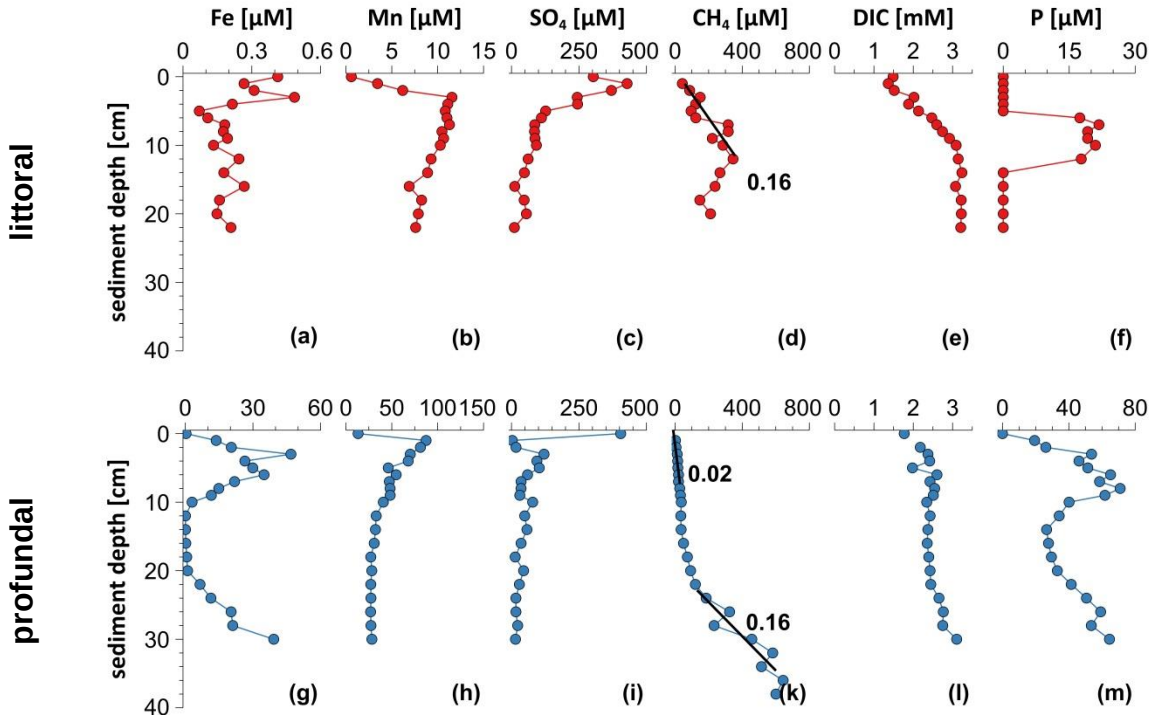

Figure 41: Geochemical pore-water profiles of selected elements in the sediments of Lake Erken taken at the littoral (a-f) and profundal (g-m) sites in August 2017. Methane diffusive fluxes calculated with Fick's 1st law (d and k) and production rates are given in mmol m^{-2} d^{-1}. Note the different scales on the x-axis for Fe, Mn and P of the profundal and littoral site.

Water characteristics

Lake Erken showed constant water temperatures in the uppermost 8 m and decreasing values below to 16 °C (Figure 42) in August 2017. The electrical conductivity was constantly low throughout the water column with values from 280 µS cm^{-1}. The uppermost 9 m of the water column were well-oxygenated, and saturation decreased down to 45% in deeper water layers. The pH values showed a similar pattern with values of 8.8 in the uppermost 9 m and decreasing values with increasing depth to pH 7.8 in 12 m water depth. Epilimnic CH_4 concentrations at the site of the continuous measurement (buoy site) were rather constant with values of 250 nM and decreased with depth to minimum values of 120 nM at 11 m water depth. Close to the lake bottom, CH_4 concentrations increased to ~ 200 nM. The CH_4 concentration profile is accompanied by an opposing trend in $\delta^{13}C$-CH_4 values with $\delta^{13}C$-CH_4 of -51‰ within the surface water layer and -48‰ in the deeper layer.

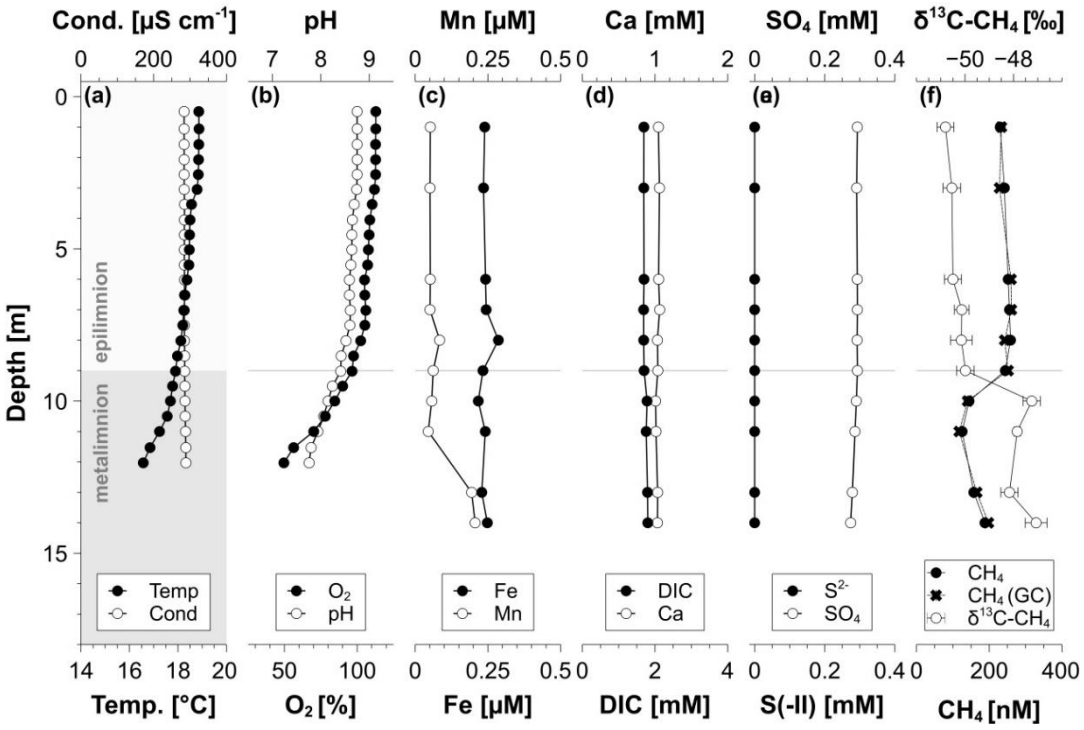

Figure 42: Geochemical profiles of selected elements in the water column of Lake Erken at the site of the continuous measurement (buoy) in August 2017.

Spatial variations of element and CH_4 concentration – Lake transects

The surface water layer of Lake Erken showed no spatial variations of most major element concentrations as shown exemplarily for Ca and DIC concentrations in Figure 43a and b. In contrast, Fe and Mn concentrations are higher in the surface water in littoral areas than at the profundal sites (Figure 43c and d). Iron and Mn concentrations are higher in the south-western bay than in the main basin of Lake Erken. The amount of suspended particulate material – based on visual impression only – was higher in the south-western bay than in the main basin of Lake Erken. Analyses in terms of the quantity and quality of suspended particulate material have not been carried out in the frame of this study.

Surface water CH_4 concentrations showed high spatial variations (Figure 43) in Lake Erken. The CH_4 concentrations of the surface water at profundal sites ranged between 200 and 350 nM, whereas the highest CH_4 concentrations (up to 1500 nM) were found at littoral sites. Highest surface water CH_4 concentration at profundal areas was found in the south-western bay of Lake Erken (350 nM).

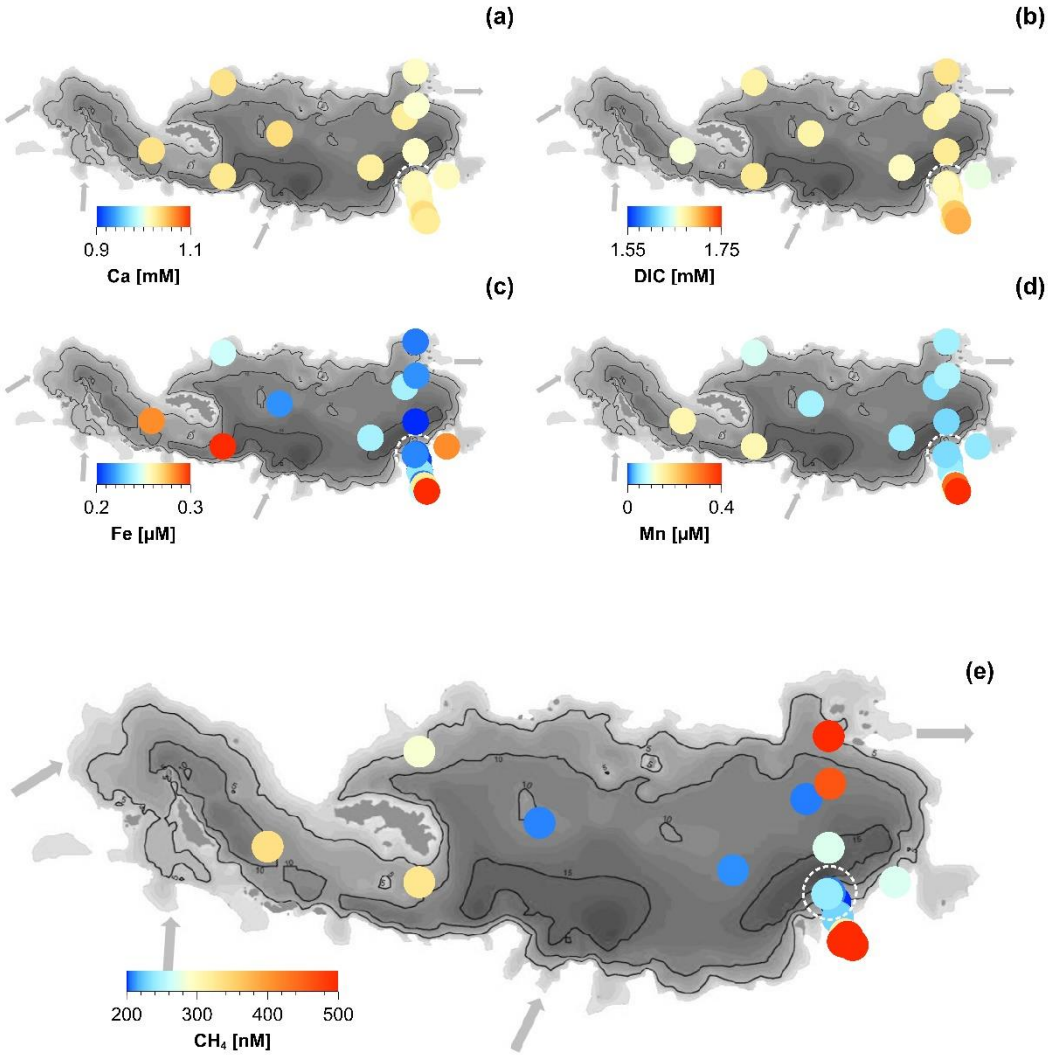

Figure 43: Spatial distribution of Ca (a), DIC (b), Fe (c), Mn (d) and CH_4 (e) concentrations in the surface water layer of Lake Erken in August 2017. The buoy site is encircled.

Temporal CH_4 variations

Uniform weather conditions dominated during the measurement period of 10 days. The wind speed was highest during day time (up to 6 m s^{-1}) and the main wind direction was north to north-east. Results for the continuously and simultaneously measured CH_4 concentrations show temporal variations during the 10 days of measurement (Figure 44). Near-shore water at *Malma Islet* showed a CH_4 concentration range between 200 and 400 nM. $\delta^{13}C$-CH_4 analyses showed values of – 54 to – 52‰. Surface water at the buoy site further offshore from the island showed lower concentrations varying between 170 nM and 270 nM. Isotopic values were generally less negative and ranged between – 50 to – 49‰.

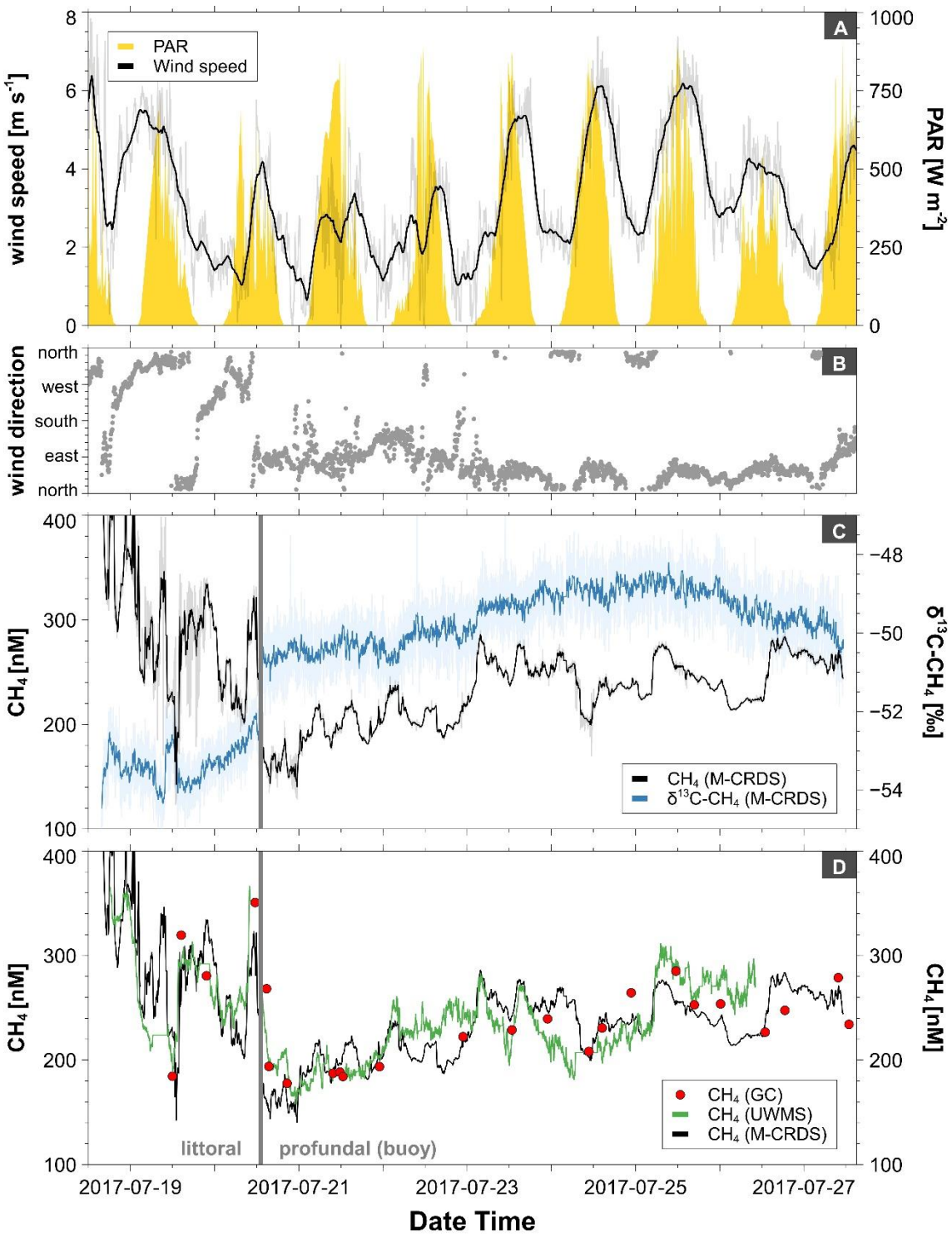

Figure 44: Temporal variations in wind speed (raw data and 2 h mean) and sunshine (expressed in PAR *Photosynthetically Active Radiation*) (A), wind direction (B), CH_4 concentration and $\delta^{13}C\text{-}CH_4$ values (raw data and 2 h mean) (C) and CH_4 concentration measured by GC, UWMS and M-CRDS (D). The pump location was changed from the littoral site a few meters offshore the island to the profundal buoy site, 50 m offshore the island, during July 20th (marked in grey).

2.3.4. Discussion

Performance during long-term measurement and method comparison

The presented results confirm the suitability of the M-CRDS for long-term *in-situ* analyses of CH_4 concentrations and $\delta^{13}C$-CH_4 values in surface waters. Methane concentrations obtained by the M-CRDS were consistent with the results of discrete water samples (GC-FID) and the UWMS for depth profile analysis as well as during the continuous measurements (Figure 45). The depth profile measurements showed an offset of less than 5 % between M-CRDS and GC-FID measurements (Figure 45a). These offsets are lower than previously reported in this study for the field application tests at Lake Stechlin (Chapter 1.4). The offset between CH_4 concentrations measured by M-CRDS, GC-FID and UWMS during continuous CH_4 concentration measurements ranged between 0 % and 60% (Figure 45b and c). Offset in CH_4 concentration was highest directly after sampling of near-shore waters with higher CH_4 concentrations and less than 15 % (GC-FID) and 20 % (UWMS) for profundal water. The analysis of short-term variations in CH_4 concentrations (e.g. by ebullition) is generally limited by the response time (average measurement time ~ 10 min) due to the rise / fall-time of the CRDS analyser during isotopic measurements. Validation measurements of $\delta^{13}C$-CH_4 values have not been carried out in the framework of this study.

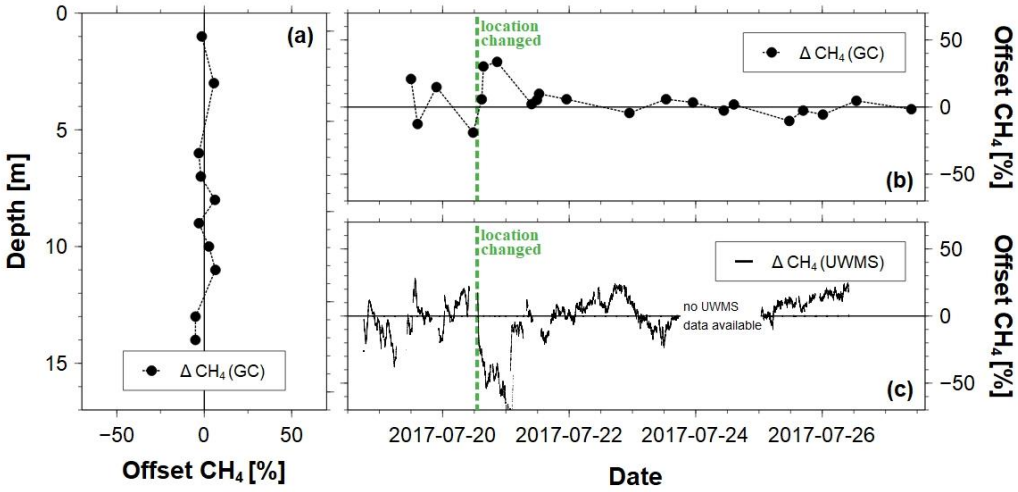

Figure 45: Offset between CH_4 concentrations measured by M-CRDS in comparison with GC-FID for depth profiles (A) as well as GC-FID (B) and UWMS (C) for continuous CH_4 concentration measurements at the buoy site (Lake Erken). The pump location was changed from few meters offshore to the profundal buoy site, 50 m offshore the island, during July 20th (marked in green).

CH_4 dynamics in Lake Erken

The calculated pore-water fluxes reveal that the surface water in Lake Erken is considerably influenced by the turnover of organic matter within the sediments. Thus, the pathways of CH_4 cycling within the sediments are essential for understanding the spatial and temporal variation in CH_4 concentration at Lake Erken. Sediments are iron-dominated and major redox-sensitive compounds showed different patterns for littoral and profundal sites, revealing different pathways of OM degradation. Profundal sediments showed the typical geochemical redox zonation of Mn, Fe and SO_4^{2-} as the main TEAs in the upper sediment layer. Methanogenic bacteria utilize the competitive substrates in the deeper areas. In contrast, methanogenesis is the dominant pathway of OM conversion at littoral sites as energetically more favourable TEAs are limited within these sediments. Methane is most likely produced via carbonate reduction at both sites as pore-water SO_4^{2-} concentrations are low and dissolved Mn and DIC are present in the entire sediment column.

Sedimentary CH_4 production rates were equal for profundal and littoral sites, however, CH_4 fluxes from the sediments into the bottom water were significantly higher at the littoral site compared to the profundal site. Hence, upward migrating CH_4 is considerably consumed by AOM in the profundal sediments. Pore-water data of profundal sediments showed intense $SO_4^{2-}$and Fe reduction within the uppermost 2 cm and 10 cm, respectively. Furthermore, Mn reduction was obvious in the entire sediment column, coinciding well with CH_4 minima in the uppermost 20 cm. The data suggest that AOM is coupled to the reduction of Fe and / or Mn in the lower parts of the profundal sediments (Beal et al. 2009; Amos et al. 2011; Crowe et al. 2011; Norði et al. 2013; He et al. 2018). Direct coupling between sulphur and carbon cycling might represent an additional pathway of anaerobic CH_4 oxidation in the uppermost 2 cm of the profundal sediments. In contrast, Mn and Fe are limited as TEAs in the littoral sediments as Fe and Mn are most likely trapped as sulphides and carbonates, respectively. Here, AOM via SO_4^{2-} is likely due to the pronounced sulphate reduction zone along with decreasing CH_4 concentrations in the uppermost 5 to 10 cm of the sediments. Even though pore-water CH_4 might be considerably consumed, CH_4 is released to a great extent via molecular diffusion into the water column.

In general, the sedimentary CH_4 flux is temporally constant in short time scales (hours to days). Nevertheless, high variations in CH_4 surface water concentrations were recorded for near-shore waters at *Malma Islet*. Temporal variations in littoral CH_4 are therefore related to external forcing, such as mixing with profundal waters (dilution) or temporarily enhanced sedimentary fluxes (enrichment) by sediment resuspension, ebullition or plant ventilation.

Dilution of littoral waters (high CH_4 concentration) with profundal waters (lower CH_4 concentration) are caused by lake-internal currents as a result from wind-driven lake circulation. Enhanced sedimentary fluxes are known to originate from ebullition (Chanton and Whiting 1995). This is generally triggered by pressure changes at the water column/sediment-interface, which often stem from wind-driven internal waves (Riedl et al. 1972; van der Loeff 1981). As a consequence, the flux of CH_4 across the sediment–water interface is enhanced by either advective transport due to "subtidal pumping" (Riedl et al. 1972) or by resuspension of sediments that was previously shown for Lake Erken (Weyhenmeyer et al. 1995; Goedkoop and Johnson 1996). Mixing, resuspension as well as ebullition will result for currents from the north as the sampling site was protected on the east and south by vegetation (reed) and on the west by the island (Figure 40). However, CH_4 concentrations and $\delta^{13}C\text{-}CH_4$ values showed no correlation with wind speed or wind direction. Plant ventilation occurs in littoral areas and leads to intense exchange between water/sediment and the atmosphere (Seiler and Holzapfel-Pschorn 1984; Schütz et al. 1989b; Ernst 1990). Correlations were found for CH_4 concentration and $\delta^{13}C\text{-}CH_4$ values with radiation and air temperature (Figure 40). Diurnal cycles of plant emissions in CH_4 concentration and $\delta^{13}C\text{-}CH_4$ values were observed for other aquatic environments and might be linked to transpiration (Schütz et al. 1989a; Chanton et al. 1997). Isotopic fractionation is thereby dependent on the pathway of ventilation and rhizosphere oxidation (Chanton et al. 1997). The mechanisms responsible for the variations in littoral CH_4 emissions might be verified by future direct measurements of plant emissions.

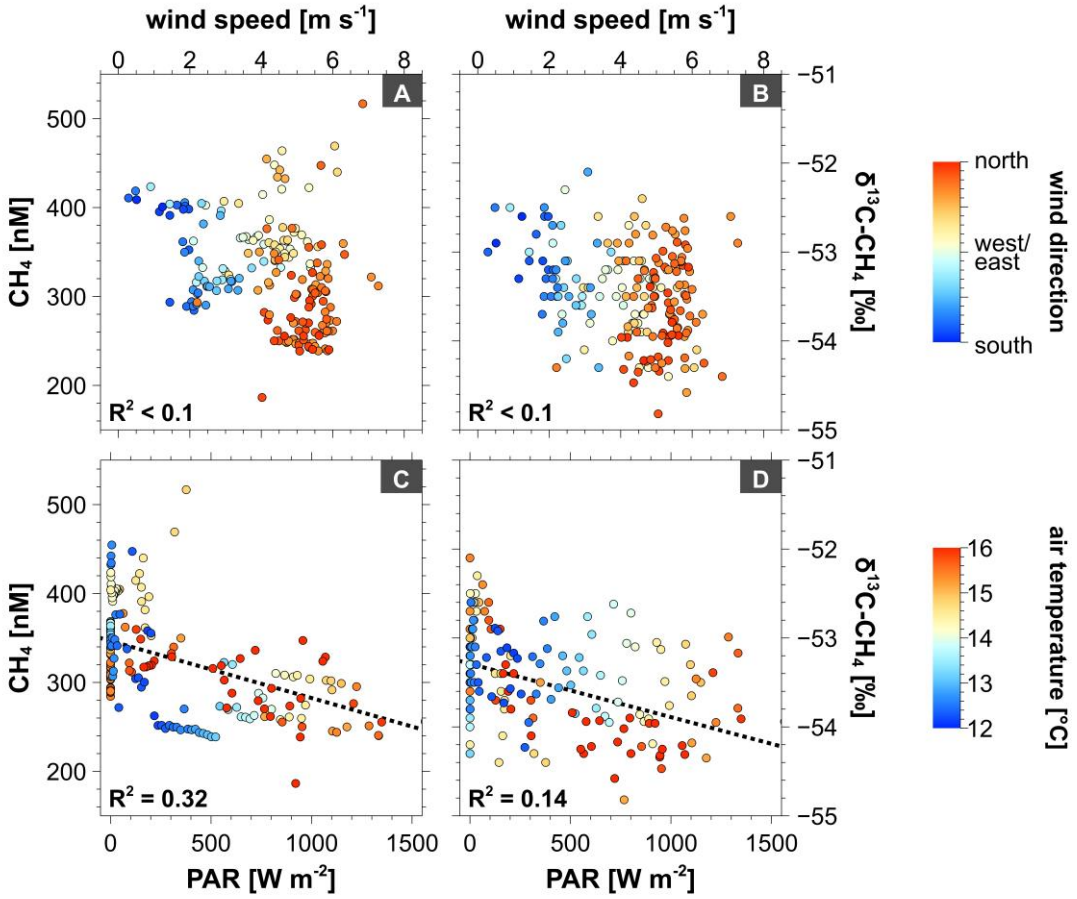

Figure 46: Correlation of wind speed (A and B) and radiation (C and D) with CH_4 concentrations (A and C) and $\delta^{13}C$-CH_4 values (B and D) of lake water at *Malma Islet*.

Surface water CH_4 concentrations of profundal areas decreased with increasing distance from the shore line (Figure 47). The rising concentration gradient with increasing distance to shore resulted from physical lateral transport processes from anoxic zones which were also shown for other lake environments (Murase et al. 2005; Hofmann et al. 2010; Encinas Fernández et al. 2016; DelSontro et al. 2017). The spatial heterogeneity of CH_4 concentrations fits very well with the model by DelSontro et al. (2017) adjusted for Lake Erken (Table 12), when assuming CH_4 oxidation (MOx) to occur within the surface water layer (Figure 47). Upper and lower bounds of the model prediction shown in Figure 47 include either no MOx or minimum and maximum MOx rates reported for moderate to high latitude lakes (Bastviken et al. 2002, 2003) since rates for Lake Erken are unknown to date. The models base on uniform littoral CH_4 production throughout the lake and show that most spatial variations in CH_4 concentrations can be explained by transport processes from littoral zones.

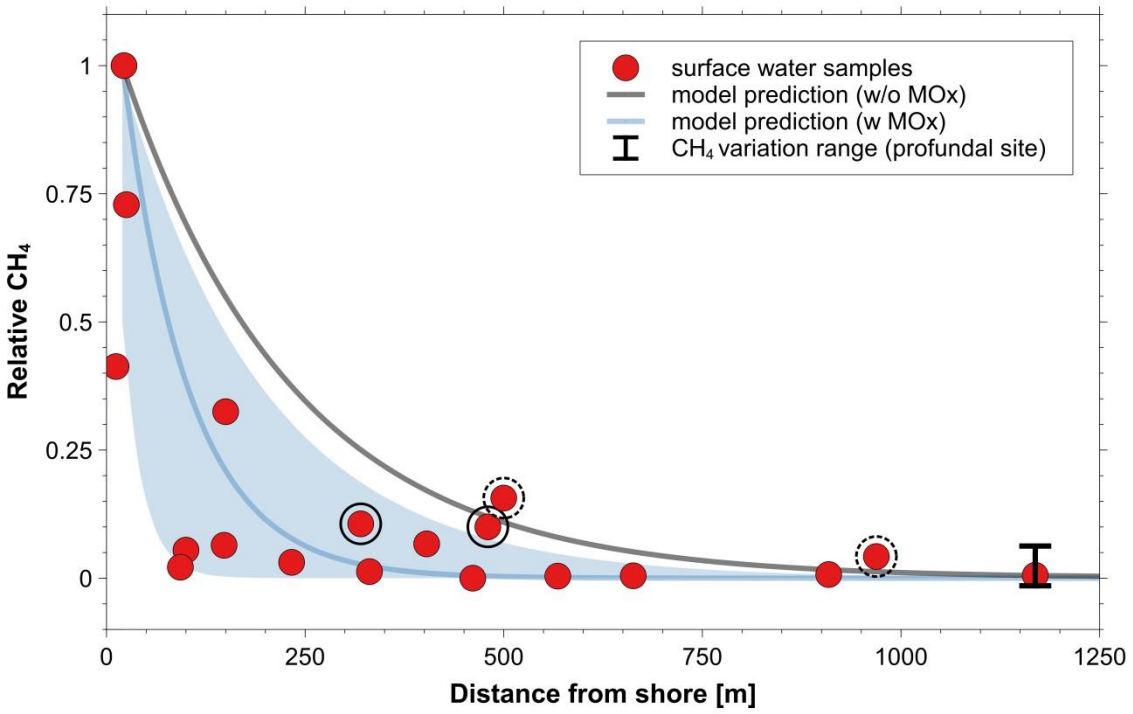

Figure 47: CH_4 concentrations of the surface water layer with distance from shore at Lake Erken. Surface water samples from the south-western (solid) and the eastern bay (dotted) of Lake Erken are encircled. The predicted concentration area was calculated after DelSontro et al. (2017) using the *elongated model* and assuming either no MOx or minimum and maximum MOx rates reported for moderate to high latitude lakes (Bastviken et al. 2002, 2003).

The predicted area covers the observed CH_4 concentrations measured in the surface water of Lake Erken. Samples from the south-western bay and the eastern part of Lake Erken are close to or above the maximum predicted concentrations based on the model calculations (Figure 47). Upwelling or diffusion of hypolimnetic CH_4 cannot be the source of the surface water CH_4, as concentrations are lower than in the epilimnion. Hence, elevated surface water CH_4 concentrations are affected by external factors such as low MOx during transport, CH_4 production in the surface water layer, littoral flux variations and / or enhanced horizontal transport processes.

Table 12: Equations and parameters adjusted for Lake Erken, used for the model calculations in Figure 47 after DelSontro et al. (2017).

Equations

$$C_X = C_{0(l)} e^{-\lambda x} + C_{0(p)} e^{-\lambda (D-x)} \quad (33)$$

$$\lambda = \sqrt{\frac{\left(\frac{k_{600}}{Z_{ML}}\right) + k_{O/P}}{k_H}} \quad (34)$$

$$k_{600} = 2.51 + 1.48 * U_{10} + 0.39 * U_{10} * log_{10}(A) \quad (35)$$

$$U_{10} = U_Z * \left[1 + \frac{\sqrt{C_d}}{\kappa} * ln\left(\frac{10}{z}\right)\right] \quad (36)$$

Parameter	Description	Value	Unit
C_X	Predicted surface water CH_4 concentration	-	[mmol m^{-3}]
$C_{0(l)}$	Littoral CH_4 concentration (surface)	1.7	[mmol m^{-3}]
$C_{0(p)}$	Profundal CH_4 concentration (surface)	0.2	[mmol m^{-3}]
λ	Physical decline in CH_4 concentration from shore to center of the lake	-	[m^{-1}]
x	Distance from shore	-	[m]
D	Shortest distance between two shores	2500	[m]
k_{600}	Standardized gas exchange coefficient from epilimnion	-	[m d^{-1}]
Z_{ML}	Thickness epilimnion	8	[m]
$k_{O/P}$	Net biological impact (negative for oxidation, positive for production)	0.005 – 0.1 (Bastviken et al. 2002, 2003)	[d^{-1}]
k_H	horizontal diffusivity coefficient	0.75 (DelSontro et al. 2017)	[m^2 d^{-1}]
U_{10}	Wind speed at 10 m height	-	[m d^{-1}]
A	Lake area	$2.4 * 10^7$	[m^2]
U_Z	Measured wind speed at height z	$3.46 * 10^5$ (mean value)	[m d^{-1}]
C_d	Drag coefficient at 10 m height	0.0013 (Stauffer 1980)	[-]
κ	Karman constant	0.4 (Andreas et al. 2006)	[-]
z	Height of wind speed measurement	4	[m]

MOx is known to depend on light exposure and the dominating types of methanotrophs (Utsumi et al. 1998; Grossart et al. 2011; Tang et al. 2014; Oswald et al. 2015). A correlation between CH_4 concentrations and external factors e.g. light exposure were not significant and specific MOx rates have not been examined in this study. Reported CH_4 oxidation rates for northern lakes range from 0.005 - 0.1 d^{-1} (Bastviken et al. 2002, 2003). Thus, estimated maximum oxidation rates might account for concentration changes of up to 30 nM d^{-1}. This broad range does not sufficiently cover the range of variation in the surface water concentrations found in Lake Erken.

Elevated surface water CH_4 concentrations might additionally result from oxic CH_4 production in the surface water layer as the recently discovered oxic pathway seems to be very common in a wide range of aquatic environments (Karl et al. 2008; Grossart et al. 2011; Bogard et al. 2014; Tang et al. 2014; Lenhart et al. 2015). The results from this study might suggest photoautotrophic CH_4 production, but they lack the evidence of this source as samples were not analysed for the photoautotroph community and $\delta^{13}C$-CH_4 values in the frame of this study. Suspended particulate material as well as Fe and Mn concentrations were higher in the south-western bay, where former studies found blooming cyanobacteria *Gloeotrichia echinulata* (Östlund et al. 2001). Oxic CH_4 production by cyanobacteria was previously shown for laboratory incubations and during field analyses at Lake Stechlin (Chapter 2.2). The predicted concentration area for lateral transported CH_4 from littoral sediment covers observed CH_4 concentrations in the western but not in the eastern part of Lake Erken. In the latter, no indication was found for blooming photoautotroph communities in the eastern Lake Erken and, hence, oxic CH_4 production might be excluded as the sole reason for elevated surface water concentrations in Lake Erken.

Littoral CH_4 concentration variations were shown exemplarily for the near-shore site at *Malma Islet*. Most profundal CH_4 would have originated from northern shores as high wind speeds were observed for northern winds. Enhanced sedimentary CH_4 fluxes by e.g. ebullition appears unlikely, since the northern shore line is sheltered from northern winds by dense forest. However, northern shore waters were not analysed for temporal variations in the frame of this study. The results of this study suggest that profundal CH_4 concentrations are probably triggered by enhanced transport processes due to wind-driven

lake circulation. Transect data showed horizontal gradients in CH_4 concentration from the shore to the buoy site. Furthermore, profundal surface water concentrations varied considerably between 150 nM and 300 nM during the 7-day measurements (buoy site) (Figure 47). Methane concentrations and $\delta^{13}C\text{-}CH_4$ values reveal dependencies on wind speed ($R^2 < 0.1$ and $R^2 = 0.16$, respectively) and wind direction ($R^2 = 0.20$ and $R^2 = 0.34$, respectively). $\delta^{13}C\text{-}CH_4$ values increased along with increasing CH_4 concentrations for northern winds (Figure 48). The results showed two probably distinct sources of CH_4 within the profundal surface water layer of Lake Erken. Surface water showed relatively constant values (~ - 50‰) for low or non-northern winds. Surface water which are influenced by northern winds tend to higher isotopic values (- 48‰).

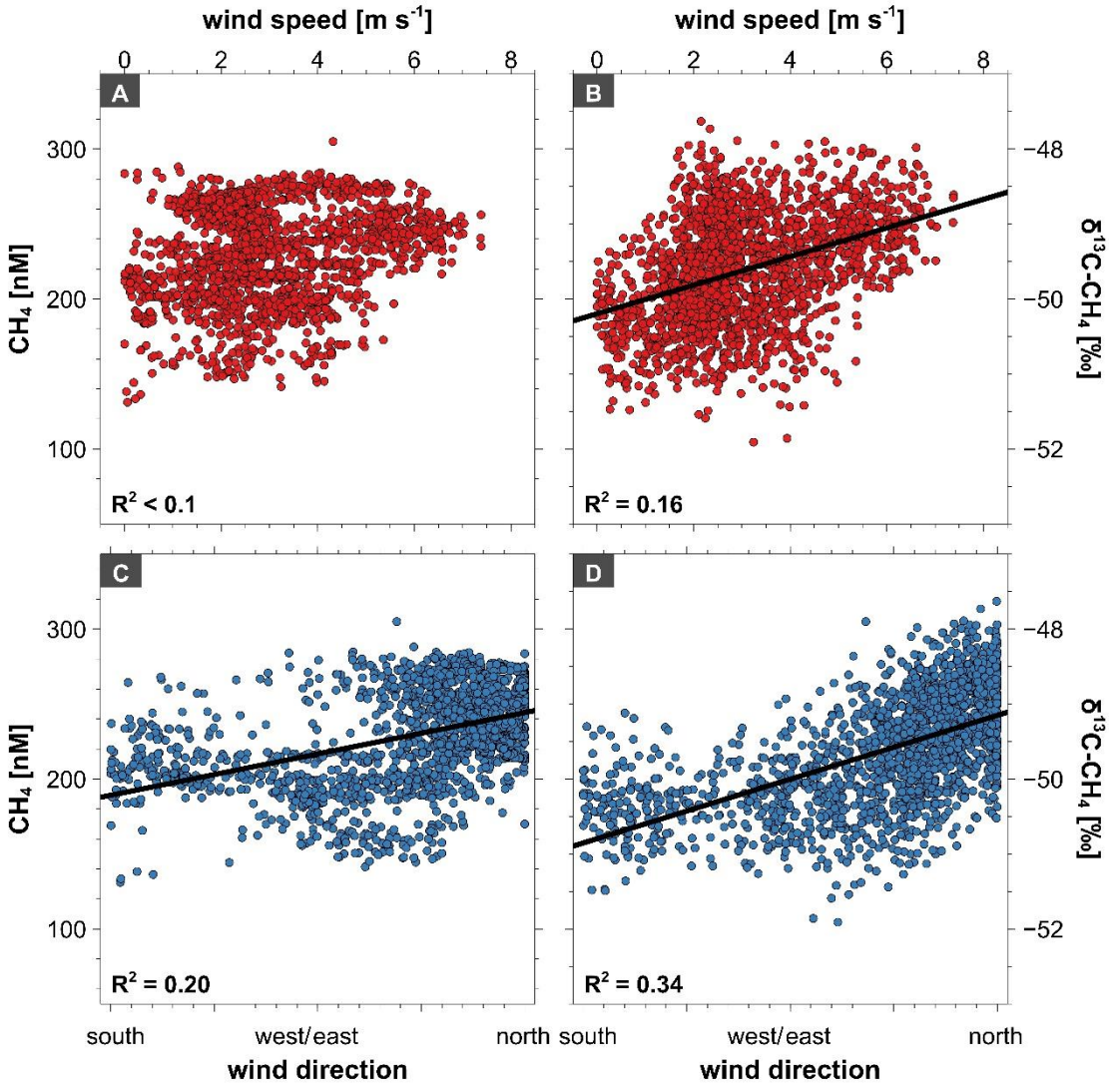

Figure 48: Correlation of wind speed (A and C) and wind direction (C and D) with CH_4 concentration (A and C) and $\delta^{13}C\text{-}CH_4$ values (B and D) at the profundal site.

Altered $\delta^{13}C\text{-}CH_4$ values in the surface water are a result of either mixing or transformation (oxidation) of CH_4. MOx is dependent on the interaction between oxygenic phototrophs and aerobic methanotrophs and leads to an uptake of lighter CH_4 and, thus, heavier values in the water (Barker and Fritz 1981). However, MOx at the profundal site appears unlikely since $\delta^{13}C\text{-}CH_4$ values increased along with increasing CH_4 concentrations. Thus, higher concentrated water has to be modulated by aerobic MOx along the transit of CH_4 in the epilimnion of Lake Erken. Profundal CH_4 is enriched with littoral CH_4 from northern shore sediments by advective horizontal transport processes during strong northern winds.

2.3.5. Conclusion

The study reveals a wide spatial and temporal variability of CH_4 concentrations in the surface water of Lake Erken. Epilimnic CH_4 concentrations showed a very good agreement with model predictions. Thus, it could be inferred that most spatial variations in CH_4 concentrations can be explained by transport processes from littoral to profundal zones at Lake Erken. Temporal variations of littoral and profundal CH_4 concentrations most likely stem from wind-driven currents in the surface water layer.

Deviations from the model predictions show that profundal waters are significantly influenced by changes in the interplay between physical processes. Surface water is enriched with littoral CH_4 from northern shore sediments by advective horizontal transport processes during strong northern winds. Methane enrichment is thereby quantitatively significant, but subordinate relative to changes in the littoral areas. Here, CH_4 concentrations are often controlled by external forcing. Mixing with profundal waters or temporarily enhanced sedimentary fluxes by ebullition or plant ventilation considerably influence aquatic CH_4 dynamics.

The results demonstrate that future whole-lake CH_4 estimations clearly need to integrate wind and wind direction as the driving factors of spatial and temporal variations of CH_4 concentrations in the surface water layer of stratified lakes. This is even more essential when considering that the emission of CH_4 from the surface water layer to the atmosphere is immediately affected by the wind speed. Future continuous-measurements of both CH_4 concentrations and $\delta^{13}C$-CH_4 values are therefore crucial for addressing the CH_4 dynamics in the surface water and its implications for CH_4 emissions of freshwater environments.

3. Conclusions and Prospective Research

3.1. The M-CRDS

The CRDS system coupled with a membrane contactor (M-CRDS) presented in this thesis enables the sensitive and simultaneous determination of short-term variations of CH_4 concentrations and $\delta^{13}C\text{-}CH_4$ values in surface waters. Laboratory and fieldwork show very good agreement of CH_4 measured simultaneously by the M-CRDS and the conventional analytical methods such as M-ICOS, UWMS, GC-FID and GC-C-IRMS analysis. The presented M-CRDS method is an easy and fast to use method and provides the continuous analyses of dissolved CH_4 concentrations and $\delta^{13}C\text{-}CH_4$ values of surface water at a very high temporal resolution.

The investigated method requires further development particularly with respect to the performance stability during measurements of several weeks and months. The different filtering units generally ensure longevity of the measuring setup. However, the lifetime of the filtering units with high mesh sizes is limited to a few days and mainly depends on the fraction of suspended particulate matter in the sampled aquatic system. Membrane alteration or aging could not be observed during the period of this work but cannot be ruled out for future continuous long term application. The installation of pressure sensors in the water and gas system for the detection of pressure changes will further provide an indication of membrane alteration and its effects on the efficiency of the gas extraction. To date, continuous sampling for GC and GC-C-IRMS validation measurements is required. The most appropriate method of validation and recalibration is the analysis of depth profiles in the field, since seasonally stratified lakes cover a broad range of physical and geochemical characteristics as well as CH_4 concentration and $\delta^{13}C\text{-}CH_4$.

Further development efforts are desirable for the calibration and characterisation of concentrations and isotopic values of CO_2 since the CRDS analyser used in this work allows the simultaneous determination of CO_2 and CH_4 concentrations and $\delta^{13}C$ values at a very high temporal resolution. Quasi-simultaneous measurements of concentrations and $\delta^{13}C$ values of CH_4 and CO_2 will then cover two of the major constituents in the carbon cycle.

The M-CRDS was successfully deployed in three different configurations: single profiling (Lake Willersinnweiher), continuous profiling (Lake Stechlin) and continuous measurement at one depth (Lake Erken). The results show that the M-CRDS is suitable for all three ways of analyses. The strength nevertheless tends to be in continuous deployment since the high temporal variability of aquatic CH_4 is not captured by traditional in-situ devices or strongly limited by the number of discrete samples. The installation and deployment of the M-CRDS is complex and single measurements at several different stations would require disproportionately much time (15-20 min) and should, thus, rather be conducted by traditional sampling and subsequent analysis by GC-FID and GC-C-IRMS. Future deployments of the M-CRDS should therefore focus on mid- to long-term measurements such as continuous profiling. In combination with the continuous in-situ analysis of the physical variations within the water column and the biological activity, the M-CRDS will essentially improve the understanding of the complex microbial pathways and transformations of CH_4 in aquatic ecosystems. In order to address CH_4 dynamics in surface waters and its implications for CH_4 emissions of freshwater environments, prospective continuous measurements of both CH_4 concentration and $\delta^{13}C$-CH_4 are critically needed. Further applications of the M-CRDS in different aquatic environments (e.g. shelves and estuaries) will also contribute to a higher temporal and spatial resolution of measurements identifying natural processes representing pathways, sources and sinks for CO_2 and CH_4 in marine, limnic and fluvial systems.

3.2. Methane in lake environments and future prospects

The combination of the new M-CRDS and conventional analytical methods revealed high spatial and temporal variability of CH_4 behaviour in the water column and the sediments in the different lake environments.

The fate of carbon in all lakes is unambiguously determined by turnover processes in sediments, where CH_4 is produced in considerable quantities. The studies at the three different lakes in different trophic states confirmed that sedimentary methanogenesis is a significant process during the degradation of organic matter (OM). Contrary to the assumptions of many studies in freshwater environments, indications for a direct coupling between sulphur and carbon cycling were found in all three lakes. Sulphate reduction (SR) generally occurred within the uppermost 10 cm of the sediments. Here, sulphate reducing bacteria (SRB) out-compete the methanogens by the utilisation of the competitive substrates. Below this depth, methanogenesis is the dominant pathway of OM conversion. The main methanogenic pathway is most likely carbonate reduction. The metabolic pathway seems to equal for all trophic states, since non-competitive substrates, such as methylated compounds are presumed to be limited in lake sediments (Capone and Kiene 1988). The presence of SR also influences the fate of CH_4 within the sediments. Methane is consumed by SO_4^{2-} in the sulphate-methane transitions zones (SMTZ) before reaching the water column. SMTZ are uncommon in freshwater environments to date, but evidence for AOM via SO_4^{2-} was found in the sediments of all three lakes. SR and CH_4 formation was highest for eutrophic lakes (Lake Willersinnweiher) and less significant in the mesotrophic and oligotrophic

lakes. AOM in the latter is mostly coupled to the reduction of Mn minerals. More than two-thirds of upwards migrating CH_4 is consumed before reaching the water column by AOM in the sediments.

However, considerable release of CH_4 across the sediment-water interface into the bottom water was found at all lakes. In lakes of lower trophic state (lake Erken and Lake Stechlin), littoral CH_4 tend to be less affected by MOx and release into bottom water was significantly higher than at the profundal sites. An opposing trend was observed for the eutrophic Lake Willersinnweiher. However, this might be the result of seasonal variation in sedimentary OM degradation, since the lakes were examined at different times of the year. Higher water temperatures and higher input of organic matter during summer will result in higher CH_4 production and release rates at the littoral sites. Temporal variations in littoral CH_4 release on shorter time scales might be related to physical forcing, such as mixing with profundal waters or temporarily enhanced sedimentary fluxes by sediment re-suspension, ebullition or plant ventilation as exemplarily shown by the application of the new M-CRDS at *Malma Islet* (Lake Erken). Released CH_4 from profundal sediments is consumed by aerobic CH_4 oxidation (MOx) in the oxic water column, which prevents sedimentary CH_4 from reaching the surface water layer. The AOM and MOx in all systems are a very effective barrier to CH_4 emission into the atmosphere in thermal stratified lakes.

The study at Lake Erken further demonstrated the wide spatial and temporal variability of CH_4 concentrations in the surface water layer of lakes. Surface water CH_4 concentrations are highest in the littoral and lower in the profundal areas of lakes. Methane oversaturation with respect to the atmosphere was observed at all three lakes during all seasons of the year. Most profundal CH_4 concentrations are best explained by horizontal transport processes from littoral zones. As littoral areas might be sheltered from prevailing winds, transport processes are coupled to both wind speed and wind direction. The predicted areas from the model by DelSontro et al. (2017) adjusted for all three lakes covers the observed CH_4 concentrations measured in the surface water of Lake Erken only. The results from Lake Willersinnweiher and Lake Stechlin are close and significantly above the maximum predicted concentrations based on the model calculations, respectively (Figure 49).

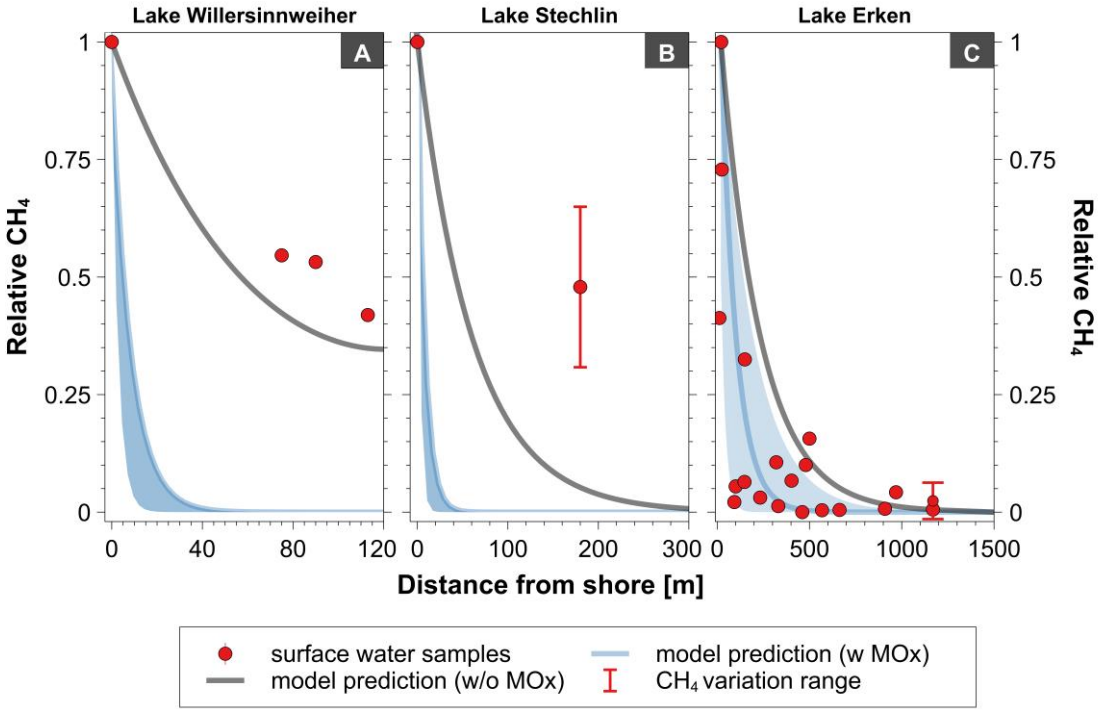

Figure 49: CH_4 concentrations in the surface water layer with distance to the shore at the different lakes studied. The predicted concentration area was calculated after DelSontro et al. (2017) using the *elongated model* and assuming either no MOx or minimum and maximum MOx rates reported for similar lakes (Bastviken et al. 2002, 2003; Bogard et al. 2014; Tang et al. 2014; Oswald et al. 2015). Equations and parameters used for the calculations are listed in the appendix.

Sedimentary CH_4 contribution to the surface water layer might be the primary cause of epilimnetic CH_4 oversaturation in winter or in nutrient-depleted lakes, such as Lake Erken during summer stratification. Groundwater-fed lakes such as Lake Willersinnweiher might also be enriched in CH_4 by groundwater contributing to the methane pool. In eutrophic and mesotrophic lakes, or lakes where nutrients, such as phosphate, are available during the period of bioproduction, aquatic CH_4 might also be produced *in-situ* by the photoautotroph community under oxic conditions. Indications for oxic CH_4 production (OMP) were found at Lake Willersinnweiher and Lake Stechlin. The study at Lake Stechlin reveals that aquatic CH_4 concentrations are directly linked to algal dynamics and algae abundances. The temporal and spatial variability of CH_4 is thereby unambiguously controlled by photoautotrophic CH_4 production within the oxic water layer and CH_4 loss to the atmosphere. Methane accumulation and pigment presence of cyanobacteria and diatoms showed good spatial and temporal coverage within the water column of Lake

Stechlin. Furthermore, laboratory incubation experiments provide evidence that all examined phytoplankton classes in Lake Stechlin produce CH_4 under oxic conditions. Thus, OMP provides a new source of CH_4 emissions that was overlooked for decades.

Methane emissions from the surface water layer to the atmosphere are known to be coupled to wind speed. The high-resolution study at Lake Stechlin revealed that increasing wind speeds also control the distribution of CH_4 in the surface water layer by lowering the CH_4 concentrations in the uppermost 5 m of the lake. Wind-induced changes in the upper water column of lakes lead to highly dynamic conditions and highly variable CH_4 concentrations in lakes. Thus, aquatic CH_4 concentrations and emissions are not predictable from single measurements. In addition, stratified lakes store significant amounts of CH_4. Estimations for the rather small eutrophic Lake Willersinnweiher amount to more than 20 kmol CH_4, stored within the anoxic hypolimnion. During the autumn overturn period, hypolimnic CH_4 is released by vertical water mass mixing, resulting in high emission rates of CH_4 to the atmosphere (e.g. Bastviken et al. 2004). Although CH_4 might be oxidised to great extent in the water column, estimated overturn emissions of Lake Willersinnweiher account for up to 50 % of the annual CH_4 emissions.

Freshwater environments have not been considered as significant CH_4 sources for a long time, and awareness has arisen only in recent years. Growing eutrophication and climate warming will both have major effects on the CH_4 pool of lakes. Nutrient availability and the diversity and composition of the microbial community might change, affecting turnover processes within the water column and the sediments of lakes. Production and turnover rates of organic matter in the lakes will increase in the future and potentially enhance methanogenesis within the sediments. Turnover rates thereby also depend on lake basin morphology, catchment characteristics and geographic location, controlling the supply of organic matter. The release of CH_4 across the sediment-water-interface thereby depends on the availability of the oxidants and the composition of microorganisms within the sediments. Concentrations of oxygen in the deep water layer will decrease and prevent CH_4 oxidation within the water column. This is even more essential when considering that increasing water temperatures might affect the intensity and duration of vertical mixing (e.g. Boehrer and Schultze 2008; Livingstone 2008). A growing

amount of hypolimnic stored CH_4 will result in increasing emission rates of CH_4 during overturn emissions. Increasing water temperatures will further result in extended stratification periods of lakes worldwide which consequently results in longer periods of bioproduction and OMP in the surface water layer (e.g. McCormick and Fahnenstiel 1999; Livingstone 2003). Climate change will also alter wind speeds and directions (e.g. Pirazzoli et al. 2006; McInnes et al. 2011). Accordingly, CH_4 emissions from freshwater environments will further increase in the future with far-reaching and self-reinforcing consequences for climate change.

To halt this development, the severe impact of human activities on aquatic environments must be reduced significantly. The use of fertiliser, for example, needs to be strictly limited since most lakes received high external loading of phosphorus and nitrogen by overfertilization and massive land use, leading to growing eutrophication of groundwater and lakes. Improving the water quality of lakes is achievable through shoreline reconstruction, biomanipulation and reestablishment of aquatic plants to limit the availability of phosphorus and nitrogen and consequently suppress phytoplankton grow (e.g. Shapiro et al. 1975; Kasprzak et al. 2002; Hansson et al. 2017). This approach was successfully adopted at Lake Willersinnweiher in the 1990s, which considerably reduced internal nutrient loading of the lake. However, regional modifications will only result in small-scale changes. In order to achieve global transformations and large-scale impacts, a reduction in worldwide CH_4 emissions together with more scientific emphasis as well as public comprehension is indispensable.

4. Related Scientific Work

Publications

Jan F. Hartmann, Marco Günthel, Thomas Klintzsch, Georgiy Kirillin, Hans-Peter Grossart, Frank Keppler and Margot Isenbeck-Schröter. 2018. Evidence for *in-situ* production of methane in the oxic surface water of an oligotrophic lake. *Nature Communications* (in prep.)

Jan F. Hartmann, Amanda Schiller, Torben Gentz, Markus Greule, Hans-Peter Grossart, Danny Ionescu, Frank Keppler, Karla Martinez-Cruz, Armando Sepulveda-Jauregui and Margot Isenbeck-Schröter. 2018. A fast and sensitive method for the continuous in-situ determination of dissolved methane and its δ^{13}C-isotope ratio in surface waters. *Limnology & Oceanography: Methods*. doi: 10.1002/lom3.10244.

Jan F. Hartmann, Amanda Schiller, Torben Gentz, Markus Greule, Hans-Peter Grossart, Danny Ionescu, Frank Keppler, Karla Martinez-Cruz, Armando Sepulveda-Jauregui and Margot Isenbeck-Schröter. 2017. Real Time Measurement of Concentration and δ^{13}C-CH_4 in Water. *Procedia Earth and Planetary Science*, Volume 17, 2017, Pages 460-463, ISSN 1878-5220, doi: 10.1016/j.proeps.2016.12.116.

Sampling campaigns & research cruises

2017 & 2018	*Lake Willersinnweiher, Ludwigshafen am Rhein, Germany* Five multi-days campaigns. Depth profiles of CH_4 concentration and its isotopic composition in the water column as well as pore-water and sediment geochemistry
08/2017	*Lake Erken, Uppsala, Sweden* Continuous in-situ measurements and depth profiles of CH_4 concentration and its isotopic composition
07/2017	*Lake Stechlin, Berlin, Germany* Continuous in-situ measurements and depth profiles of CH_4 concentration and its isotopic composition
10/2016 – 11/2016	*RV Heincke HE475, North Sea* Continuous in-situ measurements as well as pore-water and sediment geochemistry
2015 & 2016	*Upper Rhein Graben and Eiffel, Germany* Test measurements of the M-CRDS (CH_4 concentration and its $\delta^{13}C$ isotopic composition) in different aquatic systems (groundwater, lakes and rivers)
07/2015 & 08/2015	*Lake Stechlin, Berlin, Germany* Test measurements of the M-CRDS. Continuous in-situ measurements and depth profiles of CH_4 concentration and its isotopic composition

Conference Proceedings & Workshops

Tagung der Fachsektion Hydrogeologie e.V. in der DGGV e.V.

Location: Ruhr-Universität Bochum, Bochum (Germany)

Date: 21.03. – 24.03.2018

Title: "Freisetzungs- und Umsatzprozesse des Methans in einem Grundwasser-gespeisten Baggersee"

Chosen as Poster

Authors: Jan Frederik Hartmann, Yannic Wellach, Margot Isenbeck-Schröter and Frank Keppler

Workshop: Progress in PCO_2 measuring techniques

Location: Alfred-Wegener Institute (AWI), Helmholtz Centre for Polar and Marine Research, Bremerhaven (Germany)

Date: 11.09.2017

Title: "The M-CRDS System - A membran-coupled cavity-ring-down-analyser (Picarro)"

Invited Talk

Author: Jan Hartmann

15th Water-Rock Interaction International Symposium, WRI-15,

Location: Evora (Portugal)

Date: 16.10. - 21.10.2017

Title: "Real Time Measurement of Concentration and $\delta^{13}C$-CH_4 in Water"

Chosen as Poster

Authors: Jan F. Hartmann, Amanda Schiller, Torben Gentz, Markus Greule, Hans-Peter Grossart, Danny Ionescu, Frank Keppler, Karla Martinez-Cruz, Armando Sepulveda-Jauregui and Margot Isenbeck-Schröter

Published in Procedia Earth and Planetary Science, Volume 17, 2017, Pages 460-463, ISSN 1878-5220, doi: 10.1016/j.proeps.2016.12.116.

5. List of Figures

Figure 1: Global sources and sinks of CH_4 (modified after IPCC-Report 2013). Methane fluxes are given in [Tg yr^{-1}]. Natural fluxes are black, anthropogenic fluxes are red and combined natural and anthropogenic fluxes are light brown.4

Figure 2: The pathways of organic matter decomposition under anoxic conditions. Methanogenesis during the anaerobic decomposition of organic matter base on either acetate (via substitution of the methyl group) or CO_2 reduction (via H_2 or formate). Modified after Appelo and Postma (2005)..... 5

Figure 3: Classification of the various pathways of CH_4 formation using the stable isotopic composition of CH_4 ($\delta^{13}C$ and δD values). Modified after Oremland et al. (1987) and Whiticar (1999). 8

Figure 4: The CH_4 emission pathways in a stratified lake (modified after Bastviken et al. 2004). 11

Figure 5: Schematic of the cryo-trap based on thermoelectric cooling. The wet gases enter the cryo-trap, water vapour is frozen at the heat sink as well as at

the copper wool and dried gases are subsequently directed to the analyser. The heat sink was cooled by a Peltier element (*QuickCool*, QC127)..... 19

Figure 6: Schematic overview of the CRDS analyser combined with a membrane contactor setup for continuous and simultaneous determination of dissolved CH_4 concentration and $\delta^{13}C\text{-}CH_4$ in water. In the water system, water is pumped by a submersible pump (A), filtered (B) and analysed by several sensors in a bypass (C). Main water flow is adjusted by a mass flow controller (D) and directed to the membrane contactor (E). In the gas system part, gases are extracted by the membrane pump (G). The vacuum pump and tubes are flushed via two automatic 3-way-valves (Part F_1 and F_2) with ambient air avoiding condensation in the system. Depending on the CH_4 concentration, the gas sample can be diluted with synthetic air by two mass flow controllers (H_1 for gas sample flow and H_2 for synthetic air flow). Reference gases for calibration prior, during and following the experiments are introduced via 3-way-valves (I). Gases are dried by a Nafion drying tube (J) prior to analysis by the CRDS analyser (K)..... 21

Figure 7: The results of the calibration of the M-CRDS for CH_4 concentration using synthetic water standards (n = 21). Error bars (1-σ) of measurements mainly lie within symbols and reflect the noise within the measurement interval (10 min). Best fit was calculated by geometric mean regression (Sokal and Rohlf 1995)..... 25

Figure 8: The $\delta^{13}C\text{-}CH_4$ values of natural water samples (n = 15) with different stable carbon isotopic values measured both by M-CDRS and GC-C-IRMS (a). Error bars (1-σ) of measurements reflect the noise within the measurement interval (10 min). Offset of $\delta^{13}C\text{-}CH_4$ values for natural water samples (n = 15) with different $\delta^{13}C\text{-}CH_4$ values and CH4 concentration were measured by M-CRDS in comparison with GC-C-IRMS (b)..... 26

Figure 9: Keeling plot analysis of the samples used for the calibration of CH_4 concentration and $\delta^{13}C\text{-}CH_4$ by synthetic CH_4-water standards. The reference gas that was used to produce synthetic water standards represents the source of CH_4 in the Keeling plot, whereas the dilution water, used for the dilution of all synthetic water standards, displays the background concentration (encircled). The extrapolated intercept of the best fit in the Keeling plot (also shown in equation of the geometric mean regression) provides the isotope ratio of the water CH_4 source (-32.0‰). Error bars (1-σ) of measurements reflect the noise within the measurement interval (10 min) and mainly lie within symbols..... 27

Figure 10: Precision of $\delta^{13}C\text{-}CH_4$ values of the M-CRDS versus the CH_4 concentration of natural water samples (n = 520) analysed during fieldwork. Error bars (1-σ) of measurements reflect the noise within the measurement interval (10 min)..... 31

Figure 11: Exemplary response time of CH_4 concentration (a) and $\delta^{13}C\text{-}CH_4$ values (b) for low to high and high to low concentration transitions. Concentrations are normalised to 0 (1st reservoir, 130 nM) and 1 (2nd reservoir, 170 nM). Response times of the M-CRDS were assessed by the calculation of the time constant τ [s] (Johnson 1999) (n=8). $\delta^{13}C\text{-}CH_4$ data has been smoothed to 30 s averaging interval. High concentration measurement marked in grey. Spikes in CH_4 concentration arise from increased retention time of waters in the membrane contactor due to switching between water reservoirs. 32

Figure 12: Bias in the CH_4 measurements due to spectroscopic interference between water vapour (H_2O) and CH_4 in reference gas in respect to the water vapour content. The uncertainty of the software internal water correction algorithm is significantly lower than the actual measuring precision (6 ppb). Error bars (1-σ) reflect the precision of the M-CRDS. 36

Figure 13: Bias in the $\delta^{13}C\text{-}CH_4$ measurements due to effects of the gas matrix on the stable carbon isotopic values. Effects of changes in aquatic O_2 concentration

are were not detected or significantly lower than the actual measuring precision (1.7‰). Error bars (1-σ) reflect the precision of the M-CRDS. 37

Figure 14: Measured CH_4 concentration versus the temperature difference between the water temperature at the membrane and the temperature at the submersible pump during laboratory experiments. Error bars (1-σ) reflect the precision of the M-CRDS (1.1 %). 38

Figure 15: Results from first field application of the M-CRDS. Depth profiles for CH_4 were analysed by M-CRDS, M-ICOS and GC-FID analysis (a), for CH_4 and $\delta^{13}C$-CH_4 (b) and for temperature and O_2 in July 2015 (c). Results of the 24-hour measurement performed at the depth of maximum CH_4 concentration (7 m) at the LakeLab (Lake Stechlin) from August 17th to 18th, 2015 reveal high temporal variations in CH_4 concentration (d) and $\delta^{13}C$-CH_4 (e). Night time marked in grey. Keeling-Plot analysis of the 24-hour measurement (f). The extrapolated intercepts of the best fit in the Keeling plot provide the isotope ratios of the CH_4 sources (-34.55 ± 0.05‰ and -53.17 ± 0.10‰) (Sokal and Rohlf 1995; Pataki et al. 2003). 41

Figure 16: Offset between CH_4 concentrations measured by M-CRDS in comparison with GC-FID (squares) and M-ICOS (dots) (d). Error bars (1-σ) of measurements mainly lie within symbols and reflect the noise within the measurement interval (10 min). 44

Figure 17: Location of Lake Willersinnweiher in Germany and sampling locations (W1-W4) at Lake Willersinnweiher as well as groundwater wells GW-inflow and GW-outflow, sampled in May 2017, October 2017 and February 2018. Groundwater table contour modified after Wollschläger et al. (2007). 48

Figure 18: *STIFF*-diagrams of groundwater inflow and outflow as well as lake water for early-stage thermal stratification (a-c), late-stage thermal stratification (d-f) and winter circulation (g-i). The groundwater of the upstream (inflow) of Lake Willersinnweiher is classified as Ca-HCO_3^-- SO_4^{2-} type water, downstream

(outflow) of Lake Willersinnweiher as Ca-HCO_3 type water. The groundwater outflow was not analysed for early-stage thermal stratification. 55

Figure 19: The water column of Lake Willersinnweiher at all sites (W1 to W4) for the early-stage thermal stratification (a-f), late-stage thermal stratification (g-l) and winter circulation (m-r). 59

Figure 20: Geochemical pore-water profiles of selected elements at site W1 (a-f), site W2 (g-m), site W3 (n-s) and site W4 (t-y) in the sediments of Lake Willersinnweiher for the early-stage stratification (May 2017). Sedimentary fluxes of CH_4 are indicated by bold lines and are given in mmol m^{-2} d^{-1}. 63

Figure 21: Stacked fluxes of Mn, CH_4 and SO_4^{2-} in the sediments versus the respective lake depth of the sediments in Lake Willersinnweiher (A). Sedimentary conversion rates of OM (SCR) (calculated as the sum of internal production (CH_4 and Mn) and internal consumption (SO_4^{2-})) and calculated DIC fluxes with lake depth of the sampled sediments in Lake Willersinnweiher (B). Calculated rates are in the range of observed DIC fluxes in the sediments. Sulphate reduction is the main pathway of OM conversion in the sediments of Lake Willersinnweiher. Methane cycling plays an essential role within sediments of Lake Willersinnweiher. 66

Figure 22: Sulphate and methane concentrations in the pore-water at different sediment depths of the sites W1-W4 of Lake Willersinnweiher. The sulphate-methane transition zones (SMTZ) are characterised by minimum SO_4^{2-} and CH_4 concentrations in the pore-water. Data indicate the presence of anaerobic oxidation of methane (AOM) by methane-oxidizing archaea and sulphate-reducing bacteria in the upper sediment layers, consuming upward migrating CH_4. Rates for CH_4 and SO_4^{2-} consumption are indicated by the dashed and dotted lines, respectively, and are given in mmol m^{-2} d^{-1}. 68

Figure 23: The interaction of carbon and sulphur cycling in sediments. Modified after Borowski et al. (1997) for the conditions at Lake Willersinnweiher. 69

Figure 24: Percentage of produced CH_4 released across the sediment-water interface into the bottom water as well as well as AOM efficiency (percentage of produced CH_4 oxidised in SMTZ in the sediments) with respect to the lake depth of the sediments in Lake Willersinnweiher. 70

Figure 25: O_2 and CH_4 concentrations at the redoxcline in Lake Willersinnweiher during early-stage stratification (A-B) and late-stage stratification (C-D). Aerobic oxidation of methane consumes upward migrating CH_4 released from the sediments. Rates for CH_4 and O_2 consumptions are indicated by the dashed and dotted lines, respectively, and are given in mmol m^{-2} d^{-1}. 72

Figure 26: Keeling-Plot for the water samples from Lake Willersinnweiher for early-stage thermal stratification (A), late-stage thermal stratification (B) and winter circulation (C). The extrapolated intercepts of the best fit in the Keeling plot provide the isotope ratio of the different sources of CH_4 in Lake Willersinnweiher. Error bars (1-σ) of measurements reflect the noise within the measurement interval (10 min) and mainly lie within symbols. Best fit and intercepts were estimated by geometric mean regression. 73

Figure 27: Calculated $CaCO_3$ solubility by *PHREEQC* (Parkhurst and Appelo 1999) for early-stage (A) and late-stage stratification (B) of Lake Willersinnweiher. No pH data was available for the winter circulation (C). $CaCO_3$ precipitates in surface water and dissolves in deeper waters of Lake Willersinnweiher. 79

Figure 28: Air temperature and maximum wind speed at Lake Willersinnweiher for 2017 and 2018 (a). Annual CH_4 emissions from Lake Willersinnweiher based on calculations from campaigns during early-stage and late-stage stratification as well as winter circulation (b). Methane emissions during autumn overturn were conservatively estimated by calculations based on literature data (e.g. Encinas Fernández et al. 2014). Methane emission rates for autumn overturn

were calculated for minimum (45°%) and maximum (95 %) CH_4 oxidation rates reported in the literature. Wind speed and air temperature data was obtained from a nearby weather station (49.51° N / 8.55° E). Note: y-axis (Flux CH_4) in logarithmic scale. 81

Figure 29: Methane mass balance for May 2017 in Lake Willersinnweiher. Interpolated CH_4 logarithmic concentration in the water column (*QGIS Desktop 2.18.4*, TIN *(triangular irregular network*) method) as well as the estimated rates for production and consumption of CH_4 within the water column and the sediments of Lake Willersinnweiher during early-stage stratification (May 2017). Data for whole-lake CH_4 mass balance is presented in the appendix. 84

Figure 30: Position of the sampling locations (LakeLab, profundal and littoral) in June 2017 and the Leibniz-Institute of Freshwater Ecology and Inland Fisheries, Berlin (IGB). Bathymetric map of Lake Stechlin was modified after Aichner et al. (2017). 87

Figure 31: The water column at the LakeLab, exemplarily shown for June 15th 2017 (Lake Stechlin). 92

Figure 32: Continuous 2-week depth profiles at the LakeLab at Lake Stechlin. Average wind speed, CH_4 fluxes and sunshine duration (A), turbulence at 2 m and 7 m water depth as well as fluxes at the thermocline (B), temperature (C), oxygen saturation (D), cyanobacteria (E), diatoms (F) green algae (G), cryptophytae (H), CH_4 concentration (I) and $\delta^{13}C$-CH_4 values (K) interpolated from measurements at Lake Stechlin in June 2017. Grey points indicate the sampling time and depths. 94

Figure 33: Geochemical profiles of selected elements in the pore-water of the sediments at the LakeLab (a-f), at the profundal site (g-m) and the littoral site (n-s) of Lake Stechlin in June 2017. Pore-water CH_4 concentration and CH_4 diffusive fluxes calculated with Fick's 1st law. Pore-water fluxes are given in mmol m^{-2} d^{-1}. 96

Figure 34: Net oxic CH_4 production for non-steady state conditions (225 ± 170 nM d^{-1}), water-to-Air CH_4 Flux (F_S, light grey), upwards diffusion from the thermocline (F_Z, dark grey) as well as mean values of CH_4 production for Lake Stechlin, Lake Halwill (Donis et al. 2017) and Lake Cromwell (Bogard et al. 2014). Error bars represent 1-σ standard deviation. 99

Figure 35: Box-Whisker-Plots (*whisker mode:* 1 SD) for surface water CH_4 concentration (A), $\delta^{13}C$-CH_4 values (B) and oxic CH_4 production rates (C) with respect to the time of day. No significant correlations were found for oxic CH_4 production with suggested factors controlling the oxic CH_4 production such as radiation. 101

Figure 36: Correlation of *in-situ* results of cyanobacteria within the cyanobacteria bloom (A,B), diatom within the diatom bloom (C,D), green algae (E,F) and cryptophytae (G,H) with the CH_4 concentration and $\delta^{13}C$-CH_4 values in the surface water layer of Lake Stechlin. Temporally missing correlation between phytoplankton and CH_4 accumulation is most likely due to wind-induced loss of CH_4 by emission to the atmosphere. 103

Figure 37: Laboratory incubation results for diatoms (red), green algae (green) and cryptophytes (orange). Incubation of cyanobacteria was not evaluated within the frame of this study. $\delta^{13}C$-CH_4 values of headspace CH_4 from cultures ($NaH^{13}CO_3$) and WC-medium (control) incubated with or without (control) a treatment of $NaH^{13}CO_3$ (filled and empty dots, respectively). Laboratory incubations were conducted by Thomas Klintzsch (Heidelberg University)... 104

Figure 38: Correlation of the wind speed with CH_4 flux and summed epilimnic CH_4 concentration (A). Increasing wind speed (> 2 m/s) leads to decreasing CH_4 concentration in the water column and increasing CH_4 emissions. Diffusion from the thermocline to the surface water by wind-induced turbulence (B). Reduced CH_4 concentration in the uppermost 5 m by lowering the CH_4 concentration gradients within the surface water layer due to an upwelling of

colder deep water with lower CH_4 concentration and slightly lighter $\delta^{13}C$-CH_4 values. Outliers in (b) are drawn as empty circles. Error bars represent the standard deviation. 106

Figure 39: Wind speed (A), *in-situ* results of cyanobacteria (blue) and diatoms (red), the CH_4 concentration (B) and the $\delta^{13}C$-CH_4 values (C) in the water column. When merged together, the data of CH_4 accumulation and pigment presence of cyanobacteria and diatoms showed good spatial and temporal coverage. Temporally missing correlation between phytoplankton and CH_4 accumulation is best explained by wind-induced loss of CH_4 by emission to the atmosphere. 108

Figure 40: Lake Erken, 60 km north east of Stockholm, Sweden. Position of the sampling locations (*Malma Islet* and littoral site in front of *Erken Laboratoriet*), transects (red dotted) and sampling sites for continuous measurements near *Malma Islet* at Lake Erken, sampled in July 2017. The bathymetric map of Lake Erken was modified after Eidborn (2015). 110

Figure 41: Geochemical pore-water profiles of selected elements in the sediments of Lake Erken taken at the littoral (a-f) and profundal (g-m) sites in August 2017. Methane diffusive fluxes calculated with Fick's 1st law (d and k) and production rates are given in mmol m^{-2} d^{-1}. Note the different scales on the x-axis for Fe, Mn and P of the profundal and littoral site. 116

Figure 42: Geochemical profiles of selected elements in the water column of Lake Erken at the site of the continuous measurement (buoy) in August 2017. 117

Figure 43: Spatial distribution of Ca (a), DIC (b), Fe (c), Mn (d) and CH_4 (e) concentrations in the surface water layer of Lake Erken in August 2017. The buoy site is encircled. 118

Figure 44: Temporal variations in wind speed (raw data and 2 h mean) and sunshine (expressed in PAR *Photosynthetically Active Radiation*) (A), wind direction (B), CH_4 concentration and $\delta^{13}C\text{-}CH_4$ values (raw data and 2 h mean) (C) and CH_4 concentration measured by GC, UWMS and M-CRDS (D). The pump location was changed from the littoral site a few meters offshore the island to the profundal buoy site, 50 m offshore the island, during July 20th (marked in grey). 119

Figure 45: Offset between CH_4 concentrations measured by M-CRDS in comparison with GC-FID for depth profiles (A) as well as GC-FID (B) and UWMS (C) for continuous CH_4 concentration measurements at the buoy site (Lake Erken). The pump location was changed from few meters offshore to the profundal buoy site, 50 m offshore the island, during July 20th (marked in green). 121

Figure 46: Correlation of wind speed (A and B) and radiation (C and D) with CH_4 concentrations (A and C) and $\delta^{13}C\text{-}CH_4$ values (B and D) of lake water at *Malma Islet*. 124

Figure 47: CH_4 concentrations of the surface water layer with distance from shore at Lake Erken. Surface water samples from the south-western (solid) and the eastern bay (dotted) of Lake Erken are encircled. The predicted concentration area was calculated after DelSontro et al. (2017) using the *elongated model* and assuming either no MOx or minimum and maximum MOx rates reported for moderate to high latitude lakes (Bastviken et al. 2002, 2003). 125

Figure 48: Correlation of wind speed (A and C) and wind direction (C and D) with CH_4 concentration (A and C) and $\delta^{13}C\text{-}CH_4$ values (B and D) at the profundal site. 128

Figure 49: CH_4 concentrations in the surface water layer with distance to the shore at the different lakes studied. The predicted concentration area was

calculated after DelSontro et al. (2017) using the *elongated model* and assuming either no MOx or minimum and maximum MOx rates reported for similar lakes (Bastviken et al. 2002, 2003; Bogard et al. 2014; Tang et al. 2014; Oswald et al. 2015). Equations and parameters used for the calculations are listed in the appendix. 139

6. List of Tables

Table 1: Results of the characterisation of the M-CRDS for CH_4 concentration and $\delta^{13}C$-CH_4 30

Table 2: Comparison of response times for the simultaneous determination of CH_4 and $\delta^{13}C$-CH_4 in water from other studies for different devices (after Webb et al. (2016)) compared with response times calculated for the M-CRDS (this study)..... 33

Table 3: Locations sampled at Lake Willersinnweiher. Water depth for groundwater wells are expressed as groundwater level below gauge top..... 49

Table 4: Constants for the calculation of Bunsen Solubility Coefficient $\boldsymbol{\beta}$ (Wiesenburg and Guinasso 1979)..... 53

Table 5: Parameters used for the CH_4 mass balance at Lake Willersinnweiher. 54

Table 6: Concentrations of major elements in epilimnion as well as groundwater inflow and outflow of Lake Willersinnweiher for early-stage thermal stratification, late-stage thermal stratification and winter circulation.

Groundwater outflow was not analysed for CH_4 concentrations during early-stage thermal stratification. 56

Table 7: Calculated fluxes into the epilimnion for DIC and Ca^{2+} (upwards) and into the oxycline for CH_4 (upwards) and Mn and O_2 (downwards) in the water column. Methane emission from the epilimnion and internal CH_4 production in Lake Willersinnweiher were estimated from surface water CH_4 concentrations. Note: Production rates are given in [µmol m^{-3} d^{-1}]. 61

Table 8: Sedimentary conversion rates of organic carbon (SCR) calculated from redox-processes (via eq. [18] to [23]) and DIC fluxes within the sediments of Lake Willersinnweiher for early-stage stratification. Rates are given in mmol m^{-2} d^{-1}. 64

Table 9: Potential pathways for CH_4 accumulation in groundwater upstream of Lake Willersinnweiher 75

Table 10: Parameters used for the calculation of the CH_4 mass balance at Lake Stechlin 90

Table 11: Locations sampled at Lake Erken. Profundal "buoy site" and shallow shore site at *Malma Islet* was analysed by M-CRDS and GC-FID, transect locations were analysed by GC-FID only. Cores were taken at the buoy site and at the Littoral site in front of Erken Laboratoriet. 112

Table 12: Equations and parameters adjusted for Lake Erken, used for the model calculations in Figure 47 after DelSontro et al. (2017). 126

7. References

Abril, G., and N. Iversen. 2002a. Methane dynamics in a shallow non-tidal estuary (Randers Fjord, Denmark). Mar. Ecol. Prog. Ser. **230**: 171–181. doi:10.3354/meps230171

Abril, G., and N. Iversen. 2002b. Methane dynamics in a shallow non-tidal estuary. **230**: 171–181.

Aichner, B., S. Hilt, C. Périllon, M. Gillefalk, and D. Sachse. 2017. Biosynthetic hydrogen isotopic fractionation factors during lipid synthesis in submerged aquatic macrophytes: Effect of groundwater discharge and salinity. Org. Geochem. **113**: 10–16. doi:10.1016/j.orggeochem.2017.07.021

Allan, W., H. Struthers, and D. C. Lowe. 2007. Methane carbon isotope effects caused by atomic chlorine in the marine boundary layer: Global model results compared with Southern Hemisphere measurements. J. Geophys. Res. Atmos. **112**: 1–10. doi:10.1029/2006JD007369

AlNajem, S. 2016. Hydrogeochemische Charakterisierung von Grundwässern des Oberrheingrabens zur Identifizierung störungsbedingter Tiefenwasser-Einflüsse. Ruprecht-Karls-Universität Heidelberg.

Amos, R. T., B. A. Bekins, G. N. Delin, I. M. Cozzarelli, D. W. Blowes, and J. D. Kirshtein. 2011. Methane oxidation in a crude oil contaminated aquifer: Delineation of aerobic reactions at the plume fringes. J. Contam. Hydrol. **125**: 13–25. doi:10.1016/j.jconhyd.2011.04.003

Andreas, E. L., K. J. Claffey, R. E. Jordan, C. W. Fairall, P. S. Guest, P. O. G. Persson, and A. A. Grachev. 2006. Evaluations of the von Kármán constant in the atmospheric surface layer. J. Fluid Mech. **559**: 117. doi:10.1017/S0022112006000164

Appelo, C., and D. Postma. 2005. Geochemistry, groundwater and pollution, 2nd ed. A.A. Balkema Publishers.

Azadpour-Keeley, A., G. W. Sewell, and H. H. Russell. 2005. Microbial Processes Affecting Monitored Natural Attenuation of Contaminants in the Subsurface, p. 1–25. *In* Water Encyclopedia. John Wiley & Sons, Inc.

Barker, J. F., and P. Fritz. 1981. Carbon isotope fractionation during microbial methane oxidation. Nature **293**: 289–291. doi:10.1038/293289a0

Bastviken, D., J. J. Cole, M. L. Pace, and M. C. Van de Bogert. 2008. Fates of methane from different lake habitats: Connecting whole-lake budgets and CH_4 emissions. J. Geophys. Res. Biogeosciences **113**: n/a-n/a. doi:10.1029/2007JG000608

Bastviken, D., J. Cole, M. Pace, and L. Tranvik. 2004. Methane emissions from lakes: Dependence of lake characteristics, two regional assessments, and a global estimate. Global Biogeochem. Cycles **18**: n/a-n/a. doi:10.1029/2004GB002238

Bastviken, D., J. Ejlertsson, I. Sundh, and L. Tranvik. 2003. Methane as a source of carbon and energy for lake pelagic food webs. Ecology **84**: 969–981. doi:Doi 10.1890/0012-9658(2003)084[0969:Maasoc]2.0.Co;2

Bastviken, D., J. Ejlertsson, and L. Tranvik. 2002. Measurement of methane oxidation in lakes: A comparison of methods. Environ. Sci. Technol. **36**: 3354–3361. doi:10.1021/es010311p

Bastviken, D., A. L. Santoro, H. Marotta, L. Q. Pinho, D. F. Calheiros, P. Crill, and A. Enrich-Prast. 2010. Methane emissions from Pantanal, South America, during the low water season: toward more comprehensive sampling. Environ. Sci. Technol. **44**: 5450–5. doi:10.1021/es1005048

Bastviken, D., L. J. Tranvik, J. A. Downing, P. M. Crill, and A. Enrich-Prast. 2011. Freshwater Methane Emissions Offset the Continental Carbon Sink. Science (80-.). **331**: 50–50. doi:10.1126/science.1196808

Beal, E. J., C. H. House, and V. J. Orphan. 2009. Manganese- and Iron-Dependent Marine Methane Oxidation. Science (80-.). **325**: 184–187. doi:10.1126/science.1169984

Berner, R. A. 1981. A New Geochemical Classification of Sedimentary Environments. J. Sediment. Petrol. **51**: 359–365.

Biswas, H., S. K. Mukhopadhyay, S. Sen, and T. K. Jana. 2007. Spatial and temporal patterns of methane dynamics in the tropical mangrove dominated estuary, NE coast of Bay of Bengal, India. J. Mar. Syst. **68**: 55–64. doi:10.1016/j.jmarsys.2006.11.001

Blees, J., H. Niemann, M. Erne, J. Zopfi, C. J. Schubert, and M. F. Lehmann. 2015. Spatial variations in surface water methane super-saturation and emission in Lake Lugano, southern Switzerland. Aquat. Sci. **77**: 535–545. doi:10.1007/s00027-015-0401-z

Boehrer, B., and M. Schultze. 2008. Stratification of lakes. Rev. Geophys. **46**: 1–27. doi:10.1029/2006RG000210

Boetius, A., K. Ravenschlag, C. J. Schubert, and others. 2000. A marine microbial consortium apparently mediating anaerobic oxidation of methane. Nature **407**: 623–626. doi:10.1038/35036572

Bogard, M. J., P. A. Del Giorgio, L. Boutet, M. C. G. Chaves, Y. T. Prairie, A. Merante, and A. M. Derry. 2014. Oxic water column methanogenesis as a major component of aquatic CH_4 fluxes. Nat. Commun. **5**: 1–9. doi:10.1038/ncomms6350

Borges, A. V., J.-P. Vanderborght, L.-S. Schiettecatte, F. Gazeau, S. Ferrón-Smith, B. Delille, and M. Frankigoulle. 2004. Variability of the Gas Transfer Velocity of Estuary (the Scheldt) in a Macrotidal. Estuaries **0**: 593–603.

Borowski, W. S., C. K. Paull, and W. Ussier. 1997. Carbon cycling within the upper methanogenic zone of continental rise sediments: An example from the methane-rich sediments overlying the blake ridge gas hydrate deposits. Mar. Chem. **57**: 299–311. doi:10.1016/S0304-4203(97)00019-4

Borowski, W. S., C. K. Paull, and W. Ussler. 1999. Global and local variations of interstitial sulfate gradients in deep-water, continental margin sediments: Sensitivity to underlying methane and gas hydrates. Mar. Geol. **159**: 131–154. doi:10.1016/S0025-3227(99)00004-3

Botz, R., G. Winckler, R. Bayer, M. Schmitt, M. Schmidt, D. Garbe-Schönberg, P. Stoffers, and J. K. Kristjansson. 1999. Origin of trace gases in submarine hydrothermal vents of the Kolbeinsey Ridge, north Iceland. Earth Planet. Sci. Lett. **171**: 83–93. doi:10.1016/S0012-821X(99)00128-4

Boudreau, B. P. 1996. Diagenetic models and their implementation. Modelling transport and reactions in aquatic sediments,.

Boulart, C., D. P. Connelly, and M. C. Mowlem. 2010. Sensors and technologies for in situ dissolved methane measurements and their evaluation using Technology Readiness Levels. TrAC - Trends Anal. Chem. **29**: 186–195.

doi:10.1016/j.trac.2009.12.001

Broecker, W. S., and T.-H. Peng. 1974. Gas exchange rates between air and sea. Tellus **26**: 21–35. doi:10.3402/tellusa.v26i1-2.9733

Brooks, J. M., and W. M. Sackett. 1973. Sources, sinks, and concentrations of light hydrocarbons in the Gulf of Mexico. J. Geophys. Res. **78**: 5248–5258. doi:10.1029/JC078i024p05248

Brunskill, G. J. 1969. Fayetteville Green Lake, New York. II. Precipitation and Sedimentation of Calcite in a Meromictic Lake with Laminated Sediments. Limnol. Oceanogr. **14**: 830–847. doi:10.4319/lo.1969.14.6.0830

Burke, R. A., T. R. Barber, and W. M. Sackett. 1988. Methane flux and stable hydrogen and carbon isotope composition of sedimentary methane from the Florida Everglades. Global Biogeochem. Cycles **2**: 329–340. doi:10.1029/GB002i004p00329

Bussmann, I., E. Damm, M. Schlüter, and M. Wessels. 2013. Fate of methane bubbles released by pockmarks in Lake Constance. Biogeochemistry **112**: 613–623. doi:10.1007/s10533-012-9752-x

Call, M., D. T. Maher, I. R. Santos, and others. 2015. Spatial and temporal variability of carbon dioxide and methane fluxes over semi-diurnal and spring-neap-spring timescales in a mangrove creek. Geochim. Cosmochim. Acta **150**: 211–225. doi:10.1016/j.gca.2014.11.023

Capone, D. G., and R. P. Kiene. 1988. Comparison of microbial dynamics in marine and freshwater sediments: Contrasts in anaerobic carbon catabolism. Limnol. Oceanogr. **33**: 725–749. doi:10.4319/lo.1988.33.4part2.0725

Cappenberg, T. E. 1974. Interrelaions between sulfate-reducing and methane-producing bacteria in bottom deposits of a freshwater lake. I. Field observations. Antonie Van Leeuwenhoek J. Microbiol. **40**: 285–295.

Cappenberg, T. E. 1975. A study of mixed continuous cultures of sulfate-reducing and methane-producing bacteria. Microb. Ecol. **2**: 60–72. doi:10.1007/BF02010381

Casper, P., D. D. Adams, A. L. S. Furtado, O. C. Chan, T. Gonsiorczyk, and R. Koschel. 2005. Greenhouse gas cycling in aquatic ecosystems - methane in temperate lakes across an environmental gradient in northeast Germany. Verh. Internat. Verein. Limnol. **29**: 564–566.

Casper, S. J., ed. 1985. Lake Stechlin: A temperate oligotrophic lake, Springer Netherlands.

Chameides, W., and J. C. C. G. Walker. 1973. A photochemical theory of tropospheric ozone. Journa Gecophysical Res. **78**: 8751–8760. doi:10.1029/JC078i036p08751

Chanton, J. P., and G. J. Whiting. 1995. Trace gas exchange in freshwater and coastal marine environments: ebullition and transport by plants, p. 98–125. *In* Biogenic trace gases: measuring emissions from soil and water.

Chanton, J. P., G. J. Whiting, N. E. Blair, C. W. Lindau, and P. K. Bollich. 1997. Stable isotopes, diurnal variations, and C02 exchange from of belowground was correlated to the quantity of live aboveground biomass and the rate of CO were methane was observed in the floodwater overlying the. Global Biogeochem. Cycles **11**: 15–27.

Cicerone, R. J., and R. S. Oremland. 1988. Biogeochemical aspects of atmospheric methane. Global Biogeochem. Cycles **2**: 299–327. doi:10.1029/GB002i004p00299

Clayton, C. 1991. Carbon isotope fractionation during natural gas generation from kerogen. Mar. Pet. Geol. **8**.

Cole, J. J., and N. F. Caraco. 1998. Atmospheric exchange of carbon dioxide in a low-wind oligotrophic lake measured by the addition of SF_6. Limnol. Oceanogr. **43**: 647–656. doi:10.4319/lo.1998.43.4.0647

Cole, J. J., Y. T. Prairie, N. F. Caraco, and others. 2007. Plumbing the global carbon cycle: Integrating inland waters into the terrestrial carbon budget. Ecosystems **10**: 171–184. doi:10.1007/s10021-006-9013-8

Coleman, D. D., J. B. B. Risatti, and M. Schoell. 1981. Fractionation of carbon and hydrogen isotopes by methane-oxidizing bacteria. Geochim. Cosmochim. Acta **45**: 1033–1037. doi:10.1016/0016-7037(81)90129-0

Conrad, R. 1989. Control of methane production in terrestrial ecosystems, p. 39–58. *In* D.S. Andreae, M.O., Schimel [ed.], Exchange of Trace Gases between Terrestrial Ecosystems and the Atmosphere. Dahlem Konferenzen, Wiley, Chicester,.

Conrad, R. 2005. Quantification of methanogenic pathways using stable carbon isotopic signatures: A review and a proposal. Org. Geochem. **36**: 739–752. doi:10.1016/j.orggeochem.2004.09.006

Conrad, R., O.-C. Chan, P. Claus, and P. Casper. 2007. Characterization of methanogenic Archaea and stable isotope fractionation during methane production in the profundal sediment of an oligotrophic lake (Lake Stechlin, Germany). Limnol. Oceanogr. **52**: 1393–1406. doi:10.4319/lo.2007.52.4.1393

Craig, H. 1957. Isotopic standards for carbon and oxygen and correction factors for mass-spectrometric analysis of carbon dioxide. Geochim. Cosmochim. Acta **12**: 133–149. doi:10.1016/0016-7037(57)90024-8

Crowe, S. A., S. Katsev, K. Leslie, and others. 2011. The methane cycle in ferruginous Lake Matano. Geobiology **9**: 61–78. doi:10.1111/j.1472-4669.2010.00257.x

Crutzen, P. 1973. A discussion of the chemistry of some minor constituents in the stratosphere and troposphere. Pure Appl. Geophys. **106–108**: 1385–1399. doi:10.1007/BF00881092

Crutzen, P. J., and P. H. Zimmermann. 1991. The changing photochemistry of the troposphere. Tellus B **43**: 136–151. doi:10.1034/j.1600-0889.1991.t01-1-00012.x

Curry, C. L. 2007. Modeling the soil consumption at atmospheric methane at the global scale. Global Biogeochem. Cycles **21**: 1–15. doi:10.1029/2006GB002818

Dale, A. W., D. R. Aguilera, P. Regnier, H. Fossing, N. J. Knab, and B. B. Jørgensen. 2008. Seasonal dynamics of the depth and rate of anaerobic oxidation of methane in Aarhus Bay (Denmark) sediments. J. Mar. Res. **66**: 127–155. doi:10.1357/002224008784815775

Dando, P. R., J. A. Hughes, Y. Leahy, S. J. Niven, L. J. Taylor, and C. Smith. 1995. Gas venting rates from submarine hydrothermal areas around the island of Milos, Hellenic Volcanic Arc. Cont. Shelf Res. **15**: 913–929. doi:10.1016/0278-4343(95)80002-U

DelSontro, T., P. A. Giorgio, and Y. T. Prairie. 2017. No Longer a Paradox : The Interaction Between Physical Transport and Biological Processes Explains the Spatial Distribution of Surface Water Methane Within and Across Lakes. Ecosystems. doi:10.1007/s10021-017-0205-1

DelSontro, T., M. J. Kunz, T. Kempter, A. Wüest, B. Wehrli, and D. B. Senn. 2011. Spatial heterogeneity of methane ebullition in a large tropical reservoir. Environ. Sci. Technol. **45**: 9866–9873. doi:10.1021/es2005545

Denfeld, B. A., M. Ricão Canelhas, G. A. Weyhenmeyer, S. Bertilsson, A. Eiler, and D. Bastviken. 2016. Constraints on methane oxidation in ice-covered boreal lakes. J. Geophys. Res. Biogeosciences **121**: 1924–1933. doi:10.1002/2016JG003382

Deutzmann, J. S., P. Stief, J. Brandes, and B. Schink. 2014. Anaerobic methane oxidation coupled to denitrification is the dominant methane sink in a deep lake. Proc. Natl. Acad. Sci. **111**: 18273–18278. doi:10.1073/pnas.1411617111

Dlugokencky, E. J., E. G. Nisbet, R. Fisher, and D. Lowry. 2011. Global atmospheric methane: budget, changes and dangers. Philos. Trans. R. Soc. A Math. Phys. Eng. Sci. **369**: 2058–2072. doi:10.1098/rsta.2010.0341

Donis, D., S. Flury, A. Stöckli, J. E. Spangenberg, D. Vachon, and D. F. McGinnis. 2017. Full-scale evaluation of methane production under oxic conditions in a mesotrophic lake. Nat. Commun. **8**: 1661. doi:10.1038/s41467-017-01648-4

Dumestre, J. F., J. Guézennec, C. Galy-Lacaux, R. Delmas, S. Richard, L. Labroue, and J. Guezennec. 1999. Influence of light intensity on methanotrphic bacterial activity in Petit Saut reservoir, French Guiana. Appl. Environ. Microbiol. **65**: 534–539.

Dyer, K. R., M. C. Christie, and A. J. Manning. 2004. The effects of suspended sediment on turbulence within an estuarine turbidity maximum. Estuar. Coast. Shelf Sci. **59**: 237–248. doi:10.1016/j.ecss.2003.09.002

Effler, S. W., and C. T. Driscoll. 1985. Calcium Chemistry and Deposition in Ionically Enriched Onondaga Lake, New York. Environ. Sci. Technol. **19**: 716–720. doi:10.1021/es00138a010

Eidborn, A. 2015. Bathymetric map of Lake Erken.

Encinas Fernández, J., F. Peeters, and H. Hofmann. 2014. Importance of the autumn overturn and anoxic conditions in the hypolimnion for the annual methane emissions from a temperate lake. Environ. Sci. Technol. **48**: 7297–7304. doi:10.1021/es4056164

Encinas Fernández, J., F. Peeters, and H. Hofmann. 2016. On the methane paradox: Transport from shallow water zones rather than in situ methanogenesis is the major source of CH_4 in the open surface water of lakes. J. Geophys. Res. Biogeosciences **121**: 2717–2726. doi:10.1002/2016JG003586

Ernst, W. H. O. 1990. Ecophysiology of plants in waterlogged and flooded environments. Aquat. Bot. **38**: 73–90. doi:10.1016/0304-3770(90)90099-7

Ettwig, K. F., S. Shima, K. T. Van De Pas-Schoonen, J. Kahnt, M. H. Medema, H. J. M. Op Den Camp, M. S. M. Jetten, and M. Strous. 2008. Denitrifying bacteria anaerobically oxidize methane in the absence of Archaea. Environ. Microbiol. **10**: 3164–3173. doi:10.1111/j.1462-2920.2008.01724.x

Eugster, W., T. DelSontro, and S. Sobek. 2011. Eddy covariance flux measurements confirm extreme CH4 emissions from a Swiss hydropower reservoir and resolve their short-term variability. Biogeosciences **8**: 2815–2831. doi:10.5194/bg-8-2815-2011

Faure, G. 1986. Principles of Isotope Geology, 2nd ed. John Wiley and Sons.

Ferry, J. G. 2011. Fundamentals of methanogenic pathways that are key to the biomethanation of complex biomass. Curr. Opin. Biotechnol. **22**: 351–357. doi:10.1016/j.copbio.2011.04.011

Frankignoulle, M. 1988. Field measurements of air-sea CO2 exchange. Limnol. Oceanogr. **33**: 312–322.

Freundt, F. 2017. Application of helium isotopes in shallow groundwaters for geothermal energy exploration in the upper Rhine graben. Universität Heidelberg.

Froelich, P. N., G. P. Klinkhammer, M. L. Bender, and others. 1978. Early oxidation of organic matter in pelagic sediments of the eastern equatorial Atlantic: suhoxic diagenesis.

Games, L. M., J. M. Hayes, and R. P. Gunsalus. 1978. Methane producing bacteria: Natural fractionations of the stable carbon isotopes. Geochim. Cosmochim. Acta 1295–1297.

Gentz, T., E. Damm, J. Schneider von Deimling, S. Mau, D. F. McGinnis, and M. Schlüter. 2014. A water column study of methane around gas flares located at the West Spitsbergen continental margin. Cont. Shelf Res. **72**: 107–118. doi:10.1016/j.csr.2013.07.013

Giling, D. P., J. C. Nejstgaard, S. A. Berger, and others. 2016. Thermocline deepening boosts ecosystem metabolism: Evidence from a large-scale lake enclosure experiment simulating a summer storm. Glob. Chang. Biol. 1–15. doi:10.1111/gcb.13512

Goedkoop, W., and R. K. Johnson. 1996. Pelagic-benthic coupling: Profundal benthic community response to spring diatom deposition in mesotrophic Lake Erken. Limnol. Oceanogr. **41**: 636–647. doi:10.4319/lo.1996.41.4.0636

Gonzalez-Valencia, R., F. Magana-Rodriguez, O. Gerardo-Nieto, A. Sepulveda-Jauregui, K. Martinez-Cruz, K. Walter Anthony, D. Baer, and F. Thalasso. 2014. In Situ Measurement of Dissolved Methane and Carbon Dioxide in Freshwater Ecosystems by Off-Axis Integrated Cavity Output Spectroscopy. Environ. Sci. Technol. **48**: 11421–11428. doi:10.1021/es500987j

Grossart, H.-P., K. Frindte, C. Dziallas, W. Eckert, and K. W. Tang. 2011. Microbial methane production in oxygenated water column of an oligotrophic lake. Proc. Natl. Acad. Sci. **108**: 19657–19661. doi:10.1073/pnas.1110716108

Gründger, F., N. Jiménez, T. Thielemann, N. Straaten, T. Lüders, H. H. Richnow, and M. Krüger. 2015. Microbial methane formation in deep

aquifers of a coal-bearing sedimentary basin, Germany. Front. Microbiol. **6**. doi:10.3389/fmicb.2015.00200

Gülzow, W., G. Rehder, J. Schneider v. Deimling, T. Seifert, and Z. Tóth. 2013. One year of continuous measurements constraining methane emissions from the Baltic Sea to the atmosphere using a ship of opportunity. Biogeosciences **10**: 81–99. doi:10.5194/bg-10-81-2013

Hamilton, S., S. Sippel, J. Chanton, and J. Melack. 2014. Plant-mediated transport and isotopic composition of methane from shallow tropical wetlands. Inl. Waters **4**: 369–376. doi:10.5268/IW-4.4.734

Hansson, A. L., H. Annadotter, E. Bergman, and others. 2017. Biomanipulation as an Appl of Food-Chain Theory : Const Synthesis , and Recommend for Temperate Lakes. 558–574.

Hartmann, J. F., T. Gentz, A. Schiller, and others. 2018. A fast and sensitive method for the continuous in situ determination of dissolved methane and its δ^{13}C-isotope ratio in surface waters. Limnol. Oceanogr. Methods. doi:10.1002/lom3.10244

He, Z., Q. Zhang, Y. Feng, H. Luo, X. Pan, and G. M. Gadd. 2018. Microbiological and environmental significance of metal-dependent anaerobic oxidation of methane. Sci. Total Environ. **610–611**: 759–768. doi:10.1016/j.scitotenv.2017.08.140

Henry, W. 1803. Experiments on the Quantity of Gases Absorbed by Water, at Different Temperatures, and under Different Pressures. Philos. Trans. R. Soc. London **93**: 29–274. doi:10.1098/rstl.1803.0004

den Heyer, C., and J. Kalff. 1998. Organic matter mineralization rates in sediments: A within- and among-lake study. Limnol. Oceanogr. **43**: 695–705. doi:10.4319/lo.1998.43.4.0695

Hinrichs, K.-U., J. M. Hayes, S. P. Sylva, P. G. Brewer, and E. F. DeLong. 1999. Methane-consuming archaebacteria in marine sediments. Nature **398**: 802–805. doi:10.1038/19751

Ho, D. T., L. F. Bliven, R. Wanninkhof, and P. Schlosser. 1997. The effect of rain on air-water gas exchange. Tellus B Chem. Phys. Meteorol. **49**: 149–158. doi:10.3402/tellusb.v49i2.15957

Hofmann, H. 2013. Spatiotemporal distribution patterns of dissolved methane in lakes: How accurate are the current estimations of the diffusive flux path? Geophys. Res. Lett. **40**: 2779–2784. doi:10.1002/grl.50453

Hofmann, H., L. Federwisch, and F. Peeters. 2010. Wave-induced release of

methane: Littoral zones as source of methane in lakes. Limnol. Oceanogr. **55**: 1990–2000. doi:10.4319/lo.2010.55.5.1990

Holgerson, M. A., and P. A. Raymond. 2016. Large contribution to inland water CO_2 and CH_4 emissions from very small ponds. Nat. Geosci. **9**: 222–226. doi:10.1038/ngeo2654

Holmer, M., and E. Kristensen. 1996. Seasonality of sulfate reduction and pore water solutes in a marine fish farm sediment: the importance of temperature and sedimentary organic matter. Biogeochemistry **32**: 15–39. doi:10.1007/BF00001530

Holmer, M., and P. Storkholm. 2001. Sulphate reduction and sulphur cycling in lake sediments: a review. Freshw. Biol. **46**: 431–451. doi:10.1046/j.1365-2427.2001.00687.x

Holzbecher, E., G. Nützmann, and G. Ginzel. 1999. Water and component mass balances in the catchment of Lake Stechlin. Proc. Int. Assoc. Hydrol. Sci. **258**: 37–46.

Hornberger, G. M. 1995. New manuscript guidelines for the reporting of stable hydrogen, carbon, and oxygen isotope ratio data. Water Resour. Res. **31**: 2895–2895. doi:10.1029/95WR02430

Hunkeler, D., R. Aravena, K. Berry-Spark, and E. Cox. 2005. Assessment of degradation pathways in an aquifer with mixed chlorinated hydrocarbon contamination using stable isotope analysis. Environ. Sci. Technol. **39**: 5975–5981. doi:10.1021/es048464a

IPCC-Report. 2013. IPCC, 2013: Climate Change 2013: The Physical Science Basis. Contribution of Working Group I to the Fifth Assessment Report of the Intergovernmental Panel on Climate Change, T.F. Stocker, D. Qin, G.-K. Plattner, et al. [eds.]. Cambridge University Press.

Jähne, B. J., K. O. M. Münnich, R. Bösinger, A. Dutzi, W. Huber, and P. Libner. 1987. On the Parameters Influencing Air-Water Gas Exchange. J. Geophys. Res. **92**: 1937–1949. doi:10.1029/JC092iC02p01937

Jammet, M., S. Dengel, E. Kettner, F.-J. W. Parmentier, M. Wik, P. Crill, and T. Friborg. 2017. Year-round CH_4 and CO_2 flux dynamics in two contrasting freshwater ecosystems of the subarctic. Biogeosciences Discuss. 1–49. doi:10.5194/bg-2016-466

Johnson, J. E. 1999. Evaluation of a seawater equilibrator for shipboard analysis of dissolved oceanic trace gases. Anal. Chim. Acta **395**: 119–132. doi:10.1016/S0003-2670(99)00361-X

Jørgensen, B. B., and F. Bak. 1991. Pathways and microbiology of thiosulphate

transformations and sulfate reduction in a marine sediment (Kattegat,Denmark). Appl. Environ. Microbiol. **57**: 847–856.

Jørgensen, B. B., and S. Kasten. 2006. Sulfur Cycling and Methane Oxidation, p. 271–309. *In* Marine Geochemistry. Springer-Verlag.

Juutinen, S., M. Rantakari, P. Kortelainen, J. T. Huttunen, T. Larmola, J. Alm, J. Silvola, and P. J. Martikainen. 2009. Methane dynamics in different boreal lake types. Biogeosciences **6**: 209–223. doi:10.5194/bg-6-209-2009

Kaimal, J. C. 1975. Sensors and techniques for direct measurement of turbulent fluxes and profiles in the atmospheric surface layer, p. 7–14. *In* M. Maisel [ed.], Atmospheric Technology. National Center fo r Atm ospheric Research (NCAR).

Kampbell, D. H., J. T. Wilson, and S. A. Vandegrift. 1989. Dissolved Oxygen and Methane in Water by a GC Headspace Equilibration Technique. Int. J. Environ. Anal. Chem. **36**: 249–257. doi:10.1080/03067318908026878

Kankaala, P., S. Taipale, H. Nykänen, and R. I. Jones. 2007. Oxidation, efflux, and isotopic fractionation of methane during autumnal turnover in a polyhumic, boreal lake. J. Geophys. Res. **112**: G02033. doi:10.1029/2006JG000336

Karl, B., and D. Tilbrook. 1994. Production and transport of methane in oceanic particulate organic matter. Nature **368**: 732–734.

Karl, D. M., L. Beversdorf, K. M. Björkman, M. J. Church, A. Martinez, and E. F. Delong. 2008. Aerobic production of methane in the sea. Nat. Geosci. **1**: 473–478. doi:10.1038/ngeo234

Kasprzak, P., J. Benndorf, T. Mehner, and R. Koschel. 2002. Biomanipulation of lake ecosystems: An introduction. Freshw. Biol. **47**: 2277–2281. doi:10.1046/j.1365-2427.2002.01001.x

Keeling, C. D. 1958. The concentration and isotopic abundances of atmospheric carbon dioxide in rural areas. Geochim. Cosmochim. Acta **13**: 322–334. doi:10.1016/0016-7037(58)90033-4

Kelley, C. A., C. S. Martens, and J. P. Chanton. 1990. Variations in sedimentary carbon remineralization rates in the White Oak River estuary, North Carolina. Limnol. Oceanogr. **35**: 372–383. doi:10.4319/lo.1990.35.2.0372

Kelts, K., and K. J. Hsü. 1978. Freshwater Carbonate Sedimentation. Lakes 295–323. doi:10.1007/978-1-4757-1152-3_9

Keppler, F., J. T. G. Hamilton, M. Braß, and T. Röckmann. 2006. Methane emissions from terrestrial plants under aerobic conditions. Nature **439**: 187–

191. doi:10.1038/nature04420

Keppler, F., A. Schiller, R. Ehehalt, M. Greule, J. Hartmann, and D. Polag. 2016. Stable isotope and high precision concentration measurements confirm that all humans produce and exhale methane. J. Breath Res. **10**: 16003. doi:10.1088/1752-7155/10/1/016003

Kirillin, G., and C. Engelhardt. 2008. A mesoscale vortex in a small stratified lake. 349–366. doi:10.1007/s10652-008-9101-8

Kirillin, G., C. Engelhardt, and S. Golosov. 2009. Transient convection in upper lake sediments produced by internal seiching. **36**: 1–5. doi:10.1029/2009GL040064

Kirschke, S., P. Bousquet, P. Ciais, and others. 2013. Three decades of global methane sources and sinks. Nat. Geosci. **6**: 813–823. doi:10.1038/ngeo1955

Lamontagne, R. A., J. W. Swinnerton, and V. J. Linnenbom. 1974. C 1 -C 4 hydrocarbons in the North and South Pacific. Tellus **26**: 71–77. doi:10.1111/j.2153-3490.1974.tb01953.x

Lamontagne, R. A., J. W. Swinnerton, V. J. Linnenbom, and W. D. Smith. 1973. Methane concentrations in various marine environments. J. Geophys. Res. **78**: 5317–5324. doi:10.1029/JC078i024p05317

Laukenmann, S., D. Polag, H. Heuwinkel, M. Greule, A. Gronauer, J. Lelieveld, and F. Keppler. 2010. Identification of methanogenic pathways in anaerobic digesters using stable carbon isotopes. Eng. Life Sci. **10**: 509–514. doi:10.1002/elsc.201000074

Lenhart, K., T. Klintzsch, G. Langer, G. Nehrke, M. Bunge, S. Schnell, and F. Keppler. 2015. Evidence for methane production by marine algae Emiliana huxleyi and its implication for the methane paradox in oxic waters. Biogeosciences Discuss. **12**: 20323–20360. doi:10.5194/bgd-12-20323-2015

Leventhal, J. S., and G. R. Guntenspergen. 2004. Seasonal methane emissions by diffusion and ebullition from oligohaline marsh environments in coastal Louisiana, p. 389–408. *In* Geochemical Society Special Publications.

Li, Y., L. Zhan, J. Zhang, and L. Chen. 2015. Equilibrator-based measurements of dissolved methane in the surface ocean using an integrated cavity output laser absorption spectrometer. Acta Oceanol. Sin. **34**: 34–41. doi:10.1007/s13131-015-0685-9

Liikanen, A., J. T. Huttunen, T. Murtoniemi, H. Tanskanen, T. Väisänen, J. Silvola, J. Alm, and P. J. Martikainen. 2003. Spatial and seasonal variation in greenhouse gas and nutrient dynamics and their interactions in the sediments of a boreal eutrophic lake. Biogeochemistry **65**: 83–103.

doi:10.1023/A:1026070209387

Livingstone, D. M. 2003. Thermal Structure of a Large Temperate Central European Lake. Clim. Change **57**: 205–225. doi:Doi 10.1023/A:1022119503144

Livingstone, D. M. 2008. A change of climate provokes a change of paradigm: Taking leave of two tacit assumptions about physical lake forcing. Int. Rev. Hydrobiol. **93**: 404–414. doi:10.1002/iroh.200811061

van der Loeff, M. M. R. 1981. Wave effects on sediment water exchange in a submerged sand bed. Netherlands J. Sea Res. **15**: 100–112. doi:10.1016/0077-7579(81)90009-0

López Bellido, J., T. Tulonen, P. Kankaala, and A. Ojala. 2009. CO_2 and CH_4 fluxes during spring and autumn mixing periods in a boreal lake (Pääjärvi, southern Finland). J. Geophys. Res. Biogeosciences **114**: 1–12. doi:10.1029/2009JG000923

Lovley, D. R., and M. J. Klug. 1983. Methanogenesis from Methanol and Methylamines and Acetogenesis from Hydrogen and Carbon Dioxide in the Sediments of a Eutrophic Lake Methanogenesis from Methanol and Methylamines and Acetogenesis from Hydrogen and Carbon Dioxide in the Sediments of a Eutr. Appl. Environ. Microbiol. **45**: 1310–1315.

MacIntyre, S., A. Jonsson, M. Jansson, J. Aberg, D. E. Turney, and S. D. Miller. 2010. Buoyancy flux, turbulence, and the gas transfer coefficient in a stratified lake. Geophys. Res. Lett. **37**: 2–6. doi:10.1029/2010GL044164

Maeck, A., H. Hofmann, and A. Lorke. 2014. Pumping methane out of aquatic sediments – ebullition forcing mechanisms in an impounded river. Biogeosciences **11**: 2925–2938. doi:10.5194/bg-11-2925-2014

Maher, D. T., K. Cowley, I. R. Santos, P. Macklin, and B. D. Eyre. 2015. Methane and carbon dioxide dynamics in a subtropical estuary over a diel cycle: Insights from automated in situ radioactive and stable isotope measurements. Mar. Chem. **168**: 69–79. doi:10.1016/j.marchem.2014.10.017

Malmaeus, J. M., T. Blenckner, H. Markensten, and I. Persson. 2006. Lake phosphorus dynamics and climate warming: A mechanistic model approach. Ecol. Modell. **190**: 1–14. doi:10.1016/j.ecolmodel.2005.03.017

Martens, C. S., and R. A. Berner. 1974. Methane production in the interstitial waters of sulfate-depleted marine sediments. Science (80-.). **185**: 1167–1169. doi:10.1126/science.185.4157.1167

Matthews, C. J. D., V. L. St. Louis, and R. H. Hesslein. 2003. Comparison of

three techniques used to measure diffusive gas exchange from sheltered aquatic surfaces. Environ. Sci. Technol. **37**: 772–780. doi:10.1021/es0205838

McConnaughey, T. A., J. W. LaBaugh, D. . Rosenberry, R. G. Striegl, M. M. Reddy, P. F. Schuster, and V. Carter. 1994. Carbon budget for a groundwater-fed lake: Calcification supports summer photosynthesis. Limnol. Oceanogr. **39**: 1319–1332. doi:10.4319/lo.1994.39.6.1319

McCormick, M. J., and G. L. Fahnenstiel. 1999. Recent climatic trends in nearshore water temperatures in the St. Lawrence Great Lakes. Limnol. Oceanogr. **44**: 530–540. doi:10.4319/lo.1999.44.3.0530

McGinnis, D. F., J. Greinert, Y. Artemov, S. E. Beaubien, and a. Wüest. 2006. Fate of rising methane bubbles in stratified waters: How much methane reaches the atmosphere? J. Geophys. Res. **111**: C09007. doi:10.1029/2005JC003183

McGinnis, D. F., G. Kirillin, K. W. Tang, S. Flury, P. Bodmer, C. Engelhardt, P. Casper, and H. P. Grossart. 2015. Enhancing surface methane fluxes from an oligotrophic lake: Exploring the microbubble hypothesis. Environ. Sci. Technol. **49**: 873–880. doi:10.1021/es503385d

McGinnis, D. F., M. Schmidt, T. Delsontro, S. Themann, L. Rovelli, A. Reitz, and P. Linke. 2011. Discovery of a natural CO_2 seep in the German North Sea: Implications for shallow dissolved gas and seep detection. J. Geophys. Res. Ocean. **116**: 1–12. doi:10.1029/2010JC006557

McInnes, K. L., T. A. Erwin, and J. M. Bathols. 2011. Global Climate Model projected changes in 10 m wind speed and direction due to anthropogenic climate change. Atmos. Sci. Lett. **12**: 325–333. doi:10.1002/asl.341

Michmerhuizen, C. M., R. G. Striegl, and M. E. Mcdonald. 1996. Potential methane emission from north-temperate lakes following ice melt. Limnol. Oceanogr. **41**: 985–991. doi:10.4319/lo.1996.41.5.0985

Middelburg, J. J., J. Nieuwenhuize, N. Iversen, N. Høgh, H. De Wilde, W. Helder, R. Seifert, and O. Christof. 2002. Methane distribution in European tidal estuaries. Biogeochemistry **59**: 95–119. doi:10.1023/A:1015515130419

Monteil, G., S. Houweling, E. J. Dlugockenky, G. Maenhout, B. H. Vaughn, J. W. C. White, and T. Rockmann. 2011. and Physics Interpreting methane variations in the past two decades using measurements of CH 4 mixing ratio and isotopic composition. **1990**: 9141–9153. doi:10.5194/acp-11-9141-2011

Müller, B., J. S. Meyer, and R. Gächter. 2016. Alkalinity regulation in calcium carbonate-buffered lakes. Limnol. Oceanogr. **61**: 341–352.

doi:10.1002/lno.10213

Murase, J., Y. Sakai, A. Kametani, and A. Sugimoto. 2005. Dynamics of methane in mesotrophic Lake Biwa, Japan. For. Ecosyst. Environ. Scaling Up from Shoot Modul. to Watershed 143–151. doi:10.1007/4-431-29361-2_14

Nara, H., H. Tanimoto, Y. Tohjima, H. Mukai, Y. Nojiri, K. Katsumata, and C. W. Rella. 2012. Effect of air composition (N_2, O_2, Ar, and H_2O) on CO_2 and CH_4 measurement by wavelength-scanned cavity ring-down spectroscopy: Calibration and measurement strategy. Atmos. Meas. Tech. **5**: 2689–2701. doi:10.5194/amt-5-2689-2012

Natchimuthu, S., M. B. Wallin, L. Klemedtsson, and D. Bastviken. 2017. Spatio-temporal patterns of stream methane and carbon dioxide emissions in a hemiboreal catchment in Southwest Sweden. Sci. Rep. **7**: 1–12. doi:10.1038/srep39729

Neef, L., M. Van Weele, and P. Van Velthoven. 2010. Optimal estimation of the present - day global methane budget. **24**: 1–10. doi:10.1029/2009GB003661

Nicolet, M. 1970. Ozone and hydrogen reactions. Ann. Geophys. **26**: 531–546.

Niewöhner, C., C. Hensen, S. Kasten, M. Zabel, and H. . Schulz. 1998. Deep Sulfate Reduction Completely Mediated by Anaerobic Methane Oxidation in Sediments of the Upwelling Area off Namibia. Geochim. Cosmochim. Acta **62**: 455–464. doi:10.1016/S0016-7037(98)00055-6

Noble, R. D., and S. A. Stern. 1995. Membrane Separations Technology - Principles and Applications, Elsevier.

Norði, K. à., B. Thamdrup, and C. J. Schubert. 2013. Anaerobic oxidation of methane in an iron-rich Danish freshwater lake sediment. Limnol. Oceanogr. **58**: 546–554. doi:10.4319/lo.2013.58.2.0546

Norði, K., and B. Thamdrup. 2014. Nitrate-dependent anaerobic methane oxidation in a freshwater sediment. Geochim. Cosmochim. Acta **132**: 141–150. doi:10.1016/j.gca.2014.01.032

Nusslein, B., and R. Conrad. 2000. Methane production in eutrophic Lake Plusssee: Seasonal change, temperature effect and metabolic processes in the profundal sediment. Arch. fur Hydrobiol. **149**: 597–623. doi:10.1127/archiv-hydrobiol/149/2000/597

Oremland, R. S. 1979. Methanogenic activity in plankton samples and fish intestines A mechanism for in situ methanogenesis in oceanic surface waters. Limnol. Oceanogr. **24**: 1136–1141. doi:10.4319/lo.1979.24.6.1136

Oremland, R. S. L., I. Miller, and M. I. Whiticar. 1987. Sources and flux of

natural gas from Mono Lake, California. Geochim. Cosmochim. Acta **51**: 2915–2929.

Ortiz-Llorente, M. J., and M. Alvarez-Cobelas. 2012. Comparison of biogenic methane emissions from unmanaged estuaries, lakes, oceans, rivers and wetlands. Atmos. Environ. **59**: 328–337. doi:10.1016/j.atmosenv.2012.05.031

Östlund, C., P. Flink, N. Strömbeck, D. Pierson, and T. Lindell. 2001. Mapping of the water quality of Lake Erken, Sweden, from Imaging Spectrometry and Landsat Thematic Mapper. Sci. Total Environ. **268**: 139–154. doi:10.1016/S0048-9697(00)00683-5

Oswald, K., J. Milucka, A. Brand, S. Littmann, B. Wehrli, M. M. M. Kuypers, and C. J. Schubert. 2015. Light-dependent aerobic methane oxidation reduces methane emissions from seasonally stratified lakes. PLoS One **10**: 1–22. doi:10.1371/journal.pone.0132574

Paranaíba, J. R., N. Barros, R. Mendonça, A. Linkhorst, A. Isidorova, F. Roland, R. M. Almeida, and S. Sobek. 2018. Spatially Resolved Measurements of CO2 and CH4 Concentration and Gas-Exchange Velocity Highly Influence Carbon-Emission Estimates of Reservoirs. Environ. Sci. Technol. **52**: 607–615. doi:10.1021/acs.est.7b05138

Parkhurst, D. L., and C. A. J. Appelo. 1999. User's guide to PHREEQC - a computer program for speciation, batch reaction, one-dimentional transport, and inverse geochemical calcualtions, Water-Resources Investigations Report, U.S. Geological Survey.

Pataki, D. E., J. R. Ehleringer, L. B. Flanagan, and others. 2003. The application and interpretation of Keeling plots in terrestrial carbon cycle research. Global Biogeochem. Cycles **17**: 1–14. doi:10.1029/2001GB001850

Paul, D., G. Skrzypek, and I. Forizs. 2007. Normalization of measured stable isotopic compositions to isotope reference scales – a review. Rapid Commun. mass Spectrom. **21**: 3006–3014. doi:10.1002/rcm.3185

Pechlaner, R. 1970a. The phytoplankton spring outburst and its conditions in Lake Erken (Sweden). Limnol. Oceanogr. **15**: 113–130. doi:10.4319/lo.1970.15.1.0113

Pechlaner, R. 1970b. The phytoplankton spring outburst and its conditions in Lake Erken (Sweden). Limnol. Oceanogr. **15**: 113–130. doi:10.4319/lo.1970.15.1.0113

Penger, J., R. Conrad, and M. Blaser. 2012. Stable carbon isotope fractionation by methylotrophic methanogenic archaea. Appl. Environ. Microbiol. **78**: 7596–7602. doi:10.1128/AEM.01773-12

Pettersson, K. 1980. Alkaline phosphatase activity and algal surplus phosphorus as phosphorus-deficiency indicators in Lake Erken. Arch. für Hydrobiol. **89**: 54–87.

Pettersson, K. 1985. The Availability of Phosphorus and the Species Composition of the Spring Phytoplankton in Lake Erken. Int. Rev. der gesamten Hydrobiol. und Hydrogr. **70**: 527–546. doi:10.1002/iroh.19850700407

Pirazzoli, P. A., S. Costa, U. Dornbusch, and A. Tomasin. 2006. Recent evolution of surge-related events and assessment of coastal flooding risk on the eastern coasts of the English Channel. Ocean Dyn. **56**: 498–512. doi:10.1007/s10236-005-0040-3

Podgrajsek, E., E. Sahlée, and A. Rutgersson. 2014. Diurnal cycle of lake methane flux. J. Geophys. Res. Biogeosciences **119**: 236–248. doi:10.1002/2013JG002327

Prairie, Y. T., and P. A. del Giorgio. 2013. A new pathway of freshwater methane emissions and the putative importance of microbubbles. Inl. Waters **3**: 311–320. doi:10.5268/IW-3.3.542

Raghoebarsing, A. A., A. Pol, K. T. Van De Pas-Schoonen, and others. 2006. A microbial consortium couples anaerobic methane oxidation to denitrification. Nature **440**: 918–921. doi:10.1038/nature04617

Reeburgh, W. S. 1976. Methane consumption in Cariaco Trench waters and sediments. Earth Planet. Sci. Lett. **28**: 337–344. doi:10.1016/0012-821X(76)90195-3

Rella, C. W., H. Chen, A. E. Andrews, and others. 2013. High accuracy measurements of dry mole fractions of carbon dioxide and methane in humid air. Atmos. Meas. Tech. **6**: 837–860. doi:10.5194/amt-6-837-2013

Rhee, T. S., A. J. Kettle, and M. O. Andreae. 2009. Methane and nitrous oxide emissions from the ocean: A reassessment using basin-wide observations in the Atlantic. J. Geophys. Res. Atmos. **114**. doi:10.1029/2008JD011662

Rice, D. D. 1993. Composition and Origins of Coalbed Gas. Hydrocarb. from Coal **38**: 159–184. doi:10.1306/D9CB61EB-1715-11D7-8645000102C1865D

Riedl, R. J., N. Huang, and R. Machan. 1972. The subtidal pump: a mechanism of interstitial water exchange by wave action. Mar. Biol. **13**: 210–221. doi:10.1007/BF00391379

Riera, J. L., J. E. Schindler, and T. K. Kratz. 1999. Seasonal dynamics of carbon dioxide and methane in two clear-water lakes and two bog lakes in

northern Wisconsin, U.S.A. Can. J. Fish. Aquat. Sci. **56**: 265–274. doi:10.1139/f98-182

Roland, F. A. E., F. Darchambeau, C. Morana, S. Bouillon, and A. V. Borges. 2017. Emission and oxidation of methane in a meromictic, eutrophic and temperate lake (Dendre, Belgium). Chemosphere **168**: 756–764. doi:10.1016/j.chemosphere.2016.10.138

Rosenfeld, W. D., and S. R. Silverman. 1959. Carbon isotope fractionation in bacterial production of methane. Science (80-.). **130**: 1658–1659.

Rudd, J. W. M., A. Furutani, R. J. Flett, and R. D. Hamilton. 1976. Factors controlling methane oxidation in shield lakes: The role of nitrogen fixation and oxygen concentration1. Limnol. Oceanogr. **21**: 357–364. doi:10.4319/lo.1976.21.3.0357

Sander, R. 2015. Compilation of Henry's law constants (version 4.0) for water as solvent. Atmos. Chem. Phys. **15**: 4399–4981. doi:10.5194/acp-15-4399-2015

Sandler, B. 2000. Die Wirkung von Sanierungs- und Restaurierungsmaßnahmen auf die Nährstoffströme und die biotische Dynamik eines anthropogenen Gewässers am Beispiel des Willersinnweihers/Ludwigshafen. Ruprecht-Karls-Universität Heidelberg.

Saunois, M., P. Bousquet, B. Poulter, and others. 2016. The global methane budget 2000–2012. Earth Syst. Sci. Data **8**: 697–751. doi:10.5194/essd-8-697-2016

Schilder, J., D. Bastviken, M. Van Hardenbroek, P. Kankaala, P. Rinta, T. Stötter, and O. Heiri. 2013. Spatial heterogeneity and lake morphology affect diffusive greenhouse gas emission estimates of lakes. Geophys. Res. Lett. **40**: 5752–5756. doi:10.1002/2013GL057669

Schloemer, S., J. Elbracht, M. Blumenberg, and C. J. Illing. 2016. Distribution and origin of dissolved methane, ethane and propane in shallow groundwater of Lower Saxony, Germany. Appl. Geochemistry **67**: 118–132. doi:10.1016/j.apgeochem.2016.02.005

Schlüter, M., and T. Gentz. 2008. Application of Membrane Inlet Mass Spectrometry for Online and In Situ Analysis of Methane in Aquatic Environments. J. Am. Soc. Mass Spectrom. **19**: 1395–1402. doi:10.1016/j.jasms.2008.07.021

Schmid, J. 2002. Calcitfällung und Phosphor-Kopräzipitation im Phosphorhaushalt eines eutrophen Hartwassersees mit anoxischem Hypolimnion (Willersinnweiher, Ludwigshafen am Rhein).

Schmidt, K. R., T. Augenstein, M. Heidinger, S. Ertl, and A. Tiehm. 2010.

Aerobic biodegradation of cis-1,2-dichloroethene as sole carbon source: Stable carbon isotope fractionation and growth characteristics. Chemosphere **78**: 527–532. doi:10.1016/j.chemosphere.2009.11.033

Schneider von Deimling, J., J. Greinert, N. R. Chapman, W. Rabbel, and P. Linke. 2010. Acoustic imaging of natural gas seepage in the North Sea: Sensing bubbles controlled by variable currents. Limnol. Oceanogr. Methods **8**: 155–171. doi:10.4319/lom.2010.8.155

Schoell, M. 1980. The hydrogen and carbon isotopic composition of methane from natural gases of various origins. Geochim. Cosmochim. Acta **44**: 649–661. doi:10.1016/0016-7037(80)90155-6

Schoell, M. 1988. Multiple origins of methane in the earth. Chem. Geol. **71**: 1–10.

Schröder, H. 2004. Saisonale Redoxfronten im Kopplungsbereich zwischen Schwefel- Eisen- und Mangankreislauf im System Seewasser – Sediment – Grundwasser des Willersinnweihers. Ruprecht-Karls-Universität Heidelberg.

Schrum, H. N., R. W. Murray, and B. Gribsholt. 2012. Comparison of Rhizon Sampling and Whole Round Squeezing for Marine Sediment Porewater. Sci. Drill. 47–50. doi:10.2204/iodp.sd.13.08.2011

Schubert, C. J., T. Diem, and W. Eugster. 2012. Methane emissions from a small wind shielded lake determined by eddy covariance, flux chambers, anchored funnels, and boundary model calculations: a comparison. Environ. Sci. Technol. **46**: 4515–22. doi:10.1021/es203465x

Schubert, C. J., F. Vazquez, T. Lösekann-Behrens, K. Knittel, M. Tonolla, and A. Boetius. 2011. Evidence for anaerobic oxidation of methane in sediments of a freshwater system (Lago di Cadagno). FEMS Microbiol. Ecol. **76**: 26–38. doi:10.1111/j.1574-6941.2010.01036.x

Schütz, H., A. Holzapfel-Pschorn, R. Conrad, H. Rennenberg, and W. Seiler. 1989a. A 3-year continuous record on the influence of daytime, season, and fertilizer treatment on methane emission rates from an Italian rice paddy. J. Geophys. Res. **94**: 16405. doi:10.1029/JD094iD13p16405

Schütz, H., W. Seiler, and R. Conrad. 1989b. Processes involved in formation and emission of methane in rice paddies. Biogeochemistry **7**: 33–53. doi:10.1007/BF00000896

Seeberg-Elverfeldt, J., M. Schlüter, T. Feseker, and M. Kölling. 2005. Rhizon sampling of porewaters near the sediment-water interface. Limnol. Oceanogr. Methods **3**: 361–371.

Seiler, W., and A. Holzapfel-Pschorn. 1984. Methane emission from rice paddies. J. Atmos. Chem. **1**: 241–268.

Shapiro, J., V. Lamarra, and M. Lynch. 1975. Biomanipulation: an ecosystem approach to lake restoration. Water Qual. Manag. through Biol. Control 85–96.

Shen, L. dong, H. sheng Wu, X. Liu, and J. Li. 2017. Cooccurrence and potential role of nitrite- and nitrate-dependent methanotrophs in freshwater marsh sediments. Water Res. **123**: 162–172. doi:10.1016/j.watres.2017.06.075

Söhngen, N. L. 1906. Über Bakterien, welche Methan als Kohlenstoffnahrung und Energiequelle gebrauchen. Zentrabl Bakteriol Parasitenk Infekt. **15**: 513–517.

Sokal, R. R., and F. J. Rohlf. 1995. Biometry: The principles and practice of statistics in biological research, 3rd ed. WH Freeman.

Sørensen, J. 1982. Reduction of ferric iron in anaerobic, marine sediment and interaction with reduction of nitrate and sulfate. Appl. Environ. Microbiol. **43**: 319–324.

Stauffer, R. E. 1980. Windpower time series above a temperate lake. Limnol. Oceanogr. **25**: 513–528. doi:10.4319/lo.1980.25.3.0513

Stocker, T. F., G. K. C. Clarke, H. Le Treut, and others. 2001. Physical Climate Processes and Feedbacks. Clim. Chang. 2001 Sci. Bases. Contrib. Work. Gr. I to Third Assess. Rep. Intergov. Panel Clim. Chang. 881. doi:10.1256/004316502320517344

Sweerts, J. R. A., M.-J. Bär-Gilissen, A. A. Cornelese, and T. E. Cappenberg. 1991. Oxygen-consuming processes at the profundal and littoral sediment-water interface of a small meso-eutrophic lake (Lake Vechten, The Netherlands). Limnol. Oceanogr. **36**: 1124–1133. doi:10.4319/lo.1991.36.6.1124

Tang, K., D. McGinnis, K. Frindte, V. Brüchert, and H. P. Grossart. 2014. Paradox reconsidered: Methane oversaturation in well-oxygenated lake waters. Limnol. Oceanogr. **59**: 275–284. doi:10.4319/lo.2014.59.1.0275

Tang, K. W., D. F. McGinnis, D. Ionescu, and H.-P. Grossart. 2016. Methane Production in Oxic Lake Waters Potentially Increases Aquatic Methane Flux to Air. Environ. Sci. Technol. Lett. **3**: 227–233. doi:10.1021/acs.estlett.6b00150

Thullner, M., P. Regnier, and P. Van Cappellen. 2007. Modeling microbially induced carbon degradation in redox-stratified subsurface environments: Concepts and open questions. Geomicrobiol. J. **24**: 139–155.

doi:10.1080/01490450701459275

Timmers, P. H. A., D. A. Suarez-Zuluaga, M. Van Rossem, M. Diender, A. J. M. Stams, and C. M Plugge. 2016. Anaerobic oxidation of methane associated with sulfate reduction in a natural freshwater gas source. ISME J. **10**: 1400–1412. doi:10.1038/ismej.2015.213

Tranvik, L. J., J. A. Downing, J. B. Cotner, and others. 2009. Lakes and reservoirs as regulators of carbon cycling and climate. Limnol. Oceanogr. **54**: 2298–2314. doi:10.4319/lo.2009.54.6_part_2.2298

Trotsenko, Y. A., and J. C. Murrell. 2008. Metabolic Aspects of Aerobic Obligate Methanotrophy⋆, p. 183–229. *In* Allen I. Laskin, S. Sariaslani, and G.M. Gadd [eds.], Advances in Applied Microbiology.

Utsumi, M., Y. Nojiri, T. Nakamura, T. Nozawa, A. Otsuki, and H. Seki. 1998. Oxidation of dissolved methane in a eutrophic, shallow lake: Lake Kasumigaura, Japan. Limnol. Oceanogr. **43**: 471–480. doi:10.4319/lo.1998.43.3.0471

Wahlen, M. 1993. The Global Methane Cycle. Annu. Rev. Earth Planet. Sci. **21**: 407–426. doi:10.1146/annurev.earth.21.1.407

Wankel, S. D., Y. W. Huang, M. Gupta, R. Provencal, J. B. Leen, A. Fahrland, C. Vidoudez, and P. R. Girguis. 2013. Characterizing the distribution of methane sources and cycling in the deep sea via in situ stable isotope analysis. Environ. Sci. Technol. **47**: 1478–1486. doi:10.1021/es303661w

Wanninkhof, R. 1992. Relationship between wind speed and gas exchange over the ocean. J. Geophys. Res. **97**: 7373. doi:10.1029/92JC00188

Webb, J. R., D. T. Maher, and I. R. Santos. 2016. Automated, in situ measurements of dissolved CO_2, CH_4, and $\delta^{13}C$ values using cavity enhanced laser absorption spectrometry: Comparing response times of air-water equilibrators. Limnol. Oceanogr. Methods 1–15. doi:10.1002/lom3.10092

Weiss, R. F. 1974. Carbon dioxide in water and seawater: The solubility of a non-ideal gas. Mar. Chem. **2**: 203–215.

Weyhenmeyer, G. A., M. Meili, and D. C. Pierson. 1995. Simple method to quantify sources of settling particles in lakes—Resuspension versus new sedimentation of material from planktonic production, Mar. Fresh- water Res. , 46 , 223–231. Mar. Freshw. Res. **46**: 223–231. doi:10.1071/MF9950223

Whiticar, M. J. 1999. Carbon and hydrogen isotope systematics of bacterial formation and oxidation of methane. Chem. Geol. **161**: 291–314.

doi:10.1016/S0009-2541(99)00092-3

Wickert, F., K. R. Schmidt, and A. Tiehm. 2009. LCKW-Verteilung , Redoxparameter und mikrobiologischer Abbau im Porengrundwasserleiter des Oberrheingrabens bis 50 m Tiefe , dargestellt an einem Fallbeispiel. 193–199.

Widell, A. 1965. Narsalterna i sjon Erken soinmaren 1965. Scr. Limnol. Ups. **250**: 24.

Wiesenburg, D. A., and N. L. Guinasso. 1979. Equilibrium solubilities of methane, carbon monoxide, and hydrogen in water and sea water. J. Chem. Eng. Data **24**: 356–360. doi:10.1021/je60083a006

Wik, M., R. K. Varner, K. W. Anthony, S. MacIntyre, and D. Bastviken. 2016. Climate-sensitive northern lakes and ponds are critical components of methane release. Nat. Geosci. **9**: 99–106. doi:10.1038/ngeo2578

Winfrey, M. R., and J. G. Zeikus. 1977. Effect of sulfate on carbon and electron flow during microbial methanogenesis in freshwater sediments. Appl. Environ. Microbiol. **33**: 275–281.

Wollschläger, U., J. Ilmberger, M. Isenbeck-Schröter, A. M. Kreuzer, C. Von Rohden, K. Roth, and W. Schäfer. 2007. Coupling of groundwater and surface water at Lake Willersinnweiher: Groundwater modeling and tracer studies. Aquat. Sci. **69**: 138–152. doi:10.1007/s00027-006-0825-6

Yamamoto, S., J. B. Alcauskas, T. E. Crozier, J. B. B. Alcauskas, and T. E. Crozier. 1976. Solubility of methane in distilled water and seawater. J. Chem. Eng. Data **21**: 78–80. doi:10.1021/je60068a029

Yao, M., C. Henny, and J. A. Maresca. 2016. Freshwater Bacteria Release Methane as a By-Product of Phosphorus Acquisition J.E. Kostka [ed.]. Appl. Environ. Microbiol. **82**: 6994–7003. doi:10.1128/AEM.02399-16

Zappa, C. J., P. A. Raymond, E. A. Terray, and W. R. McGillis. 2003. Variation in surface turbulence and the gas transfer velocity over a tidal cycle in a macro-tidal estuary. Estuaries **26**: 1401–1415. doi:10.1007/BF02803649

8. Appendix

Data calibration and characterisation work

Calibration – Concentration

STD Gas	CH_4 (GC-FID)	Absorption of light in the cavity of (M-CRDS)		CH_4 (M-CRDS)		$\delta^{13}C\text{-}CH_4$ (M-CRDS)	
	Value	Value	+-	Value	+-	Value	+-
	[nM]	[ppm cm^{-1}]		[ppm}		[‰]	
5	0.00	3.98	0.02	2.89	0.01	-52.1	2.18
5	0.23	4.21	0.06	3.05	0.04	-51.6	2.20
5	0.60	4.49	0.02	3.26	0.02	-51.4	1.84
100	11.4	10.5	0.05	7.56	0.04	-46.0	0.91
100	22.9	17.9	0.39	12.9	0.28	-45.3	0.62
100	33.5	23.2	0.45	16.7	0.33	-44.6	0.59
100	41.0	28.6	0.26	20.5	0.19	-45.1	0.53
100	50.8	36.0	0.27	25.9	0.20	-45.4	0.48
100	62.5	41.4	0.80	29.8	0.58	-45.7	0.46
100	68.0	46.8	0.45	33.6	0.32	-45.9	0.37
1000	95.7	66.8	0.30	48.3	0.22	-53.0	0.39
1000	193	134	0.58	97.0	0.43	-53.4	0.41
1000	300	203	3.79	147	2.74	-53.5	0.37
1000	367	250	4.31	181	3.13	-53.5	0.40
1000	421	292	4.54	212	3.29	-53.5	0.35
1000	486	343	5.30	249	3.84	-53.4	0.38

Calibration – Isotopic values

Sample ID	$\delta^{13}C\text{-}CH_4$ (GC-C-IRMS)		$\delta^{13}C\text{-}CH_4$ (M-CRDS)	
	Value	+-	Value	+-
	[‰]		[‰]	
1	-47.4	0.2	-48.9	0.83
2	-47.4	0.2	-48.6	0.83
3	-47.7	0.2	-48.7	0.81
4	-47.4	0.2	-48.5	0.77
5	-46.7	0.2	-47.5	0.57
6	-46.1	0.2	-46.0	0.82
7	-44.4	0.2	-44.5	1.29
8	-41.4	0.2	-43.7	1.44
9	-40.2	0.2	-42.7	2.05
10	-48.8	0.2	-47.6	0.72
11	-84.4	0.2	-82.9	1.30
12	-82.9	0.2	-82.9	1.30
13	-43.4	0.2	-44.5	1.30
14	-48.2	0.2	-50.0	1.30
15	-58.3	0.2	-58.7	1.30

Calibration – Keeling plot

Sample ID	$1 / CH_4$		$\delta^{13}C\text{-}CH_4$	
	Value	+-	Value	+-
	[L nmol^{-1}]		[‰]	
1	0.24	0.01	-45.1	0.21
2	0.21	0.01	-43.2	0.31
3	0.22	0.01	-44.2	0.34
4	0.19	0.01	-42.3	0.22

Potential sources of error

Sample ID	H_2O		CH_4		CH_4 (dry)		$\delta^{13}C$-CH_4	
	Value	+-	Value	+-	Value	+-	Value	+-
	— [%] —		— [ppm] —		— [ppm] —		— [‰]—	
1	2.25	0.01	1.94	< 0.01	2.00	< 0.01	-53.7	0.6
2	1.47	0.03	1.96	< 0.01	2.00	< 0.01	-53.2	0.5
3	0.06	0.01	2.00	< 0.01	2.00	< 0.01	-53.3	0.6

Sample ID	O_2	CH_4	$\delta^{13}C$-CH_4				
			GC-C-IRMS	+-	M-CRDS	+-	Offset
	[%]	[nM]	——— [‰] ———				
1	110	490	-47.4	0.2	-48.9	0.83	1.48
2	114	504	-47.4	0.2	-48.6	0.83	1.15
3	110	511	-47.7	0.2	-48.7	0.81	1.00
4	113	511	-47.4	0.2	-48.5	0.77	1.09
5	131	583	-46.7	0.2	-47.5	0.57	0.90
6	140	324	-46.1	0.2	-46.0	0.82	-0.11
7	123	238	-44.4	0.2	-44.5	1.29	0.09
8	80.2	407	-48.8	0.2	-47.6	0.72	-1.16
9	0.00	1120	-84.4	0.2	-82.9	1.3	-0.80
10	20.0	108	-43.4	0.2	-44.5	1.3	1.11
11	100	540	-48.2	0.2	-50.0	1.3	1.80
12	100	144	-58.3	0.2	-58.7	1.3	0.40

Sample ID	ΔT	CH_4		Offset
		Value	+-	
	[°C]	——— [nM] ———		[nM]
1	0	110	1.21	0.00
2	2.2	109	1.20	1.13
3	3.5	109	1.20	1.02
4	5.6	110	1.21	0.18
5	6.6	110	1.21	0.22
6	7.8	110	1.21	0.22
7	9.8	110	1.21	0.04
8	10.5	110	1.21	-0.29
9	11.1	110	1.21	-0.11
10	11.9	110	1.21	-0.07

Field application at Lake Stechlin

Water depth	M-ICOS		GC-FID	M-CRDS			
	CH_4	+-	CH_4	CH_4	+-	$\delta^{13}C$-CH_4	+-
[m]	[nM]			[nM]		[‰]	
0	469	2.17	443	494	3.54	-49.9	1.3
2	486	2.09	479	494	4.25	-49.9	1.3
4	492	3.21	498	502	6.92	-50.1	1.0
4.5	498	1.91	502	500	0.93	-50.0	1.0
5	501	1.94	505	498	2.01	-49.9	1.2
5.5	501	2.25	500	500	3.63	-49.9	1.1
6	509	3.16	491	498	3.78	-49.8	1.2
6.5	522	2.77	521	501	4.02	-49.8	1.1
7	515	1.04	533	504	7.98	-50.0	1.1
7.5	594	6.21	574	577	12.4	-40.5	1.1
8	342	20.5	269	379	27.4	-35.2	1.2
10	124	0.92	158	70.3	1.73	-37.5	2.3
12	92.0	3.50	88.0	60.2	1.46	-46.4	2.5
14	80.0	4.16	76.0	63.7	2.43	-49.4	2.9
16	104	2.95	184	134	0.56	-50.2	2.9
17	151	1.70	165	116	5.10	-52.1	2.3
18	155	2.92	114	111	7.00	-53.0	1.8
18.5				63.7	22.1	-50.1	2.5

Data Lake Willersinnweiher

Lake Willersinnweiher **Early-stage stratification 05.17** **Site W1**
Water Column

Water Depth	T	pH	O_2	Ca	DIC	Mn	Fe	NO_3^-	SO_4^{2-}	S (-II)$^-$	CH_4	$\delta^{13}C$-CH_4
[m]	[°C]	–	[mM]			[µM]			[mM]		[µM]	[‰]
2	14.2	8.85	0.36	1.82	1.47	n.d.	0.27	12.3	2.13	n.d.*	0.12	-52.4
4	12.9	8.74	0.33	1.88	1.56	n.d.	n.d.	35.8	2.12	n.d.	0.14	-52.4
5	10.9	8.35	0.28	2.13	2.09	n.d.	n.d.	8.7	2.10	n.d.	0.11	-51.1
6	8.9	7.41	0.04	2.25	2.23	0.36	n.d.	26.7	2.06	n.d.	0.14	-48.3
7	7.6	7.44	0.01	2.21	2.22	2.91	n.d.	10.0	2.03	n.d.	0.10	-44.9
8	7.7	7.42	0.01	2.18	2.21	2.28	n.d.	9.9	2.08	n.d.	0.08	-49.4
10	7.1	7.35	0.01	2.21	2.18	0.36	n.d.	11.5	2.06	n.d.	0.07	-47.8
12	7.0	7.34	0	2.22	2.19	6.01	n.d.	16.3	2.07	n.d.	0.42	-57.6
13.5	7.4	7.4	0	2.15	2.24	20.84	n.d.	11.9	2.11	n.d.	1.61	-69.6
15	6.9	7.49	0	2.25	2.43	58.34	0.36	9.8	2.09	n.d.	6.39	-74.7
17	6.9	7.52	0	2.26	2.45	64.34	0.63	20.1	2.05	n.d.	8.21	-75.4

* n.d. indicates below detection limit

Lake Willersinnweiher			**Early-stage stratification 05.17**						**Site W2** **Water Column**			
Water Depth	T	pH	O_2	Ca	DIC	Mn	Fe	NO_3^-	SO_4^{2-}	S (-II)$^-$	CH_4	$\delta^{13}C$-CH_4
[m]	[°C]	–	[mM]			[µM]			[mM]		[µM]	[‰]
1	15.1	8.86	0.36	1.90	1.44	n.d.	n.d.	9.29	2.10	n.d.	0.15	-53.0
2	14.4	8.87	0.35	1.87	1.46	n.d.	n.d.	17.23	2.08	n.d.	0.14	-52.9
4	13.0	8.71	0.33	1.96	1.57	n.d.	n.d.	12.60	2.09	n.d.	0.13	-53.0
5	10.5	8.08	0.22	2.25	2.12	n.d.	n.d.	33.39	2.09	n.d.	0.14	-51.3
6	8.7	7.55	0.05	2.26	2.18	n.d.	n.d.	13.60	2.07	n.d.	0.09	-47.2
7	7.8	7.41	0.02	2.18	2.18	1.46	n.d.	8.98	2.07	n.d.	0.13	-44.5
8	7.8	7.39	0.03	2.21	1.83	1.27	n.d.	98.68	2.03	n.d.	0.08	-46.7
10	7.7	7.39	0.04	2.22	2.14	1.00	n.d.	10.32	2.08	n.d.	0.07	-46.5
12	6.9	7.38	0.04	2.18	2.15	0.46	n.d.	20.97	2.05	n.d.	0.01	-47.9
13.5	7.0	7.36	0.00	2.21	2.20	8.92	n.d.	17.42	2.03	n.d.	0.47	-61.8
15	7.0	7.37	0.00	2.27	2.44	36.40	0.63	0.00	1.98	n.d.	10.11	-76.7

Lake Willersinnweiher			**Early-stage stratification 05.17**						**Site W3** **Water Column**			
Water Depth	T	pH	O_2	Ca	DIC	Mn	Fe	NO_3^-	SO_4^{2-}	S (-II)$^-$	CH_4	$\delta^{13}C$-CH_4
[m]	[°C]	–	[mM]			[µM]			[mM]		[µM]	[‰]
1	18.0	8.78	0.36	1.86	1.39	0.36	0.18	10.5	2.06	n.d.	0.18	-53.4
2	16.2	8.81	0.37	1.85	1.43	n.d.	n.d.	25.8	2.06	n.d.	0.17	-53.0
4	13.6	8.55	0.32	1.95	1.61	n.d.	n.d.	14.1	2.04	n.d.	0.15	-52.2
5	11.6	8.05	0.24	2.15	2.04	n.d.	n.d.	10.6	2.01	n.d.	0.13	-51.7
6	9.2	7.47	0.09	2.20	2.19	n.d.	n.d.	26.9	2.01	n.d.	0.14	-47.5
7	8.1	7.31	0.01	2.21	2.17	0.55	n.d.	25.5	2.02	n.d.	0.16	-43.5
8	7.8	7.26	0.01	2.18	2.18	1.82	n.d.	10.1	2.04	n.d.	0.11	-46.7

Lake Willersinnweiher **Early-stage stratification 05.17** **Site W4**
Water Column

Water Depth	T	pH	O_2	Ca	DIC	Mn	Fe	NO_3^-	SO_4^{2-}	S (-II)$^-$	CH_4	$\delta^{13}C$-CH_4
[m]	[°C]	–	[mM]			[µM]			[mM]		[µM]	[‰]
0.5	17.6	8.90	0.38	1.86	1.44	n.d.	n.d.	n.d.	2.10	n.d.	0.27	-56.1

Lake Willersinnweiher **Early-stage stratification 05.17** **Groundwater**
Inflow and Outlow

Water Depth	T	pH	O_2	Ca	DIC	Mn	Fe	NO_3^-	SO_4^{2-}	S (-II)$^-$	CH_4	$\delta^{13}C$-CH_4
[m]	[°C]	–	[mM]			[µM]			[mM]		[µM]	[‰]
Inflow	14.4	7.28	n.d.	3.04	3.31	11.4	39.7	13.9	2.07	n.d.	0.84	–
Outflow*	–	–	–	–	–	–	–	–	–	–	–	–

*GW outflow not analysed in May 2017

Lake Willersinnweiher			**Early-stage stratification 10.17**						**Site W1** **Water Column**			
Water Depth	T	pH	O_2	Ca	DIC	Mn	Fe	NO_3^-	SO_4^{2-}	S (-II)$^-$	CH_4	$\delta^{13}C$-CH_4
[m]	[°C]	–	[mM]			[µM]			[mM]		[µM]	[‰]
2	15.6	8.30	0.30	1.92	1.34	n.d.	n.d.	4.84	2.12	n.d.	0.60	-51.5
4	15.4	8.30	0.30	1.92	1.36	n.d.	n.d.	3.23	1.30	n.d.	0.51	-51.0
6	15.0	8.29	0.29	1.90	1.34	n.d.	n.d.	2.26	1.89	n.d.	0.53	-51.0
7	14.4	8.25	0.25	1.86	1.35	n.d.	n.d.	7.10	1.79	n.d.	0.13	-50.8
8	13.5	7.36	0.02	2.16	2.18	0.40	n.d.	2.42	1.61	n.d.	0.21	-54.0
9	10.5	7.30	n.d.	2.41	2.27	32.4	n.d.	2.24	1.20	n.d.	1.42	-58.0
10	9.1	7.34	n.d.	2.21	2.48	38.2	3.26	2.90	1.51	0.21	26.9	-75.8
12	8.1	7.37	n.d.	2.18	2.65	34.2	2.11	2.37	1.60	0.50	38.6	-76.5
15	7.8	7.40	n.d.	2.23	2.90	33.9	1.81	1.94	1.66	–	71.6	-77.0
18	7.8	7.33	n.d.	2.27	2.97	33.9	1.59	1.13	1.69	1.35	84.0	-77.5

Lake Willersinnweiher			**Early-stage stratification 10.17**						**Site W2** **Water Column**			
Water Depth	T	pH	O_2	Ca	DIC	Mn	Fe	NO_3^-	SO_4^{2-}	S (-II)$^-$	CH_4	$\delta^{13}C$-CH_4
[m]	[°C]	–	[mM]			[µM]			[mM]		[µM]	[‰]
2	15.5	8.21	0.28	1.88	1.36	n.d.	n.d.	5.48	1.41	n.d.	0.73	-52.5
4	15.4	8.19	0.28	1.85	1.30	n.d.	n.d.	2.58	2.05	n.d.	0.70	-52.3
6	15.3	8.18	0.27	1.91	1.35	n.d.	n.d.	2.10	1.87	n.d.	0.68	-52.5
7	15.2	8.13	0.27	1.84	1.58	n.d.	n.d.	2.74	2.11	n.d.	0.65	-51.7
8	13.8	7.33	0.02	2.02	2.18	n.d.	n.d.	2.42	2.09	n.d.	0.12	-50.0
9	10.6	7.28	n.d.	2.31	2.25	6.24	n.d.	2.58	1.91	n.d.	0.18	-53.0
10	9.0	7.33	n.d.	2.26	2.35	46.6	0.98	2.58	1.88	0.06	6.87	-74.0
12	7.6	7.33	n.d.	2.30	1.36	36.4	3.01	1.77	1.93	0.34	29.8	-76.6
15	7.3	7.28	n.d.	2.23	–	32.2	1.25	0.00	1.99	–	89.6	-78.0

Lake Willersinnweiher			**Early-stage stratification 10.17**						**Site W3** **Water Column**			
Water Depth	T	pH	O_2	Ca	DIC	Mn	Fe	NO_3^-	SO_4^{2-}	S (-II)$^-$	CH_4	$\delta^{13}C$-CH_4
[m]	[°C]	–	[mM]			[µM]			[mM]		[µM]	[‰]
2	15.8	8.28	0.29	1.84	1.11	n.d.	n.d.	22.19	2.13	n.d.	0.75	-53.5
4	15.5	8.27	0.29	1.81	1.09	n.d.	n.d.	10.94	2.13	n.d.	0.71	-52.7
6	15.3	8.25	0.29	1.81	1.10	n.d.	n.d.	25.18	2.13	n.d.	0.69	-51.5
7	15.1	8.05	0.26	1.85	1.15	n.d.	n.d.	13.15	2.13	n.d.	0.70	-51.8
8	14.0	7.30	0.03	2.07	1.77	n.d.	n.d.	3.37	2.09	n.d.	0.45	-50.6

Lake Willersinnweiher **Early-stage stratification 10.17** **Site W4**
Water Column

Water Depth	T	pH	O_2	Ca	DIC	Mn	Fe	NO_3^-	SO_4^{2-}	S (-II)$^-$	CH_4	$\delta^{13}C$-CH_4
[m]	[°C]	–	[mM]			[µM]			[mM]		[µM]	[‰]
0.5	16.1	8.29	9.71	1.85	1.12	n.d.	n.d.	35.2	2.12	n.d.	1.32	-60.0

Lake Willersinnweiher **Early-stage stratification 10.17** **Groundwater**
Inflow and Outlow

Water Depth	T	pH	O_2	Ca	DIC	Mn	Fe	NO_3^-	SO_4^{2-}	S (-II)$^-$	CH_4	$\delta^{13}C$-CH_4
[m]	[°C]	–	[mM]			[µM]			[mM]		[µM]	[‰]
Inflow	13.7	7.30	n.d.	2.89	3.06	10.7	39.2	10.2	2.22	n.d.	1.94	-6.3
Outflow	13.4	7.26	n.d.	2.77	3.74	15.5	43.7	5.48	1.36	n.d.	1.73	-18.2

Lake Willersinnweiher **Early-stage stratification 02.18** **Site W1**
Water Column

Water Depth	T	pH	O_2	Ca	DIC	Mn	Fe	NO_3^-	SO_4^{2-}	S (-II)$^-$	CH_4	$\delta^{13}C$-CH_4
[m]	[°C]	–	[mM]			[µM]			[mM]		[µM]	[‰]
1	0.7	–	0.43	1.97	2.02	0.59	n.d.	n.d.	2.09	n.d.	0.08	-50.0
3	2.5	–	0.42	2.09	2.08	0.53	n.d.	n.d.	2.17	n.d.	0.06	-50.0
6	2.4	–	0.42	2.05	2.06	0.52	n.d.	n.d.	2.11	n.d.	0.09	-50.6
9	2.4	–	0.43	1.90	2.02	0.51	n.d.	n.d.	1.93	n.d.	0.04	-51.2
12	2.3	–	0.43	2.06	2.02	0.50	n.d.	n.d.	2.09	n.d.	0.07	-51.0

Lake Willersinnweiher **Early-stage stratification 02.18** **Site W4**
Water Column

Water Depth	T	pH	O_2	Ca	DIC	Mn	Fe	NO_3^-	SO_4^{2-}	S (-II)$^-$	CH_4	$\delta^{13}C$-CH_4
[m]	[°C]	–	[mM]			[µM]			[mM]		[µM]	[‰]
0.5	–	–	–	1.96	2.03	0.21	n.d.	n.d.	2.11	n.d.	–	–

Lake Willersinnweiher **Early-stage stratification 02.18** **Groundwater Inflow and Outlow**

Water Depth	T	pH	O_2	Ca	DIC	Mn	Fe	NO_3^-	SO_4^{2-}	S (-II)$^-$	CH_4	$\delta^{13}C$-CH_4
[m]	[°C]	–	[mM]			[µM]			[mM]		[µM]	[‰]
Inflow	12.7	8.0	n.d.	3.18	3.47	11.8	43.0	n.d.	2.31	n.d.	1280	-10.9
Outflow	12.1	8.3	n.d.	2.80	3.94	15.0	45.9	n.d.	1.53	n.d.	128	1.10

Lake Willersinnweiher			**Early-stage stratification 05.17**			**Site W1 Pore-water**			
Sediment Depth	Ca	DIC	NO_3^-	Mn	Fe	SO_4^{2-}	S (-II)$^-$	CH_4	Porosity
[cm]	[mM]		[µM]			[mM]			[Vol. %]
0	2.25	2.81	n.d.	83.2	1.16	2.12	0.14	0.24	1.21
1	2.15	3.49	n.d.	161	0.27	1.59	0.24	0.31	0.97
2	2.03	4.70	n.d.	178	0.18	0.89	2.17	0.71	0.93
3	2.15	4.88	n.d.	166	0.36	0.82	2.31	0.70	0.96
4	2.20	5.13	n.d.	158	0.11	0.59	3.10	0.32	0.94
6	2.10	5.48	n.d.	102	0.10	0.44	2.90	0.29	0.92
7	2.17	5.83	n.d.	102	0.19	0.18	3.02	0.26	0.93
8	2.18	4.63	n.d.	101	0.18	0.16	1.86	0.17	0.92
9	2.18	6.16	n.d.	100	2.06	0.15	2.85	0.08	0.87
10	–	–	–	–	–	–	–	0.21	0.89
11	–	5.68	n.d.	–	–	0.21	–	0.12	0.86
13	2.20	6.21	n.d.	92.8	0.09	0.04	3.44	0.08	0.92
15	2.20	6.37	n.d.	86.8	0.13	n.d.	2.85	0.08	0.88
17	2.17	6.45	n.d.	80.7	0.03	0.02	2.82	0.08	0.85
19	2.21	6.39	n.d.	76.7	1.07	0.04	2.37	0.02	0.86
21	–	–	–	–	–	–	–	0.13	0.80
23	–	–	–	–	–	–	–	0.11	0.82
25	–	–	–	–	–	–	–	0.10	0.71
27	–	–	–	–	–	–	–	0.02	0.81

Lake Willersinnweiher			**Early-stage stratification 05.17**			**Site W2 Pore-water**			
Sediment Depth	Ca	DIC	NO_3^-	Mn	Fe	SO_4^{2-}	S (-II)$^-$	CH_4	Porosity
[cm]	—— [mM] ——		——— [µM] ———			——— [mM] ———			[Vol. %]
0	2.33	2.72	n.d.	49.1	1.34	2.00	0.07	0.10	1.00
1	2.23	5.28	n.d.	76.3	0.18	0.57	1.71	0.07	0.98
2	2.30	5.86	n.d.	64.1	0.18	0.37	2.51	0.12	0.98
3	2.30	5.87	n.d.	58.6	0.18	0.32	2.63	0.15	0.93
4	2.36	6.18	n.d.	56.4	0.18	0.29	2.51	0.19	0.96
5	2.35	6.27	n.d.	53.8	0.18	0.19	2.18	0.22	0.95
6	2.40	6.33	n.d.	53.9	0.45	0.16	1.96	0.38	0.91
7	2.43	6.40	n.d.	54.2	0.18	0.10	2.02	0.42	0.92
8	2.46	6.66	n.d.	51.1	0.36	0.08	2.06	0.44	0.86
9	2.43	6.72	n.d.	50.8	0.18	0.05	1.45	0.54	0.84
10	2.50	6.74	n.d.	52.6	0.18	0.10	1.32	0.63	0.75
12	2.53	7.08	n.d.	54.4	0.36	0.07	0.72	0.63	0.73
14	2.48	7.09	n.d.	55.7	0.45	n.d.	0.20	0.89	0.68
16	2.62	7.34	n.d.	60.9	0.72	0.02	0.02	1.26	0.73
18	2.62	7.52	n.d.	57.3	0.63	n.d.	0.05	1.83	0.75
20	2.59	6.90	n.d.	53.1	0.09	0.20	n.d.	1.89	0.68
26	2.58	7.45	n.d.	59.3	31.2	0.02	n.d.	3.49	0.66
29	2.66	7.69	n.d.	65.1	49.9	n.d.	n.d.	1.35	0.64
33	–	7.57	n.d.	72.2	107	0.02	n.d.	1.87	0.65
37	2.67	7.69	n.d.	73.5	56.4	n.d.	n.d.	4.67	0.61
41	2.76	8.09	n.d.	49.1	1.34	0.03	n.d.	–	–

Lake Willersinnweiher		**Early-stage stratification 05.17**			**Site W3 Pore-water**			
Sediment Depth	Ca	DIC	NO_3^-	Mn	Fe	SO_4^{2-}	S (-II)$^-$	CH_4	Porosity
[cm]	—— [mM] ——		——— [μM] ———			——— [mM] ———			[Vol. %]
0	–	2.46	n.d.	1.22	0.33	1.93	0.00	0.02	0.70
1	–	2.80	n.d.	–	–	1.54	0.02	0.08	0.67
2	–	3.26	n.d.	48.4	5.12	1.36	0.00	0.08	0.60
3	–	4.69	n.d.	50.8	0.23	0.63	1.72	0.12	0.41
4	–	5.04	n.d.	48.1	0.36	0.41	0.62	0.23	0.43
5	–	5.16	n.d.	–	–	0.35	0.01	0.30	0.46
6	–	5.55	n.d.	42.4	0.11	0.32	2.73	0.34	0.65
7	–	5.48	n.d.	39.5	0.90	0.42	0.71	0.39	0.61
8	–	5.61	n.d.	35.9	0.60	0.38	1.18	0.80	0.49
9	–	5.75	n.d.	32.4	0.38	0.37	1.27	0.40	0.47
10	–	5.12	n.d.	–	–	0.48	–	0.53	0.47
12	–	6.35	n.d.	23.5	0.19	0.11	0.97	0.48	0.43
14	–	6.55	n.d.	14.8	0.52	0.02	0.41	0.70	0.43
16	–	6.65	n.d.	13.7	0.30	0.05	0.03	–	0.70

Lake Willersinnweiher		**Early-stage stratification 05.17**			**Site W4 Pore-water**			
Sediment Depth	Ca	DIC	NO_3^-	Mn	Fe	SO_4^{2-}	S (-II)$^-$	CH_4	Porosity
[cm]	—— [mM] ——		—— [μM] ——			—— [mM] ——			[Vol. %]
0	1.92	2.62	n.d.	1.91	0.18	2.18	–	0.02	0.86
1	-	2.11	n.d.	-	-	2.01	–	0.02	0.88
2	2.10	2.10	n.d.	19.3	0.36	1.99	–	0.03	0.76
3	2.11	2.42	n.d.	18.4	0.18	1.92	–	–	–
4	2.08	2.37	n.d.	15.3	0.27	1.88	–	0.03	0.76
5	2.06	2.40	n.d.	13.4	0.18	1.81	–	–	–
6	–	–	n.d.	–	–	–	–	–	–
7	2.10	2.51	n.d.	11.4	0.18	1.80	–	0.03	0.82
8	–	3.33	n.d.	-	-	1.40	–	0.06	0.78
9	–	–	n.d.	–	–	–	–	–	–
11	2.18	3.67	n.d.	13.0	0.27	1.39	–	–	–
13	–	–	n.d.	–	–	–	–	0.11	0.81
16	2.23	–	n.d.	12.4	0.45	1.59	–	0.21	0.81
21	2.37	3.46	n.d.	10.6	0.27	1.55	–	0.32	0.58

Data for whole-lake CH_4 mass balance (May 2017 in Lake Willersinnweiher)

Lake Depth [m]	Volume [m³]	Area [m²]
0 - 2	148 000	54 500
2 - 4	120 000	
4 - 6	217 000	115 500
6 - 7	191 000	
7 - 8	164 000	
8 - 9	135 000	
9 - 10	106 000	
10 - 12	77 700	
12 - 15	43 400	
15 - 18	11 600	
18 - 20	67	

Description	littoral	profundal	Unit
Sedimentary Production*	0.05 - 0.27	1.01 - 2.82	[mmol m^{-2} d^{-1}]
Sedimentary Release*	0.02 - 0.08	0.15 - 0.36	[mmol m^{-2} d^{-1}]
AOM (SMTZ) *	0.00 - 0.07	0.28 - 1.93	[mmol m^{-2} d^{-1}]
MOx*	–	0.15 - 0.29	[mmol m^{-2} d^{-1}]
Emissions*	0.02 - 0.03	0.01 - 0.02	[mmol m^{-2} d^{-1}]
Oxic Production*	5410 - 19700		[mmol d^{-1}]
C_{CH4} groundwater*	0.84		[mmol m^{-3}]
Flow groundwater**	970		[m^3 d^{-1}]

* based on presented and calculated data

** based on data from Wollschläger et al. (2007)

Data Lake Stechlin

Lake Stechlin			**06.17**						**Site LakeLab Water Column**			
Water Depth	T	pH	O_2	Ca	DIC	Mn	Fe	PO_4^{3-}	SO_4^{2-}	S (-II)$^-$	CH_4	$\delta^{13}C$-CH_4
[m]	[°C]	–	[mM]			[µM]			[mM]		[nM]	[‰]
0.5	18.5	8.54	0.33	1.04	0.85	0.86	n.d.	0.05	0.20	n.d.	495	-50.0
2.5	18.5	8.56	0.33	1.02	1.02	0.85	n.d.	0.00	0.21	n.d.	510	-49.5
5.0	18.5	8.53	0.33	1.02	1.10	0.85	n.d.	0.00	0.21	n.d.	517	-49.5
6.0	18.4	8.51	0.33	1.01	1.09	0.85	n.d.	0.00	0.23	n.d.	517	-50.0
6.5	15.3	8.72	0.42	–	–	–	–	–	–	n.d.	520	-49.2
7.0	12.3	8.68	0.45	1.00	1.54	0.85	n.d.	0.00	0.36	n.d.	626	-49.2
7.5	11.4	8.65	0.45	–	–	–	–	–	–	n.d.	590	-48.3
8.0	10.6	8.54	0.44	0.98	1.20	0.85	n.d.	0.00	0.27	n.d.	378	-48.5
8.5	10.3	8.43	0.43	–	–	–	–	–	–	n.d.	328	-48.5
9.0	9.52	8.31	0.41	1.02	1.64	0.86	n.d.	0.09	0.37	n.d.	240	-47.8
10.0	8.86	8.19	0.40	1.03	1.64	0.86	n.d.	0.05	0.37	n.d.	196	-47.5
14.0	7.19	7.77	0.35	1.01	1.63	0.86	n.d.	0.37	0.37	n.d.	153	-45.0
18.0	6.18	7.49	0.31	1.02	1.64	0.86	n.d.	0.60	0.37	n.d.	411	-50.0

Lake Stechlin		**06.17**				**Site LakeLab Pore-water**			
Sediment Depth	Ca	DIC	PO_4^{3-}	Mn	Fe	SO_4^{2-}	S (-II)$^-$	CH_4	Porosity
[cm]	—— [mM] ——		—— [µM] ——			—— [mM] ——			[Vol. %]
0	1.06	1.76	1.15	0.68	n.d.	0.32	0.02	0.58	0.98
1	1.23	2.37	6.23	nan	n.d.	0.22	–	1.16	0.99
2	1.13	2.41	26.1	4.99	n.d.	0.11	–	0.96	0.99
3	1.32	2.81	33.9	5.92	n.d.	0.11	–	1.74	0.98
4	1.42	3.23	40.6	6.13	n.d.	0.09	0.04	1.84	0.95
5	1.46	3.09	39.0	5.84	n.d.	0.11	0.04	1.93	0.93
6	1.47	3.36	45.2	6.92	n.d.	0.08	–	2.07	0.93
7	1.33	3.00	42.5	6.24	n.d.	0.06	–	2.10	0.91
8	1.30	3.03	43.2	6.53	n.d.	0.04	–	2.09	0.89
9	1.41	3.09	45.7	6.83	n.d.	0.07	0.03	2.15	0.90
10	1.67	3.76	46.9	7.68	n.d.	0.06	0.04	2.15	0.93
12	1.37	3.29	45.9	6.99	n.d.	0.04	0.05	2.31	0.91
14	1.46	3.51	47.1	7.64	n.d.	0.02	0.05	2.14	0.93
15	1.72	3.64	50.1	8.25	n.d.	0.05	0.06	1.83	0.93
18	1.46	3.51	47.6	8.41	n.d.	0.04	0.07	1.88	0.93
20	1.51	3.49	46.2	9.10	n.d.	0.02	0.07	1.91	0.93
23	1.36	3.17	45.0	9.01	n.d.	0.03	0.06	1.83	0.93
26	1.31	3.28	39.7	8.72	n.d.	0.03	0.05	1.70	0.94
29	1.46	3.44	39.7	8.81	n.d.	0.02	0.04	1.80	0.98
32	1.40	3.39	37.4	8.14	0.21	0.02	0.02	1.75	0.93
36	1.25	3.17	34.2	6.32	0.20	0.01	0.01	1.74	0.92
40	1.15	2.87	33.2	5.46	0.21	0.01	–	1.74	0.93
44	1.37	3.32	34.2	5.48	0.81	0.01	–	1.93	0.94
48	1.06	1.76	1.15	0.68	n.d.	0.32	0.02	1.42	0.91

Lake Stechlin		**06.17**				**Site Profundal Pore-water**			
Sediment Depth	Ca	DIC	PO_4^{3-}	Mn	Fe	SO_4^{2-}	S (-II)$^-$	CH_4	Porosity
[cm]	—— [mM] ——		——— [μM] ———			——— [mM] ———			[Vol. %]
0	0.96	1.49	0.00	n.d.	n.d.	0.35	0.01	0.02	0.88
1	0.99	1.26	0.23	n.d.	n.d.	0.52	–	0.05	0.91
2	0.98	1.32	1.15	n.d.	n.d.	0.48	–	0.11	0.93
3	1.02	1.48	1.85	1.50	n.d.	0.39	–	0.19	0.89
4	1.03	1.61	2.54	1.52	n.d.	0.34	–	0.33	0.92
5	1.11	1.75	3.46	1.48	n.d.	0.35	–	0.44	0.92
6	1.06	1.73	3.92	1.02	n.d.	0.30	0.02	0.51	0.90
7	1.12	1.92	5.08	1.13	n.d.	0.27	–.	0.64	0.91
8	1.06	1.74	6.23	1.19	n.d.	0.25	0.02	0.61	0.86
10	1.11	1.97	7.39	1.71	n.d.	0.22	0.06	0.56	0.91
12	1.13	2.04	9.23	2.17	n.d.	0.17	0.07	0.67	0.93
14	1.10	2.06	10.8	2.80	n.d.	0.14	0.10	0.90	0.93
16	1.17	2.26	11.3	3.37	n.d.	0.10	0.04	0.77	0.91
18	1.14	2.23	11.1	3.64	n.d.	0.10	–	0.73	0.90
21	1.11	2.25	10.8	3.86	n.d.	0.03	–	0.67	0.93
24	1.12	2.35	11.3	4.00	n.d.	0.02	–	0.87	0.95
27	1.13	2.31	12.2	3.95	n.d.	0.02	0.03	0.85	0.92
31	1.22	2.46	14.3	3.95	n.d.	0.02	0.06	1.04	0.94
35	1.15	2.32	15.7	3.59	n.d.	0.02	0.02	1.17	0.92
39	1.12	2.35	15.7	3.24	0.31	n.d.	0.02	1.49	0.96
44	1.03	2.25	15.0	3.80	4.49	n.d.	0.02	1.24	0.92
48	–	–	–	–	–	–	–	1.32	0.93

Lake Stechlin		**06.17**				**Site Littoral Pore-water**			
Sediment Depth	Ca	DIC	PO_4^{3-}	Mn	Fe	SO_4^{2-}	S (-II)$^-$	CH_4	Porosity
[cm]	—— [mM] ——		——— [µM] ———			——— [mM] ———			[Vol. %]
0	0.96	1.59	0.00	n.d.	n.d.	0.34	–	–	0.98
1	1.19	1.71	0.00	n.d.	n.d.	0.40	–	0.09	0.95
2	1.46	2.78	0.23	2.93	n.d.	0.15	0.02	0.11	0.95
3	1.38	2.81	1.39	2.46	n.d.	0.06	0.03	0.21	0.97
4	1.38	2.57	1.85	1.09	0.38	0.15	–	0.17	0.96
5	1.36	2.59	3.46	1.51	n.d.	0.09	0.05	0.24	0.96
6	1.33	2.67	4.39	1.70	n.d.	0.07	0.20	0.22	0.91
7	1.30	2.61	6.23	1.38	n.d.	0.08	0.08	0.30	0.92
8	1.30	2.64	8.31	1.32	n.d.	0.06	–	0.38	0.91
9	1.36	2.70	4.16	1.14	n.d.	0.05	0.07	0.47	0.88
10	1.46	2.81	4.62	1.25	n.d.	0.04	0.13	0.64	0.89
12	1.43	2.97	5.08	1.08	n.d.	0.05	0.12	0.72	0.89
14	1.42	2.84	5.54	1.02	n.d.	0.06	0.13	1.13	0.90
16	1.58	3.08	6.46	0.96	n.d.	0.05	0.11	1.31	0.88
18	1.75	3.40	7.39	1.09	n.d.	0.05	0.23	1.43	0.87
20	1.73	3.56	7.62	1.00	n.d.	0.03	0.19	1.61	0.88
23	2.05	4.01	8.08	1.66	0.30	0.02	–	1.67	0.87
26	2.15	4.49	7.85	1.20	n.d.	0.03	0.25	1.72	0.85
29	2.05	4.33	5.77	1.30	n.d.	0.03	–	1.68	0.98

Data Lake Erken

Lake Erken			**07.17**						**Site Buoy** **Water Column**			
Water Depth	T	pH	O_2	Ca	DIC	Mn	Fe	PO_4^{3-}	SO_4^{2-}	S (-II)$^-$	CH_4	$\delta^{13}C$-CH_4
[m]	[°C]	–	[mM]			[µM]			[mM]		[nM]	[‰]
1	18.9	8.75	0.33	1.05	1.69	n.d.	0.24	n.d.	0.29	n.d.	230	-50.8
3	18.8	8.74	0.33	1.06	1.69	n.d.	0.23	n.d.	0.29	n.d.	242	-50.5
6	18.4	8.59	0.31	1.05	1.70	n.d.	0.24	n.d.	0.29	n.d.	252	-50.5
7	18.2	8.61	0.31	1.06	1.69	n.d.	0.24	n.d.	0.29	n.d.	256	-50.1
8	18.1	8.52	0.30	1.03	1.69	n.d.	0.29	n.d.	0.29	n.d.	258	-50.1
9	17.9	8.41	0.29	1.04	1.70	n.d.	0.23	n.d.	0.29	n.d.	244	-50.0
10	17.7	8.15	0.25	1.01	1.78	n.d.	0.22	n.d.	0.29	n.d.	144	-47.2
11	17.2	7.94	0.21	1.01	1.76	n.d.	0.24	n.d.	0.29	n.d.	125	-47.8
13	16.6	7.76	0.15	1.04	1.79	0.19	0.23	n.d.	0.28	n.d.	158	-48.2
14	–	–	–	1.03	1.80	0.21	0.25	n.d.	0.27	n.d.	188	-47.1

Lake Erken		**07.17**			**Site Buoy Pore-water**			
Sediment Depth	Ca	DIC	P	Mn	Fe	SO_4^{2-}	S (-II)$^-$	CH_4
[cm]	[mM]		[μM]			[mM]		
0	1.11	1.77	n.d.	13.3	0.35	0.40	n.d.	–
1	1.19	0.36	19.4	87.4	13.7	0.00	n.d.	n.d.
2	1.14	2.18	26.1	81.2	20.4	0.02	n.d.	0.01
3	1.29	2.37	53.7	70.2	46.8	0.12	n.d.	0.01
4	1.30	2.42	46.1	67.9	26.4	0.09	n.d.	0.02
5	1.17	1.98	51.5	46.1	29.9	0.10	n.d.	0.02
6	1.31	2.60	65.2	54.8	34.9	0.06	n.d.	0.02
7	1.26	2.43	58.5	47.3	21.8	0.04	n.d.	0.02
8	1.32	2.54	71.0	48.1	14.9	0.04	n.d.	0.03
9	1.30	2.51	61.8	48.2	11.6	0.03	n.d.	0.03
10	1.27	2.34	40.2	40.8	3.02	0.08	n.d.	0.04
12	1.23	2.43	34.2	33.0	n.d.	0.05	n.d.	0.03
14	1.26	2.37	26.6	32.2	n.d.	0.06	n.d.	0.04
16	1.22	2.35	27.7	30.9	0.24	0.04	n.d.	0.05
18	1.12	2.39	29.5	27.1	0.65	n.d.	n.d.	0.07
20	1.17	2.43	33.1	28.2	1.03	0.04	n.d.	0.09
22	1.17	2.45	41.5	27.1	6.55	0.03	n.d.	0.12
24	1.21	2.65	50.6	27.3	11.4	0.02	n.d.	0.19
26	1.22	2.76	59.2	26.9	20.3	0.02	n.d.	0.33
28	1.25	2.75	53.5	27.3	21.0	0.02	n.d.	0.23
30	1.31	3.10	64.5	28.3	39.2	n.d.	n.d.	0.46
32	–	–	–	–	–	–	–	0.58
34	–	–	–	–	–	–	–	0.51
36	–	–	–	–	–	–	–	0.64
38	–	–	–	–	–	–	–	0.60

Lake Erken		**07.17**			**Site Littoral Pore-water**			
Sediment Depth	Ca	DIC	P	Mn	Fe	SO_4^{2-}	S (-II)$^-$	CH_4
[cm]	[mM]		[μM]			[mM]		
0	0.98	1.49	n.d.	0.59	0.41	0.30	n.d.	–
1	1.05	1.36	n.d.	3.45	0.27	0.43	n.d.	0.04
2	1.10	1.52	n.d.	6.19	0.31	0.37	n.d.	0.09
3	1.14	2.02	n.d.	11.6	0.49	0.24	n.d.	0.15
4	1.10	1.88	n.d.	11.1	0.22	0.24	n.d.	0.12
5	1.16	2.13	n.d.	10.8	n.d.	0.13	n.d.	0.10
6	1.20	2.47	17.4	11.0	n.d.	0.11	n.d.	0.12
7	1.30	2.60	21.8	11.3	n.d.	0.09	n.d.	0.32
8	1.34	2.74	19.2	10.5	n.d.	0.09	n.d.	0.32
9	1.42	2.92	19.2	10.6	n.d.	0.09	n.d.	0.22
10	1.50	3.09	21.0	10.3	n.d.	0.09	n.d.	0.29
12	1.50	3.14	17.7	9.28	0.24	0.06	n.d.	0.35
14	1.55	3.24	n.d.	8.90	0.18	0.05	n.d.	0.27
16	1.36	3.07	n.d.	6.90	0.27	n.d.	n.d.	0.24
18	1.50	3.22	n.d.	8.25	n.d.	0.05	n.d.	0.15
20	1.46	3.22	n.d.	7.89	n.d.	0.06	n.d.	0.21
22	1.42	3.21	n.d.	7.60	0.21	n.d.	n.d.	–

Lake Erken		**07.17**				**Transects**			
Site		Ca	DIC	NO_3^-	Mn	Fe	SO_4^{2-}	S (-II)$^-$	CH_4
Northing	Easting	— [mM] —		——— [µM] ———			——— [mM] ———		
59°50,395' N	18°31,145' E	1.03	1.66	2.24	0.14	0.28	0.27	n.d.	336
59°50,276' N	18°32,596' E	1.03	1.68	0.88	0.14	0.30	0.31	n.d.	328
59°51,830' N	18°33,070' E	1.03	1.67	2.10	0.09	0.25	0.26	n.d.	285
59°50,452' N	18°34,214' E	1.04	1.67	0.82	0.06	0.22	0.31	n.d.	206
59°50,305' N	18°36,367' E	1.03	1.66	0.44	0.06	0.24	0.31	n.d.	208
59°50,535' N	18°37,264' E	1.03	1.67	0.25	0.05	0.24	0.30	n.d.	205
59°50,287' N	18°37,390' E	1.02	1.66	0.55	0.04	0.22	0.26	n.d.	239
59°50,244' N	18°37,426' E	1.01	1.65	0.34	0.05	0.28	0.31	n.d.	270
59°50,269' N	18°38,269' E	1.02	1.67	0.30	0.06	0.24	0.31	n.d.	227
59°50,960' N	18°37,527' E	1.02	1.67	0.20	0.11	0.24	0.31	n.d.	895
59°51,119' N	18°37,419' E	1.01	1.68	0.59	0.06	0.21	0.31	n.d.	746
59°50,575' N	18°37,430' E	1.01	1.67	0.19	0.06	0.22	0.31	n.d.	462
59°50,380' N	18°37,419' E	1.01	1.68	0.32	0.04	0.20	0.31	n.d.	270
59°50,244' N	18°37,426' E	1.02	1.68	0.67	0.04	0.21	0.31	n.d.	206
59°50,215' N	18°37,466' E	1.02	1.68	0.70	0.04	0.20	0.31	n.d.	199
59°50,172' N	18°37,480' E	1.02	1.68	0.42	0.06	0.21	0.31	n.d.	221
59°50,118' N	18°37,530' E	1.03	1.69	1.03	0.08	0.21	0.31	n.d.	307
59°50,110' N	18°37,548' E	1.04	1.70	0.47	0.32	0.26	0.31	n.d.	1426
59°50,850' N	18°37,584' E	1.03	1.70	0.75	0.41	0.32	0.30	n.d.	1684

Data for model calculations in Chapter "Methane in lake environments and future prospects"

Parameter	Description	Value		Unit
		Lake Willersinnweiher	Lake Stechlin	
C_X*	Predicted surface water CH_4 concentration	-		[mmol m^{-3}]
$C_{0(l)}$**	Littoral CH_4 concentration (surface)	1.32	1.20 ***	[mmol m^{-3}]
$C_{0(p)}$**	Profundal CH_4 concentration (surface)	0.55	0.50	[mmol m^{-3}]
λ*	Physical decline in CH_4 concentration from shore to center of the lake	-		[m^{-1}]
x*	Distance from shore	-		[m]
D	Shortest distance between two shores	180	650	[m]
k_{600}*	Standardized gas exchange coefficient from epilimnion	-		[m d^{-1}]
Z_{ML}**	Thickness epilimnion	6	7	[m]
$k_{O/P}$	Net biological impact (negative for oxidation, positive for production)	0.1 – 0.5 (Bogard et al. 2014; Tang et al. 2014)		[d^{-1}]
k_H	horizontal diffusivity coefficient	0.06 (DelSontro et al. 2017)		[m^2 d^{-1}]
U_{10}*	Wind speed at 10 m height	-	-	[m d^{-1}]
A	Lake area	$0.27 * 10^6$	$4.3 * 10^6$	[m^2]
U_Z	Measured wind speed at height z	$3.45 * 10^5$ (mean value)		[m d^{-1}]
C_d	Drag coefficient at 10 m height	0.0013 (Stauffer 1980)		[-]
κ	Karman constant	0.4 (Andreas et al. 2006)		[-]
z	Height of wind speed measurement	4	2	[m]

* calculated from equations presented in Table 12

** obtained from presented data

*** pers. comm. HP Grossart (IGB)

Eidesstattliche Versicherung gemäß § 8 der Promotionsordnung

der Naturwissenschaftlich-Mathematischen Gesamtfakultät der Universität Heidelberg

1. Bei der eingereichten Dissertation zu dem Thema

   Methane Dynamics in Lakes

   handelt es sich um meine eigenständig erbrachte Leistung.

2. Ich habe nur die angegebenen Quellen und Hilfsmittel benutzt und mich keiner unzulässigen Hilfe Dritter bedient. Insbesondere habe ich wörtlich oder sinngemäß aus anderen Werken übernommene Inhalte als solche kenntlich gemacht.
3. Die Arbeit oder Teile davon habe ich wie bislang nicht an einer Hochschule des In- oder Auslands als Bestandteil einer Prüfungs- oder Qualifikationsleistung vorgelegt.
4. Die Richtigkeit der vorstehenden Erklärungen bestätige ich.
5. Die Bedeutung der eidesstattlichen Versicherung und die strafrechtlichen Folgen einer unrichtigen oder unvollständigen eidesstattlichen Versicherung sind mir bekannt.

Ich versichere an Eides statt, dass ich nach bestem Wissen die reine Wahrheit erklärt und nichts verschwiegen habe.

Heidelberg, _____ _____

(Ort Datum) (Unterschrift)